

**Optimisation of the HVOF Thermal Spray Process
For Coating, Forming and Repair of Components**

by

Jit Cheh Tan, BSc (Eng)

Ph.D

1997

**Optimisation of the HVOF Thermal Spray Process
For Coating, Forming and Repair of Components**

by

Jit Cheh Tan, BSc (Eng)

A thesis submitted in fulfilment of the requirement for the degree of

Doctor of Philosophy

Supervisors:

Professor M.S.J. Hashmi

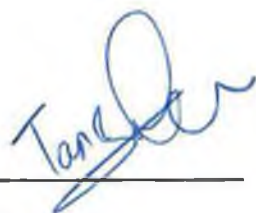
Dr L. Looney

Dublin City University
School of Mechanical & Manufacturing Engineering
September 1997

DECLARATION

I hereby certify that this material, which I now submit for assessment on the programme of study leading to the award of Doctor of Philosophy is entirely my own work and has not been taken from the work of others save and to the extent that such work has been cited and acknowledged within the text of my work.

Signed: _____



I.D. No.: 93700571

Date 8th September 1997

ACKNOWLEDGEMENTS

I would like to express my sincere thanks to Professor M.S.J. Hashmi and Dr Lisa Looney for their continued support and supervision throughout the course of the project.

I would also like to thank Mr Martin Johnson for his co-operation and assistance in preparing all the experimental specimens. I must also thank Mr Liam Dominican and Mr Ian Hopper from the workshop for their help at various stages of this work.

I would like to thank my girlfriend, Janet , for her love, support and encouragement during these long years. And last, but not least, a very special thanks to my parents and my family for their constant love and support.

Table of Contents

Declaration	I
Acknowledgements	II
Table of Contents	III
Abstract	VII
CHAPTER 1 INTRODUCTION	1
CHAPTER 2 LITERATURE SURVEY	4
2.1 Introduction to Surface Engineering	4
2.2 Overview Of Coating Technologies	6
2.3 Thermal Spraying	10
2.3.1 Wire Spraying	10
2.3.2 Electric Arc Spraying	12
2.3.3 Plasma Spraying	12
Atmospheric Plasma Spraying (APS)	12
Vacuum Plasma Spraying (VPS)	14
2.3.4 Flame Thermal Spraying	16
Pulse Combustion HVOF (Detonation Gun) Process	18
Continuous Combustion HVOF Process	18
2.4 The HVOF Process	20
2.4.1 Combustion and Gas Dynamic of the HVOF System	20
2.4.2 Advantages and Disadvantages of the HVOF System	26
2.4.3 Characteristics of HVOF Coatings	26
2.4.4 Comparison of HVOF and Plasma Thermal Spraying	28
2.4.5 Future Potential and Markets	29
2.5 Thermally Sprayed Coatings	31
2.5.1 Composition of Thermal Sprayed Coatings	34
2.5.2 Residual Stress	34
2.5.3 Bond Strength	35
2.5.4 Hardness	37
2.5.5 Anisotropy in Thermally Sprayed Coatings	37

2.6 Spray Forming	38
2.6.1 Current Conventional Sinterforming Processes for Particulate Materials	38
2.6.2 History of Spray Forming Techniques	38
2.6.3 Thermal Spray Forming of Solid Components	39
2.6.4 The HVOF Forming Process	39
2.6.5 Osprey Forming	42
CHAPTER 3 EXPERIMENTAL EQUIPMENT AND PROCEDURES	44
3.1 HVOF Thermal Spraying System	44
3.1.1 Diamond Jet Gun	44
3.1.2 Powder Feed Unit	49
3.1.3 Gas Flow Meter Unit	50
3.1.4 Gas Regulator and Manifolds	51
3.1.5 Air Control Unit	52
3.2 Procedure for HVOF Spraying	53
3.2.1 Spraying Substrate and Surface Preparation	53
3.2.2 Spraying Process	54
3.2.3 Post Spray Treatment Process	55
3.3 Thermal Spray Safety Measures	57
3.3.1 Gas Cylinder Use	57
3.3.2 "Diamond Jet Equipment" Safety	58
3.3.3 Metal Dust	58
3.3.4 Eye Protection	59
3.3.5 Reduction of Noise Hazard	59
3.3.6 Personal Protection	59
3.3.7 Reduction of Respiratory Hazards	60
3.3.8 General HVOF Gun Operational Precautions	60

CHAPTER 4 COATING PROPERTIES AND MEASUREMENT METHODS	61
4.1 Coating Thickness Control and Measurement Method	61
4.2 Hardness Measurement	63
4.3 Porosity Measurement	65
4.4 Adhesion Bond Strength Measurement	66
4.5 Optical Microscope	70
4.6 Residual Stress Measurement	70
4.6.1 X-Ray Diffraction Stress Determination	71
4.6.2 The Hole Drilling Method	78
4.6.2.1 THE HOLE DRILLING PROCEDURE WITH RS-200 MILLING GUIDE	79
4.6.2.2 Strain Gauges and Strain Indicator	80
4.6.2.3 Drilling Samples	83
4.6.2.4 Data and Calculation	84
4.7 Three Point Bend Test	86
CHAPTER 5 EXPERIMENTAL WORK AND RESULTS	88
5.1 Fabrication of Free Standing Components	88
5.1.1 Fabrication of Free Standing Solid Components	88
5.1.2 Characterisation of Free Standing Components	95
5.2 HVOF Sprayed coatings	107
5.2.1 Experimental Matrix - Coatings	109
5.2.2 Results:	110
5.3 Repair of damaged components using the HVOF Process	140
5.3.1 Machinability of repaired components	144
5.3.2 The optimisation of HVOF repair process	152
5.4 Statistical Analysis of Results	186

CHAPTER 6 CONCLUSIONS AND RECOMMENDATIONS	196
6.1 Conclusion:	196
6.2 Recommendations for future work	197
References	198
Publications	206
Appendices	207
Appendix A	207
Appendix B	209
Appendix C	210
Appendix D	217

Abstract:

Optimisation of the HVOF Thermal Spray Process for Coating, Forming and Repair of Components

by Jit Cheh Tan BSc (Eng)

The High Velocity Oxy-Fuel (HVOF) Thermal Spraying technique has been widely adopted in many industries due to its flexibility, and cost effectiveness in producing superior quality of coating. The demand of high-technology industries and the availability of new advanced materials have generated major advances in this field. The HVOF thermal spray process has been utilised in many industries to apply coatings on components to protect against wear, heat and corrosion, and also to build up worn components. This spraying technology is not limited to coating substrates but also encompasses the manufacture of net shaped component from materials which are sometimes difficult to form by conventional methods.

A knowledge of coating properties, testing and evaluation methods is essential in order to apply coating technology to a specific application. While spraying parameters and substrate surface preparations directly impact the coating properties, it is equally important to know the spraying technique required to deposit coating having these properties and the processing parameters which have to be applied.

The thesis reports the development and optimisation of the HVOF thermal spray process for coating, forming and repair of components. A die was designed to manufacture free standing WC-Co inserts, and a similar technique was then followed to fabricate free standing annular rings and solid discs. The effects of spraying parameters on the components properties such as residual stresses and hardness were investigated and limitations identified.

Experiments to assess the coatings properties involved the combinations of three spraying powders, (1) Austenitic stainless steel (2) WC-Co and (3) Tool steel match powder on stainless steel 316L and D2 tool steel substrates. Investigations were carried out on the effect of spraying distance, sprayed coating thickness and pre-spray heat treatment on coating properties including hardness, bond strength and residual

stress. Results reveal that there are strong correlations between the bonding strength, coating thickness and residual stress in coatings. The tensile residual stresses coupled with increasing coating thickness cause the degradation of bond strength with increasing coating thickness.

Optimisation of the repair of damaged components using the HVOF technique involved the use of similar combinations of powder and substrate materials. Tests were carried out to identify the adhesion strength of the repaired material sprayed under various conditions which were varied, including (1) repair thickness (2) pre-repair and post-repair heat treatment (3) repair wall angle and (4) substrate surface preparation. In addition, the finish machining possibility of these repaired components was evaluated.

CHAPTER 1 INTRODUCTION

The recognition that the vast majority of engineering components can potentially degrade or catastrophically fail in service because of such surface related phenomena as wear, corrosion and fatigue, led in the early 1980's to the rapid development of surface engineering. Surface engineering involves, amongst other processes, the application of traditional and innovative coating technologies to engineering components and materials, in order to produce a composite material with properties unattainable in either the base or surface materials.

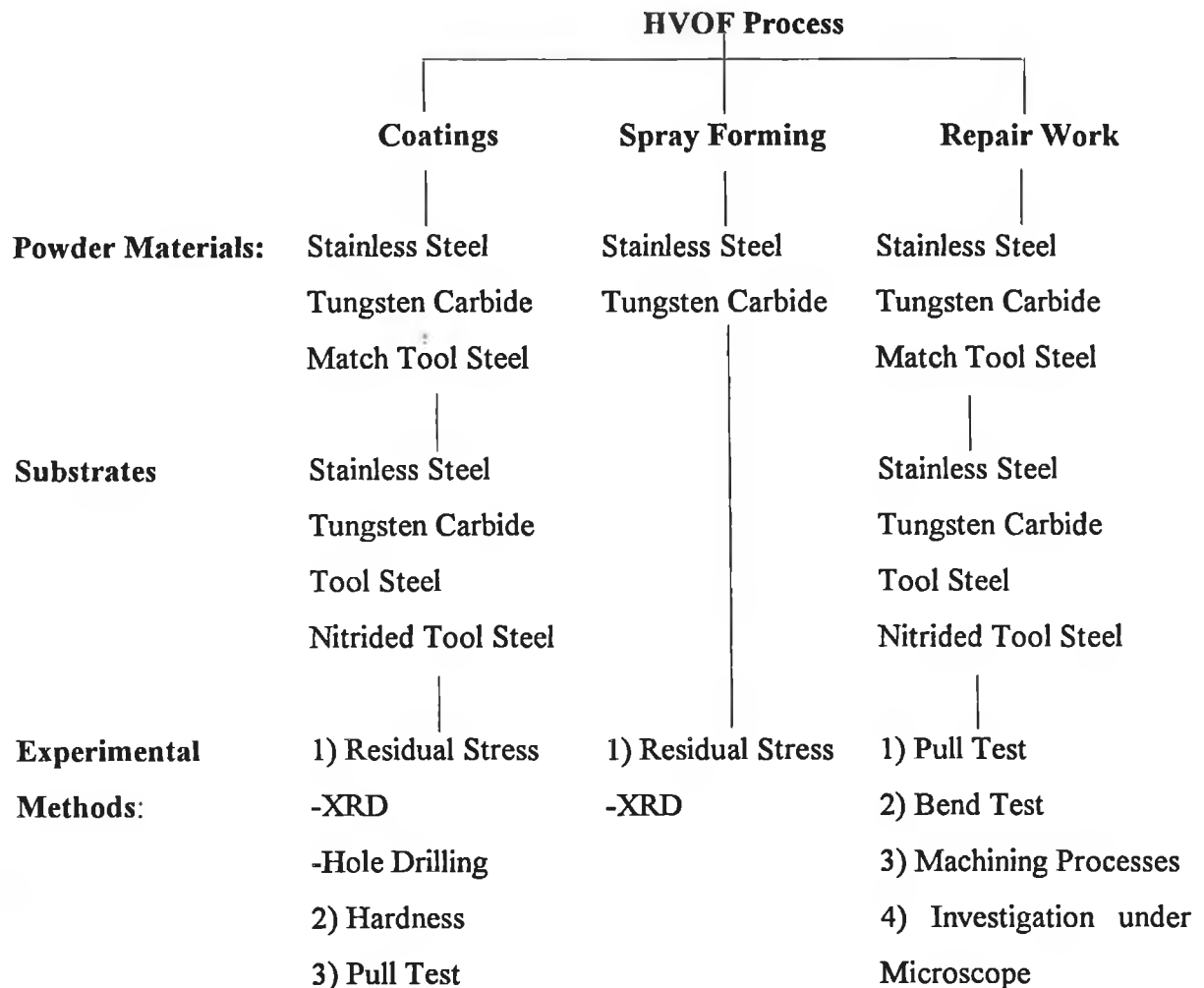
Of all the advanced coating techniques, the thermal spraying process is one of the most successful and versatile because of the very wide range of coating materials and substrates that can be processed, e.g. from tape recording heads, to print rollers, and bridge structures. The High Velocity Oxy-Fuel (HVOF) process is one of the most popular thermal spray technologies and has been utilised in many industries because of its flexibility, and the superior quality of coatings produced compared to other thermal spraying techniques.

The demands of high-technology industries, and the availability of new particulate materials have generated major advances in this field. The need for selection of matching substrate and spraying materials, and the determination of optimised spraying parameters and substrate surface preparation methods are the main problems associated with the HVOF spraying process.

The main objective of this research is to investigate and optimise spray parameters for a number of different applications of the technique, namely:

1. Fabrication of solid WC components using the HVOF process
2. Reduction of residual stresses in HVOF formed and coated components
3. Repair of damaged components using the HVOF process.

The work programme of this project is outlined in the following schematic diagram.



The remainder section of this thesis is divided into a number of chapters. Chapter 2, the literature review, gives a general introduction to surface engineering focusing mainly on flame thermal spraying technology. The spray forming process, its history background are discussed. This chapter also details the characteristics of the High Velocity Oxy-fuel (HVOF) process and coatings.

The experimental equipment and procedures of the HVOF thermal spraying system are presented in chapter 3. It includes brief descriptions of individual units within the whole HVOF system, and the safety aspects of this system.

Measurement methods are described in chapter 4. These include detailed descriptions of residual stress measurement on coatings and free standing components using both the X-ray diffraction and Hole drilling methods. Data, results and calculations are also included. Coating adhesion strength and bend test methods are also detailed in this chapter.

Chapter 5 presents the experimental results, including results of free standing components fabricated using the HVOF process. The effects of substrate pre-spray heat treatment on the residual stresses of the components sprayed are analysed and discussed. The effects of pre-spray substrate surface temperature, substrate surface treatment and post-spray heat treatment on coating bond strength are also discussed. This chapter also includes the results of a study carried out on the effect of component defect angle on the adhesion and bend strengths of repairs. Tests were also carried out on the effect of different substrate surface preparations on the adhesion strength of the sprayed coatings.

Statistical analysis of the results are also presented in this chapter.

Conclusions for the present work and suggestion for further work are included in Chapter 6.

CHAPTER 2 LITERATURE SURVEY

2.1 Introduction to Surface Engineering

Surface engineering in today's engineering world embraces the design, evaluation and performance in service of a total system including a substrate through the interface to a coating [1]. It is a branch of science that deals with methods for achieving desired surface requirements and assessing surface behaviour in service for engineering components [2]. The behaviour of a material is greatly dependent upon the surface of the material, the shape of the contact surface, the environment and the operating conditions.

Surface properties for certain engineering applications can be selected on the basis of a subjective judgement, i.e. colour or texture for decoration. However, surfaces not only define the outer limits of bodies, they are also called upon to perform a variety of engineering functions, possibly completely different from those required of bulk materials. Modern process environments which contribute to wear of machine tools in industry can be very complex, usually involving a combination of chemical and physical degradation. Surface properties of the components used in a particular working environment have to be designed in accordance to that working environment. Various surface properties that are relevant to the behaviour of engineering components are shown in Figure 1.

The surface properties of the materials of a component may change noticeably as a result of the environment in which it operates. The outer surface of bulk material is known to consist of several zones having different physical and chemical characteristics particular to bulk material itself [3]. The construction of a metal surface is shown schematically in Figure 2. Above the worked layer, there is a region of amorphous or microcrystalline material called the Bilby Layer, resulting from the surface melting and flowing during work hardening. Above this is an oxide layer, the formation of this layer depending on the environment and surface oxidation mechanism. Outermost is a layer of adsorbate, which is generally a layer of water vapour or hydrocarbon from the surroundings which may condense and become physically adhered to the surface.

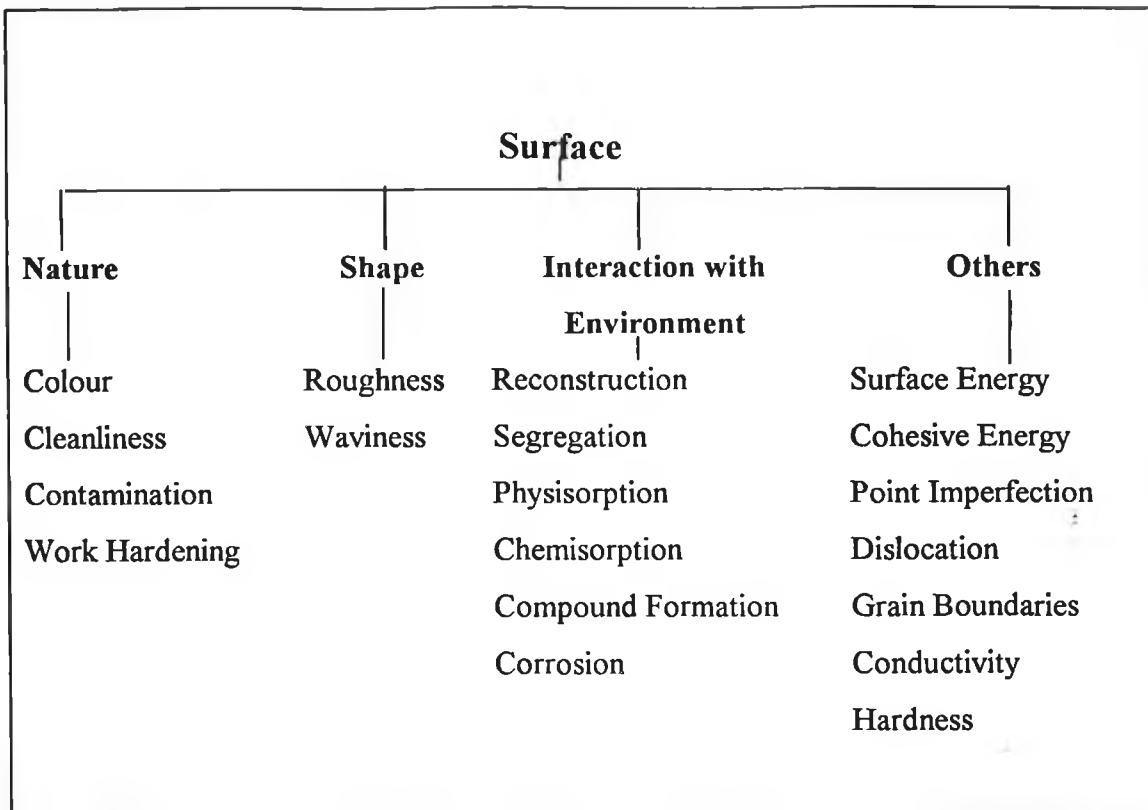


Figure 1 Various surface properties

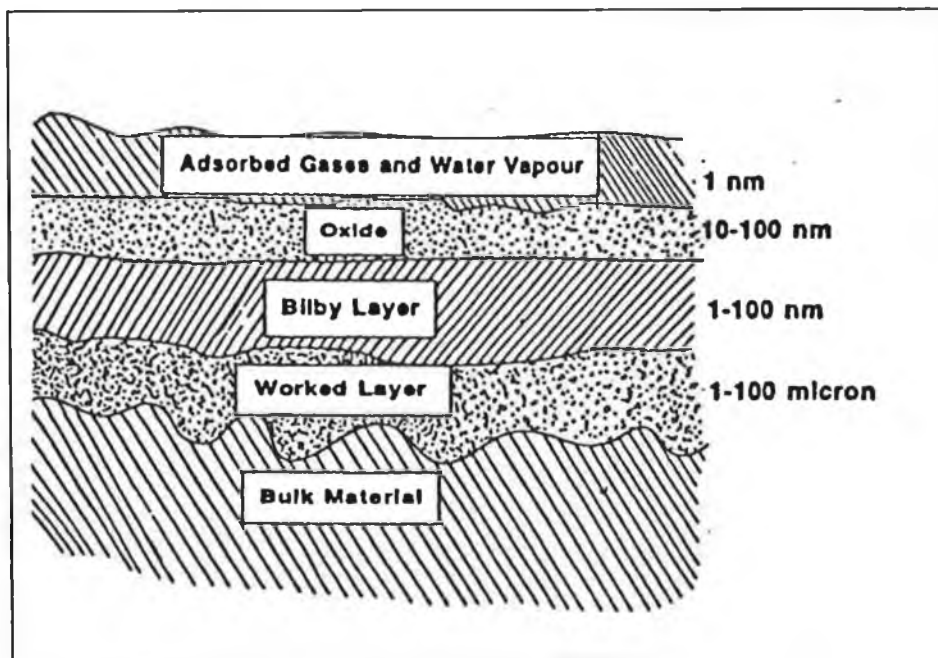


Figure 2 Schematic representation of metal surface [3].

2.2 Overview Of Coating Technologies

A coating may be defined as a near surface region with properties different from the bulk material it is deposited on. Thus the material system (coating and substrate) form a composite where one set of properties are obtained from the bulk substrate and another from the coating itself. In short, the complex coating-substrate combination fulfils the desired coating property requirement. Figure 3 illustrates some of the inter related properties of the complex system including processing and environment which may be controlled within specified limits to ensure that the overall engineering requirements of the system are fulfilled.

A coating process involves the selection of deposition material, the transport of the material and the accumulation of the material on the substrate. These steps can be completely separate from each other, or may be superimposed on each other depending upon the process used. The methods of depositing coating materials can be grouped into three distinct types viz. Vapour (gaseous) Phase, Liquid Phase and Molten or Semi-molten Phase. Figure 4 shows the wide variety of surface coating techniques in use. Figure 5 details the classification of various flame spraying processes.

The selection of a particular deposition process depends on several factors, including:

- 1) The material to be deposited,
- 2) rate of deposition required,
- 3) limitations imposed by the substrate (eg. maximum allowable deposition temperature),
- 4) adhesion of the deposited material to substrate,
- 5) process energy,
- 6) purity of target material since this will influence the impurity content in the film,
- 7) apparatus required and availability of same,
- 8) cost, and
- 9) ecology considerations

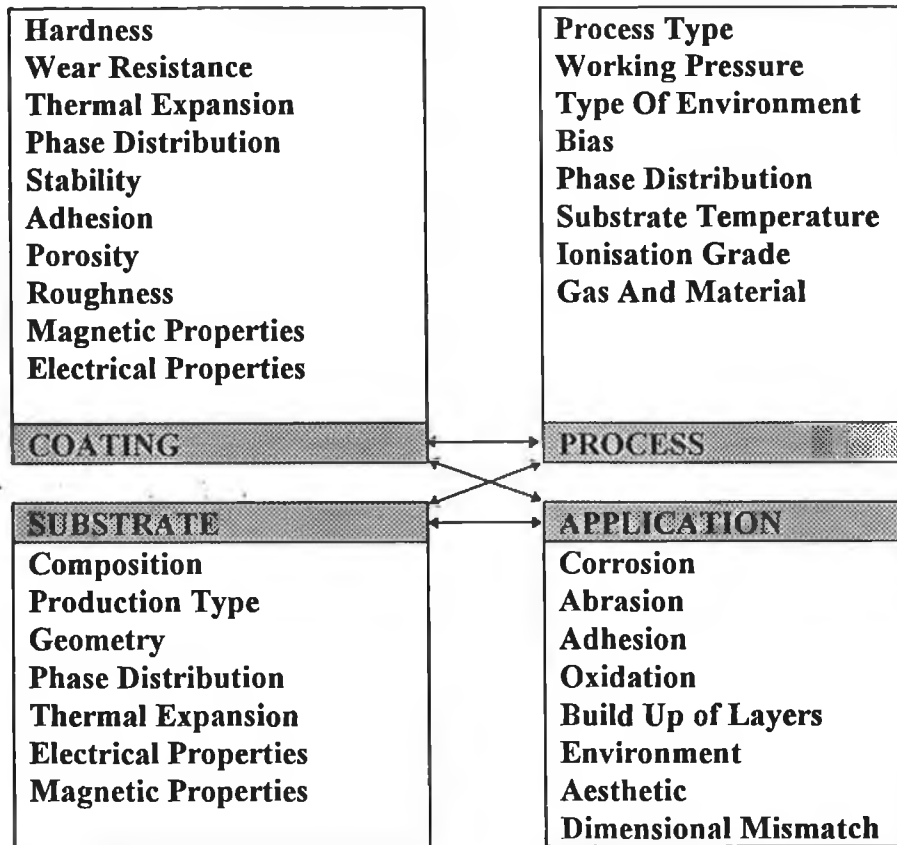


Figure 3 The inter-relationship of coating, substrate, process and application

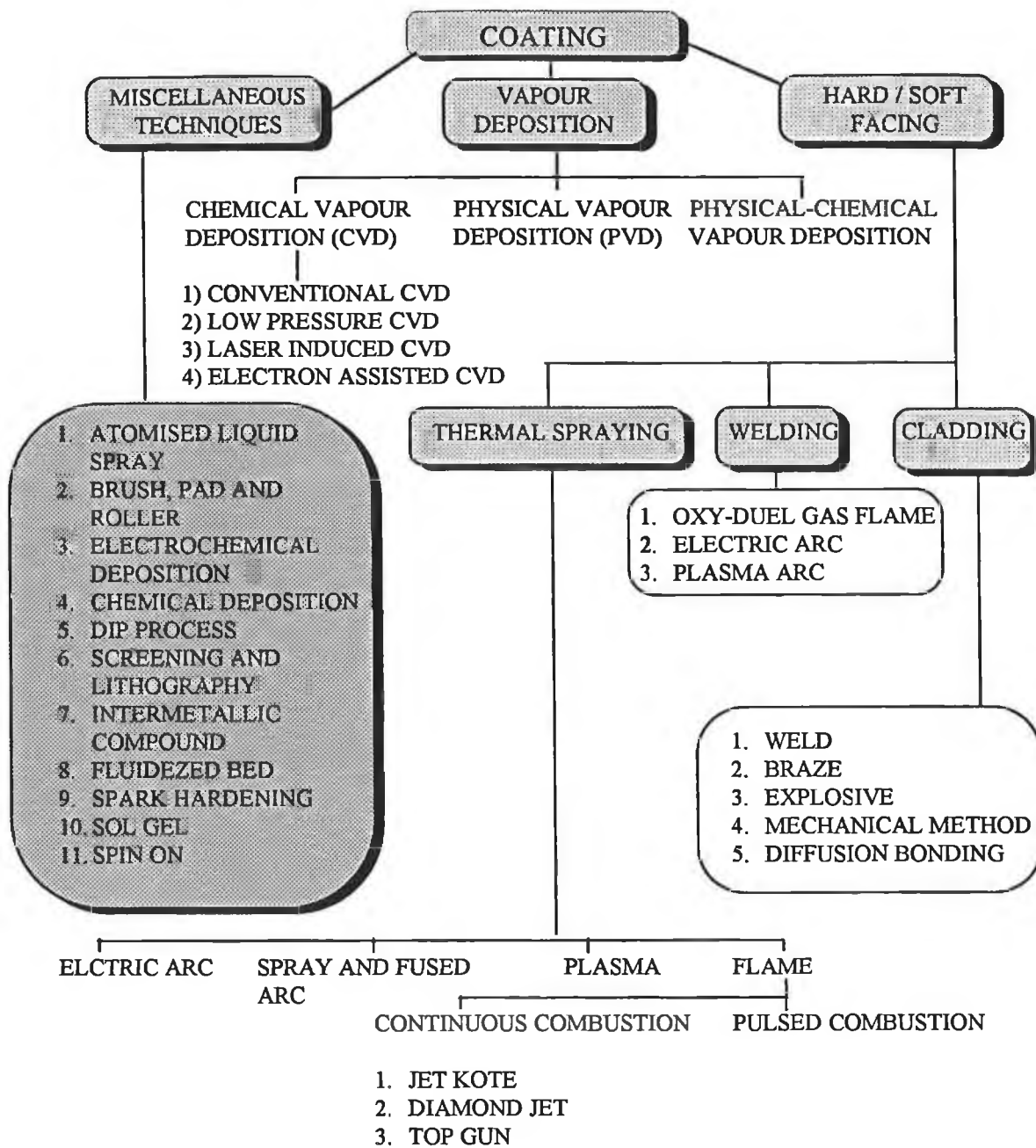


Figure 4 Classifications of various coating techniques

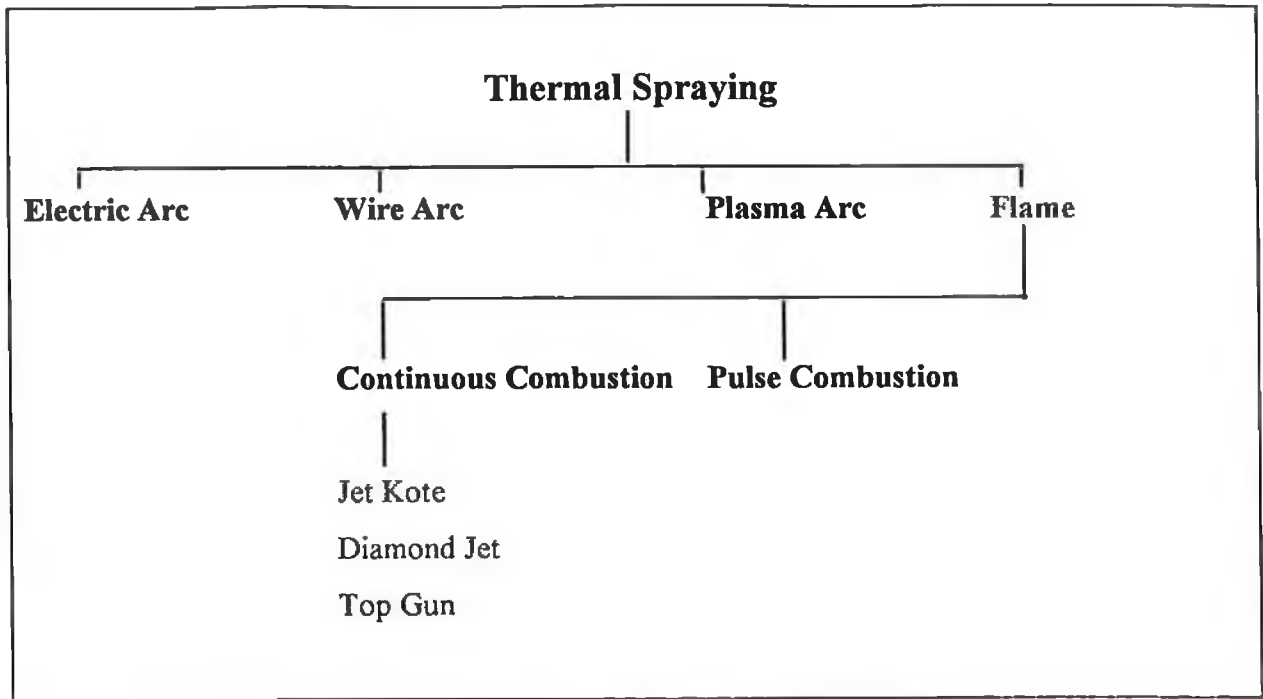


Figure 5 Classification of various flame thermal spraying

2.3 Thermal Spraying

Thermal spraying is the generic name for a family of coating processes in which a coating material is heated rapidly in a hot gaseous medium, and simultaneously projected at high velocity onto a prepared substrate surface where it builds up to produce the desired coating. It has a long history beginning with work carried out in the late nineteenth century . The earliest commercial application is attributed to Schoop in Switzerland who by 1910 [4] had developed devices for melting tin or zinc and projecting the molten metal with compressed air. By the mid-1920s metal spraying had found use in at least 15 countries [4]. In the last three decades the demands of high technology industries, eg. the aerospace industry, have lead to major advances in this field. New materials used in these industries require higher energy to process them and this challenge has been met with considerable success. It is now possible to spray virtually any material provided that it melts (or becomes substantially molten) without significant degradation during a short residence in a heat source. A further improvement of coating properties, in particular the reduction of coating porosity, is being attempted by the use of new methods for the post-treatment of thermally sprayed coatings, ultrasonic compression, hot isostatic pressing and shot peening or hammering. Thus, as will be described later, most metals, alloys, many ceramics, cermets and even plastics can be thermally sprayed. There are numerous thermal processes which can be classified under specific headings, and these are now considered in some detail .

2.3.1 Wire Spraying

Although this process was the first to be developed from the pioneering work by Schoop, it still maintains a prominent position in surface technology. Wire-spraying 'guns' operating on the same basic principle are marketed by various manufacturers [5]. A wire, typically 3-5 mm in diameter, is fed by a variable-speed motor or air turbine through the centre of a multi-jet combustion flame (Figure 6) . The tip of the wire melts and an annular gas jet (usually of compressed air) strips molten particles from it, and propels them to the substrate at a velocity of approximately 100m/s. The fuel gas used is generally acetylene, although for some metals propane or hydrogen is preferred (e.g. copper reacts with acetylene). Wire-spraying equipment is portable, and the guns can be used manually making them attractive for on-site applications. Nevertheless, for the most reliable results the gun are manipulated automatically by a

traversing unit or robot. Extension devices are also available which enable inside diameters to be coated.

A fairly wide selection of ferrous and non-ferrous metals can be sprayed successfully with this method, as shown in Table 1. Wire feed rates can be quite high, eg. approximately 20kg/hr for copper which gives a coverage of some 20m² at a coating thickness of 0.1mm. Attempts have been made to extend the application of wire spraying to non-metallic materials. Thus, in the 'Rockkide ®' process, rods of oxides such as alumina and chromia are sprayed to produce oxide coatings [6]. An alternative approach, which has met with limited acceptance, is to use a plastic tube filled with powder for spraying. The plastic has to burn away to allow the ceramic to be sprayed effectively. Cermet coatings have been produced by spraying wires containing particulate ceramic, e.g. aluminium plus 10 vol% alumina or silicon carbide [6].

Material	Application
Mild Steel	Reclamation and machine element work
Carbon and low alloy steel (1)	Reclamation, corrosion resistance and medium wear resistance
Martensitic stainless steel	Corrosion and wear resistance
Austenitic stainless steel	Corrosion resistance and machinability
NiCu (Monel)	Marine corrosion
NiCrBSi	Wear and corrosion resistance, hot hardness
NiCr (80/20)	Corrosion and high temperature oxidation resistance
NiCrFe	High temperature corrosion resistance
NiAl	Intermediate layer used to improve the adhesion of ceramic coatings
Mo	Wear resistance. anti galling, arc erosion, bonding
Al*	Resistant to atmospheric and marine corrosion, resistant to oxidation after heat treatment
Zn*	Atmospheric and marine corrosion resistance
Bronze	Medium wear resistance, high strength, used in bearings
Aluminium Bronze*	Corrosion resistance, bond coat, bearing applications
Copper	High electrical and heat conduction, radio frequency shielding
Babbitt	Journal bearing applications

* Indicates material can also be deposited by arc spraying

Table 1 Material deposited using wire and arc spraying [5].

2.3.2 Electric Arc Spraying

In this process two wires of opposite polarity are fed through angled electrode holders so that their tips are almost in contact and generate an electric arc. The latter, at a temperature of about 6000°K, provides sufficient thermal energy to melt the wires, and the molten metal is atomised by a jet of high-pressure gas (usually compressed air) to provide a spray stream (Figure 7). Arc torches are powered by 3-phase transformers, the characteristics of which are designed to accommodate metals of widely varying electrical conductivity and melting point. Typically they operate at 20-40 V, and arc currents of 200-300 A, and can process material wire at up to 50kg/hr. Attachments are available which by means of a secondary gas flow, deflect the spray stream at angles of up to 90°, so allowing cylindrical bores to be coated. Many metals can be sprayed with this process, (see Table 1) and this technique has the potential to produce 'pseudo-alloy' coatings by feeding in wires of dissimilar metals. For any metal the size of the droplets in the spray stream is directly proportional to the wire diameter and arc voltage, but inversely proportional to the atomising gas pressure [7]. Recently Steffens et. al. [8] have reported the development of an arc gun capable of stable operation in a low-pressure chamber atmosphere, so sensitive metals can be sprayed to give high density deposit, free of oxide inclusions.

2.3.3 Plasma Spraying

Atmospheric Plasma Spraying (APS)

In Plasma spraying, a pilot arc is generated by means of a high frequency ignition or high voltage between an anodic, water-cooled nozzle, generally made of copper, and a tungsten cathode. The plasma gases (often a mixture of Ar, He, N₂ and H₂), are led through the pilot arc where they are dissociated and ionised (Figure 8).

The advantage of plasma spraying is the high flame temperature which measures between 6000°K and approximately 15000°K [9-10]. In contrast to other thermal spraying techniques, plasma spraying achieves high deposition rates even in material with a high melting temperature. In addition to metallic materials and cermets, some plastics can also be sprayed.

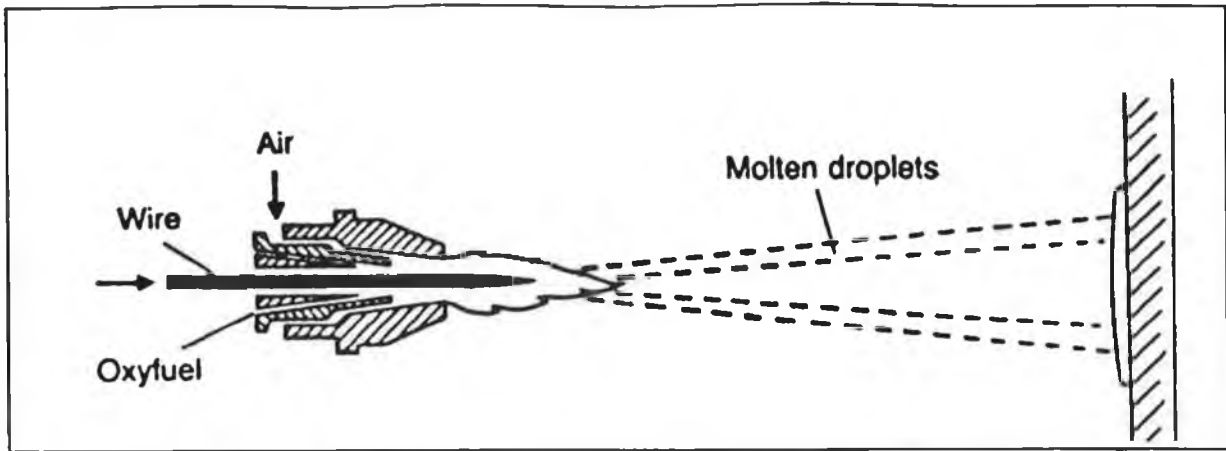


Figure 6 Schematic diagram of a combustion flame wire gun

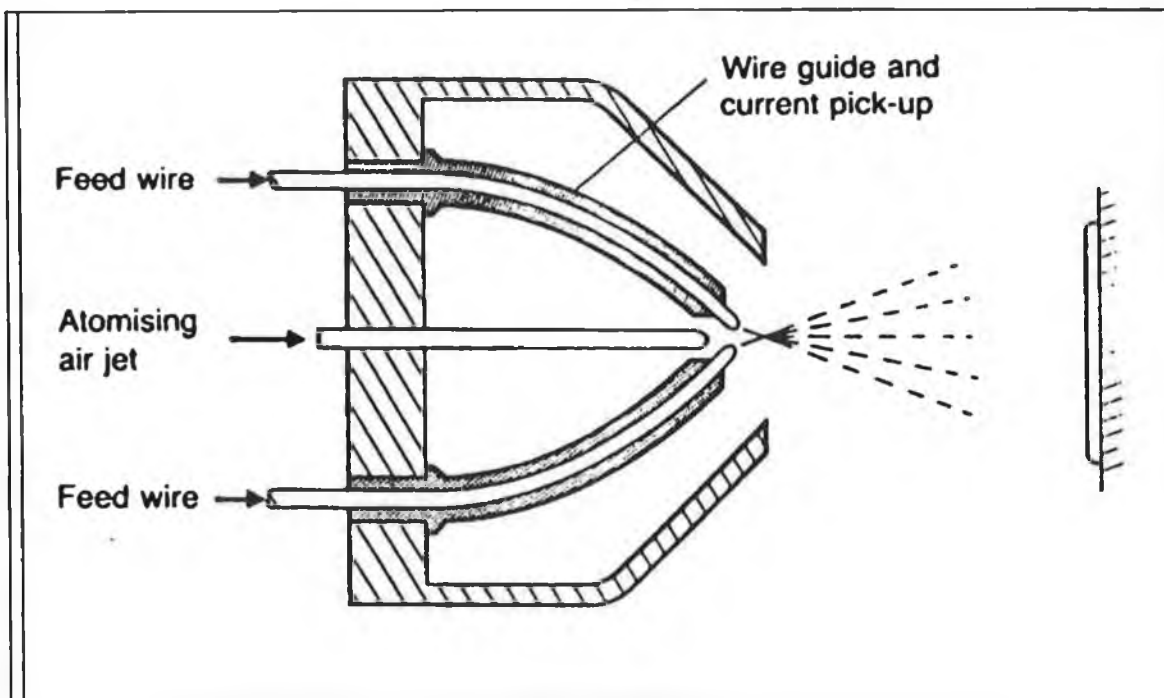


Figure 7 Schematic diagram of an electric arc wire spray gun

A requirement for the surfacing material is the existence of a liquid state. Material subjected to thermal decomposition or sublimation, as for example SiC and Si_3N_4 cannot be deposited by conventional spray techniques.

The range of commercially available plasma torches includes small burners of less than 10kW power, water-stabilised plasma torches exceeding 200kW power, and computer controlled plasma spraying plants and manipulators for the automatic and reproducible coating of mass

products and components of complex geometry. At present, high velocity torches with individually formed nozzles are being developed [11].

The latest patented invention is a rotating plasma torch, for which the work piece stands still while the plasma torch rotates. This plasma spray unit allows coating of internal surfaces e.g. bore holes of diameters between 35 - 500 mm.

Vacuum Plasma Spraying (VPS)

In the vacuum plasma spray process, spraying takes place in a closed chamber containing a defined atmosphere at reduced pressure. The torch and the workpiece are positioned by a handling system. The main industrial application of vacuum plasma spraying is the coating of super-alloy turbines blades with MCrAlY alloys ("M" here represents the elements Ni,Co,Fe and their mixtures). Such coatings have the function of protecting the substrate material from hot-gas corrosion and thus improving the component lifetime. The MCrAlY coatings are characterised by a dense, nearly oxide free, homogeneous structure and a broad diffusion zone [12]. Furthermore, such coatings often serve as bond coatings for ceramic thermal barrier coatings.

Recently, there have been increased efforts to extend the range of application of this spray process [8]. Apart from the spraying of combustion-sensitive materials (eg. nitrides and carbides), the spraying of reactive material (eg. titanium and tantalum) is included. The spraying of corrosion resistant coatings composed of such reactive material is not possible in atmospheric conditions because of the high reactivity and high gas absorption. Therefore titanium coatings for medical applications are suitably produced by VPS. For example a porous coating structure is often used on a bone implant to allow the bone cell to grow into the controlled porosity.

Additional fields of application are the synthesis of diamond coatings and alloying of surface material during the plasma process.

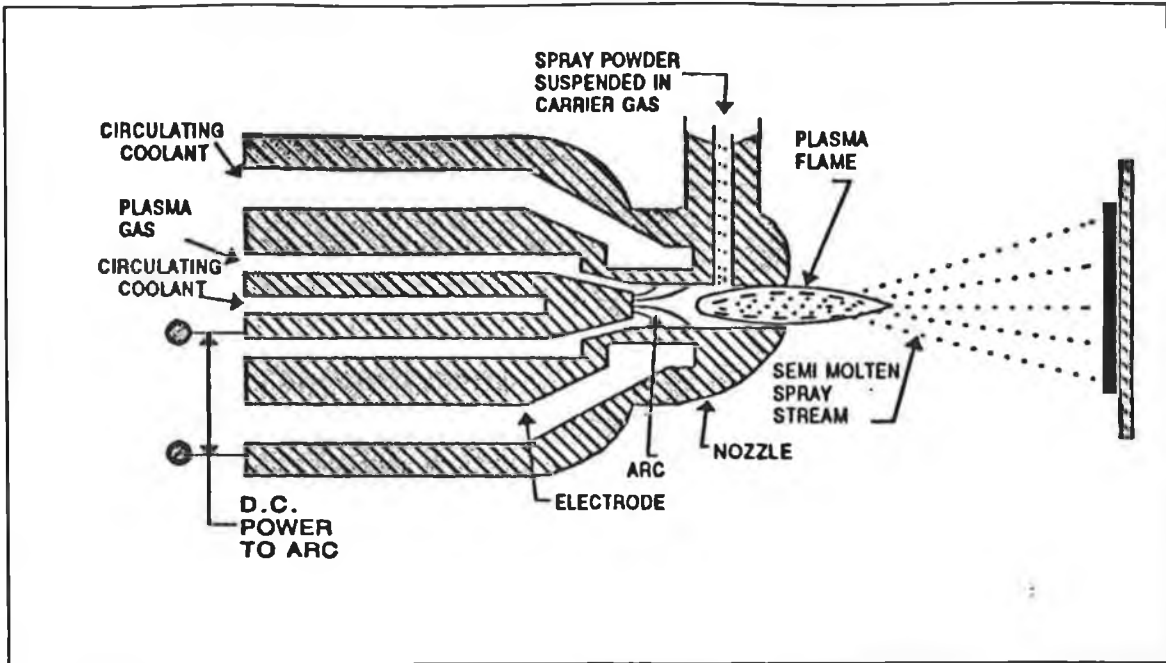


Figure 8 Schematic diagram of a plasma spray gun

2.3.4 Flame Thermal Spraying

As Figure 9 shows, in a flame-spraying torch the nozzle configuration is such that the combustion gases are mixed and burnt in the region around a central powder injector. In a basic system, powder is aspirated into the gas stream by gravity feed, although better control is obtained by utilising specially designed feed units. Depending upon their morphology and coating properties required, the particles usually become partially or fully molten and acquire the velocity of the jet stream of about 100m/s. In some devices compressed air is employed to further accelerate the particles (ie. to increase their kinetic energy). However, while the resultant coatings are of better integrity, the deposit efficiency (coating weight/weight of powder sprayed) is drastically reduced for ceramics because some of the particles are re-solidified before impact and consequently do not adhere to the substrate. With a temperature of $\sim 3000^{\circ}\text{K}$, the oxy-fuel flame (usually acetylene) can melt most materials, and so flame spraying is a useful technique for processing materials not available as wires [13]. Many metals, some oxides and a few carbides can be sprayed with this method, as shown in Table 2. Modified torches are extensively used for applying plastic coatings onto large components. A particular market which also exists is for the so-called self-fluxing alloys which, after deposition, are fused to produce dense, metallurgical bonded overlays. Spray rates of the material of this self-fluxing alloy process are about 1-2 kg/hr, which is much lower than the wire or arc processes, but again torches can be machine mounted or manually manipulated. Like their wire-spraying counterparts, an extra extension for treating internal surface can be fitted to the torches.

Material	Application
Low carbon steel	Reclamation and machine element work
Martensitic stainless steel	Corrosion and wear resistance
Austenitic steel	Corrosion resistance and machinability
NiAl	Wear resistance and intermediate layer used to improve the adhesion of ceramics
NiCrAl	High temperature resistance and bonding
NiCrBSi	Self-fluxing, wear and corrosion resistance, hot hardness
NiCr (80/20)	Corrosion and high temperature oxidation resistance
NiCrFe	Corrosion and high temperature oxidation resistance
WC/NiCrBSi	high wear resistance
Cr ₂ O ₃	Wear and corrosion resistance
Al ₂ O ₃	Electrical and wear resistance
Al ₂ O ₃ /TiO ₂	Wear resistance

Table 2 Material used in the powder flame process

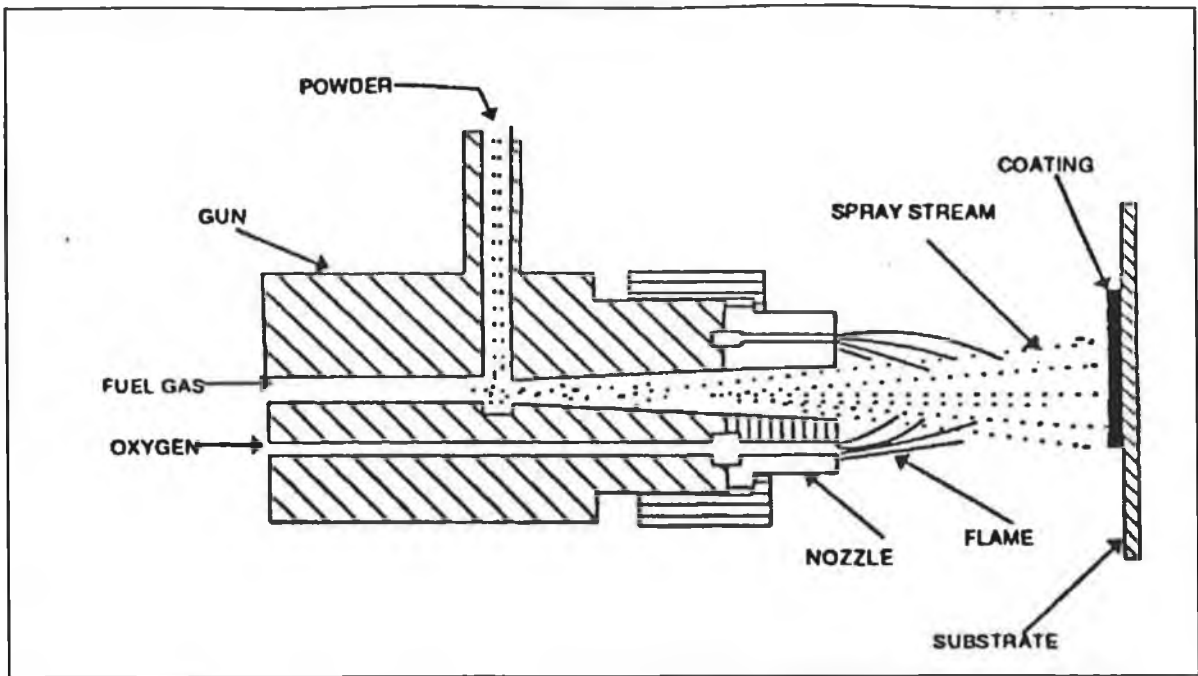


Figure 9 Schematic diagram of flame spray gun

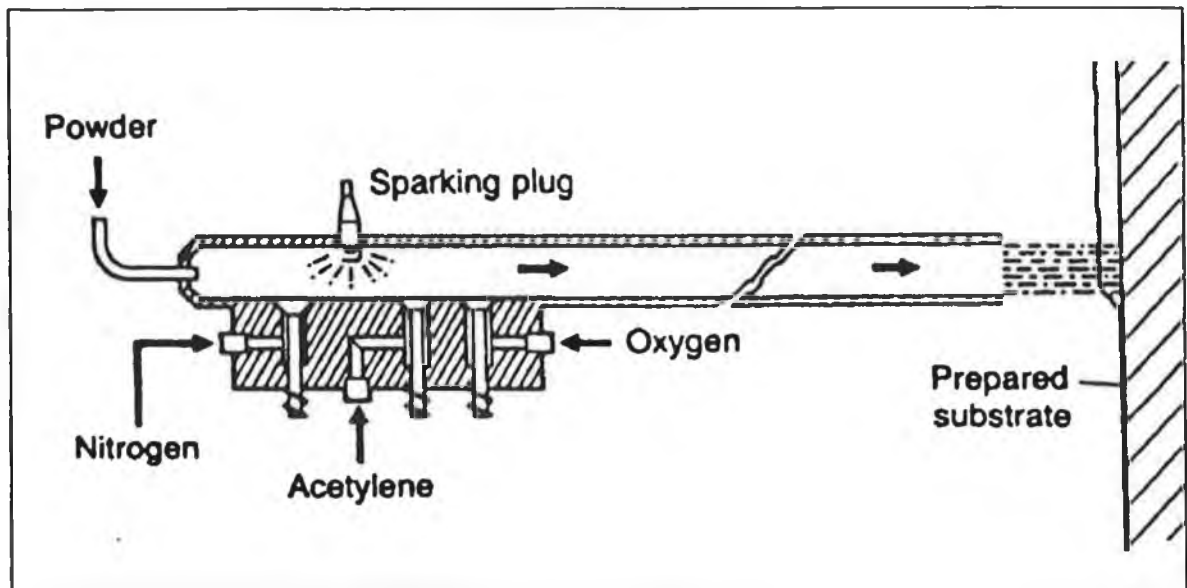


Figure 10 Schematic diagram of a detonation gun

Pulse Combustion HVOF (Detonation Gun) Process

This process was developed in the middle 1950's [14] by Union Carbide Corporation from experiments involving the controlled detonation of an oxy-acetylene mixture. The 'D' Gun consists of a barrel, 1 - 1.5 m long and 20 - 30 mm internal diameter, into which a gas mixture is injected and ignited by a spark plug (Figure 10). During a short burn period the flame front accelerates, compressing and heating the unreacted gases in front of it. When a critical temperature is reached, self-ignition produces a detonation or shock wave. For an equi-molar ratio of oxygen and acetylene the shock wave travels at a constant velocity of $\sim 3000\text{m/s}$, and at a maximum temperature of 3500°K . Powder particles of the coating material (carried in nitrogen) are streamed into the unreacted gas mixture before ignition. As the detonation wave passes through the suspended particles, they are heated and can be accelerated to a velocity exceeding 700m/s . The large kinetic energy attained by the particles is released as heat on impact with the substrate, and helps to produce the best bonded and highest density thermally sprayed coatings.

The D gun fires between four and eight times per second yielding a circular area of coating $\sim 250\text{mm}$ in diameter, and $6\ \mu\text{m}$ thick per detonation, with a nitrogen purge between each cycle. It produces high noise levels (150 dB) and is operated remotely in acoustically insulated cells. It has been used very successfully to spray thin coatings from a range of carbides, oxides, cermets and high temperature alloys [15]. However, like most thermally sprayed coatings, D gun deposits possess residual tensile stress which can result in considerable reduction in the fatigue strength of certain substrates such as titanium alloys.

Continuous Combustion HVOF Process

The high velocity oxy-fuel spray process (as described in detail in section 2.4) is a subsequent version of the conventional oxy-fuel process (Figure 11). Although the HVOF process was established on an industrial basis only in the middle 1980's, it is the most significant development in the thermal spraying industries [16]. It is generally used to produce cemented carbide coatings, and can achieve the best quality in terms of density, adhesion and phase stability within the coatings. Due to the fact that the deposited coatings can be machined to excellent smooth surfaces, numerous applications for coating production on new parts and

repair of worn out parts have been exploited [17]. There are different types of continuous combustion available in the market, including Jet Kote, Diamond Jet and the CDS Gun.

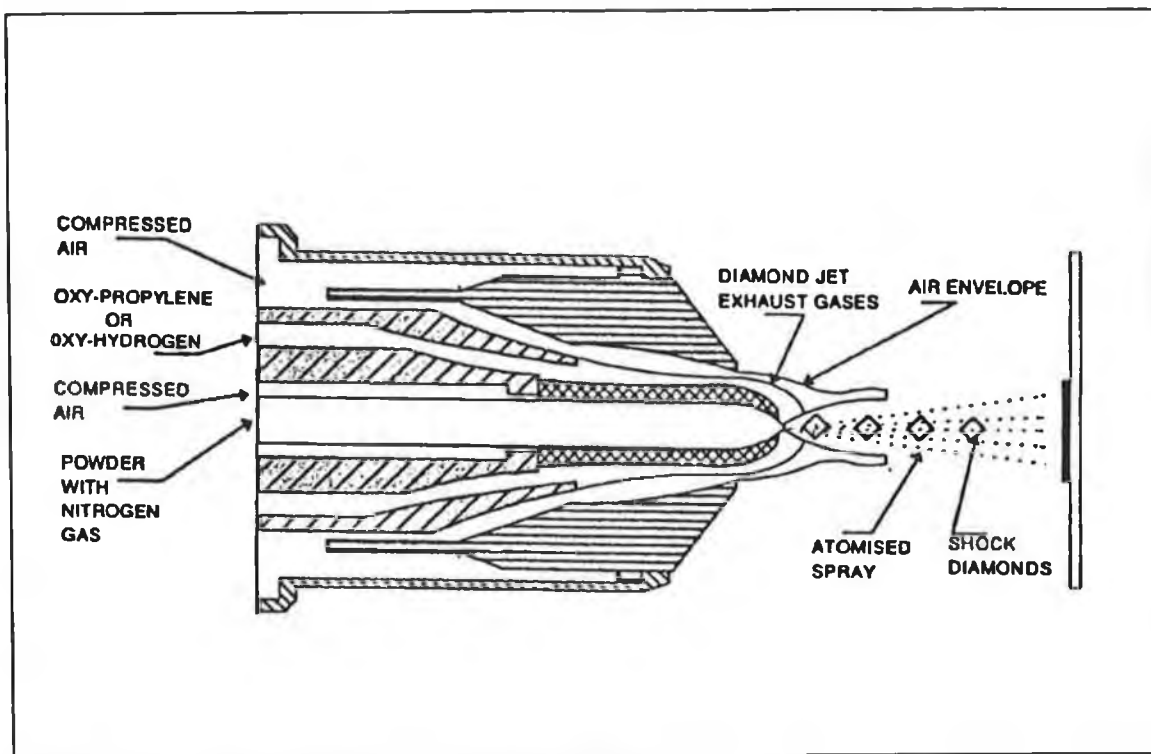


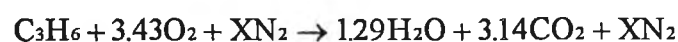
Figure 11 Schematic diagram of Diamond Jet HVOF spray gun

2.4 The HVOF Process

The HVOF process is based on using a combination of thermal and kinetic energy for melting and accelerating powder particles, to deposit desired coatings. Carbon-hydrogen gases (propane, propylene, acetylene) or pure hydrogen are mainly used as fuel gases and the gas temperature depends on the choice of fuel gas and the ratio of the oxygen and fuel gas flow rates. Powder particles of the desired coating material are fed axially into the hot gas stream, melted and propelled to the surface of the workpiece to be coated. The gun consists of three sections: a mixing zone, combustion zone and the nozzle. During operation the body is cooled by air or water. The fuel and oxygen are mixed by means of co-axial jets and guided to the combustion zone where a pilot flame or external igniter initiates combustion. During combustion the gas is allowed to expand in the nozzle, where it is accelerated. The powder is accelerated by the carrier gas and injected into the flame. The powder has the same direction of flow as the direction of the surrounding expanded gas. On entering the combustion zone through the nozzle the powder particles are heated and are further accelerated. Due to the high velocity and high impact of the sprayed powder, the coating produced is less porous and has higher bond strength than that produced by other methods [18-22].

2.4.1 Combustion and Gas Dynamic of the HVOF System

Oxygen and fuel gas at certain pressures, usually recommended by the gun manufacturer, are mixed in the mixing zone of the gun and then directed towards the combustion zone. After ignition a chemical reaction takes place which releases heat energy from the combustion process. As combustion continues, the pressure inside the combustion chamber increases and the hot gas flows with high velocity. Propylene, propane or acetylene and oxygen are used for combustion. In spraying carried out using propylene and oxygen, with nitrogen as the powder carrier gas, according to Kowalsky et al. [23] the simple chemical reaction of the gases at stoichiometry (theoretically required for complete combustion) in terms of mass is as follows:



The stoichiometric oxygen fuel ratio is 4.5 to 1. The energy released by the chemical reaction of the combustion gases is used to heat and accelerate both the emerging gases, and the spraying powder. The resulting gas velocity is a function of variables such as gas composition, pressure, temperature, density and the area through which the gas travels. However, the

maximum obtainable gas velocity through the minimum cross sectional area is related to the local sound velocity [23].

The local velocity of sound in a perfect gas is defined by:

$$C = \sqrt{KRT}$$

where,

C = sound velocity

K = ratio of specific heats of oxygen to fuel

R = gas constant

T = local temperature

The local Mach number is defined as the ratio of the local gas velocity (V) to local sonic velocity;

$$M = \frac{V}{C}$$

Basic flow regimes are defined relative to the Mach number as;

Subsonic flow $M < 1$

Sonic flow $M = 1$

Supersonic flow $M > 1$

Hypersonic flow $M > 5$

The condition in which the gas velocity is equal to the sonic velocity where $M = 1$ is called the "critical state". Associated with the critical state are the critical gas state conditions, critical mass flow rate, and critical area. When the local gas speed is equal to the sonic velocity the nozzle can discharge the maximum mass flow rate, m . The critical mass flow rate can be defined as:

$$m = \rho VA$$

where,

ρ = critical density

V = critical gas velocity

A = critical area

This equation can be written in terms of the total pressure and total temperature as [23]:

$$m = \left[\frac{K}{R} \left(\frac{2}{K+1} \right)^{\frac{K+1}{K-1}} \right]^{\frac{1}{2}} \cdot \frac{P_0 A}{T_0^{\frac{1}{2}}}$$

where,

P_0 = total pressure at critical state

T_0 = total temperature at critical state

When the critical condition is reached, the flow is said to be choked. From the above equation it can be seen that by increasing the gas pressure, the critical mass flow rate increase, whereas by increasing the temperature the critical mass flow rate decreases. Figure 12 shows the variation of gas flow velocity with the chamber pressure [24]. The chamber is usually maintained at a certain pressure which differs for different design of the HVOF system

Beyond the point of combustion, the combustion gases are expanded in a converging and diverging nozzle to achieve supersonic speed. The adiabatic flame temperature of the stoichiometric combustion gases is about 2900°C (if propylene is the fuel gas). Jet and flame temperatures also vary with the oxygen/fuel ratio as shown in Figure 13 [24]. Within the HVOF device, heat due both to combustion and friction along the nozzle surface tend to choke the flow at the nozzle exit. As the combustion products pass the nozzle, the jet expands because the static pressure in the nozzle is greater than the ambient pressure, and expansion and compression waves occur in the free jet (Figure 14). The intersection of these waves form the bright regions in the jet stream, commonly known as shock diamonds [25-27].

During combustion, coating particles are injected into the centre of the combustion chamber using a carrier gas, are then turbulently mixed, and accelerated to a high speed and heated within the hot gases. The gas powder mixture leaves the barrel as a high velocity jet. Since the particles are injected with supersonic speed, each particle will pass through shock waves. From the measurement taken of the velocity of powder particles of different size and different materials (Figure 15) it is shown that the velocities are highest at the central axis and decrease radially outward [23]. This decrease is caused by viscous forces acting between the jet and the ambient air.

The correct choice of fuel gas is mainly governed by economics, by the coating material itself and by the desired coating properties. Propane is mainly used as a fuel gas. When processing oxygen sensitive materials, hydrogen as a fuel gas offers some advantages in terms of low

oxygen pick-up. If higher heat input is necessary to melt powder particles, propylene should be used. High-melting, oxide-based ceramics can only be sprayed by the HVOF process when acetylene is used as the fuel gas. A summary of the material classes which are commonly processed using the HVOF method, including recommended fuel gas, and achieved coating hardness is shown in Table 3 [28].

Type of Material	Spray Material	Fuel Gas	Hardness - HV _{0.3}
Metal	Cu	Propane	150 -250
	Al	Propane	>120
	Mo	Propane, acetylene	600 -900
Metallic alloy	Steel	Propane, hydrogen	160 - 500
	Nickel based alloy	Propane, hydrogen	400 - 750
	cobalt based alloy	Propane, hydrogen	400 - 750
Hard alloy	Nickel based alloy	Propane, hydrogen	250 - 800
	cobalt based alloy	Propane, hydrogen	400 - 700
Hard metal	WC-12 Co	Propane	1200 - 1700
	WC-10 Co-4 Cr	Propane	1000 - 1100
	WC-13Ni	Propane	about 1000
	Cr ₃ C ₂ -25 NiCr	Propane	about 900
Oxide ceramic	Cr ₂ O ₃	Acetylene	1200 - 1700
	Al ₂ O ₃	Acetylene	1200 - 1400
	Al ₂ O ₃ -40 TiO ₂	Acetylene	about 950

Table 3. Summary of the spraying materials which can be used in the HVOF Process [28].

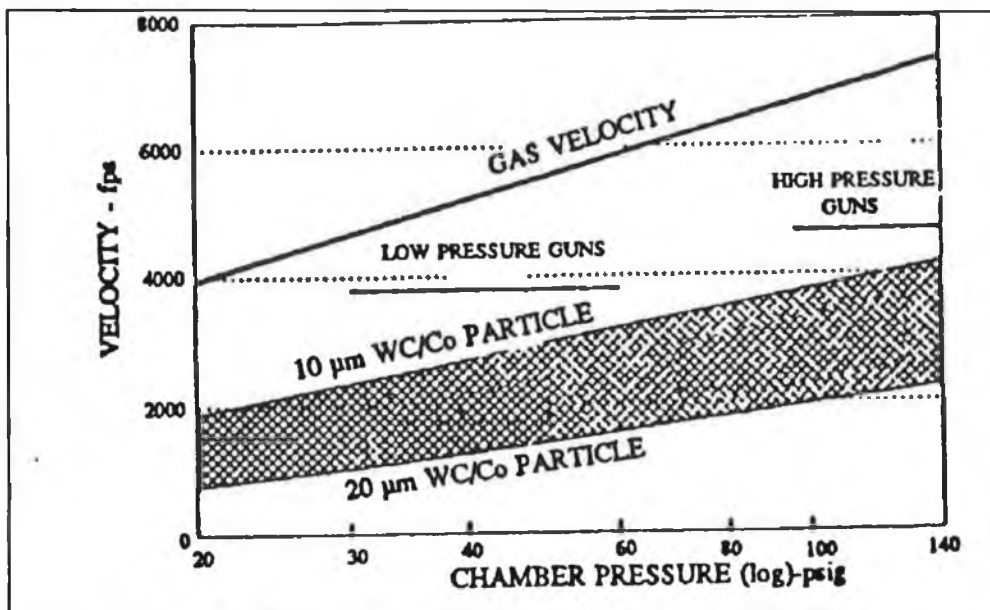


Figure 12 Gas velocity in HVOF system Vs gun chamber pressure [24]

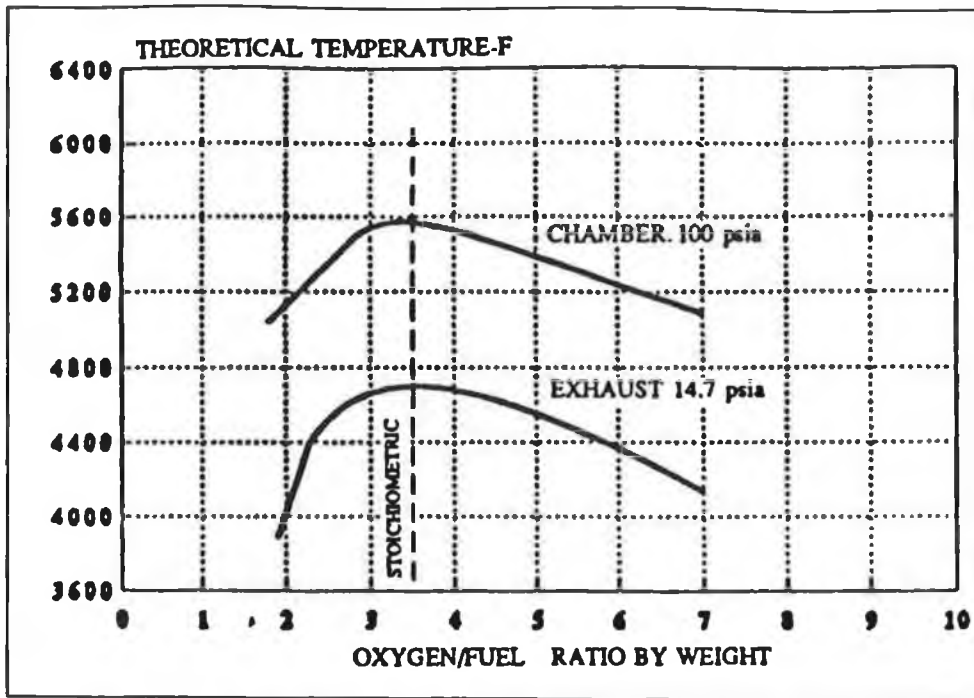


Figure 13 Variation of theoretical flame temperature with oxygen/fuel ratio [24]

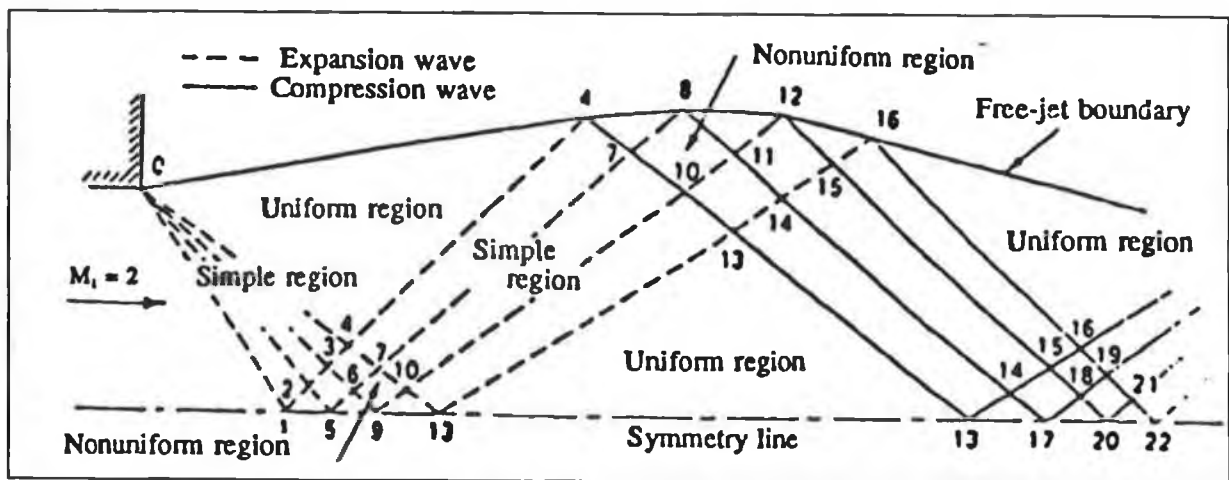


Figure 14 shock formation of an under expanded jet [24].

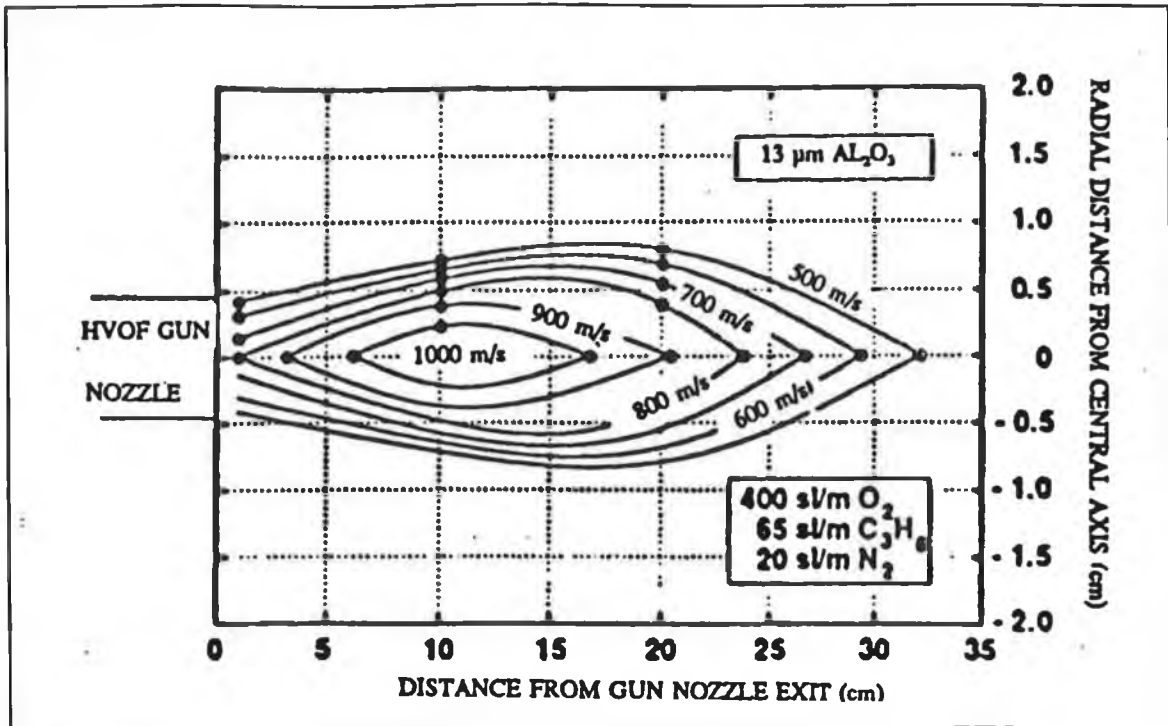


Figure 15 Laser velocimeter 2-D particle velocity distribution [23]

2.4.2 Advantages and Disadvantages of the HVOF System

Particle velocity is a critical factor in all thermal spraying processes. Quality of the coatings improves with the velocity of the sprayed particles. HVOF guns can produce particle velocities of 800m/s, which is considerably higher than those provided by the other currently available commercial thermal spray processes. Additional benefits of the HVOF process are:

- 1) short particle exposure time in flight due to the high speed
- 2) low surface oxidation due to relatively short particle exposure time
- 3) uniform and efficient particle heating due to high turbulence
- 4) low mixing with ambient air once jet and particles leave the gun
- 5) low ultimate particle temperature compared to plasma or arc guns.

All the above advantages will lead to coatings with a higher density, improved corrosion resistance, higher hardness, better wear resistance, higher bond and cohesive strength, lower oxide content, less unmelted particle content, better chemistry and phase retention, greater thickness of coating and smoother as-sprayed surfaces than the other thermal spray methods.

The main disadvantages are:

- 1) the amount of heat content in the HVOF stream is very high, so over heating of the substrate is quite likely. Therefore extra cooling of the substrate is necessary, and cooling with liquid CO₂ is now a standard with new HVOF processes.
- 2) masking of the part is still a great problem as only mechanical masking is effective. It is very difficult and time consuming to design an effective mask for a complex component with areas which do not need coating.

2.4.3 Characteristics of HVOF Coatings

The hard metals (WC-Co, Cr₃C₂-NiCr) representing approximately 70% of the current coating materials used with HVOF, occupy a position of great importance in the coating industry. Hard metals sprayed by HVOF show superior density (typically >97%), a more homogenous phase distribution and less formation of undesired brittle carbide phases in comparison with those results produced with other thermal spray variants [28].

Deposition efficiency, which describes the ratio of the particle stream which leads to the formation of the coating and the total particle stream, can be increased to the order of 70% to 80% using HVOF. Some HVOF processes, when utilising acetylene, are able to produce ceramic coatings of remarkable high quality, eg. chromia (Cr_2O_3) coatings [28]. The quality of chromia coating is based on high kinetic energy in combination with the moderate particle temperature which leads to the formation of a dense structure with a low thermally induced oxygen loss. Contrary to metallurgical advantages, the low deposition rate and low deposition efficiency of 25% and in turn higher production costs, have to be noted as disadvantages of the process when applied to some ceramics.

HVOF, as do other thermal spray variants, allows processing of combined materials, which are often called pseudo alloys. Self fluxing nickel base alloys are often mixed with hard metals, like WC-Co and simultaneously sprayed, in order to combine the corrosion resistance of the nickel base alloy with the wear resistance of the hard metal.

Although the HVOF process can produce coatings of high density sometimes the coating may be penetrated by some corrosive media, and special sealing methods need to be applied to further enhance the protective properties of the coating to withstand corrosive attacks.

Branch Of Industry	Application	Material
Paper Industry	Various Rolls	WC-Co-Cr
	Ductors	Cr_2O_3
Steel Industry	Furnace Rollers	Cr_3C_2 -NiCr
	Conveyor Rollers	Cr_3C_2 -NiCr
Printing Industry	Metering Rollers	Cr_2O_3
Textile Industry	Galettes	Al_2O_3 - TiO_2
Fittings	Isolating Valves	WC-Co + WC-Ni
	Bail Cocks	Cr_3C_2 -NiCr
Electronics	Conductor Tracks	Cu
Plant Construction	Mills	Al_2O_3 , Mo, Different Steels
	Separtrs	Al_2O_3 , Mo, Different Steels
	Chemical Equipment	Al_2O_3 , Mo, Different Steels
Automotive Industry	Friction Disks	Mo

Table 4 Possible applications of HVOF coatings in various branches of industry [28]

Coating thickness for hard metals is generally in the range of 0.1 to 0.2 mm. Thickness above 0.3 mm are possible, but due to the higher residual stress state in such coatings, deposits of more than 0.3mm are not recommended by the powder manufacturer. However, a coating of 10 mm has been successfully produced with HVOF using a liquid CO₂ cooling system [29-30]. The surface roughness of the sprayed coatings depends largely on the spray powder used. When fine spray powders are used, the surface roughness in the as-sprayed condition is as low as Ra = 1-2 μm, and can be less than 0.1 μm after mechanical treatment by superfinishing with diamond grinding.

HVOF coatings are used in different areas of industry, summarised in Table 4, and characteristics of HVOF thermally sprayed coatings are further discussed in section 2.5.

2.4.4 Comparison of HVOF and Plasma Thermal Spraying

As seen in Table 5, the advanced features of the HVOF process give better results over plasma processes. Higher bond strength, lower oxide content, improved wear resistance and lower porosity are some examples.

Table 6 shows the difference in spraying parameters of these two processes. The HVOF process is relatively simple, and thus enhances coating reproducibility.

	HVOF	Standard Plasma	D-Gun	High vel. Plasma
Hardness (DPH 300)	1,050	750	1,050	950
Porosity (%)	<1	<2	<1	<1
Oxide content (%)	<1	<3	<1	<1
Bond strength psi	10,000	8,000	10,000	10,000
Max. thickness (in)	0.060	0.025	0.3	0.015

Table 5 Coating Characteristics of various thermal spraying process for WC_CO [31].

	HVOF	Plasma
Flame Temperature	3000 ⁰ C	11,000 ⁰ C
Gas Velocity	Mach 4	Subsonic to Mach 1
Torch of Substrate Distance	130-350 mm	75-150 mm
Angle of deposition	45 ⁰	60 ⁰
Deposition Efficiency %	75	45

Table 6 Comparison of HVOF and Plasma spraying process parameters [31].

2.4.5 Future Potential and Markets

New developments will boost the introduction of HVOF sprayed coatings in new markets. Currently these developments largely deal with special powder modification, such as grain size and chemical composition, which have to be tailored to the requirement of the individual HVOF applications. A new line of agglomerated and sintered spray powder offers advantages in terms of phase distribution in HVOF coatings of complex material [32]. In addition the use of simulation models represents a promising alternative for tailoring spray parameters to the needs of the particular application which minimises experimental efforts.

New markets are also achieved by combining HVOF coatings with other coating processes, which are at the present under intensive research. The processes and the additional materials which can be combined with HVOF coatings include the following [28,32]:

Sealing

Utilising different kinds of liquid waxes and resins, which penetrate the sprayed coating and then harden. This increases corrosion resistance, especially in aqueous solutions.

PTFE deposits

PTFE offers excellent gliding and anti-sticking properties. A wear resistance coating with low coefficient of friction is achieved by combining a HVOF coating with a PTFE coating.

PVD deposits

PVD coatings of materials like TiN, or CrN are extremely hard and can be applied to different kinds of tools. When combined as a top deposit over a HVOF coating, the sprayed coating

provides the base strength and base hardness to avoid a skin effect, ie. undesired fracture of the very hard PVD coating on a soft base material. In future it is foreseen that the combination of HVOF/PVD coating will be applied to substrate such as copper, aluminium, and other light metals and their alloys.

Despite the fact that new coating materials will be available for the HVOF process, hard metals are expected to keep their dominance of the market. Each application needs certain and careful development, including critical consideration of the economic aspects. Future markets for HVOF coatings, with or without further combined deposits, will be focused on high priced products. Promising developments are being made in the area of textile machinery, rolls used in steel making and processing or in the paper industry, and certain components subjected to high loads in the general engineering sector and in the aircraft industry [33].

2.5 Thermally Sprayed Coatings

A thermally sprayed coating produced in open air is a heterogeneous mixture of sprayed material, oxide inclusion and porosity [34-35]. During flight from the gun to the substrate, the particles interact chemically and physically with the surrounding environment. Thermal spray coatings consists of lenticular splats whose boundaries are generally parallel to the substrate surface. On solidification, within each lamellae fine-grained equiaxed crystals form. The spraying torch moves over the substrate and the first layer composed usually of 5-15 lamellae, depending on the processing parameters (powder feed rate, spray distance, particles diameters and torch linear speed) is formed [35].

The columnar orientation gradually decreases as the thickness of the coating increases. The change from columnar to random grain morphology is believed to be produced by the effective lowering of the cooling rate, which gives the structure time to reform and change [36]. Radially elongated grains are rarely observed in thick coatings, this is due to the high thermal conductivity of metals. Thin regions under the impact of the subsequently arriving molten droplets probably recrystallize into randomly oriented grains [37]. Another feature of the rapid solidification in thermal spraying is the formation of structural defects such as vacancies, coagulation and dislocations. However, the structure depends heavily on quench rate. A perfect morphological form of lamellae splatted on the substrate is shown in Figure 16 [38]. Figure 17 shows the schematic diagram of the cross section of the microstructure of thermally sprayed coatings [39].

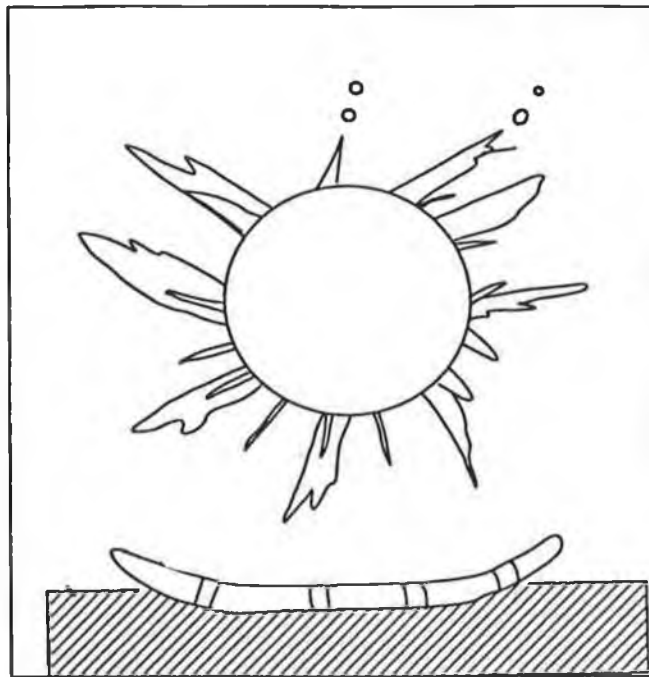


Figure 16 A perfect morphological forms of lamellae splashed on the substrate [38].

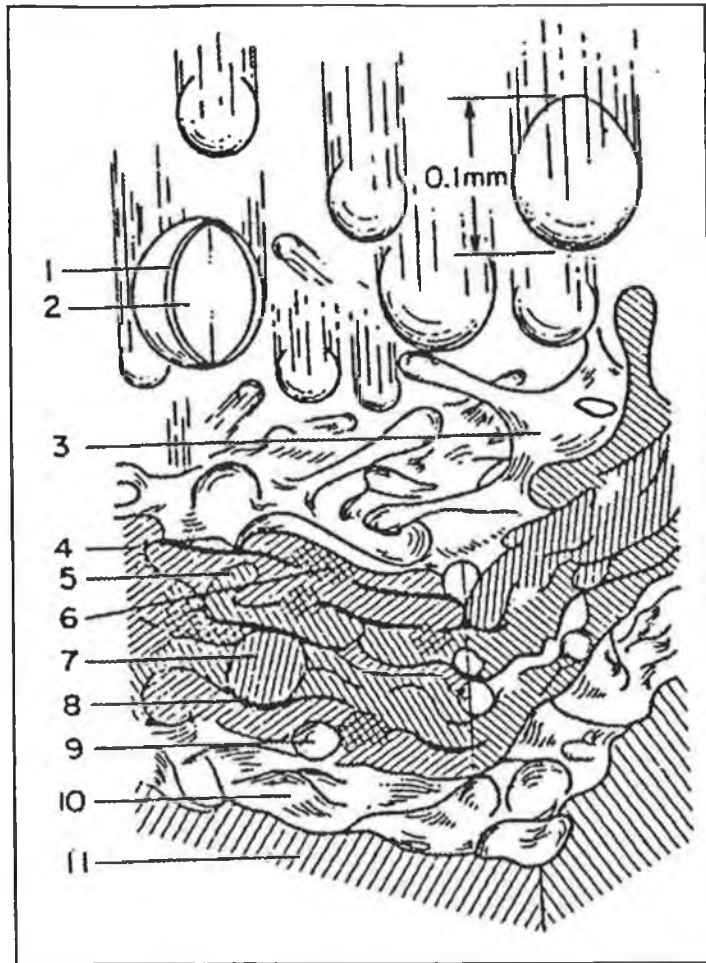


Figure 17 Schematic cross section of the microstructure of thermally sprayed coatings [39]

1. Partially sectioned oxide layer formed on a metal droplet in flight;
2. Metal particle with its centre still in the liquid state;
3. Impinging metal droplet, partially splashing away;
4. Burst oxide sheet situated between two metal layers;
5. Interconnection (keying) of two particles that have splashed out;
6. Partial alloying of two simultaneously impinging particles;
7. Encapsulated presolidified spherical particle;
8. Microcavity formed by uneven flow of splatted particles;
9. Micropore caused by entrapped gases;
10. Bond layer with roughened (grit blasted) surface;
11. Substrate material.

2.5.1 Composition of Thermal Sprayed Coatings

In thermal spraying, the composition of coatings may vary from the composition of the original sprayed material due to the reaction of the molten particles with the gaseous environment. In particular the extent of this oxidation is very important to the properties of the coating. In a study of the effect of oxidation on deposited aluminium and bronze, it was found that even minor oxidation during deposition is detrimental to compressive strength both parallel and perpendicular to the surface. However, discrete oxide particles not only strengthen the coating but also add wear resistance [40]. The loss of carbon from tungsten carbide coatings through oxidation has been reported [41-43]. Metallic or cermet coatings may also react with air, forming oxides scales on the particle and dissolving the impurities in the molten droplet. The extent of these reactions varies with process parameters. As a result of rapid quenching, non-equilibrium phases may be present. In alumina coatings, slightly superheated particles on impact on a highly thermally conductive substrate, give delta and theta phases in addition to gamma, with the alpha phase suppressed [44].

2.5.2 Residual Stress

In thermal spraying, residual stress develops as a result of cooling of individual powder particles from above their melting point to room temperature, on splat. The magnitude of the residual stress is a function of spray gun parameters, deposition rate, the thermal properties of both the coating and substrate materials and the amount of auxiliary cooling used [45-47]. The use of finer powder also leads to higher residual stress [48]. In thick coatings residual stress increases linearly with coating thickness, and this shearing stress can cause cracking and spalling [48]. Normally coatings suffer tension as a result of residual stress [49,43]. Methods which reduce tensile stress in the HVOF spraying and hence shear stress at the interface are [49] :

- 1) expanding the substrate prior to spraying by preheating
- 2) selecting a coating material with low shrinkage properties
- 3) building up a part with material of low thermal expansion value.

2.5.3 Bond Strength

The bonding mechanism of thermally sprayed coatings is the subject of much debate. Because of rapid cooling there can only be limited inter-diffusion between the deposition and substrate material, so bonding is predominantly physical in nature rather than metallurgical or chemical.

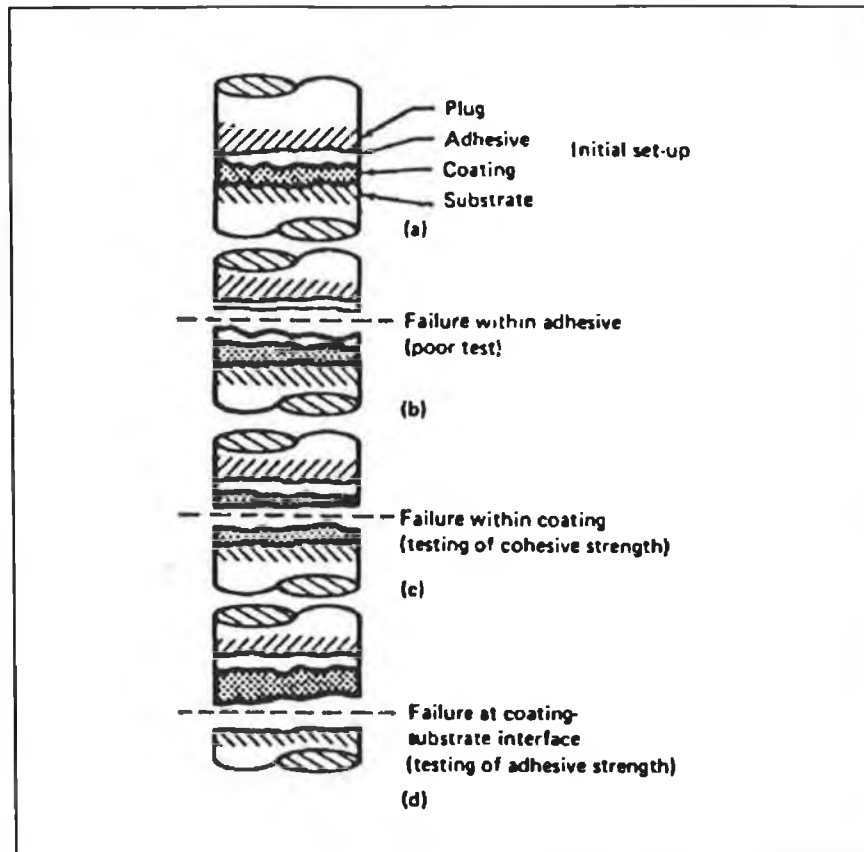


Figure 18 Modes of coating failure by standard pull test ASTM C633-79

Although the molten particles will deform to the substrate surface roughness producing a degree of mechanical interlocking, grit blasting does not significantly increase the surface area of the interlocking [50]. It does, however create a very active surface. For example, Moss and Young [51] calculated that a flame sprayed tin particle travelling at only 100m/s had sufficient combined thermal and kinetic energy to exceed the plastic yield stress on grit blasted mild steel. The resulting shear action of grit blasting would rupture the surface oxide layer providing a clean region for metal - metal contact. Other evidence [52] showed that plasma sprayed aluminium also breaks through the oxide layer on steel. The bond strength of sprayed coatings, as measured by standard pull-off tests (Figure 18) should only be taken as a guide [39]. The actual bonding values depend greatly on the substrate and process parameters.

Another interesting area to study regarding the bond strength of coatings is the build-up of individual particles that strike the substrate, and the effect the substrate temperature has on the impact of each particle deposited. The substrate temperature prior to spraying directly affects the flattening process of impinging molten particles onto the substrate, and thus affects the mechanical and physical properties of thermal spray coatings [53]. The flattening process is one of the most important processes in thermal spraying as it defines the characteristics of the sprayed layers. Many models of molten or liquid particle impingement on flat surfaces have been proposed [54-55].

Flattening processes on rough surfaces have also been investigated recently by Moreau et al. [56], who claimed that the flattening ratio and spreading rates become smaller with increasing surface roughness.

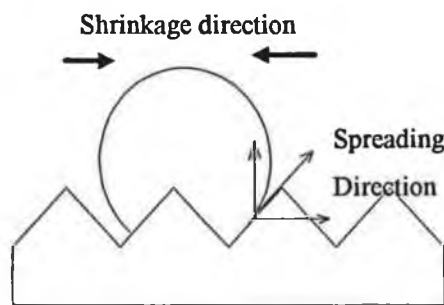


Figure 19 Schematic cross section of particle impact on a large mountain of roughened surface[53].

Many lamella on the roughened surface are, to a degree attached to the substrate by the force resulting from the shrinkage of the liquid wrapped around the surface irregularities.

Inside the contact area between the lamella and the substrate, adhesion results from the following mechanisms:

- physical interaction and,
- metallurgical interaction.

The conditions prerequisite to the physical interaction between the contacting surfaces are as follows:

- surfaces are clean
- surfaces are in a state of high energy (eg. by plastic deformation)
- the contact is closed (this occurs readily if the lamella is liquid)

There are two possible mechanisms of metallurgical interaction; diffusion and chemical reaction between the lamella and substrate.

The time taken for deformation for each sprayed particle has been studied by various researchers [57], as have the effect of the spraying parameters and the substrate material [58-59]. It has been proven that with the higher substrate temperature of 300°C prior to spraying, aluminium oxide powder deposited on mild steel substrate, produces an almost perfect lenticular shape[53].

2.5.4 Hardness

A thermally sprayed coating has a heterogeneous structure consisting of the coating material, oxide and voids. As a result, macrohardness values are less than those of equivalent material in either a cast or a wrought form. Hardness is usually reduced for a given material if the coating is applied in an inert atmosphere as compared to spraying in air [60-61]. Although oxidation may increase the hardness of the coating, it reduces internal strength of the coating and thus may be detrimental to the coating performance. Hardness in thermal sprayed coatings is normally measured in a test specimen which may differ from that on actual parts due to differences in angle of deposition and stand off distance, and in some cases due to differences in residual stress.

2.5.5 Anisotropy in Thermally Sprayed Coatings

Successive particles in thermal spraying acquire the same lenticular shape over the material already deposited. As a result, coatings develop with an anisotropic lamella structure parallel to the interface. The mechanical as well as other properties of thermal sprayed coating are anisotropic because of this structure and directional solidification. This anisotropy is probably more pronounced for cermet and metallic coatings [62].

2.6 Spray Forming

2.6.1 Current Conventional Sinterforming Processes for Particulate Materials

Currently sinterforming is the principal method used for the production of a number of high premium products from refractory material. Carbides, cermet cutting tool inserts, carbide washers and some electronic ceramic components are typical products which are produced using this forming technique. This technique involves a long production time and high costs.

The operation stages are:

- 1) Compaction of the constituent powder using a pre-shaped die
- 2) Sintering (firing)
- 3) Final finishing by precision grinding.

The compaction stage is a very energy intensive process; and for some components, the sintering process may take up to 70 hours to be completed. Both of these factors lead to high processing costs, therefore if a spray forming technique could be used instead, it would not only simplify the solid component fabrication process, but also substantially improve product quality, while lowering cost.

2.6.2 History of Spray Forming Techniques

The spray forming technology was suggested by Brennan in 1958 [63] for the production of strip but was not used in practice. The principal developer of the spray forming process was Singer [64]. He developed a variant forming process applied to strip. Research on the manufacture of free standing components using various film coating techniques had been carried out by different researchers since the early '80s. This application is of considerable value if conventional methods of ceramic manufacture cannot be used. For example, Fulmar Research Ltd. designed a CVD method for manufacturing tubes from BN [65]. The precursor gases are reacted over a graphite mould held at 1900°C, followed by mechanical separation of the coating from the substrate. Since then this technique has been employed widely to fabricate various free standing components ranging from thick film circuits made of ceramic to manufacturing of cutting tool insert with various refractory materials.

2.6.3 Thermal Spray Forming of Solid Components

The thermal spraying process was originally developed for hardfacing of engineering components to improve their wear resistance, eg. a tungsten carbide layer on a stainless steel or mild steel substrate. Due to the capability of this process to produce very dense coatings, it is suitable for manufacturing free standing solid components. Spray forming is a near-net shape fabrication technology in which a spray of finely atomised liquid droplets is deposited onto a suitably shaped substrate or a mould which is subsequently removed leaving a coherent solid. The technology offers unique opportunities for simplifying the processing of materials, while substantially improving product quality. Spray forming can be performed for a wide range of metals and non-metals, and offers great improvements on the properties of the fabricated components, as a result of rapid solidification (eg. refined microstructures, extended solid solubility and reduced segregation). This forming process also offers substantial economic benefits over more conventional methods as a result of process simplification and the reduction of process stages.

2.6.4 The HVOF Forming Process

As mentioned in the previous sections, the HVOF thermal spraying process has been utilised in many industries because of its flexibility and the superior quality of coatings produced compared to some other thermal spraying techniques. It can also be employed advantageously to manufacture free standing solid components from materials which are difficult to produce by conventional forming. Free standing components of various sizes and shapes have been manufactured by different research groups using the HVOF process [66]. This method has introduced a new means of production of free standing solid components by combining the superiority of HVOF coating quality and the simplicity of few manufacturing process stages. Any material can potentially be used to manufacture free standing components with this method as long as the sprayed material can be melted, and the component die for the desired geometry can be designed. Figure 20 shows various sizes and shapes of components manufactured with the HVOF process [67].



Figure 20 Pictures of cylindrical components manufactured with HVOF process

One of the goals of this project is to use the HVOF process to spray form solid WC components. This material is chosen because the method currently used for manufacturing of carbide components is powder metallurgy, which consists of a number of processing stages and is therefore expensive. Cemented carbides belong to the family of hard, wear-resistant refractory materials, in which the hard carbide particles are bonded together or cemented by a soft and ductile metal binder. WC was first synthesised by a French chemist in 1890, and the study of WC in powder metallurgy was first carried out by Schrocter in 1923, who introduced a new way for obtaining a fully consolidate product [68]. Fine WC particles are mixed with the metallic binder by intensive milling, so that every carbide particle is coated with binder material, and then this powder mixture is used to manufacture solid components by compacting, sintering and post sintering operations. Unlike other metal powders, cemented carbide does not deform during the compaction process; it cannot be compressed to above 65% of the theoretical upper limit density. In order to achieve good dimensional tolerances the compacted components are sintered in a vacuum hydrogen atmosphere. During this operation cobalt melts and draws the carbide particles together causing a shrinkage of 17% - 25% to the compacted product. The product can then be final finished to the required dimensions. This forming operation is very time consuming and expensive.

From the above paragraph on the history and method of manufacturing of WC solid components, it is quite obvious that spray forming may be a viable alternative forming process for the production of WC solid components. Development of HVOF thermal spraying processes has offered opportunity for replacing the conventional sinterforming manufacturing process.

2.6.5 Osprey Forming

A more conventional way to form refractory material from its powder is called Osprey Forming. This method has been used for quite some time already. In the Osprey process as shown in Figure 21, material is melted and is subjected to gas atomisation under inert conditions. Nitrogen and argon gases are commonly used for production of the inert atmosphere. The atomised droplets are collected in a mould, or group of moulds in which final solidification occurs. A key part of this process is the achievement of partial solidification before impingement. The liquid droplet size, the droplet velocity, metal flow rate, gas to metal flow rate ratio and flight distance are carefully controlled to achieve the required conditions of cooling of the liquid. Upon impingement on the deposition surface, the viscous semi-solid droplets spread laterally by a rather high velocity shearing process. This shearing process breaks up any dendrites formed in the droplets before impact, thereby supplying many new nucleation spots in the under cooled liquid. The material then solidifies at a high velocity by heterogeneous nucleation followed by the formation of equiaxed grains. This spray forming process can achieve quite high deposition rates of about 15 and 100 kg/ min for aluminium and steel respectively. Osprey forming of thick sections of stainless steels followed by hipping and heat treatment results in an excellent combination of properties. These properties are isotropic due to the preservation of hipping of the equiaxed as-cast grain structure. The tensile strength, ductility and toughness of the spray formed and hipped material appear to be as good or better than sinterforming by the osprey process. Suitable materials include stainless steels, high speed steels, nickel based superalloys. Experiments to co-spray aluminium atomised droplets with SiC particles to form an *in situ* metal matrix composite have been reported [64]. The advantage of the HVOF thermal spray forming process over the osprey forming process is its simplicity and involves less manufacturing process stages

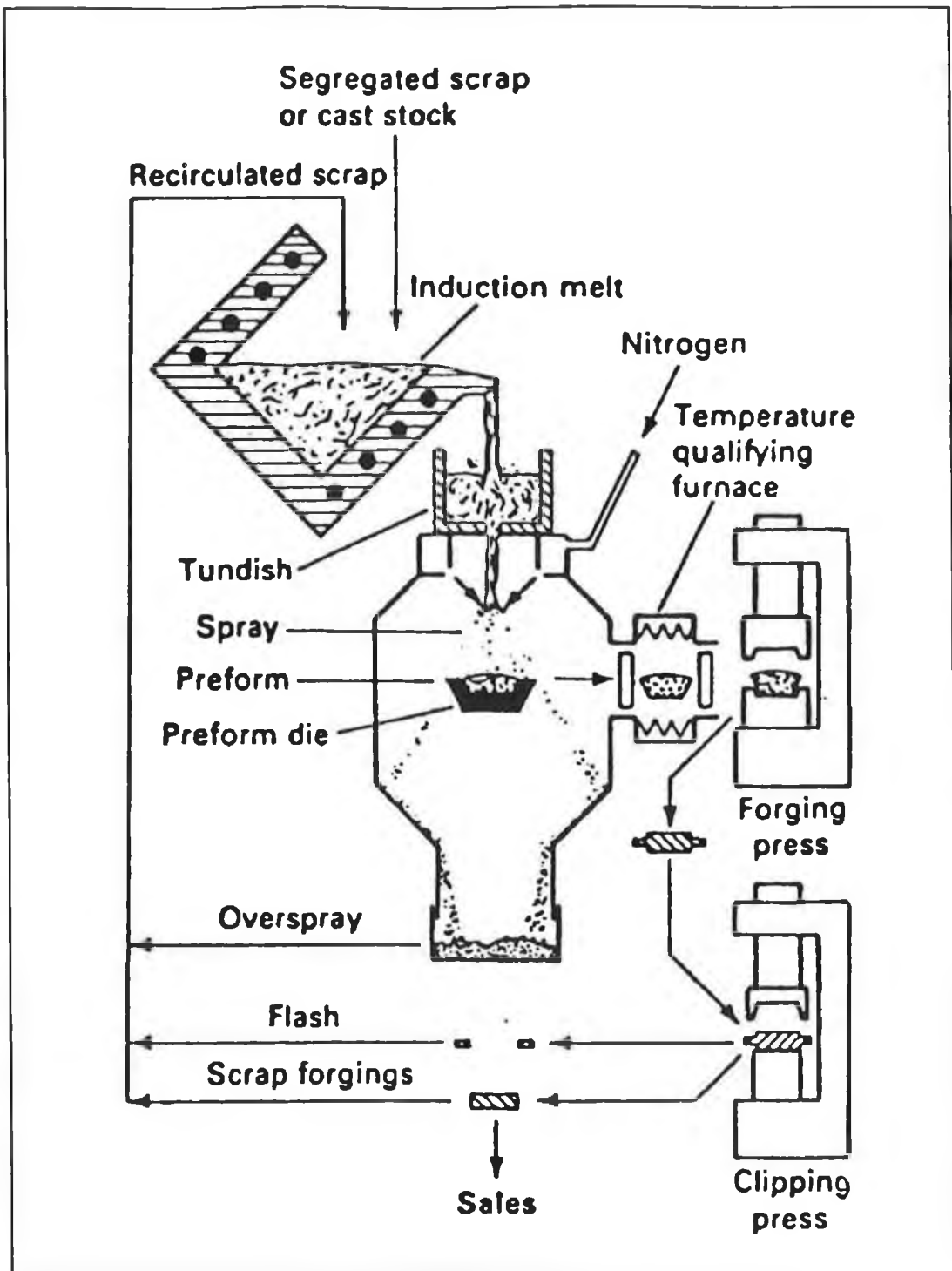


Figure 21 Schematic diagram of osprey spraying process [64]

CHAPTER 3 EXPERIMENTAL EQUIPMENT AND PROCEDURES

3.1 HVOF Thermal Spraying System

The equipment used in this project is a High Velocity Oxy-Fuel (HVOF) Thermal Spraying System (Figure 22). It consists of two units ie. the spraying system and the support system. The spraying system alone should not be used to deposit coatings unless it is equipped with some supporting facilities to ensure the safety of the equipment and the operator. This is a manual control continuous combustion Diamond jet thermal spraying system, manufactured by Metco Ltd. The complete system includes: diamond jet gun, powder feed unit, gas flow meter unit, gas regulator and manifolds, and air control unit.

3.1.1 Diamond Jet Gun

Figures 23 and 24 show two schematic diagrams of the Diamond Jet gun. Diamond Jet is its commercial name, and the gun consists of the air cap body, air cap, nozzle nut, and a button on-off switch which controls the flow of powder from the feed unit. The hose connection block consists of the air, fuel and oxygen hose connections and gas tight plungers to make the connections leak-proof, and to allow the gases to be transferred to the valve core. The valve core shown in Figure 24, is a cylindrical part consisting of a series of passages and grooves and o-rings, housed within the gun body. A lever type handle is attached to the end of the valve core. Rotational movement of the valve core permits the flow of gases through the gun. Oxygen and propylene enter the gun from different positions of the valve core. To turn off the flame of the gun, the valve handle must be rotated to the 'full up' position. All these parts are attached to the gun body, and work together to generate and control spray of molten or semi-molten metal powder with high kinetic and thermal energy.

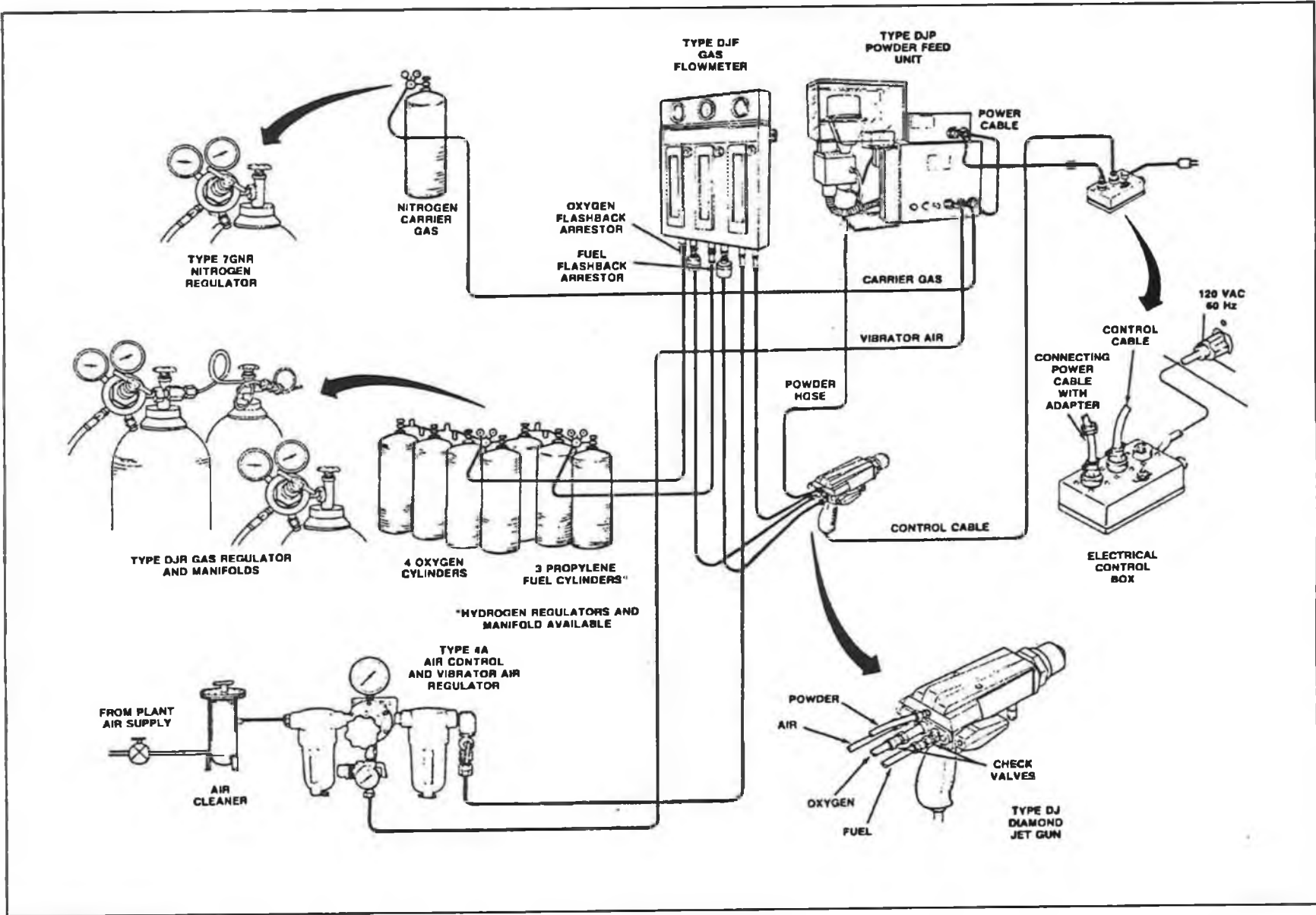


Figure 22 High Velocity Oxy-Fuel Thermal Spraying System

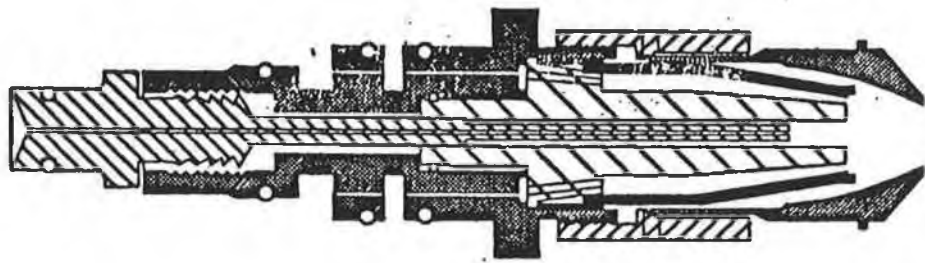
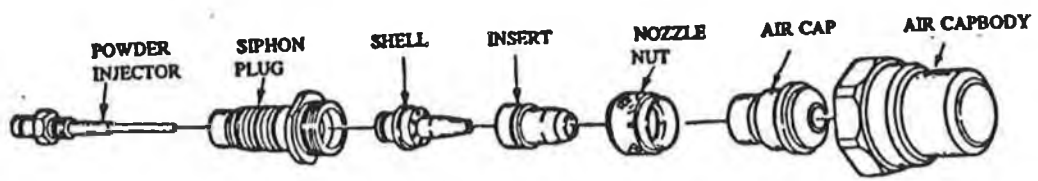


Figure 23 Schematic and cross section diagram of the front end assemblies of HVOF DJ gun.

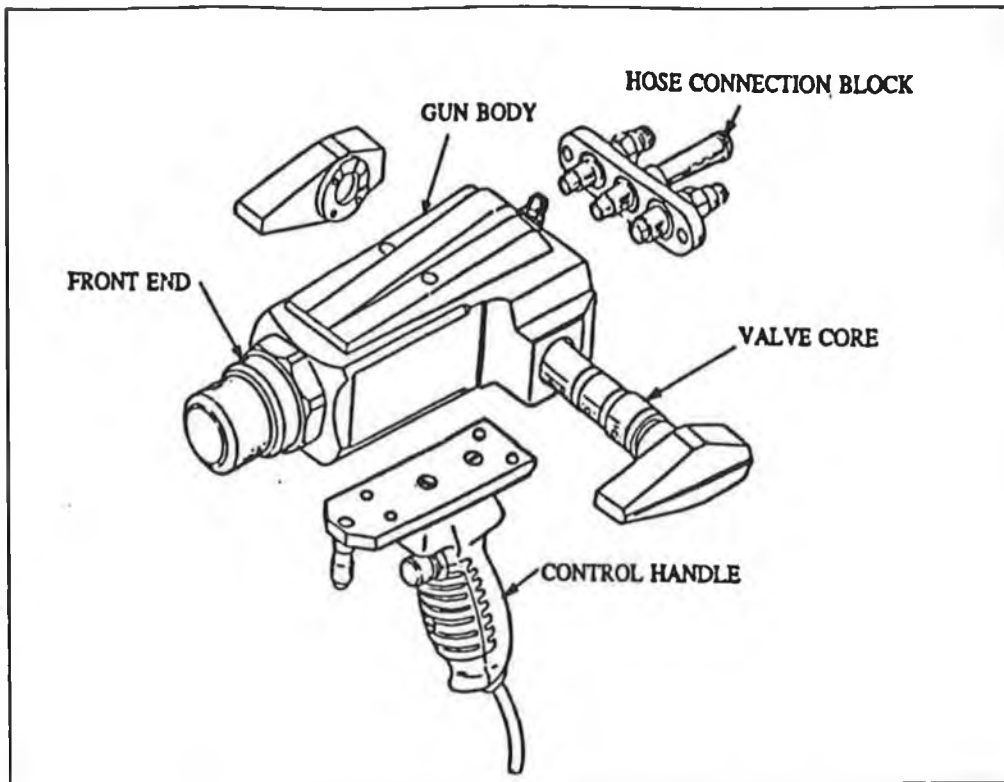


Figure 24 Schematic diagram of the assemblies of the HVOF DJ Gun

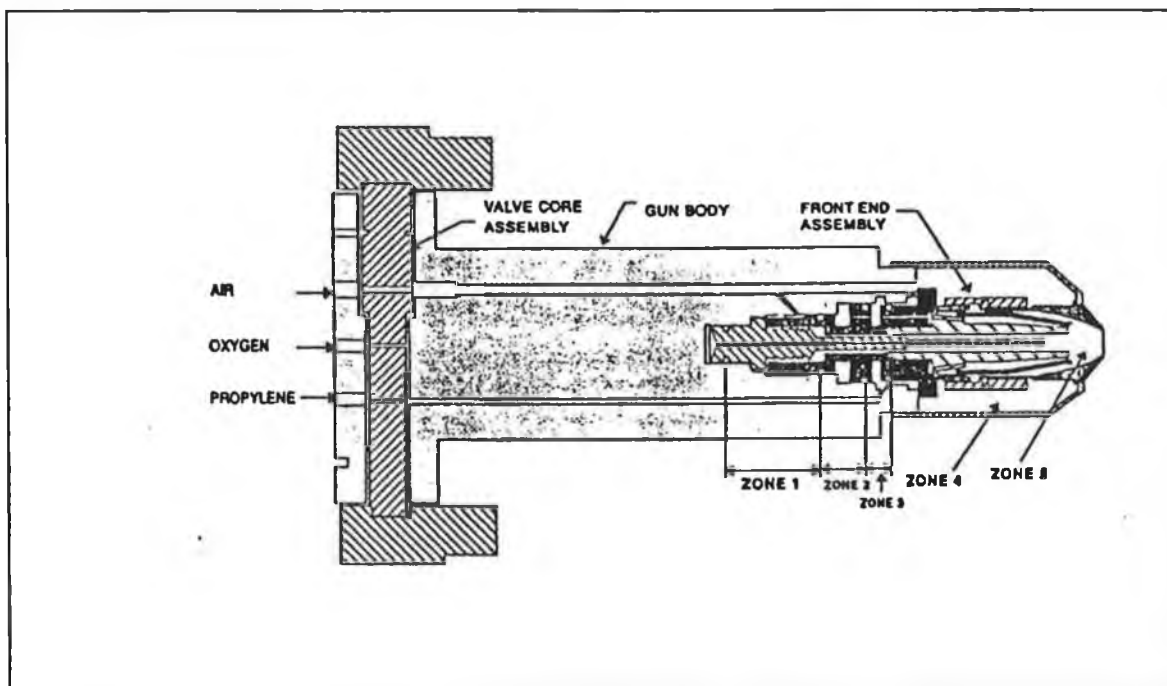


Figure 25 Schematic diagram of the top view of the DJ Gun. Zone 1-5 are the regions where the fuel gas, air and oxygen are mixed and burned.

Figure 25 shows the schematic diagram of the top view of the gun and the cross section view of its front end assemblies. The front end assemblies were grouped as different zones, the fuel gas and oxygen are mixed and burned at various stages at these zones. The combustion product is also accelerated from here due to nozzle effects. Powder particles are injected into the combustion zone by the carrier gas during combustion. The central part of this assemble (Figure 25) is the siphon plug. Holes for propylene and air run parallel to the gun body, and holes for oxygen are obliquely placed through zone 2. Both the gases are mixed in zone 3 and the mixture passes through the hole of the insert to the tip of the shell. At the tip of the shell and insert the combustion takes place within zone 5. The pressure at the combustion zone is about 35 psi [69]. Due to the high back pressure of all incoming gases the flame front moves outward, and because of the nozzle action, the velocity of the combustion product increases up to approximately 1500m/sec [70]. The nozzle effect arises due to the internal surface profile of the air cap. With the change of profile in the air cap the kinetic energy is changed.

Compressed air enters zone 4 from zone 3, and enters the combustion zone through the holes in the nozzle nut. Air is guided by the outer surface of the shell and the inner surface of the air cap in such a manner that it creates a layer of air over the inner surface of the air cap. Due to this air layer the air cap is thermally insulated from the hot combustion products of the combustion zone. The powder injector connected with the powder feed unit is fitted at the back of the siphon plug. The front end of the powder injector is extended up to the tip of the insert, which helps to inject the powder at the very centre of the combustion stream.

The nozzle nut is used to fix the shell and insert together with the siphon plug (Figure 23). Proper tightening of the nozzle nut is important for proper working of the gun. The air cap, siphon plug, insert, shell and nozzle nut are fitted to the air cap which is in turn fitted to the gun body.

3.1.2 Powder Feed Unit

The powder feed unit is a completely self contained unit, designed to deliver powder to the gun at a precise flow rate (Figure 26) . This system is equipped with an integral powder feed rate meter, which continuously displays the spray rate. The unit comprises of a hopper assembly, control cabinet and control panel. Carrier gas flows to the gun via the hopper assembly and gas flow meter. There is a pressure gauge in this line. With the help of the control unit the pressure and flow of the carrier gas can be controlled. The hopper assembly comprise of a hopper, powder port shaft (pickup shaft), air vibrator and control valves. The powder port shaft is located in the throat of the hopper, and at the mid span of this shaft there is a radial hole. The air vibrator is mounted in the base of the hopper. A load cell is used to weigh the hopper assembly, and control valves are used to control the carrier gas.

Working principle of the powder feed unit:

Powders enter the powder port shaft under the action of gravity; by controlling the valve, carrier gas is allowed to pass through the powder port shaft. While passing through the shaft, carrier gas picks up the powder and injects it to the very centre of the combustion zone through the powder injector. The amount of powder flowing with the carrier gas is controlled by the rate of carrier flow, hole size of the powder port shaft, amplitude of the vibration of the air vibrator, and the differential pressure between the hopper and the carrier flow line. The amplitude of the vibration can be controlled by varying the flow of air into the air vibrator. With the increase of hopper pressure the flow of powder with the carrier gas will increase and this increased pressure is indicated on a dial of the powder feed unit. The fluidity of the powder is maintained by passing pressurised gas through a filter placed at the entrance of the shaft hole. The controlled vibration of the hopper and the gas pressure ensure a constant supply of powder at the vicinity of the hole opening. The amount of powder delivered from the hopper is determined by the rate at which the hopper loses weight. The load cell fixed to the hopper assembly continuously weighs the hopper. This result is calculated against a certain period of time and the flow rate of powder in pounds per hour or

gram per minute is displayed. Unfortunately, as a result any change of flow rate cannot be detected instantly.

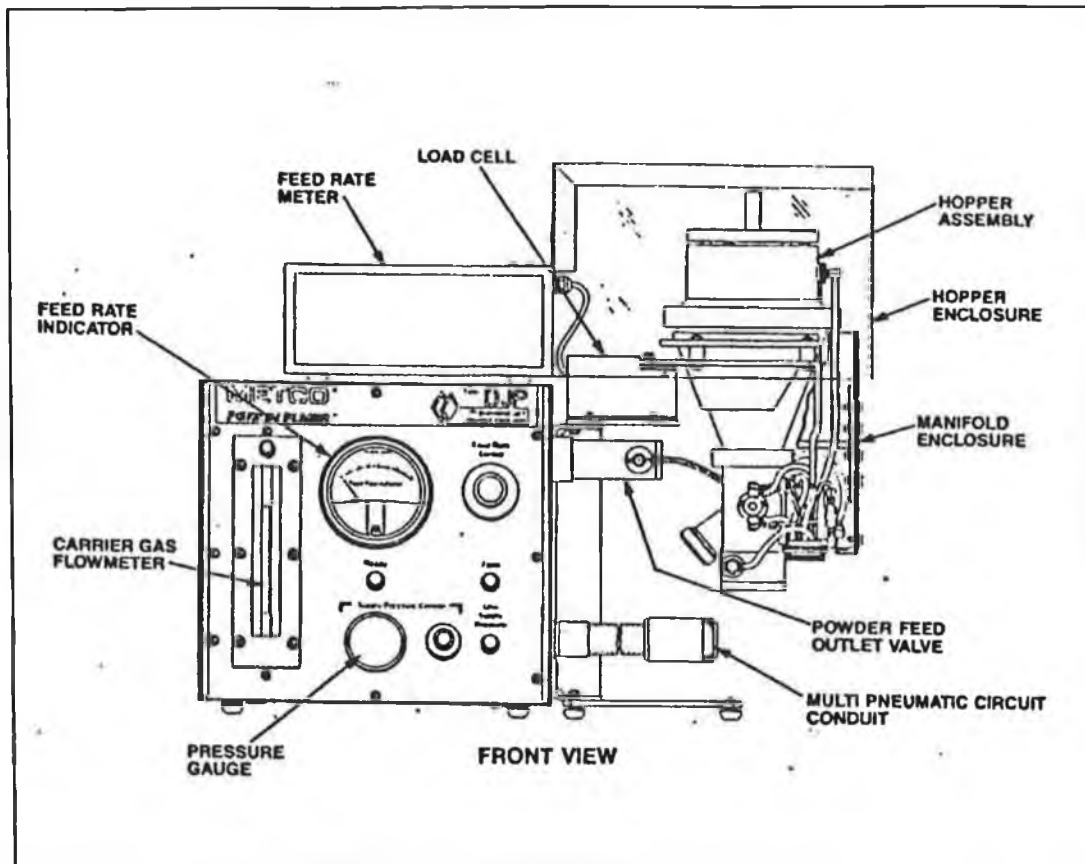


Figure 26 DJ powder feed unit

3.1.3 Gas Flow Meter Unit

The gas flow meter unit shown in Figure 27 controls and monitors the fuel gas, oxygen and air required by the gun. It consists of flow measuring glass tubes, close coupled pressure gauges and accurate flow adjustment valves. There is a float located within each flow measuring tapered glass tube, free to travel up and down. Gas flowing through the flowmeter causes the float to rise to a point of dynamic balance, which is a true indication of the flow. As flow area increases the float rises, and it descends when flow area decreases. The use of

the close coupled pressure gauges and the flow adjustment valves allows maintenance of accuracy of the gas flow required. To guard against any danger of backfire, flashback arrestor and check valves are installed in both the oxygen and propylene lines. Flash back arrestors are fixed at the outlet of the flow meter unit and are designed to stop the flow of gas from the flowmeter to the gun in the event of a sudden pressure rise in the hose line due to an increase in temperature. Check valves are also provided at the inlet of the gun body to prevent a back flow of gases.

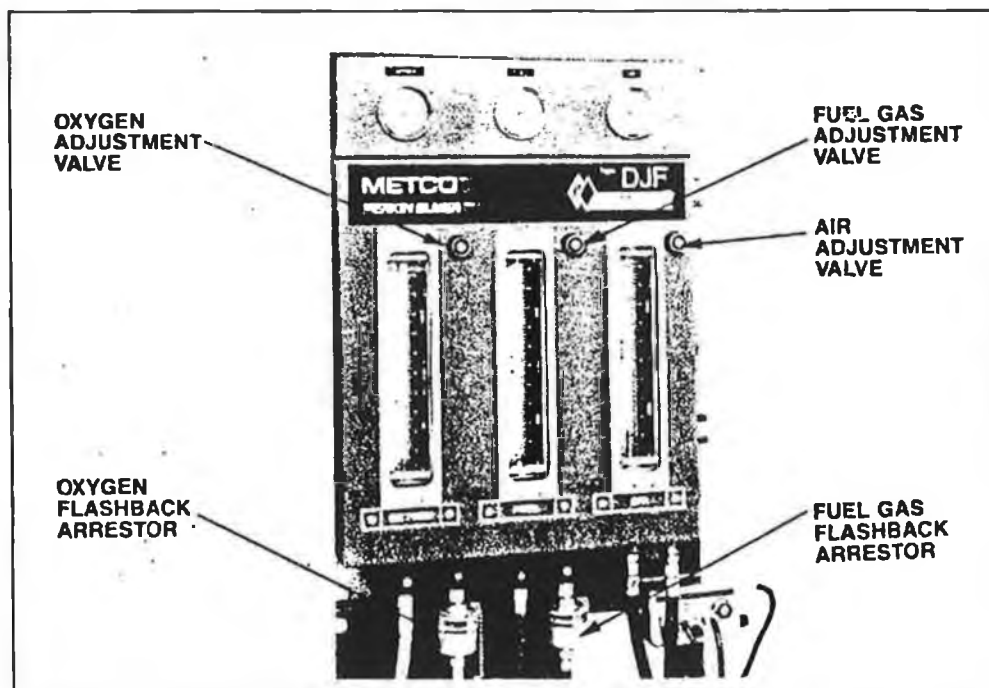


Figure 27 DJ flow meter unit

3.1.4 Gas Regulator and Manifolds

The compressed gas cylinders used with the Diamond jet system are equipped with pressure regulators (with gauges) to adjust the supply gas pressure of the gas cylinder to a correct working pressure. These gas regulators consist of a high pressure regulator, and metallic tube manifolds which enable several gas cylinders to be connected together. Some of the manifolds are fitted with non-return valves.

3.1.5 Air Control Unit

This unit consists of a pressure regulator and two filters. The regulator provides a means for adjusting air pressure to the gun. It holds the required pressure constant regardless of fluctuation in the line pressure. A filter which is mounted in front of the regulator is used to remove water which condenses out as a result of the pressure drop through the regulator. The filter bowls are transparent to show the level of trapped liquid, and also have a manual drain to permit removal of the liquid without shutting down the system. An unregulated air line is provided at another outlet after the first filter. The air is controlled by a shut off valve. From here air is supplied to the air vibrator of the powder feed unit through a "Y" connector. A regulator is provided to control the air pressure as required by the vibrator.

3.2 Procedure for HVOF Spraying

The HVOF process can be used to produce good quality coatings if every step leading to the final coating is carried out with care. The entire thermal spray coating process can be divided into three steps: surface preparation, spraying process and post spray treatment.

3.2.1 Spraying Substrate and Surface Preparation

In most coating processes the integrity of the deposit is critically dependent on the condition of the substrate surface. HVOF thermal spraying is no exception, but unlike other methods it is often applied on site in ambient atmosphere, or in dusty workshops. Thus surface cleanness in the true scientific sense is never achieved. Nevertheless, the widespread acceptance of sprayed coatings reflects the fact that adequate bond strength can be obtained for many practical applications. Experience has shown that without exception, all sprayed coatings have significantly higher bond strength on roughened surfaces [39]. In fact, negligible adhesion may occur on a smooth surface. Heavy duty applications require the use of large (25 mesh) metallic grits which, because of their momentum, can remove surface scale as well as providing a coarse texture to support the thick coatings typically deposited by wire or arc processes. For thinner coatings applied by high energy techniques, eg. the HVOF process, grit blasting is usually carried out with finer ceramic (Al_2O_3 , SiC, etc.) materials.

Grit blasting has some disadvantages, eg. some substrate materials may be too hard to roughen, while others can work harden, and thin sections may distort. Inevitably a few grit particles remain embedded in the surface. A freshly prepared surface is also very reactive, and the spraying operation must be carried out as soon as possible after blasting.

There are, however, some materials which when thermally sprayed adhere strongly even to a smooth or poorly prepared surface [50]. Such self-bonding materials include molybdenum and nickel- aluminium thin coatings (~ 0.1 mm) which are extensively used as bond (key) layers beneath other materials (especially ceramics) to improve the overall adhesion. An

exothermic reaction between nickel and aluminium contributes additional thermal energy which is partly responsible for the good bond.

Areas not requiring coatings are usually masked during grit blasting and spraying to prevent build-up of over-sprayed material. The design of components to accommodate thermally sprayed coatings is very important in order to get the best coating possible.

3.2.2 Spraying Process

Immediately prior to deposition of the powder, the substrate has to be preheated to remove moisture and condensation from the substrate. Preheating will also help in reducing the thermal stress that may arise due to the difference in the coefficient of thermal expansion between the substrate material and the coating material. The pre-spray heating temperature can also improve the coating adhesion strength by encouraging more diffusion between the substrate and the coating. According to the system manufacturer, the pre-spray heating temperature of a steel substrate should be 90-150°C and should never exceed 200°C [70], if the gun is used to heat up the substrate surface. Temperatures higher than 200 °C, generated from the flame from the gun will cause oxidation to the substrate surface and the subsequently sprayed coating will have less adhesion strength to the substrate due to the oxide inclusion. But sometimes higher pre-spray temperature eg. 250°C is needed in order to further reduce the thermal tensile residual stresses within the coating due to the difference in the coefficient of thermal expansion between the substrate and the deposited material. It has also been found that higher pre-spray heating temperatures encourage more diffusion to occur between the coating and the substrate [28]. Higher pre-spray substrate temperature can also be obtained by heating the substrate in a furnace to the desired temperature prior to spraying.

Spray process parameters for the HVOF system depend on the type of application, coating material and substrate. The rotational speed of the substrate and traverse of the gun should be such that the deposition rate of the coating thickness per spray is less than 75µm for

general metallic materials, and for carbide it should be about $15\mu\text{m}$ [70]. In general, it is a good practice to traverse the gun as fast as possible. However, any sign of spiral build up of deposition on rotating cylindrical substrate should be avoided. Before carrying out spraying, the spraying process parameters are to be adjusted. These process parameters include pressure and flow rate of gases, air pressure and flow rate, spray rate, spray distance and spray gun setting. All these spraying parameters vary depending on the type of coating material to be deposited. Appendix A details the spraying parameters and gun settings for different powder recommended by the powder manufacturer.

During spraying, cooling may be required in order to prevent the coating and the substrate from overheating, and to allow continuous spraying, especially when applying a thicker coating. During spraying the temperature of the process should be carefully monitored.

3.2.3 Post Spray Treatment Process

The as-sprayed coatings are seldom ready for use. In most practical applications they have to be ground and polished to get the required surface roughness. Heat treatment could be necessary to change the coatings' phase composition, to decrease porosity or to improve another coating property. Impregnation (sealing) proves necessary for electrical application of the deposits (such as corona rolls) [71]. Post-spray treatment such as grinding, polishing and laser engraving is an integral part of the production of ceramic coatings and many others.

Among the heat treatment processes, furnace treatment seems to be the most usually applied, especially in research laboratories. The laser treatment or HIPing are less frequent owing to the cost of the equipment.

The HVOF thermally sprayed coatings can also be machined by different machining processes, the machining of these material can be a tedious task, and sometimes is troublesome for the inexperienced operator. Materials that are abrasion resistant, are difficult to grind. For certain materials, the structure of the sprayed mass is porous; highly reflective finishes are difficult to achieve. The bond between the sprayed particles is primarily

mechanical; therefore, individual particles can be pulled out if cutting pressures are excessive. Sprayed coatings are composed of well defined particles and have poor thermal conductivity compared to the same material in wrought form. Heat transfer away from the cutting point is slow. The acceptable methods, practices and techniques used for machining materials in their wrought form do not apply to the same materials when sprayed. Factors which influence the choice of finishing method include type of material to be finished, shape of part, finish and tolerance required and economics.

Carbide tools are generally used to machine hard coating materials such as ceramics, carbides and cermets. Tool angles, surface speed and feeds are critical in the success of machining these coatings. Improper tool angles and tool pressure can result in excessive particle pull-out and destruction of the coating substrate bond.

3.3 Thermal Spray Safety Measures

Potential hazards are always associated with thermal spraying, including the preparation and finishing processes. Due to the gases, temperature and toxic nature of the powders used, it is essential that all personnel concerned with thermal spraying should be familiar with safety regulations contained in an established standard set by the local, and/or state health authorities. The following sections discuss some safety practices applicable to thermal spraying.

The Metco Diamond Jet System hardware has been designed for operation only in areas which are maintained " Non- Hazardous " by means of proper and adequate ventilation from a source of clean air, to ensure a dangerous accumulation of combustible gas does not occur. It is the responsibility of the operator to be familiar with the operation manual before using this system. Proper training from a Metco Representative or from an experienced operator is essential before the use of this system. Although this system is considered as potentially hazardous (like many industrial tools), it incorporates built-in safety features to protect the operator and equipment. This process can be safe when performed by a properly trained operator with an understanding of spraying practices, knowledge of the equipment, who operate with care, and is familiar with recommended precautionary measures.

3.3.1 Gas Cylinder Use

Charged gas cylinders are potentially dangerous. The storage, handling and use of oxygen and fuel gas cylinders should be in accordance with "Safety in Welding and Cutting", American National Standard Z49.1 and Compressed Gas Association Pamphlet P.1, " Safe handling of Compressed Gasses." [72]. The relevant guidelines can be summarised as follows:

Never put a gas cylinder in a hazardous position. Keep cylinders away from heat and water. Always chain cylinders to keep them from toppling. Put the valve caps on the cylinders when they are not connected for use. All damaged cylinders should be reported to the gas distributor without hesitation. It is very dangerous to hang a spray gun or its hoses on regulators or cylinder valves, as a fire or explosion may result. Before moving any cylinder, shut the valve, discharge and remove the regulator and put on the valve cap.

Never use oil or grease in or near oxygen equipment. Before attempting to increase the fuel consumption of propylene through means of pressurising the cylinder, consultation is needed with the local gas supplier. Fuel gases of this type are heavier than air. The use of these gases should be only in a well ventilated room. All gas cylinders should be stored in an isolated open store room.

3.3.2 "Diamond Jet Equipment" Safety

All equipment must be maintained in accordance with the maintenance procedures outlined by Metco. Use only approved Metco replacement parts. Use of the parameters provided is important to ensure that the equipment operates correctly. All hoses and fittings must be maintained. Any worn or damaged hose should be removed from operation. Prevent hoses from damage by preventing over-bending, twisting, tension or being run over and stepped on.

Equipment maintenance has to be carried out on a regular basis follow recommendations in the Metco instruction manuals [73].

3.3.3 Metal Dust

All dust having considerable calorific value can be explosive. Aluminium and magnesium dust are particularly hazardous. The greatest care should be used in handling them. To minimise the danger of dust explosion resulting from spraying, adequate ventilation must be provided for spray booths, and other confined spaces, to prevent the accumulation of fumes and dust. Good house-keeping in the work area is essential. Inspection and regular cleaning to ensure that there is not a potentially dangerous accumulation of dust, helps reduce risks. All dust must be wetted down and kept in water using a water wash wet collector.

When cleaning the booths, pipes etc., the ventilating fan must be kept running to prevent the accumulation of fumes or dust in the system. Non-sparking tools should be used in the cleaning and repair operation.

3.3.4 Eye Protection

All persons in the vicinity of an operating system must wear a suitable eye glasses, to provide protection against any flying particles caused by the jet flow and against ultra-violet radiation from the spraying flame. The choice of glasses shade may be based on visual sensitivity and sharpness (acuity) and may vary widely from one individual to another. A grade 9 lens is recommended for protection against ultra-violet radiation up to 40 kW.

Eyes protectors should be inspected frequently. Lenses and cover plates which are scratched, pitted, or damaged can impair vision and seriously reduce protection.

3.3.5 Reduction of Noise Hazard

The noise from the DJ spray gun exceeds the maximum permitted by the Occupational Safety and Health Administration [73]. The operator and other personnel close to the system must be protected from the excessive noise. If possible, the spray operation should be isolated. If this is not possible, personnel should be rotated. Hearing protectors must be used at all times, keeping in mind that the use of cotton ball for hearing protection is ineffective against high-intensity noise.

Noise level at any location depends on factors such as equipment operating parameters, background noise, room size and wall, floor and ceiling material. To determine the exact noise level, it is necessary to measure the sound level.

3.3.6 Personal Protection

Possible allergic reaction to dust, fumes, or other unknown causes of health impairment due to contact with the body cannot, in most cases, be predicted. To avoid such reaction, never permit spray dust to enter the eyes, mouth, cuts, scratches, or open wounds. After spraying, and especially before eating or handling food, hands must be washed thoroughly. If available, fireproof

or flame resistance protective clothing should be worn. This includes gloves to protect hands from continuous exposure to spray dust. Ultra-violet protected gloves should be wore by operators who hold the gun during operation.

3.3.7 Reduction of Respiratory Hazards

A suitable spray booth and an adequate exhaust system are required to control the toxic or noxious effect of dust, fumes and mist which may be generated by flame spraying. A proper breathing mask should be worn at all time during operation of the gun. The mask filter should be such that the smallest particles being worked with are excluded from inhaled air.

3.3.8 General HVOF Gun Operational Precautions

Before spraying, all equipment should be inspected to ensure that the system is correctly assembled with Metco supplied components. The maintenance recommendation in the Metco instruction manual should be followed.

It should be remembered that the stream of sprayed metal is very hot. The lighted gun should be pointed away from the operator, and away from material which will burn. Carelessness in pointing the gun at paper or wood can result in fire. Special care is needed not to spray on the hoses when operating the gun as hoses will burn and should be kept out of the way. All air lines, compressor, regulator etc., should be inspected regularly for leaks and loose connections.

CHAPTER 4 COATING PROPERTIES AND MEASUREMENT METHODS

In this project, studies were carried out to investigate the characteristics of the coatings produced using the HVOF process. Properties of coatings such as hardness, bond strength, residual stress, bend strength and coating morphology were studied using various characterisations and measurement techniques.

The following paragraphs describe the measurement methods used and working principles of each. Discussion on the porosity measurement technique is also included in this chapter, although tests on porosity were not carried out on any of the test samples in this project.

4.1 Coating Thickness Control and Measurement Method

The control of the deposition of coatings precisely to the desirable thickness is very difficult due to the manual handling of the spraying process. Trial samples are usually sprayed first with the same powder and spraying parameters for test specimens, the number of spraying passes and time to deposit the coating upto the require thicknesses are noted. The procedure is then repeated to spray the test specimens. Experimental specimens for this project sprayed following this method are within $\pm 10\%$ of the target thicknesses.

The thermal spraying process is normally used to deposit coatings of thickness from 50 μm to more than 1000 μm . Eddy current and magnetic induction measurement methods are very effective at measuring the coating thickness within this range. A Fisherscope Multi thickness measuring instrument based on the eddy current and magnetic induction working principles is used in this project. A schematic of eddy-current gauge is shown in Figure 28. A high frequency current is passed through the sensing coil of the instrument, when it is brought close to a conductive material, an eddy current is induced in that material. This will then cause the back emf energy loss and change the impedance of the coil. This change in impedance is measured and converted into thickness proportional

electronics signals. This instrument has to be calibrated with standard specimens of known thicknesses provided by the manufacturer before use. The accuracy was found to be within $\pm 5\%$ of the known thickness value. The standard test practices for this method are described in detail in ASTM Designation E 376-69 [74]. A micrometer was also used to measure coating with higher thicknesses.

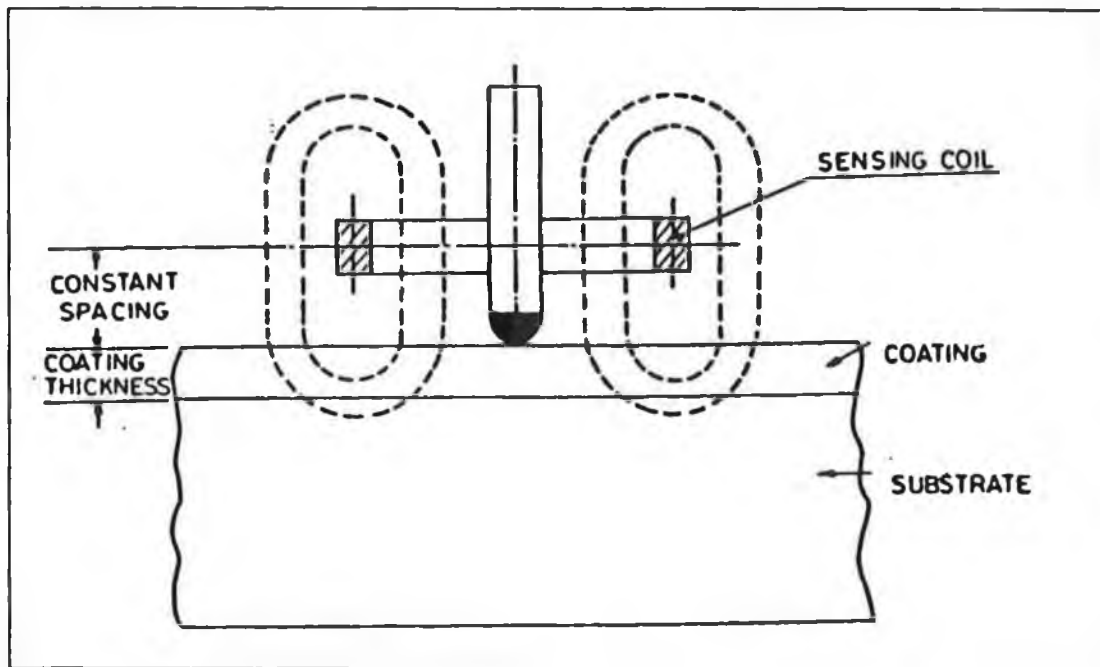


Figure 28 Operating principle of thickness measurement by eddy-current.

4.2 Hardness Measurement

Hardness and microhardness tests are often used for the first approximation of coating wear resistance, which is by far the most important property in present applications of thermal spray technology. The measurement also enables a quick estimation of coating strength and the quality of spraying, because specific defects, such as porosity and unmelted grains, lower the coating hardness value.

Hardness is usually measured in one of three different methods, ie. static indentation, rebound or dynamic and scratch methods. In the static indentation method a ball or a diamond cone or a pyramid is forced onto the material being tested using a known load. The relationship between the total load and the area or depth of indentation provides the measurement of hardness. This method has served quite well for hardness tests performed using loads of 200g and higher. Hardness tests with a load range less than 200g give widely scattered values and the scatter increasing as the load decreases. Scatter of approximately 10% is usually found with this method, this is due to errors involved in applying load, dimension measurements and the hardness definition [75].

Two types of hardness measurement machines were used for this project, one is a static indentation hardness tester called Leitz Miniload 2 Vickers and the other is a Rockwell hardness tester. The range of test loads that can be used by the Vickers hardness instrument is from 5g to 2000g. Hardness of thermally sprayed coatings are normally measured along the cross-section of the coating, therefore a coated sample has to be sectioned and mounted for grinding and polishing before testing. The polished sample is then positioned on the platform of the hardness tester, and indented with a known load. By focusing the microscope to the width of the indentation the hardness can be measured.

Rockwell hardness values are expressed as a combination of a hardness number and a scale symbol representing the indenter and the minor and major load. The hardness number is expressed as the symbol HR and the scale designation, eg. 64 HRC represents

the Rockwell hardness number of 64 on the Rockwell C scale. There are 30 different scales, defined by the combination of the indenter and the minor and major loads [76]. The majority of applications (for steel, brass and other alloys) are covered by Rockwell C and B scales

The relationship between the Vickers and Rockwell scales is known to be non-linear, this is shown in Figure 29 [76].

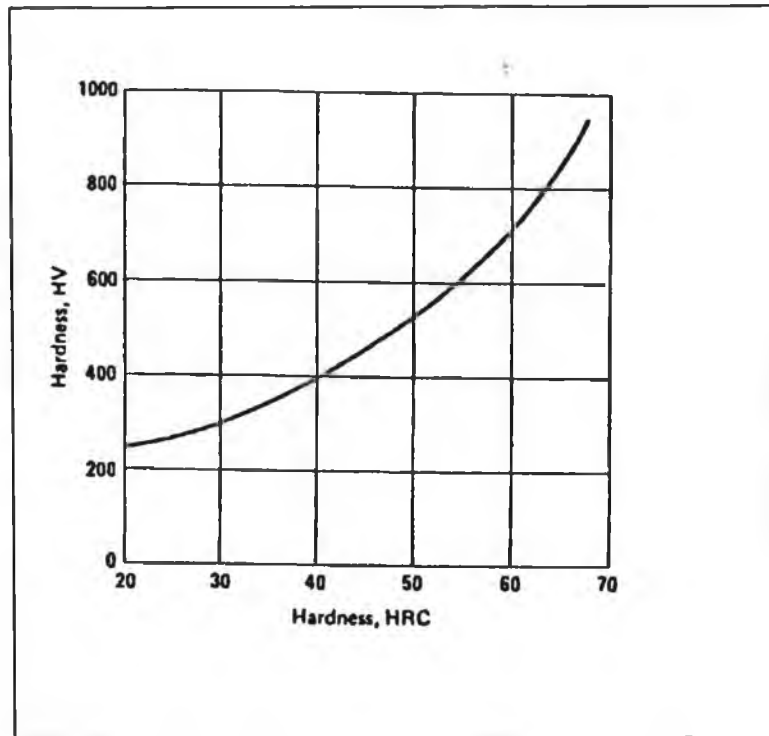


Figure 29 The relationship of HRC and Vickers Hardness Scales [76].

4.3 Porosity Measurement

The common techniques used to measure porosity are direct observation methods and indirect detection methods which allow observation of both isolated voids (closed porosity) and through pores (open porosity). Indirect detection methods include the use of a mercury porosimeter, the optical dielectric constant test, the pore corrosion test, the radiography method and density measurement. Direct observation techniques use optical microscopy, scanning electron microscopy, transmission electron microscopy and x-ray scattering.

By using an optical microscope, porosity of a coating can be measured by comparing micro-photographs of the sample with another micro-photograph of a sample of known porosity. Porosity can be measured by optical microscopy by directly measuring the pore area in the view field of a microscope, and comparing this area with the total viewing area. A microscope equipped with a computerised analysis system is generally used to determine the area of the pores on any specified size of field within the focus area of the microscope. The instrument works by projecting the focused area of the microscope to a video camera, which converts the light image into an electronic signal. The computer then processes the signal by digitising the electronic signals, and the microscope image can be seen on a computer screen. The pores on the sample are seen as darker area, and a computer program is used to calculate the darker area by assessing the difference in colour to the brighter area. For this measurement, metallographic preparation of the coating is required. This is often difficult because a coated sample is a combination of hard and soft materials, which normally require different polishing techniques. Pull-out is a common problem that can substantially increase the apparent porosity in brittle coatings, such as carbides and ceramics.

4.4 Adhesion Bond Strength Measurement

Adhesion strength is the most desirable property of a thermally sprayed coating. The adhesion of a thermally sprayed coating to a substrate is the principal property which determines its quality. Coatings on metal substrate are tested using a method described by ASTM C633-79, 'Standard Test Method for Adhesion or Cohesive Strength of Flame Sprayed Coatings'. The test consists of coating one face of the substrate, and then bonding a loading fixture to the coating with a suitable adhesive. The coating is then ground around the base of the loading fixture so that shear stresses are avoided during the tensile test of the assembly. The test is performed at room temperature due to the limitations of the adhesives. The coating should be more than 0.015in (0.38mm) in thickness because of adhesive penetration into the coating. The tensile adhesion test is useful in quality control as it provides a ranking of various types of spray systems and resulting coatings. The mode of coating failure, (see Figure 18) will be either cohesive or adhesive. An adhesive failure occurs when the entire coating separates from the substrate. True adhesive failure rarely occurs because of the rough nature of the substrate surface. Failure in this case takes place near the interface where the fracture surface exhibits areas devoid of coating. A fracture occurring entirely within the coating is called cohesive failure. Figure 30 is a diagram of tensile adhesion test configuration as specified by ASTM C633-79 [77].

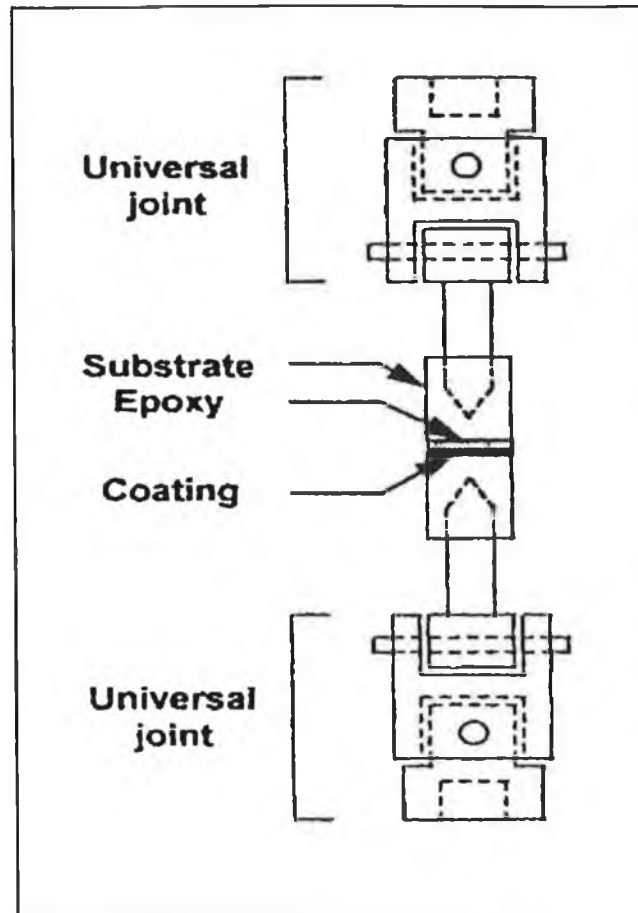


Figure 30 Tensile adhesion test configuration specified by ASTM C633-79 [77].

Scotch Weld Brand structural adhesive EC1386 was used to glue the test samples together for the pull tests. The product specification and technical data is shown in Appendix A. The glued samples were then cured in an oven at 165°C to 180 °C for three hours. Pressure is needed during the cure of this glue in order to keep parts aligned and to overcome distortion and thermal expansion in the glued parts. A clamp block designed to carry out this task is shown in diagram A in Figure 31, where pressure can be applied at one end by tightening the screw, the cavity in the middle is designed as a channel for any excessive glue to flow. Diagram B in Figure 31 shows the holder for the test samples. To carry out tests, the whole fixture is attached to a tensile tester. The travelling speed of the cross head of the tensile tester was set at 0.02mm/sec until rupture occurred, and the maximum load applied was recorded.

The bond strength is found from the simple relation:

$$UTS = L / A$$

Where: UTS = cohesive or adhesive strength - force per unit of surface area

L = load to failure (force)

A = cross sectional area of specimen.

This method is useful for comparing adhesion or cohesive strength of coatings of similar types of flame sprayed materials. The test should not be considered to provide an intrinsic value for direct use in making calculations such as to determine whether a coating will withstand specific environmental stresses. Residual stresses in flame spraying coating develop in a much more complicated manner than that for a standardised test.

Like many others test methods, this method also suffers from the possibly of test error and disadvantages such as the following:

1. If failure occurs within the adhesive only, the area within the coating is used in the calculation to find the stress at failure. This method is inaccurate because the test result has indicated either defective bonding of adhesive to the sample or non-axial loading of the sample.
2. The manner in which the coating is loaded is not typical of stresses observed during its service life.
3. The value of measurement is influenced by the symmetry of the experimental setup, and by the penetration of epoxy into pores of the coating.
4. The adhesive must have a greater tensile strength than the coating.
5. The elevated curing temperature of the adhesive may affect the adhesion of the coating, since the residual stress distribution may be altered.
6. The fracture surface of a test specimen may exhibit both adhesive and cohesive failure. The tensile adhesion test yields only an average value when both of these failure modes act together. It does not establish which failure mode limits the strength of the coating.

7. Flaws in the form of microcracks, porosity and second phase inclusion within the coating will affect adhesion. The role of these microstructural features of the coating cannot be examined by the tensile adhesion test.

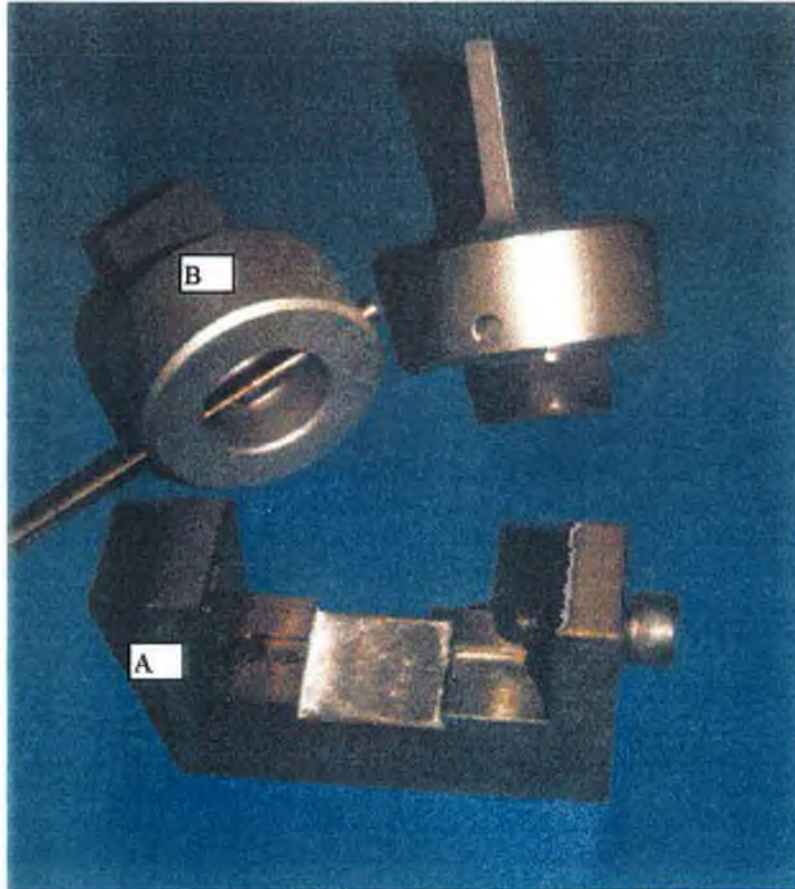


Figure 31 Fixtures for tensile adhesion test.

4.5 Optical Microscope

The optical microscope provides a source of basic information about the coating and substrate microstructure. The optical microscope makes it possible to analyse;

- fraction and size of voids in the coating
- fraction and size of unmelted particles in the coating
- deformation (mechanical or thermal) of substrate near the coating
- distribution of phases in the coating.

Prior to the microscopic observation the sprayed piece must be prepared metallographically. As the total field of microscopic observation is no greater than a few square millimetres, it is important to select a typical part of the sprayed piece or the part in which microstructure defects are to be expected such as edges or sharp angles.

The selected part might be impregnated within a low viscosity resin, and the mounted pieces are usually polished until a mirror like finish is achieved.

The optical microscope used for this project is Reichert Universal Camera Microscope.

4.6 Residual Stress Measurement

It is probably true to say that all engineering components contain stress; which varies in magnitude and sign. These stresses which are produced as a result of mechanical working of the material, heat treatment, joining procedures, etc. are called residual stresses, and they can have a very significant effect on the fatigue life of components. These residual stresses are “locked into” the component in the absence of external loading, and represent a datum stress over which the service stresses are subsequently superimposed. If, by fortune or design, the residual stresses are of the opposite sign to the service stresses then part of the service load overcomes the residual stress and thereafter the combined stress can rise towards a failure value. In such cases, residual stresses are thus extremely beneficial to the component and a

significantly higher fatigue strength can result. If however, the residual stresses are of the same sign as the applied stress, eg. both tensile, then a smaller service load is required to produce failure than would have been the case for a component with a zero stress level initially. The strength and fatigue life in this case is therefore reduced. Thus both magnitude and sign of residual stresses are important to component life considerations, and the two most common methods for determining these quantities are described below:

4.6.1 X-Ray Diffraction Stress Determination

The X-Ray Diffraction technique is probably the most highly developed non-destructive measurement technique currently available for measuring residual stresses. The principle of the X-ray procedure is to use a diffractometer to measure the relative shift of X-ray diffraction lines produced on an irradiated surface. The individual crystals within any polycrystalline material are made up of families of identical planes of atoms, with a fairly uniform interplanar spacing d (Figure 32a). The so-called lattice strain normal to the crystal planes is then $\Delta d/d$. At certain angles of incident, (known as Bragg's angles) X-ray beams will be diffracted from a given family of planes.

Diffraction occurs at an angle 2θ , defined by Bragg's Law:

$$n\lambda = 2d \sin \theta$$

where:

n = integer

d = lattice spacing of crystal planes

λ = wavelength of X-ray beam

θ = the angle of diffraction.

Any change in the lattice spacing, d , results in a corresponding shift in the diffraction angle 2θ . Figure.32a shows a sample in the $\psi=0$ orientation. The presence of a tensile stress in the sample results in a Poisson's ratio contraction, reducing the lattice spacing, and slightly

increasing the diffraction angle, 2θ . If the sample is then rotated through some known angle ψ , (Figure.32b) the tensile stress present in the surface increases the lattice spacing over the stress-free state, and hence 2θ decreases. By measuring the change in the angular position of the diffraction peak for at least two orientations of the sample defined by the angle ψ , the residual stresses on the sample surface can be calculated [78].

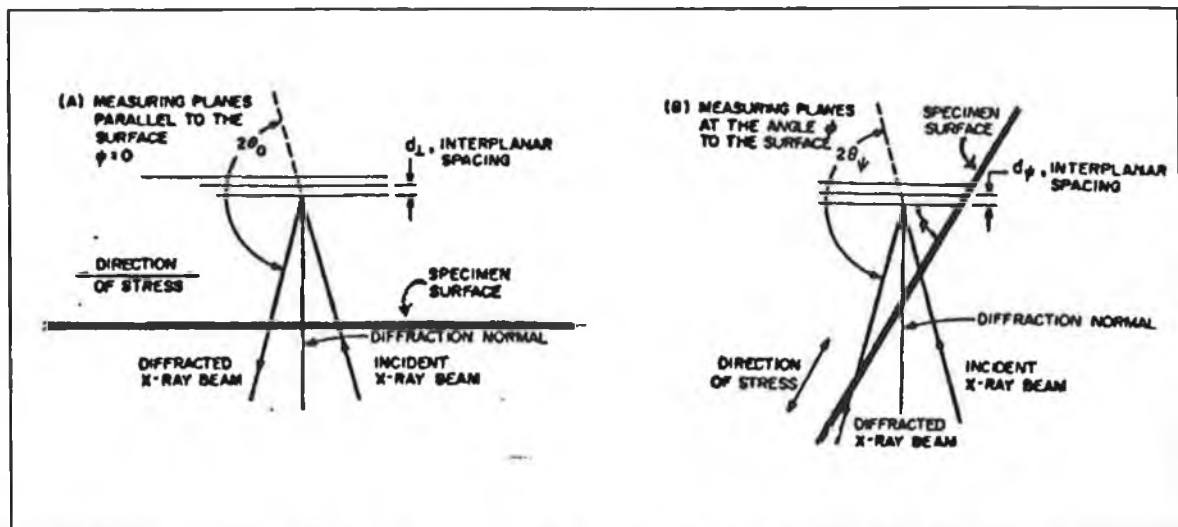


Figure 32 Schematic diagram of orientation of measured lattice planes with respect to specimen structure (a) specimen at $\psi = 0$ exposure (b) specimen rotated ψ degree [78]

Figure.33 shows a plane stress elastic model of a flat specimen. As X-ray diffraction stress measurement is confined to the surface of the sample, in the exposed surface layer, a condition of plane stress is assumed to exist. That is, a stress distribution described by principal stresses σ_1 , and σ_2 exists in the plane of the surface, and no stress is assumed perpendicular to the surface, $\sigma_3=0$. However, a strain component perpendicular to the surface ϵ_3 exists as a result of the Poisson's ratio contraction caused by the two principal stresses [78].

The strain $\epsilon_{\phi\psi}$, in the direction defined by the angles ϕ and ψ is:

$$\epsilon_{\phi\psi} = \frac{1+\nu}{E} (\sigma_1 \cos^2 \phi + \sigma_2 \sin^2 \phi) \sin^2 \psi - \frac{\nu}{E} (\sigma_1 + \sigma_2) \quad \text{Eqn 1}$$

where ν is Poisson's Ratio and E is the Young's Modulus.

If the angle ψ is taken to be 90 degrees, the strain vector lies in the plane of the surface, and the surface stress component, σ_ϕ is :

$$\sigma_\phi = (\sigma_1 \cos^2 \phi) + (\sigma_2 \sin^2 \phi) \quad \text{Eqn 2}$$

Substituting Eqn.2 into Eqn.1 yields the strain in the sample surface at an angle ϕ from the principle stress σ_1 :

$$\epsilon_{\phi\psi} = \frac{1+\nu}{E} \sin^2 \psi - \frac{\nu}{E} (\sigma_1 + \sigma_2) \quad \text{Eqn.3}$$

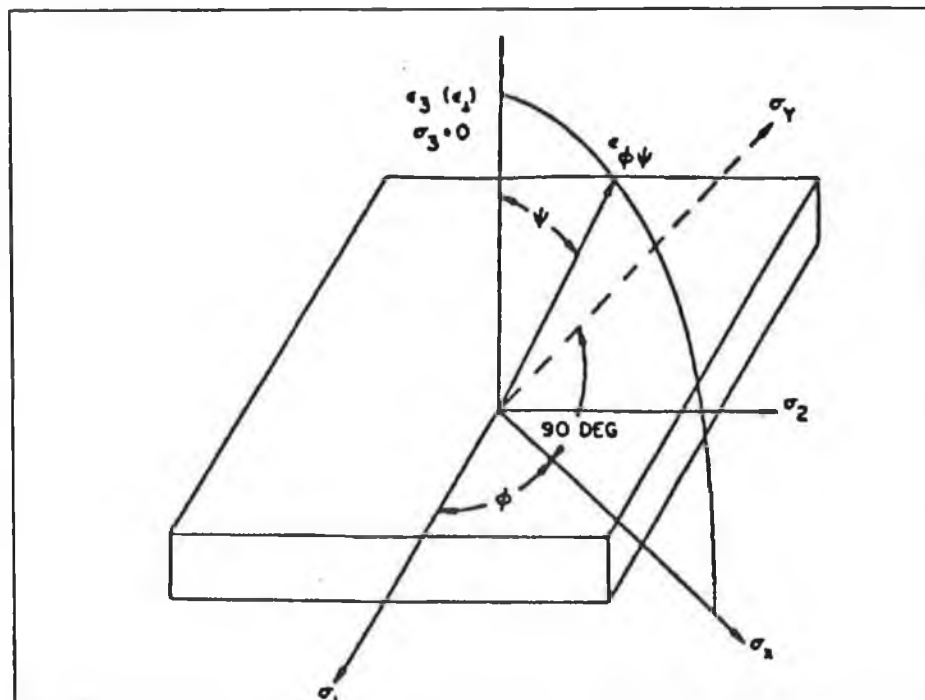


Figure 33 Plane stress elastic model of a flat specimen [78]

Multiple Exposure / Sin²ψ Technique

The multiple or Sin²ψ technique utilises the above Eqn.3 for strain and thus stress determination. It involves the measurement of several values of lattice strain in multiple ψ directions, where ψ is chosen so that the corresponding values of Sin²ψ are equally spaced. For example for ψ angles of 0, 20, 29 and 36.3 degrees, the corresponding Sin²ψ values are 0, 0.1170, 0.2340 and 0.3505 respectively and intervals between successive value of Sin²ψ are all approximately 0.117. This Sin²ψ interval should be selected to yield a suitable plot of Sin²ψ Vs ε_{φψ}, as in Figure 35 [78]. Figure 34 shows a typical XRD profile with 2θ₀, corresponding to initial incident angle 2θ and shifted peak of 2θ_ψ.

From the Figure.35 it is seen that:

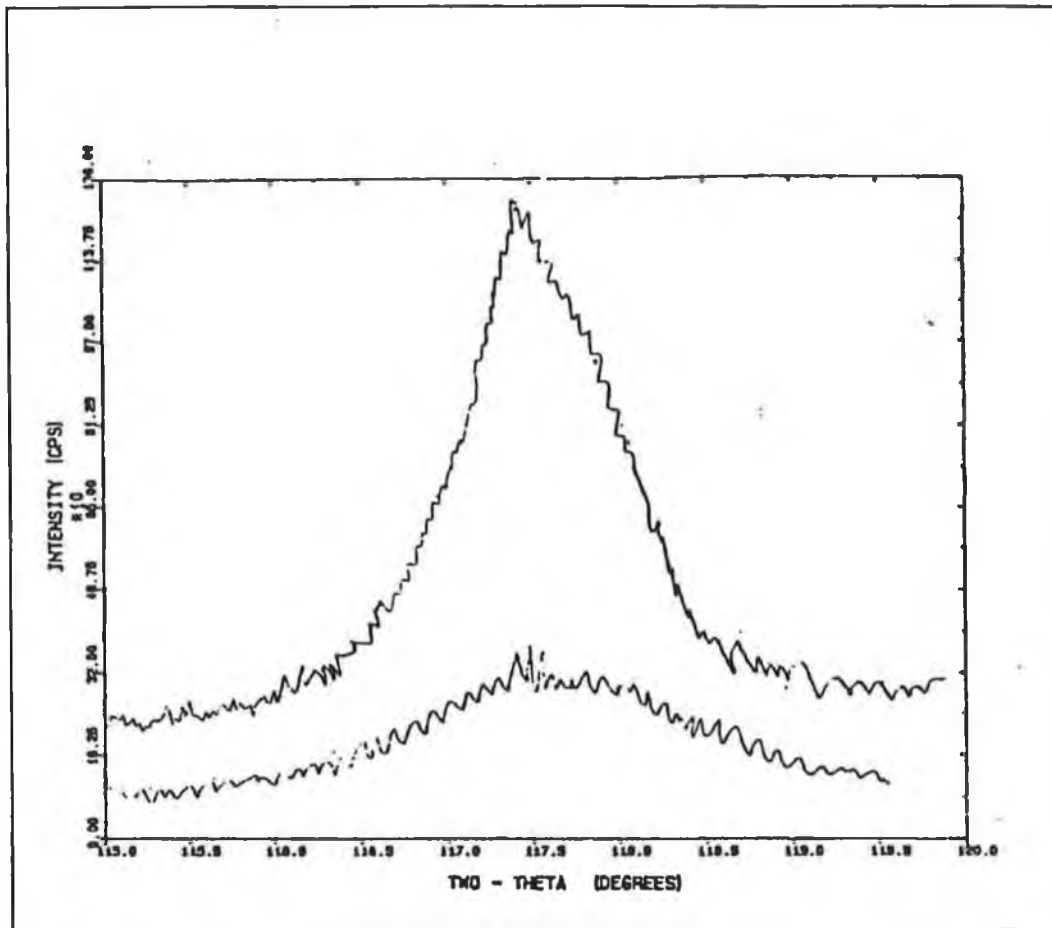
- 1) The intercept at ψ = 0 is equivalent to ε_{φ0} = ε_⊥ = -ν/E [σ₁+ σ₂]
- 2) The strain values vary linearly with Sin²ψ
- 3) The slope of the line is equivalent to ((1+ν)/E)σ_φ and thus σ_φ can be determined if the correct elastic constants are used.
- 4) A zero strain will be indicated for a ψ angle when

$$\text{Sin}^2 \psi = \left(\frac{\nu}{1 + \nu} \right) \left(\frac{\sigma_1 + \sigma_2}{\sigma_\phi} \right)$$

- 5) The strain values being measured must be reported in term of Δd/d_⊥

To summarise the method, by plotting the graph of Sin²ψ Vs ε_{φψ}, it is possible to determine the slope of line which best fits the measured points, and thus employ Eqn. 3 to determine stress as

$$\sigma_\phi = E/(1+\nu) * \text{slope.}$$



A slow scan of peak from 115 degree to 120 degree with $\psi = 0$ and $\psi = 45$ degree

Figure 34 A typical X-Ray diffraction measurement X-Ray profile

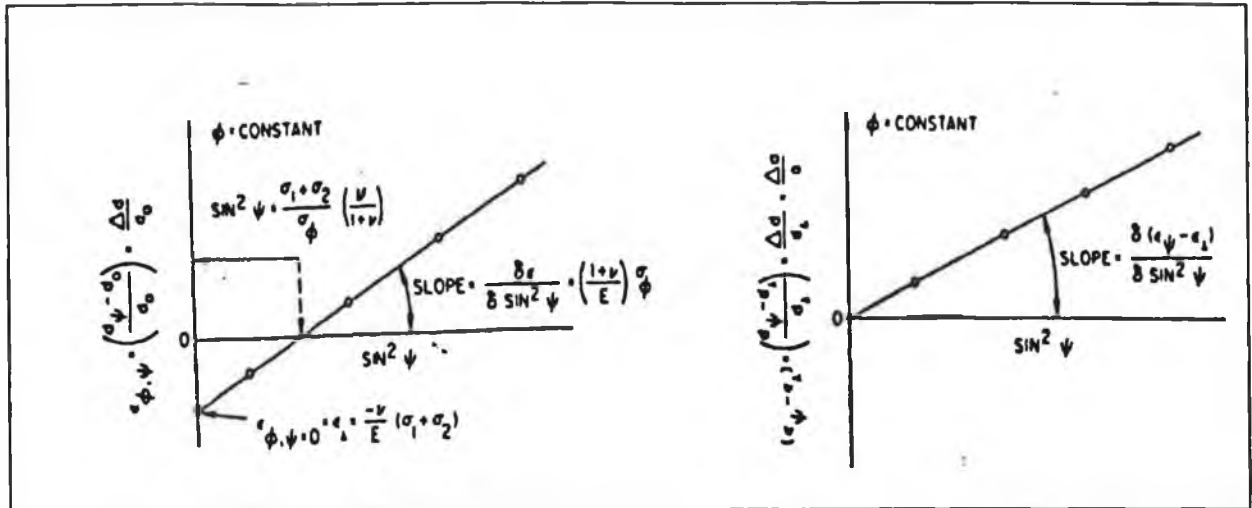


Figure 35 Multiple exposure / $\text{Sin}^2 \psi$ Technique for residual stress measurement

X-Ray Diffractometer

The diffractometer used in this experimental work is a Siemens Diffrac 500 XRD. As with most X-ray diffractometers it is provided with a scanning goniometer which allows scanning from negative 2θ angles as large as -110 degrees, to positive angles up to 165 degrees. The centre of the goniometer contains a specimen platform which is adjustable in three directions so that the desired point on the specimen surface can be made to coincide very precisely with the true axis of rotation of the diffractometer. The specimen holder is able to rotate about the diffractometer axis independently of the detector motion so that the strain ($\Delta 2\theta$ or $\Delta d/d$) can be measured at different ψ angles. The value of λ (wave length of x-ray beam) was determined by the available target material, $\text{CrK}\alpha$.

X-Ray Diffractometer Scanning Procedure

For the scanning procedure, a sample is placed in the sample holder and the machine adjusted to the parameters given in Table 7. A broad scan over the entire sample is initially carried out. A slow scan was then made over on a chosen peak which is of highest intensity, and which is within a high Bragg's angle (2θ) region. The specimen is then tilted

by first 15 and then 45 degrees, in order to get the shifted peak value caused by the residual stresses. Resident software locates the peak centre using a parabola fitting method. The change in peak location is then used to calculate the residual stress on the specimen.

Characteristics of X-ray	CrK α
Tube Voltage	30Kv
Tube Current	10 mA
Divergence Slit (deg.)	1
Receiving Slit (deg.)	0.2

Table 7: Siemens Diffrac 500 parameters

4.6.2 The Hole Drilling Method

This test method is often described as “semi-destructive” because the damage that it causes is very localised and in many cases does not significantly affect the usefulness of the specimen.

The principle is as follow:

A hole is drilled at the geometric centre of a strain gauge rosette, and this causes the residual stresses in the area surrounding the drilled hole to relax. The relieved strains are measured with a suitable strain-recording instrument. Within the close vicinity of the hole, the relief is almost complete when the depth of the drilled hole approaches 0.4 of the mean diameter of the strain gauge circle.

The calculation of the residual stresses is based on Kirsch’s theory [79]. Kirsch calculated the strain distribution around a circular hole, made upon a infinite plate, loaded with plane stress. The hypothesis are:

- 1) The material itself is an isotropic and linear elastic material
- 2) The tension perpendicular at the surface is negligible
- 3) The main tension direction are constant along the depth
- 4) The internal tensions are not in excess of one third of the yield strength
- 5) The hole is concentric with the rosette

The method which was based on Kirsch's theory to establish a relationship between the relieved strains and residual stresses is shown in Appendix C.

4.6.2.1 THE HOLE DRILLING PROCEDURE WITH RS-200 MILLING GUIDE

The RS-200 milling guide is a high precision instrument for analysing residual stress by the hole drilling method (Figure 36), but the destructive nature of this measuring method is its main disadvantage compared to others.

The base of the Milling Guide assembly is supported by three levelling screws with swivel pads which facilitate attachment to curved surfaces. Four adjusting screws are provided for alignment of the guiding hole over the rosette. A locking ring is an added safety to restrict movement of the guiding hole after final alignment. The microscope assembly consists of a highly polished housing, an eyepiece, a reticule, and an objective lens. All of these components are pre-aligned and set. A nylon collar, with a lock screw, is fitted over the microscope housing to fix its height above the installed rosette.

Two fixed-depth gauges are provided for setting the depth of the milled hole. If increment boring is required, the depth setting micrometer is used. To ensure a rigid fixture, the swivel pads are glued to the support area with adhesive cement. An alignment template, made of clear plastic, is used for initial alignment of the Milling Guide assembly over the installed rosette.

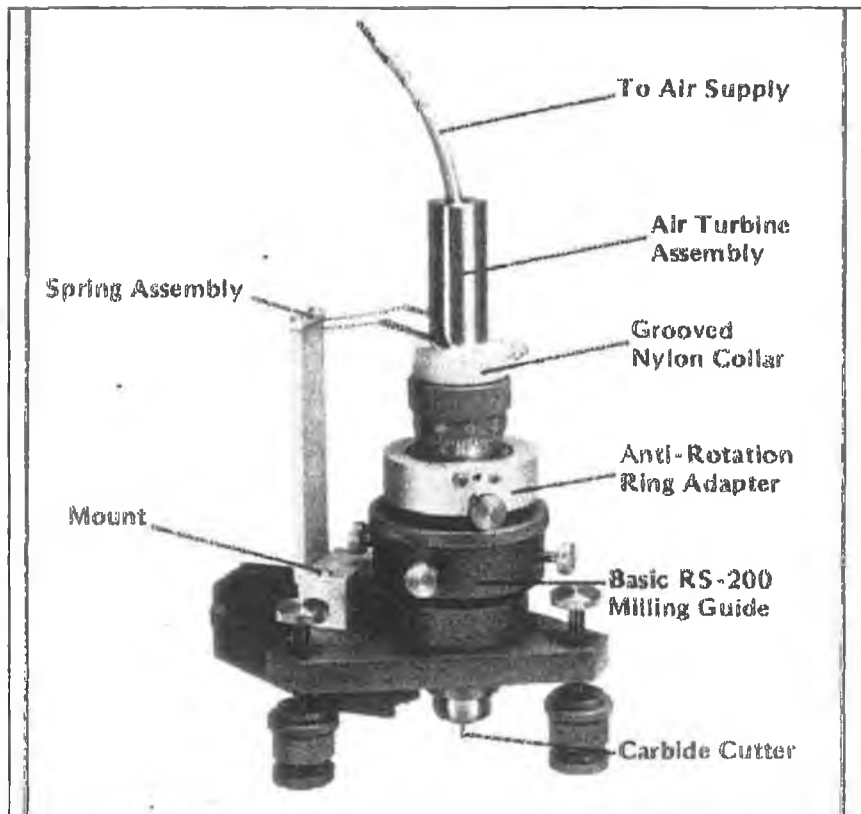


Figure 36 Hi-Speed Accuracy components assembled on the milling guide base

The Hi Speed Turbine Accessory is designed to produce an accurately drilled hole via high speed air turbine, the air turbine can rotate a precision carbide cutter at speed of up to 300,000 rpm.

4.6.2.2 Strain Gauges and Strain Indicator

The principle of operation of a strain gauge is that the resistance of an electrical conductor changes with a ratio of $\Delta R/R$ if a stress is applied, causing its length to change by a factor $\Delta L/L$. Here ΔR is a change in resistance from the unstressed value, and ΔL is the change in length from the original unstressed length.

The change in resistance is brought about mainly by the physical change in the conductor, and an alteration of the conductivity of the material due to changes in the materials structure.

Copper nickel alloy is commonly used in strain gauge construction because the resistance change of the foil is virtually proportional to the applied strain ie.

$$\frac{\Delta R}{R} = K\varepsilon$$

where K is a constant known as gauge factor and ε is the strain, and is equal to $\Delta L/L$.

$$K = \frac{\Delta R / R}{\Delta L / L}$$

The change in the resistance of the strain gauge can therefore be utilised to measure strain accurately when these gauges are connected to an appropriate measuring and indicating circuit.

In order to obtain the best possible result from a strain gauge it is important to thoroughly prepare the gauge and the surface of the specimen to which the gauge is to be attached.

The strain gauge measuring grid is manufactured from a copper nickel alloy and it is accurately produced by a photo-etching technique. Thermoplastic film is used to encapsulate the grid, which helps to protect the gauge from mechanical and environmental damage, and also acts as a medium to transmit the strain from the test object to the gauge material.

The strain gauge used in the current experiment is of the type TEA-XX-062RK-120 (Figure.37); TEA series gauges are a family of encapsulated constant strain gauges to which have been added printed circuit terminals. These types of gauges are mostly used for general strain tests and the following are their general characteristics:

Resistance in ohms at 24⁰ C = 120.0 ± 0.4%

Gauge factor at 24⁰ C = 2.06 ± 1%

Temperature range: -75⁰ C to 120⁰ C for continuous use in static measurements

Mean gauge circle diameter: 5.14 mm.

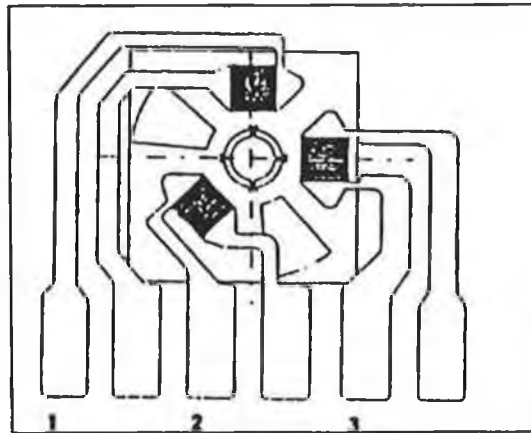


Figure 37 Strain gauge Model MMTEA-XX-062-120

The strain gauge was attached to the coating surface using the following procedure:

- Surface preparation: an area larger than the installation is smoothed with fine grade emery paper to remove any physical contamination. Then the area is degreased with solvent cleaner and neutralised with MN 5-5 M - Prep neutraliser.
- Bonding of the strain gauge: The strain gauge is glued on the desired spot with a thin layer of M-Bond 200 Adhesive, and a reasonable pressure is applied by pressing down on the gauge manually for about one minute to ensure proper bonding.

Finally, the connecting wires are soldered to each strain gauge element, and a gauge installation tester model 1300 is used to ensure that there are no faults in the connection of wires and the whole installation.

For the present work each strain gauge is connected to a Digital Strain Indicator P-3500 and a Vishay Switch and Balance Unit for strain reading. This is a battery powered precision instrument, which accepts full, half or quarter bridge inputs, and the required bridge completion components for 120 ohms and 350 ohms bridge are provided. This instrument accepts gauge factor of 0.500 to 0.900 with accuracy of $\pm 0.05\%$, and reading of $\pm 3\mu\epsilon$ for gauge factor greater than 1.00.

The Switch and Balance Unit SB-10 is used to set each channel of the strain gauge initially to zero, and to provide a direct reading from each channel of the strain gauge by switching the channel key. This unit is capable of reading ten different strain gauge channels at the same time, which means that it can be connected to several strain gauges simultaneously.

4.6.2.3 Drilling Samples

Before the attachment of the base of the milling guide on the table, an alignment template to facilitate final positioning is used. Cement is used to attach the base onto the surface of the table, and with the help of the microscope and four adjusting screws the Milling Guide is aligned with the centre of the strain gauge. A micrometer depth set attachment is used so that the gradual increments of the drilling depth can be adjusted. Finally, the Hi-Speed Accessory is placed on the Milling Guide with a carbide cutter of 1.6mm diameter. Drilling is powered by compressed air, an on/off mechanism being controlled by a pneumatic foot switch.

According to ASTM Standard E 837-92 [80], the diameter D_0 , of the drilled hole should be related to the diameter of the gauge circle, D , by $0.3 < D_0 / D < 0.5$. In this test the cutter used is 1.6mm in diameter, so the ratio value of the D_0 / D is 0.311. To protect the strain gauge grids, a margin of at least 0.3mm should be allowed between the hole boundary and the strain gauge grids. As the ratio D_0 / D increases, the sensitivity of the method increases approximately proportionally to $(D_0 / D)^2$. In general, larger holes are

recommended because of the increased sensitivity. In a material whose thickness is at least 1.2D, the final depth of the hole should be 0.4D. In the case of a material whose total thickness is less than 1.2D, a hole passing through the entire thickness should be made. As the mean gauge circle diameter of the strain gauge is 5.14mm, therefore the hole depth must be about 2.0574 mm, if it is used for material of thickness of minimum 1.2D.

The centre of the drilled hole should coincide with the centre of the strain gauge circle to within $\pm 0.004D$ or $\pm 0.025\text{mm}$ whichever is greater.

The calibration constants A_0 and B_0 can be obtained from a table in which numerical values were derived from finite element analysis and are found to be in excellent agreement with experiment results [81]. However the constants A_0 and B_0 can be established using a calibration experiment as reported on the ASTM- Designation E 837-92.

4.6.2.4 Data and Calculation

To calculate the residual stress, the equations suggested by ASTM E 837-92 were used, but with some modification for the calibration constants. The three strain gauge grids used were numbered in counterclockwise, such as shown in Figure.37, and for this reason the appropriate equations are:

$$\sigma_{\min}, \sigma_{\max} = \frac{\epsilon_3 + \epsilon_1}{4A} \pm \frac{\sqrt{[(\epsilon_3 - \epsilon_1)^2 + (\epsilon_3 + \epsilon_1 - 2\epsilon_2)^2]}}{4B} \quad \text{Eqn 4}$$

$$A = -\frac{1 + \nu}{2E} \cdot a \quad \text{Eqn 5}$$

$$B = -\frac{1}{2E} \cdot b \quad \text{Eqn 6}$$

$$\tan 2\gamma = \frac{\varepsilon_3 + \varepsilon_1 - 2\varepsilon_2}{\varepsilon_3 - \varepsilon_1}$$

Eqn 7

where \bar{a} and \bar{b} are constant for the blind holes according to the data supplied by the gauge manufacturer.

4.7 Three Point Bend Test

In three point bend test, a rectangular coupon is rested on two points (knife edges) and a third point applies a load at the midspan location. During the test, the upper half of the specimen is under compression, while the complementary half is under tension. Failure is by propagation of a crack parallel to the direction of loading, between coating and substrate.

The fracture mechanics approach to the evaluation of crack propagation is based on defining adhesion in terms of stress intensity factor, K , or strain release rate G . These apply to crack propagation through a homogeneous material. The approach has been adapted for coatings, establishing the resistance to debonding in terms of equivalent parameters K' and G' in three point bend test. In this case the crack propagates through the interface of two materials.

The use of the concept of the mechanics of fracture in the determination of the adherence of a coating was developed by Suga et al [82]. The adherence was correlated to the mechanical interlocking of the deposited material on the substrate surface. In the three point bending experiments, if the curve of load versus deformation was linear, the energy of fracture is given by :

$$G_C' = F_C^2 \cdot \frac{9(e/2)^2 \cdot \pi \cdot Y_G}{B^2 \cdot H^3 \cdot E}$$

where the following parameters are described in reference 82:

F_C = Fracture load

Y_G = Geometry Correction

B = Specimen Width

H = Specimen Height

e = Span distance

E = Modulus of elasticity

Y_G is the geometry correction for the specimen and can be calculated from [83-84];

$$Y_G = 1.93 - 3.07\left(\frac{a}{H}\right) + 13.66\left(\frac{a}{H}\right)^2 - 23.98\left(\frac{a}{H}\right)^3 + 25.22\left(\frac{a}{H}\right)^4$$

Where:

H = specimen height

a = crack length

The coating adherence strength or the fracture resistance can thus be calculated from:

$$K_c' = \sqrt{\frac{EG_c'}{1 - \nu^2}}$$

Chapter 5 Experimental Work And Results

In this chapter, HVOF thermal spraying experiments and results are presented and analysed. Experimental work is grouped under three categories:

1) Fabrication of free standing components, 2) Surface coatings and 3) Build-up repair.

Different tests were carried out for each category of experiment, and the experimental matrices, results and discussion for each are presented in separate sections in this chapter.

5.1 Fabrication of Free Standing Components

This section consists of details of the fabrication process of free standing components, the experimental tests and results.

5.1.1 Fabrication of Free Standing Solid Components

Free standing solid components made from various materials had been fabricated successfully by Helali [66]. As seen in Figure 38, all the fabricated components in his work were of hollow cylindrical shape. These components were manufactured by depositing the spraying material onto a rotating pre-shaped die/core. Masking was not necessary on these dies because the whole die surface was covered by the depositing material. This outer shell thus formed was then separated from the die as a free standing hollow component.

In the present work, all the WC solid components were formed by depositing the spraying material onto an open cavity fixed die. The depositing process was carried out on one side of the die only. The depositing material was allowed to build up, until it filled the whole die cavity. Masking of the die is difficult but essential in order to prevent excess material from adhering to the edges of the die.

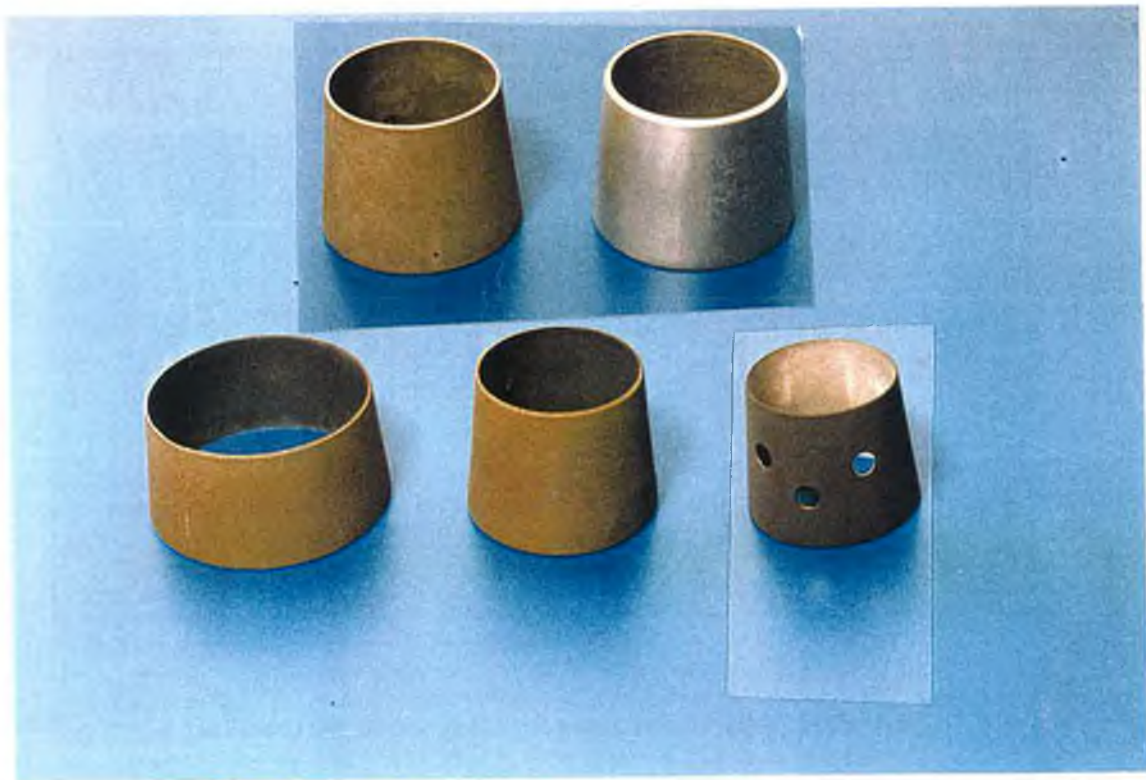


Figure 38 Hollow, free standing components produced by Helali [85].

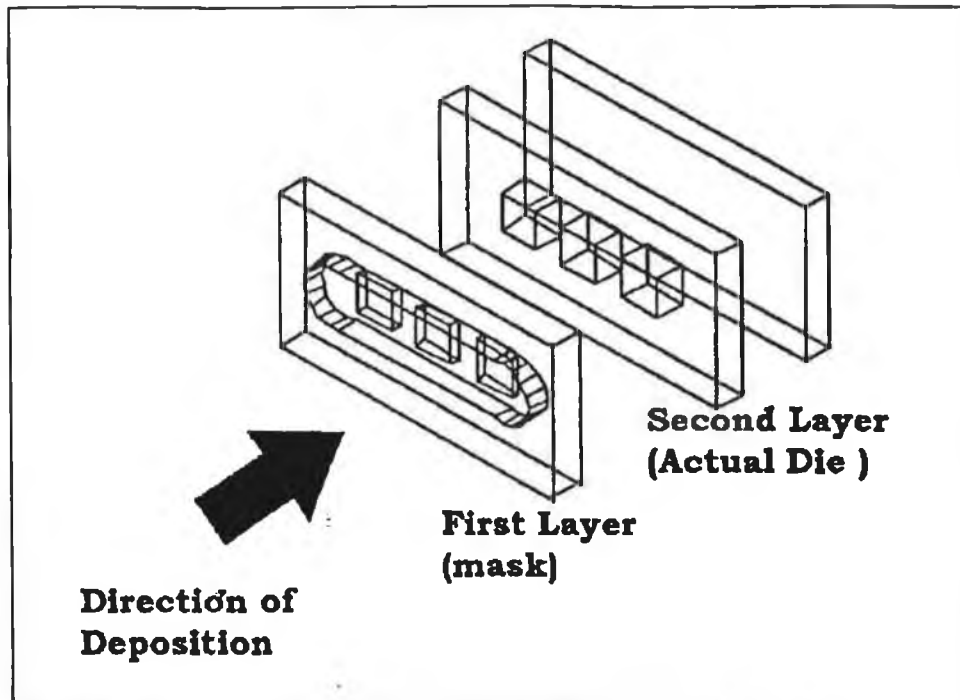


Figure 39 Diagram of die used to fabricate solid components

Small inserts, similar to cutting tool inserts were manufactured using a Diamond Jet HVOF Gun. The spraying parameters were set at values according to the values recommended by the gun and the WC-Co powder manufacturer. These data are presented in detail in Appendix A. Each gun setting is designed to have different geometry and they are chosen to suit individual types of powder. Due to each powder having particular powder size, density and composition, it requires different air and fuel level combinations, and particle dwell times inside the nozzle during spraying so that good coating quality can be produced.

The dies designed to produce the shapes required, consist of three layers as shown in Figure 39. The first layer separates the deposited material inside the die from that deposited at its edge (it acts like a mask), the second layer is the actual die, which is made in two halves to facilitate separation. The last layer acts as a base for supporting the deposited material. During the manufacturing process, aluminium powder (a releasing agent) was sprayed to a thickness of about 75 micron onto the die. Surface

preparation such as sand blasting is not needed for this process because any adhesion between the deposited material and the base will make the separation very difficult. The die was then preheated to 400°C with the flame from the gun, and was subsequently sprayed with final tool material. Tests carried out by Helali [66] suggest that the ideal pre-spray temperature range for hollow cylindrical free standing WC-Co material is between 400°C-500°C. A pre-spray temperature higher than 500°C will cause too much oxidation to the cylindrical core; high temperatures will also cause the aluminium releasing layer to melt and be dispersed away from the die by the high velocity flame jet. These factors will cause the spray formed components to fracture during the cooling stage. At temperature of lower than 400°C, the deposited component usually fracture during cooling due to the difference in the rates of thermal contraction of the sprayed material and the die during cooling [66]. The pre-spray temperature of the die is also strongly related to the microstructure and stress condition of the final product.

For this test, it was found that the pre-heating temperature of 400°C is sufficient to minimise the thermal expansion difference between the die and the sprayed material.

As the die was maintained stationary, it was very important to apply cool air to the die, or to increase the spraying distance, in order to reduce the heat which builds up under continuous spraying conditions. The temperature of the deposited die has to be kept at around 475 °C, as higher temperatures might change the phase composition of the deposited material [66]. The temperature of the whole process was carefully monitored using a pyrometer with an accuracy of 0.2%, and was kept at around 475 °C. Immediately after spraying, the whole die assembly was transferred to a preheated furnace for separation.

The post heating temperature and soaking time of the deposited die are very critical for the ease of separation of the fabricated component from its die [66]. For this test, the

die assembly was soaked in a furnace for 20 minutes at 600 °C. During this the aluminium releasing layer was melted away leaving a gap between the deposited material and the die. Figure 40 shows the relationship between the thickness of the releasing agent and the post heating temperature for separation of the deposit from its die. These results were obtained on the basis of about 100 tests on the carbide components by Helali [66]. The post heating treatment of the die assembly (soaked in a furnace for 20 minutes at 600 °C) which places it in zone S of Figure 40.

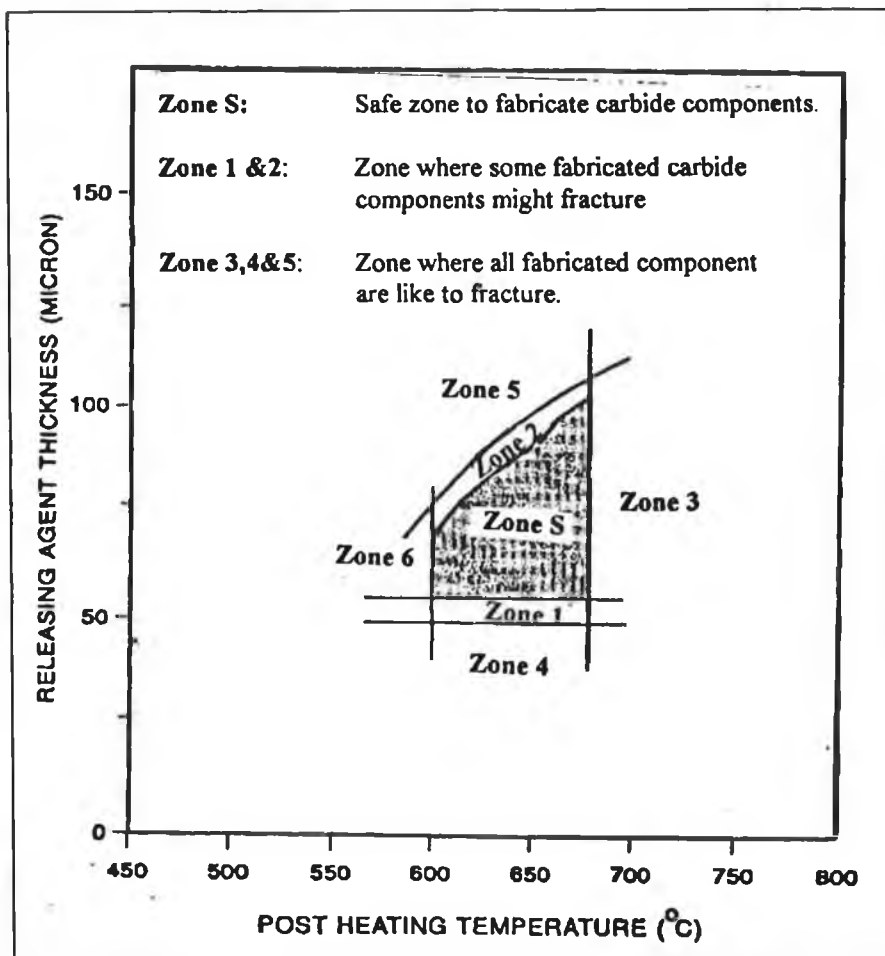


Figure 40 Post heating temperature for various releasing agent thicknesses with 20 minutes of soaking period.[66].

It was found that it is more difficult to build up within a small stationary die, than to spray onto a rotating die. This is due to the deposition process being concentrated on a small area, with overheating likely to occur. The heat generated on that small spot has

to be dissipated from the die by applying cool air to the die. Another method to reduce the heat is by increasing the spraying distance, where occasionally the spraying process also has to be interrupted to avoid overheating. However, it was also found that too much interruption to spraying will cause the final product to consist of layers rather of a homogeneous material throughout the formed piece [86].

Subsequent to heat treatment, the separated components were surface finished to the desired shapes and sizes using a diamond grinding wheel.

Annular free standing rings were made using similar technique, with the exception of masking which was not required for those dies used to form rings. Spraying material was deposited directly onto the top face of an annular hollow die. Figure 41 shows pictures of the WC-Co free standing components fabricated: cutting tool inserts, flat annular washers and solid discs.

Table 8 describes the types of powder material and the spraying parameters used for the fabrication of the free standing components. These data were recommended in the Metco Application Data Chart and Literature [87] for optimum spraying quality. The spraying distance and spray rate were varied in order to study their effect on the property of the components fabricated.

A detail chemical composition for the type of powder, gun settings and gases level used for these tests are presented in Appendix A.

Powder Material		Spraying parameters	
Powder Material	Metco WC-Co (WC-Co)	Spray distance	152 mm
Powder Composition	Tungsten Carbide 88.5%	Spray rate	38.0 g/min
	Cobalt 11.5%	Coverage*	3.4 m ² /hr/0.1mm
Die material	Stainless steel 316L	Powder required	0.83 Kg/m ² /0.1mm
		Deposit efficiency**	87%

Table 8 Spraying parameter for WC-Co powder.

*Coverage means the area of coating with coating thickness of 0.1mm which can be achieved per hour.

**Deposition efficiency is the ratio, usually expressed in percent, of the weight of spray deposit to the weight of the material sprayed.

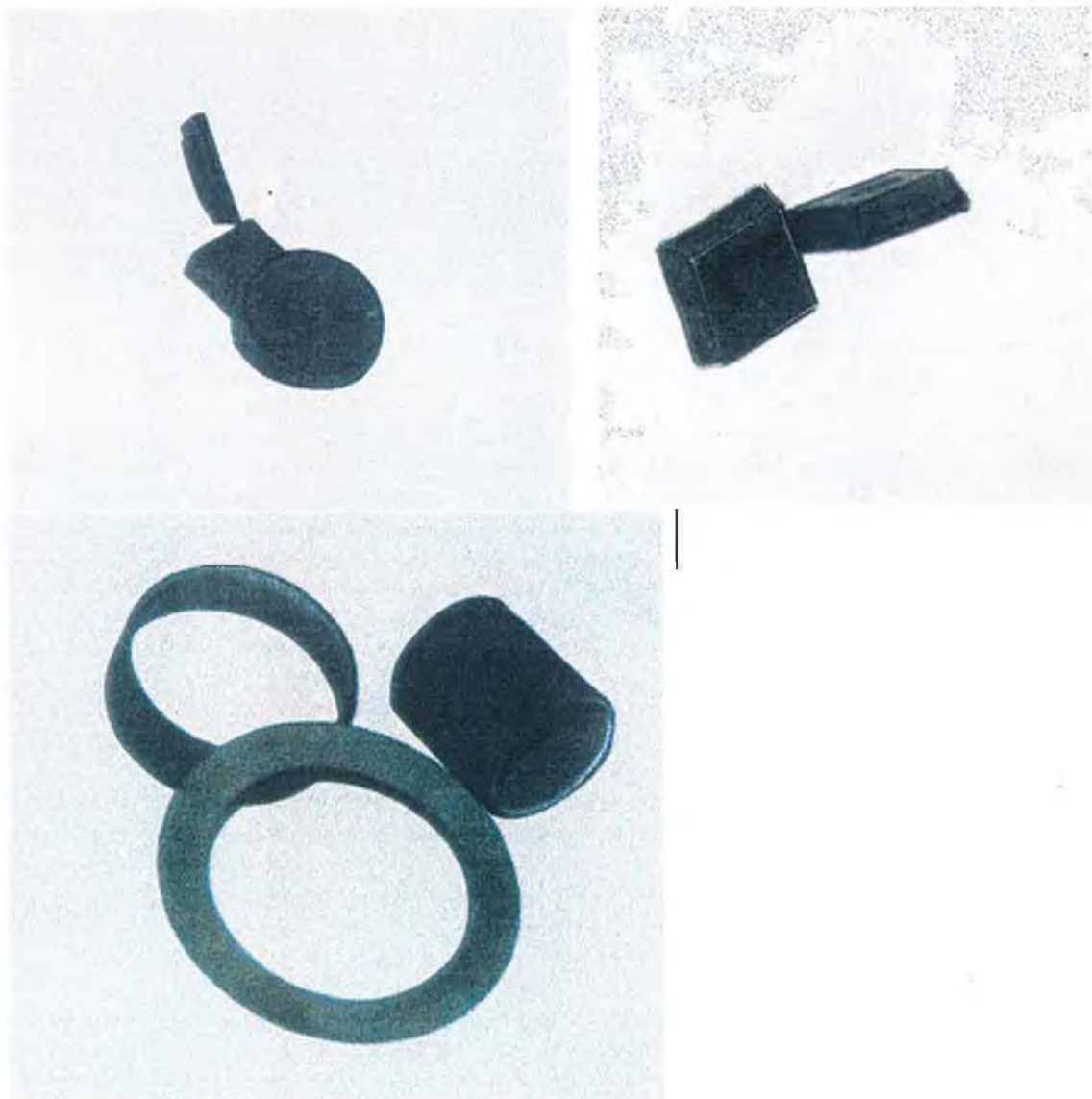


Figure 41 Pictures of Free Standing Components manufactured using the HVOF process

5.1.2 Characterisation of Free Standing Components

Free standing WC-Co annular rings were manufactured using the spraying parameters described in the previous section. These components were then sectioned, mounted and polished for XRD analysis. Tests were carried out to identify the effects of the post-spray temperature on the residual stress of the components manufactured. Tests were also carried out to study the effect of spraying distance and powder flow rate on the residual stress and hardness of the components produced. The hardness of samples were measured using a Vicker's Hardness Tester.

Experimental Test Matrix - Free Standing Components

The following table details the experimental matrix.

Sample type	Pre-Analysis Treatment	Spray Distance (mm)	Powder Flow Rate(g/s)	Pre/Post Spray Heat Treatment	Sample No.
WC/Co Annular Rings	Sectioned For Analysis	152.4	45.3	none	A1,A2,A3
		127	45.3	none	B1,B2,B3
		177.8	45.3	none	C1,C2,C3
		152.4	37.7	none	D1,D2,D3
		152.4	52.9	none	E1,E2,E3
		152.4	45.3	post separation: 600°C,4Hrs	F1,F2,F3
	-	152.4	45.3	none	G1,G2,G3

Table 9 Experimental matrix for free standing components.

Samples were prepared with three experimental parameters varied: (a) post-pray heat treatment (b) spraying distance and (c) powder flow rate.

Post-spray heat treatment temperature of 600°C and soaking time of 4 hours were chosen based on the study carried out by Helali [66]. The results of this test were then used to confirm his work. In his work, WC-Co free standing cylindrical components were heat treated within the range of 620°C to 690°C, with soaking period which ranges from 5 minutes to 200 minute. The residual stresses in the components were

significantly transformed from compressive state to tensile after the process of heat treatment.

The spraying distance was limited within the range of 127mm to 178mm. If the spraying distance is too short, the component will overheat, thus leading to fracture. Where as if the spraying distance is too long, this will cause the fabricated component to contain high porosity.

The powder flow rate was varied in between 37.7g/min to 52.9 g/min. Longer time is needed to fabricate the components to the desired thickness for lower powder spraying rate, thus generating higher temperature during the spraying process. Components fabricated with low powder flow rate will also contain high porosity level.

Characterisation

All the WC-Co solid components but one were sectioned, mounted and polished for XRD residual stress analysis. The remaining single complete ring was examined with XRD to identify any changes in residual stress due to the sectioning processes.

The residual stress results of the XRD method were then compared with results obtained by Helali [66] using the bend test method from samples produced using the same spraying parameters and deposition material.

Table 9 details the experimental matrix. All samples with the same identifying letter came from the same original annular ring. The XRD measured stress values given in the results (Table 10) are based on the average from these 'sister' samples. For each XRD sample, values of 2θ were measured at three orientations, ψ (0° , 15° and 45°). All readings were taken from the top face of the components, and the WC XRD peak was chosen to measure the stress because it was the most broad peak available within

the scanned 2θ range. Using Bragg's law the values of 2θ were taken to calculate three values of the lattice spacing d_0 , d_{15} and d_{45} respectively. The changes in spacing over the initial spacing were plotted against $\sin^2\psi$, and were fitted with a straight line using a least square regression technique. Deviation of measured points from the fitted line was no more than 4% for any of the samples. From the slope of the line, stress was calculated using the expression introduced earlier: $\sigma_{\psi} = \{E/(1+\nu)\} \times \text{slope}$. (section 4.6.1)

The value of the elastic constant, $E/(1+\nu)$, is important for calculating the residual stress, however it is not considered appropriate to use values derived for bulk material for material which has undergone the thermal spray process [62]. The values for Young's Modulus for the thermally sprayed materials have been given as about one third less than the bulk material value [62]. In the present case, in the absence of measured values, $E/(1+\nu)$ was estimated using XRD readings from a cylindrical WC/Co component of 'known' stress (i.e. measured using a bend test) [62]. While this method is not ideal, it is an improvement on using bulk data to calculate E for sprayed material.

For this cylindrical component, lattice spacing change was plotted against $\sin^2\psi$, and let $E/(1+\nu)$ to be equal to the known stress divided by the slope. For WC/Co components the value was found to be 104.2GPa. By comparison with at least one reference [62], this is approximately 2/3 that for bulk material (150.7GPa). As Poisson ratio does not generally vary outside the limits 0.26-0.3, it was expected that the factor $E/(1+\nu)_{\text{thermal spray}}$ would be approximately 2/3 that for bulk material.

Results:

Table of Results

	Sample type	Heat Treatment	XRD method (MPa)	Bending Test method (MPa)	Hardness (HV 3)
G	Complete WC ring. Same parameters as sample A	none	-210		
A	WC ring	none	-230.1	- 170	1132
B	WC ring, spray distance 127 mm	none	-310.2		1169
C	WC ring, spray distance 177.8 mm	none	-298.6		1107
D	WC ring, powder flow rate 37.7 g/min	none	-329.4		1139
E	WC ring, powder flow rate 52.9 g/min	none	-350.0		1146
F	WC parameters as sample A	post heat at 600°C for 4 hrs	274.7	190	

unless otherwise specified spray distance was 152.4 mm, and powder flow rate 45.3 g/min.

Table 10 Results Comparison of Residual Stresses Measurement by Various Methods

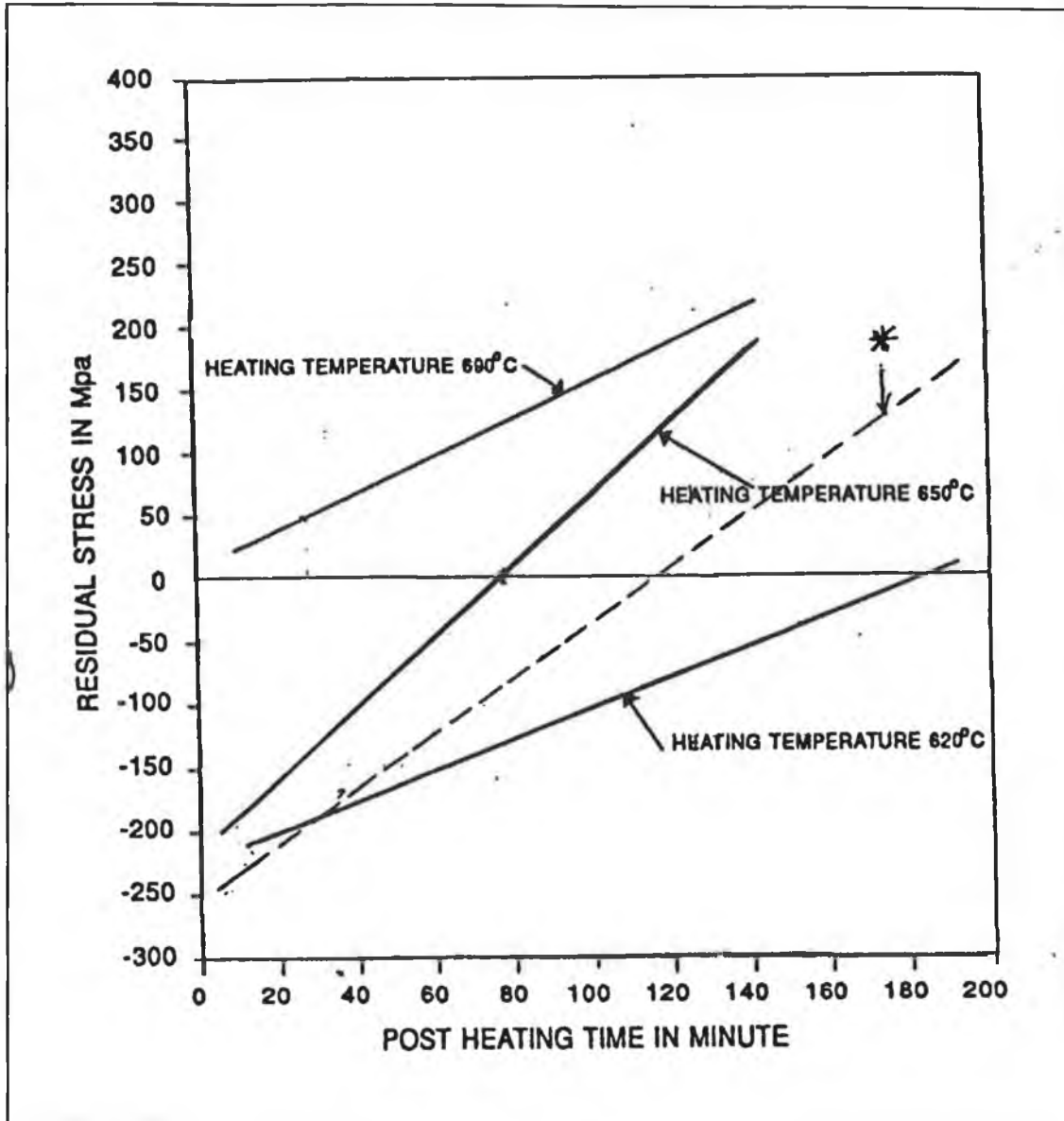
The XRD results given in Table 10 are average values, calculated on the basis of three samples from each component. Scatter between values was small (<5%) in the case of most WC/Co components but was 8% in the case of specimen E. The bend test results given for comparison are for split cylindrical components formed using similar spraying parameters to those indicated for the flat rings.

a) Post Heat Treatment

Post spraying heat treatment had the largest effect on the residual stress of the free standing WC/Co components, changing the significant compressive stress to a tensile stress of marginally larger magnitude, from 230MPa compressive stress to 274 MPa tensile. The reason for the transition lies in the microstructural changes occurring during heating. Within the component the energy supplied by the heating allows movement on a microstructural scale, relieving the stress. Grain growth may also have occurred. A satisfactory mechanistic based explanation of why, once the compressive stress is relieved, a tensile stress should developed has not been identified. Figure 42 shows the curve of the relation between residual stress and post heating time for various post-spray heating temperature for the test carried out by Helali [66].

According to the work done by Helali , he showed that by heat treating the sample at a certain temperature, the stress vs the time shows a linear straight line relation. With the exception that within the temperature range, the slopes calculated for different temperatures do not show a linear trend, ie. slopes of different times do not show an increasing or decreasing trend with temperature. At 620°C, 650°C and 690°C the slopes were calculated to be approximately 1.1, 2.8 and 1.6 respectively.

In this study, it was found that the residual stress results obtained after heat treating the components at 600°C for upto 4 hours also follow a straight line, shown in Figure 42, which conforms to what Helali found. The slope of this line is calculated to be approximately 2.1. It is confirmed that if an appropriate post sprayed heat treatment is applied to the free standing components, it is possible to manufacture components totally free of residual stress.



* This line represent the results from the present study.

Figure 42 Curve showing relationship between residual stress and post heating time.

b) Residual Stress Results of XRD compared to Bend Test

For the two comparative samples in which stress was evaluated using both these methods, the magnitude of the stress was larger using the XRD method. However, both methods were qualitatively consistent, indicating the nature of the stresses (i.e. compressive or tensile), confirming that the postheat treatment can not only reduce compressive stresses to zero, but may 'over-correct' into tensile stress. The difference in measurement may have arisen because of the fact that in the bend test, the sample geometry can limit the amount of deformation possible for stress relief. The two sample types were not of the same geometry.

c) Spraying Distance

Figure 43 shows the result of the effect of spraying distance on the compressive residual stress. From the graph, the experimental data plotted shows a parabolic trend. A parabolic equation was obtained by curve fitting. The results show the optimum spraying distance of 150 mm (close to the value recommended by the powder manufacturer). Changing this optimum distance to either a lower value (eg. 127mm) or a higher value (eg. 177mm), a higher compressive stress (up to 30% greater) was generated. For short spraying distance, the sprayed particles have a shot peening effect on the substrate [88]. This is essentially a mechanical working process in which the high velocity stream of hard cermet spray particles is directed to the substrate. Impact of the shot causes plastic deformation of the surface which induces compressive residual stress. A compressive stress is associated with a lower temperature as the coating is produced. With longer spray distances the particles have time to cool down significantly during the flight.

As evident from Figure 43, the compressive stress will be greater for either an increased or a decreased spraying distance

It has been found that the spraying distance is the dominant factor influencing the hardness of the depositing material [66, 89]. Figure 44 shows the effect of the spraying distance on the hardness. The graph shows a linear relationship with a negative slope of the value 1.2432, valid for spraying distance range of about 120mm to 180mm.. Similar work carried out by Helali also showed a negative slope but with a higher slope value of 2.13, over the spraying distance range from 120mm to 220mm. Both set of tests confirm that the component hardness reduces with longer spray distance. It is thought that the higher temperature reached with the shorter distance may cause the production of a hard amorphous carbon/cobalt phase in the material [88].

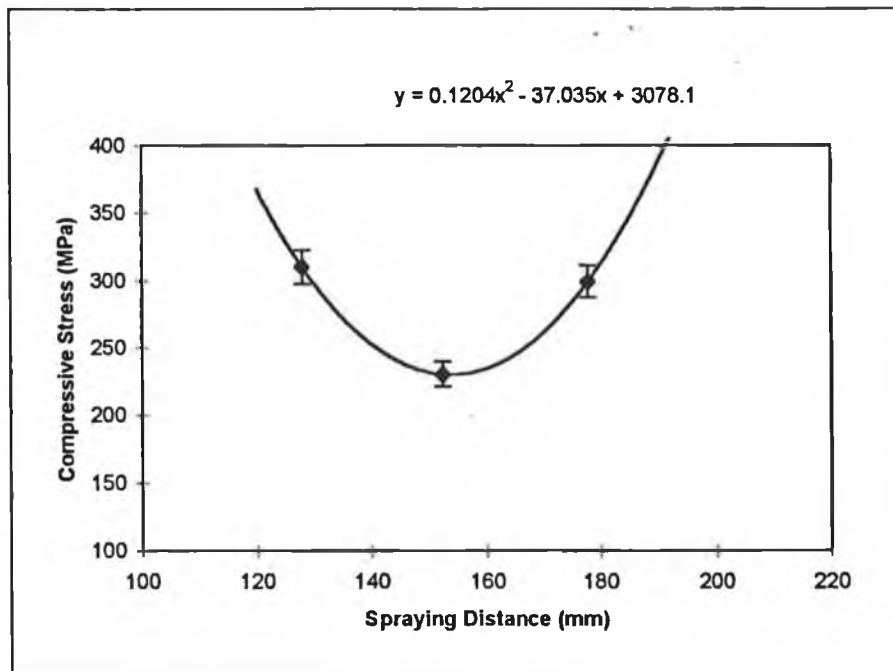


Figure 43 Compressive Stress (MPa) Vs Spraying Distance (mm).

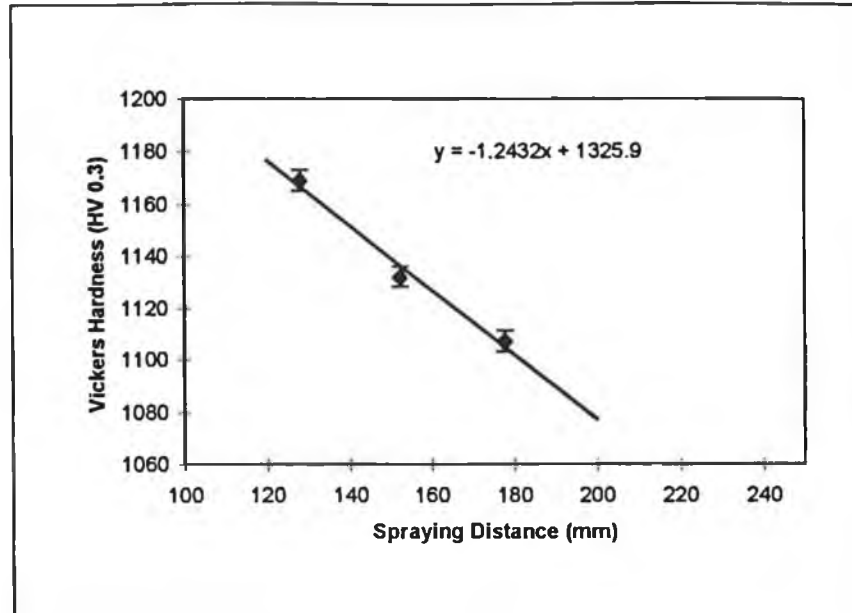


Figure 44 Hardness (HV 0.3) Vs Spraying Distance (mm)

d) Powder Flow Rate

The results show that varying the powder flow rate either above or below of about 45.0 g/min leads to an increase in average compressive residual stress. The graph shown in Figure 45 is fitted with a parabolic trend line, higher compressive stress was found for either side of the optimum spraying powder flow rate. For example, the compressive stress increases by 50 percent if the powder flow rate is either decreased or increased by about 8 g/min. The design of the gun settings allows for only a certain amount of powder to melt at the optimum rate. Too high a powder flow rate results in incomplete melting of some particles, thus some of the heat generated on the component surface was dissipated by these unmelted particles. At low powder flow rates, all the particles are fully melted due to the lower amount of powder present in the combustion zone. The particularly wide ‘splattering’ of the particles results in quick loss of heat and thus lower temperature. Compared with at least one reference by Brandt [88], where he studied the effect of different powder grain size on the residual stresses of HVOF process sprayed WC-Co coating, higher compressive residual stress was found for smaller particles size. The temperature of the particles with a smaller

diameter are heated on to a higher level as it passing through the nozzle of the gun. All the sprayed particles were fully melted before hitting the surface of the substrate. The disadvantage of spraying with a low powder flow rate is that the sprayed component usually has a high porosity level. A porosity level of almost 3.8% was found in the WC-Co component sprayed with powder flow rate of 25 g/min in the study carried out by Helali [66].

Figure 46 shows the effect of spraying powder flow rate on the hardness. There was a very small difference in hardness value over the flow rate values tested. The line fitted with the data shows a negative slope of the value 0.33. From the graph, it is noted that the hardness value is lower for higher spray powder flow rate. For higher powder flow rate, some of the powder grains are not melted, it has been reported that unmelted grains can also lower the hardness of coatings [71]. Although there is a slight decreased in the hardness value as the powder flow rate is increased, but if compared to the effect of spray distance, the change of hardness values changes in this test parameter can be considered relatively insignificant.

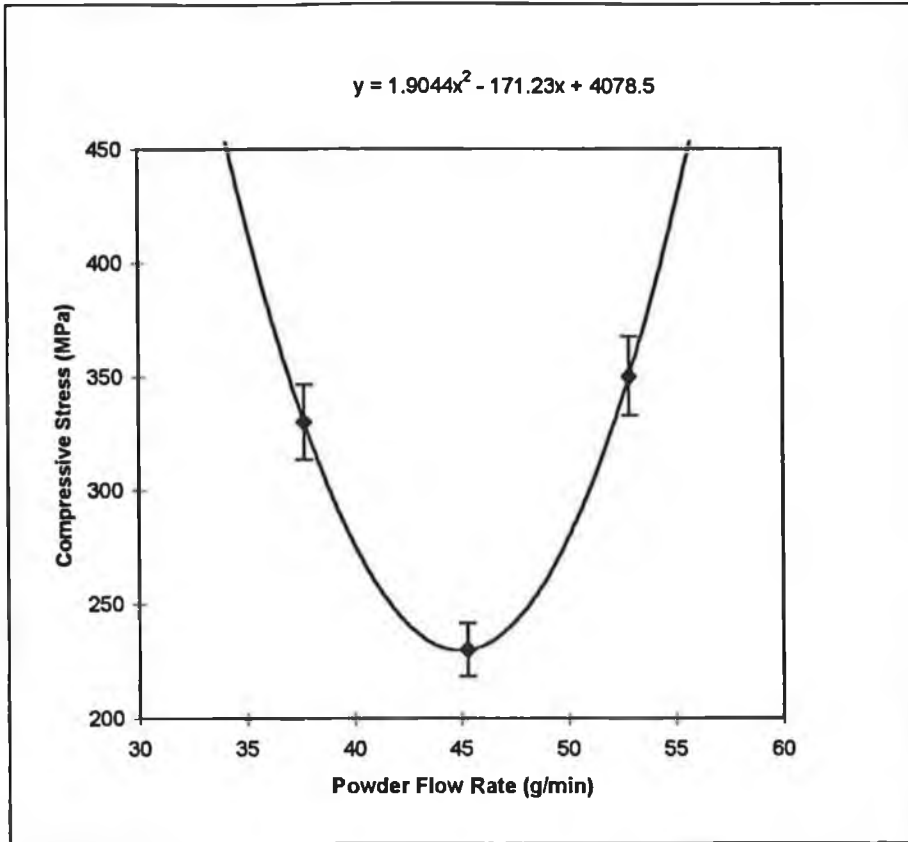


Figure 45 Compressive Stress (Mpa) Vs Powder Flow Rate (g/min)

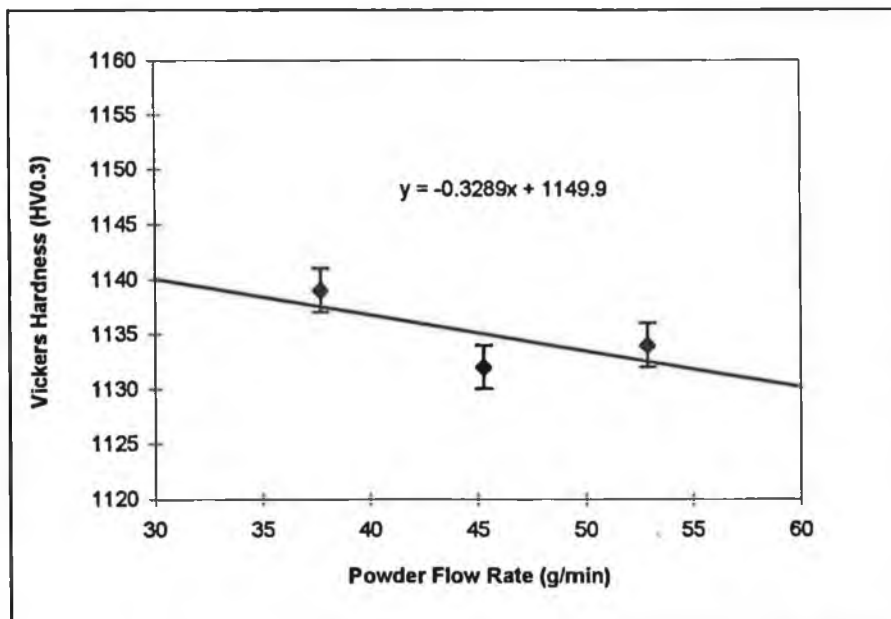


Figure 46 Hardness (HV 0.3) Vs Powder Flow Rate (g/min)

e) Sectioning of the Specimen

Comparing the residual stress results of a complete ring, with those from a sectioned sample spray formed under the same conditions indicates that the effect of cutting the original ring is small in comparison with other effects. The 10% larger compressive stress measured in the sectioned sample is close to being within the range of scatter noted for other samples.

Summary:

Of the parameters investigated, post heat treatment has been identified as having the most significant effect on the residual stress, changing a large compressive stress to a tensile one of similar magnitude. Spray distance and powder flow rate can affect the residual stresses by 30% to 50 % in the range of tests carried out. Optimum conditions of both powder flow rate and spray distance were confirmed. Comparing Figure 43 (compressive stress Vs spraying distance) and Figure 45 (compressive stress Vs powder flow rate), it can be seen that Figure 43 has a wider parabolic curve. By differentiating both equations, it was found that the equation for the powder flow rate has a steeper slope. This shows that the powder flow rate has a more restricted varying range value.

Figures 43 and 46 show the effect of the spraying distance and powder flow rate against the hardness of the deposited material respectively. It was found that the spraying distance has more influence on hardness than on powder flow rate.

5.2 HVOF Sprayed coatings

The experimental objective was to study the effect of spraying distance, sprayed coating thickness and pre-spray heat treatment on coating properties including hardness, bond strength and residual stress. Three types of coating materials were used, 1) Austenitic stainless steel powder 2) WC-Co powder and 3) Matching tool steel powder (chemical composition close to tool steel material). These powders were deposited on two different substrate materials, stainless steel 316 L and D2 tool steel. A detailed data table on the chemical composition of each type of powder is given in Appendix A.

In this section, all the coatings are grouped and discussed according to the type of test carried out. For example, the results, results discussion and summary for hardness tests are presented under one section for all types of substrate and spraying powder combinations.

Microhardness tests are often used to establish a first approximation of coating wear resistance, which is by far the most important property for present applications of thermal spray technology. This measurement also enables quick estimation of coating strength and the quality of spraying. Because a few specific defects, such as porosity and unmelted particles within coatings may result in lower hardness value. Carbides, together with oxides, are the hardest thermally sprayed coatings [71].

The Vickers Microhardness test was used to measure the hardness of WC-Co coating material and Rockwell hardness test was used for both stainless steel and matching tool steel coating materials. The Vickers microhardness was used for WC-Co because the Rockwell method was not suitable for measuring a very hard coating like WC-Co. The Vickers microhardness, HV3, of tungsten carbide is generally well above 1000. The Rockwell hardness test is used mainly for alloy coatings, and test samples don't have to be sectioned and metallographically polished for this method. There are two different scales for Rockwell hardness, HRB (Rockwell B) for less hard material and HRC

(Rockwell C) for harder material. The relationship between the Rockwell and Vickers scales is known to be non-linear, as shown in Figure 28 in Chapter 4.

Two methods have been used for residual stresses detection in this study. The theory upon which the XRD and hole drilling methods are based is detailed in Chapter 4. Both measurement methods were carried out on the same sample in order to compare the differences in stress value.

In addition, the effect of varying the depth of the drilled hole for the hole drilling measuring method was assessed.

Tensile bond strength tests were carried out according to ASTM standard 633-79. The test sample fixtures and failure modes have been described in detail in Chapter 4.

The following table details the experimental matrix. All samples with the same identifying letter had the same combination of substrate and spraying powder. Four types of tests were carried out to study the properties of coatings produced using different spraying parameters. On the hardness measurement of coating, the spraying distance was the only varying parameter because preliminary tests have established that spraying distance has the most significant effect on coating hardness. Both the coating thickness and pre-spray temperature were varied to study their effect on residual stresses and bond strength of coatings.

5.2.1 Experimental Matrix - Coatings

Sample Type	Spraying distance (mm)	Sample no.	Method of Characterisation	Coating Thickness (mm)	Pre-spray heat treatment
WC-Co on Stainless Steel	101.6 (4 in)	A1	Hardness	1 mm	200°C
	127 (5 in)	A2			
	152.4 (6 in)	A3			
	177.8 (7 in)	A4			
	203.2 (8 in)	A5			
	228.6 (9 in)	A6			
	254 (10 in)	A7			
Stainless steel powder on Stainless Steel	101.6 (4 in)	B1	Hardness	1 mm	200°C
	127 (5 in)	B2			
	152.4 (6 in)	B3			
	177.8 (7 in)	B4			
	203.2 (8 in)	B5			
	228.6 (9 in)	B6			
	254 (10 in)	B7			
Tool steel base powder on D2 Steel	203.2 (8 in)	D1	Hardness	1 mm	200°C
	228.6 (9 in)	D2			
	254 (10 in)	D3			
	279.4 (11 in)	D4			
	304.8 (12 in)	D5			
	330.2 (13 in)	D6			
	355.6 (14 in)	D7			
WC-Co on Stainless Steel	152.4 (6 in)	A8	Bond Strength	0.5	200°C
		A9		1.0	
		A10		1.5	
		A11		2.0	
Stainless steel powder on Stainless Steel	152.4 (6 in)	B9	Bond Strength	0.5	200°C
		B10		1.0	
		B11		1.5	
		B12		2.0	
		B13		2.5	
		B14		3.0	
		B15		3.5	
		B16		4.0	
B17	4.5				
Tool steel base powder on Stainless Steel	254 (10 in)	C1	Bond Strength	0.5	200°C
		C2		1.0	
		C3		1.5	
		C4		2.0	
		C5		2.5	
		C6		3.0	
		C7		3.5	
		C8		4.0	
WC-Co on D2 Steel	152.4 (6 in)	D1	Bond Strength	0.5	200°C
		D2		1.0	
		D3		1.5	
		D4		2.0	

Experimental Matrix - Coatings (continued.)

Sample Type	Spraying distance (mm)	Sample no	Method of Characterisation	Coating Thickness (mm)	Pre-spray heat treatment
Tool steel base powder on D2 Steel	254(10 in)	E1	Bond Strength	0.5	200°C
		E2		1.0	
		E3		1.5	
		E4		2.0	
		E5		2.5	
		E6		3.0	
		E7		3.5	
		E8		4.0	
		E9		4.5	
Stainless steel powder on Stainless Steel	152.4 (6 in)	B18	Hole Drilling	0.5	none
		B19			100°C
		B20			150°C
		B21			200°C
Stainless steel powder on Stainless Steel	152.4 (6 in)	B22	Hole Drilling	0.2	200°C
		B23		0.3	
		B24		0.6	
Stainless steel powder on Stainless Steel	152.4 (6 in)	B25 B26	XRD	0.5	none 200°C

5.2.2 Results:

a) Hardness test

Hardness tests were carried out for three different combinations of substrate and coating powder: 1) WC-Co on stainless steel substrate 2) stainless steel powder on stainless steel substrate 3) matching tool steel powder on D2 tool steel.

All the samples were prepared using the spraying parameters shown in Appendix A for individual type of powder, with only spraying distance being varied. Spraying distance was chosen as it has been proven to be the most influential spraying parameter on

hardness in coatings [66,89-91]. The pre-spray temperature of the substrate was 200°C.

The hardness values used to plot the following graphs are the average values from three samples coated under the same spraying conditions. Scatter between values was relatively small, with the greatest amount of scatter being 5.8 % from the average value. Figures 47 to 49 show the result plotted for each of the substrate and coating powder combinations.

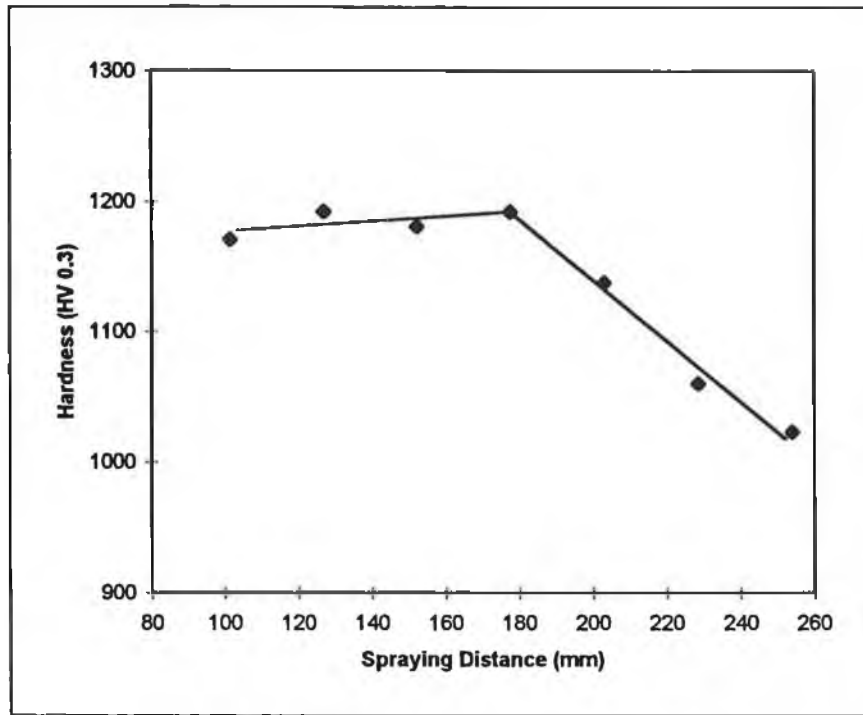


Figure 47 Hardness Vs Spraying Distance for WC-Co on stainless steel substrate.

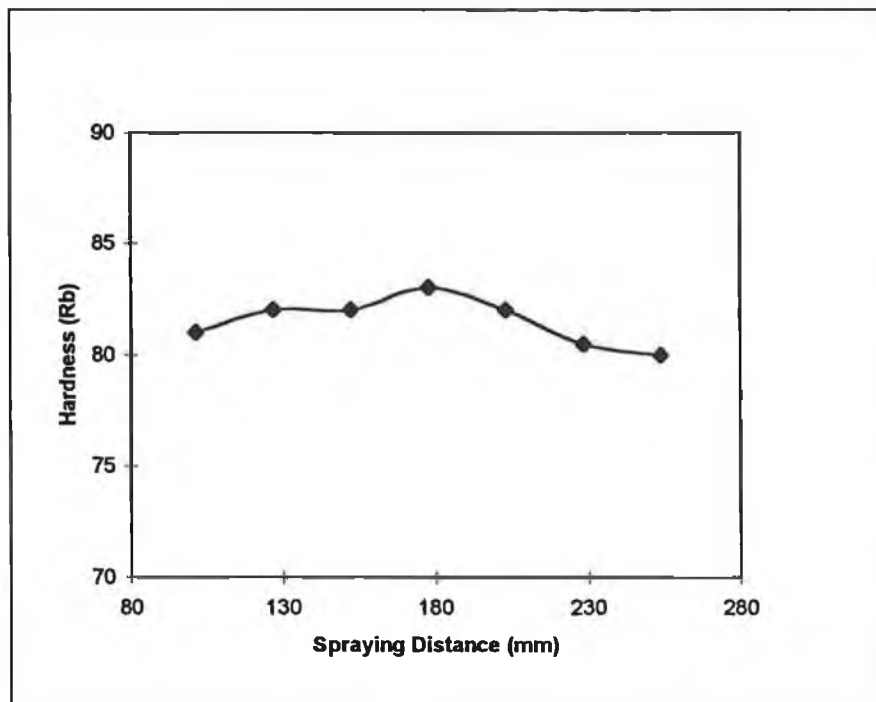


Figure 48 Hardness Vs Spraying distance for stainless steel powder on stainless steel substrate

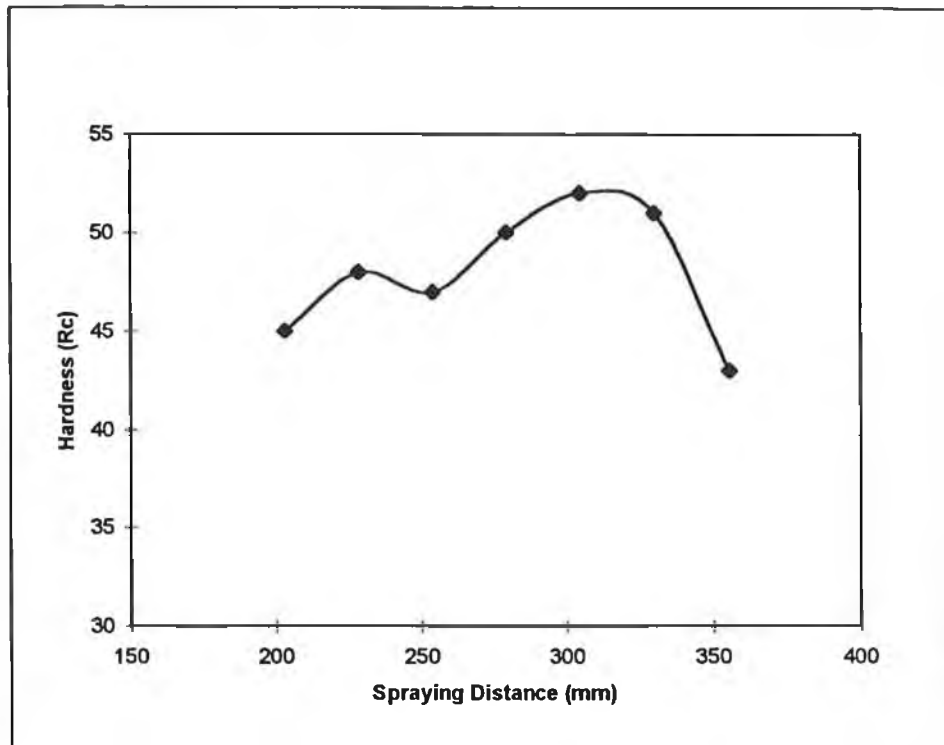


Figure 49 Hardness Vs Spraying distance for tool steel match powder on D2 tool steel substrate.

Discussion of results for hardness test

Figure 47 shows the effect of spraying distance on hardness of WC-Co coatings on a stainless steel substrate. By comparing Figure 47 to Figure 44 (the effect of spraying distance on hardness of Spray formed WC-Co solid components), it is clear that the coating samples have a different dependency of hardness on spray distance. It is difficult to explain why, but is probably related to the different residual stress conditions on both types of samples. The highest hardness values are found between the spraying distances of 120mm and 180mm, the hardness value significantly drops (about 14%) when the spraying distance is increased to 254 mm from 180mm. An explanation for this may be that higher temperature generated with the shorter spraying distance cause the production of a hard amorphous tungsten carbide phase in the material. Jarosinski et al [19] found that WC-Co coatings which contain higher levels of WC have higher hardness values. To clarify this, the X-ray diffraction method

was used to compare the amount of WC phase present in samples which were produced at 177.8mm and 254mm spraying distance respectively. Table 12 shows the relative intensity of XRD traces for these two samples. It was found that the coating sprayed at a shorter spray distance has 8.5% more WC phase presence within its coating than that sprayed from 254mm. Figure 50a and Figure 50b show the XRD pattern for these two coatings. There were more traces of WC phase, the main contributor to the hardness, in coatings sprayed at a distance of 177.8mm than 254mm.

	% of Phase present		
	WC	W ₂ C	W
Initial powder	69	24.8	6.2
Coating sprayed from distance 254mm	47	38	15
Coating sprayed from distance 177.8mm	55.5	32	12.5

Table 12 XRD relative intensity traces of composition in the powder and WC-Co coating.

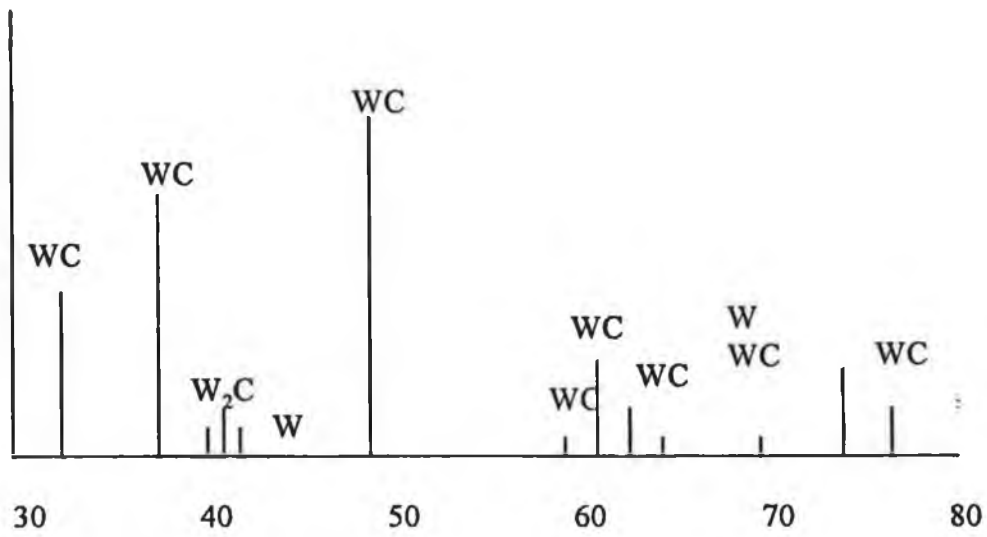


Figure 50(a) XRD pattern of WC-Co sprayed from a distance of 177.8mm

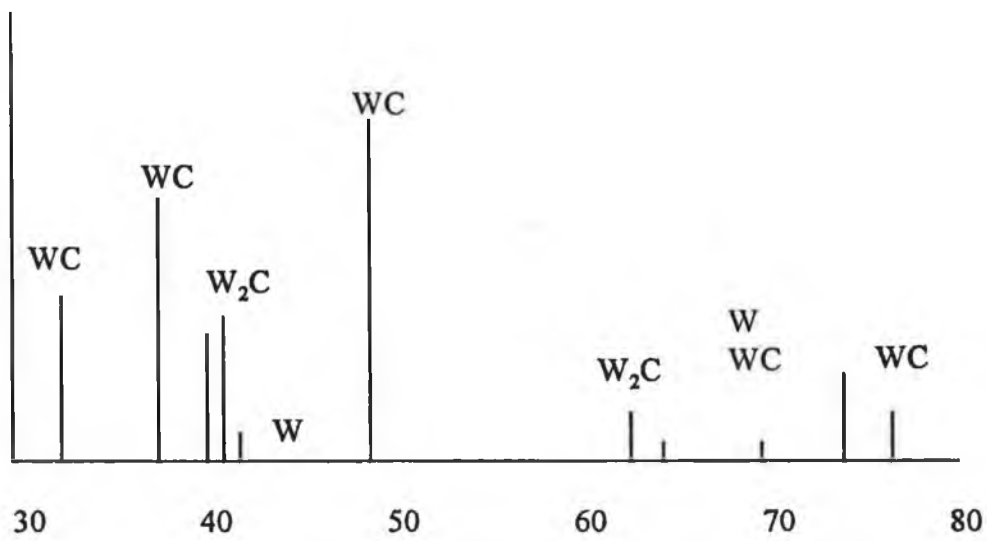


Figure 50(b) XRD pattern of WC-Co sprayed from a distance of 254mm

Figure 48 shows the hardness of stainless steel powder sprayed on a stainless steel substrate for various spraying distances. The highest hardness value was found between the spraying distances of 160mm and 190mm. For stainless steel coatings, there was only a slight drop in hardness for samples coated from spraying distance outside 160mm and 190mm range. The spraying distance of around 180mm was found to produce coatings with the highest hardness value. This spraying distance is also close to the recommended spraying distance (180mm -200mm) by the powder manufacturer for stainless steel powder. At this spraying distance, the sprayed particles may reach the optimum temperature and velocity as they reach the substrate surface. Proper melting and splatting of the sprayed particles will promote oxidation of the individual sprayed particle. This finding coincides very well with the results of a study made by Borisov et.al. [92]. These authors found that the degree of fusion of the particles and the presence of an oxide phase have effect on the microhardness of the coatings.

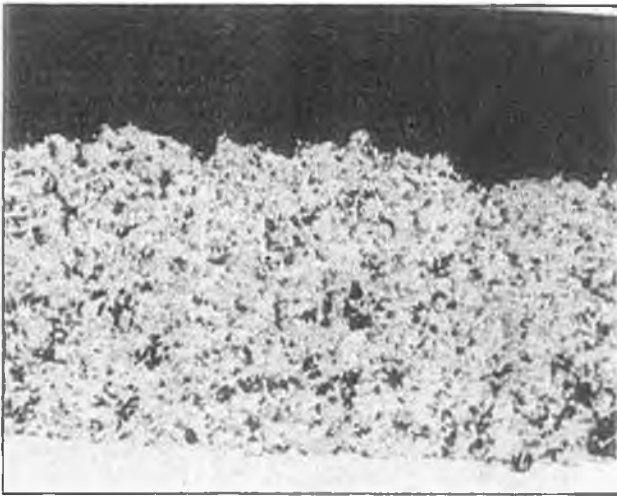
They also carried out tests on the effect of the degree of fusion and oxidation on the hardness of plasma sprayed 316L stainless steel coatings. Their results showed that the zones with the low degree of fusion and oxidation have microhardness of (HV0.1) 2400-2600, and an increase in the fusion degree and oxidation leads to the increase of microhardness to (HV0.1) 3200-5000. Borisov et.al. [92] also carried out X-ray phase analysis on the 316L stainless steel coatings containing oxide phases, and found that they were mostly the complex oxides of the type of Cr_2O_3 , Fe_2O_3 , NiO , Fe_2NiO_3 , etc., ie, there was no clearly defined selectivity of oxidation of individual elements. This may prove a hypothesis of the oxidation of a spraying material primarily at the moment of collision of a particle at the surface of a substrate due to an intensive interaction of thin films and fine droplets formed from its splatting with oxygen [93].

Too short a spraying distance for stainless steel powder will cause the sprayed particles to splat excessively, leaving voids in each lamella. A longer spraying distance will also

reduce the momentum required by the sprayed particles to splat fully. The interlamellar contact strength and porosity, which influence hardness, are improved if the sprayed particles splat at an optimum rate when impacting at the right velocity.

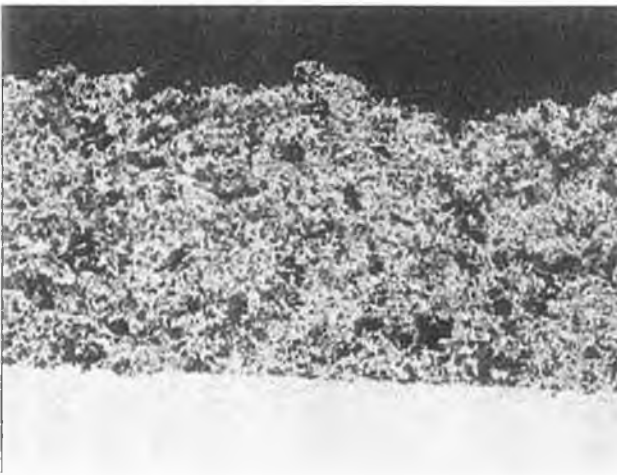
Figure 49 shows the hardness of D2 steel substrate coated with matching D2 powder for various spraying distances. The highest hardness value was found for spraying distances of between 275mm to 330mm. There was a drop of 10% in hardness from the highest hardness value, for coatings sprayed with spraying distance of 203mm and 13% reduction in hardness when the spraying distance was increased to 335mm. The reduction in hardness values are mainly due to the influence of the inferior interlamellar contact strength and high porosity levels created by incorrect spraying distances.

As the interlamellar structure of coating, coating density, amount of voids and oxide content also influence the coating hardness, some of the coated samples were selected and sectioned for examination under optical microscope. Observation under optical microscope reveal that the coatings produced with excessively short or long spray distances contain either more voids or oxide inclusions than coatings sprayed with the optimum spraying distance. Figure 51a and 51b show the optical micrographs of cross sectioned sample of tool steel powder sprayed on a D2 steel substrate, from distances of 279mm and 356mm respectively. The diffusion is unlikely to happen in these coatings due to the relatively low spray temperature and the presence of an oxide layer between coating and substrate. The coating sprayed from a 356mm distance shows more evidence of voids within the coating than that sprayed from 279mm distance. Similar results were observed for the samples of WC-Co coating on stainless steel substrate (Figure 53a and Figure 53b). Figure 52a and 52b show micrographs of cross sectioned stainless steel powder on stainless steel substrate sprayed at distances of 177.8mm and 254mm respectively. The coating sprayed from a longer spraying distance (Figure 52b) has more voids and oxide inclusions due to the long spraying distance and thus leading to high porosity level.



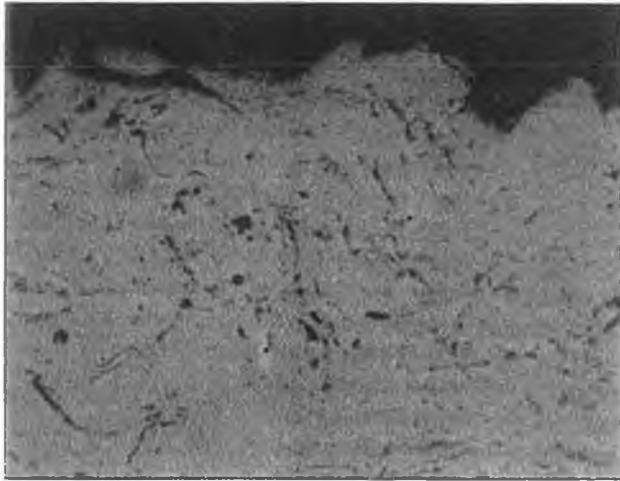
Mag. x 200

Figure 51a. D2 Steel coated with Tool steel base powder from 279.4mm spraying distance (optimum).



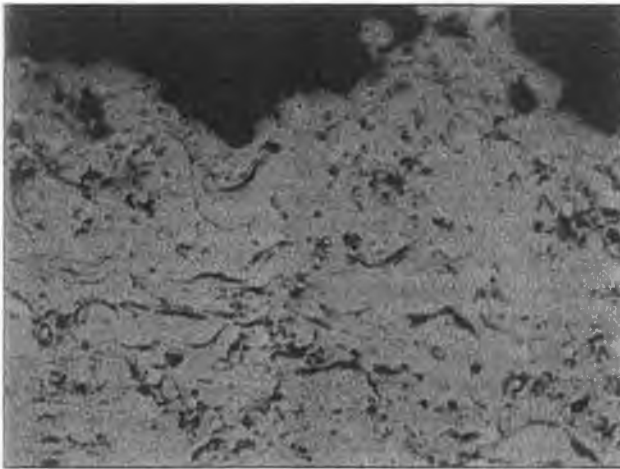
Mag. x 200

Figure 51b. D2 Steel coated with Tool steel base powder from 355.6mm spraying distance (too long).



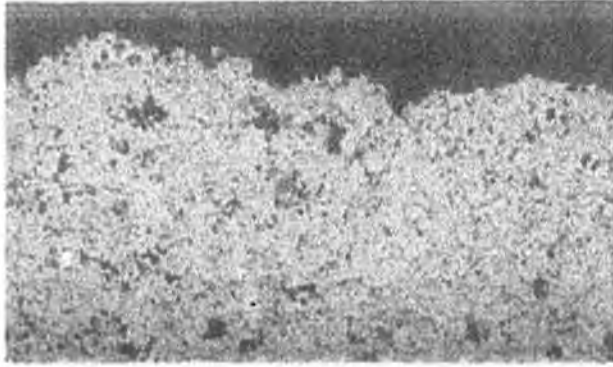
Mag. x 200

Figure 52a. Stainless Steel Coated with Stainless steel powder from 177.8 spraying distance (optimum).



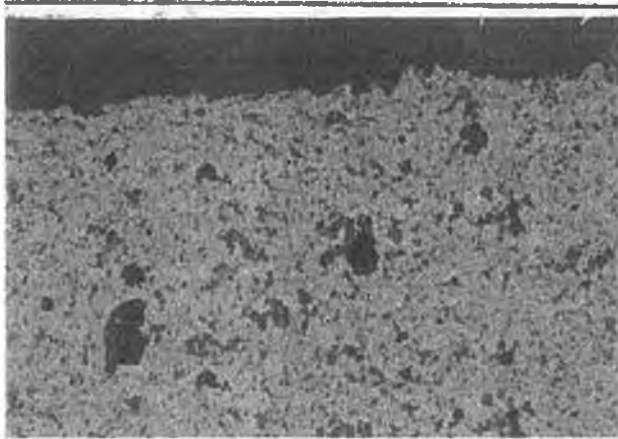
Mag x 200

Figure 52b Stainless Steel Coated with Stainless steel powder from 254mm spraying distance (too long).



Mag x 150

Figure 53a .Stainless Steel Substrate coated with WC-Co from spraying distance 177.8mm (optimum)



Mag x 150

Figure 53b Stainless Steel Substrate coated with WC-Co from spraying distance 254mm (too long).

(b) Tensile Bond Strength

Tensile bond strength tests were carried out for five different combinations of substrate and coating powder. 1) WC-Co on stainless steel substrate 2) Stainless steel powder on stainless steel substrate 3) Tool steel match powder (composition close to D2 tool steel) on stainless steel substrate 4) WC-Co on D2 tool steel substrate 5) Tool steel match powder on D2 tool steel substrate.

For all the materials, the spraying process was carried out with spraying parameters as shown in Appendix A for the relevant types of powder, unless otherwise stated.

The bond strength values used to plot graphs are average values, calculated on the basis of four samples coated under the same spraying conditions. The results include a mixture of coating failure modes. The few cases of glue failure due to misalignment of sample fixtures during experiments are not included in the calculation of the results.

The adhesion strength or cohesion strength of thermal spray coatings can be influenced by many factors. Some of these factors are intrinsic - ie., related to the spray variables, such as powder characteristics, spray parameters and substrate preparation. Others are extrinsic, including post treatment and service conditions, such as hot corrosion, thermal shock, and so on. However, adhesion test are usually performed at room temperature and do not consider in -service conditions that may decrease adhesion strength. It is important for materials designers to keep in mind that strength is strongly related to service conditions. Also, the estimation of confidence intervals for such coatings enables the reliability of the so-determined property to be ascertained. The measurement of the adhesion of thermal spray materials is, at least on the conceptual level, a routine operation. The tensile adhesion method detailed in ASTM C633 is simple and is often used in industry to rank different coatings. However, the shortcoming of this test is that it does not promote any understanding of coating

performance, ie., how coatings can be designed to be more functional. And the coating should be considered as one part of the overall system.

Sample	Coating Thickness (mm)								
	0.5	1	1.5	2	2.5	3	3.5	4	4.5
A1	75	62	42	35					
A2	79**	59	34	***					
A3	79	62**	***	***					
A4	82	61	40	30					
Scatter of A	4.8%	3.3%	12.1%	7.7%					
B1	48	57	57**	52	50	48	25*	24*	22*
B2	57	60	56	58	54	49	49	21*	20*
B3	58**	59	54	57	52	52	30*	24*	18*
B4	59	58	60	60	54	52	42	22*	19*
Scatter of B	13.5%	2.6%	5.7%	8.4%	4.8%	4.5%	34.2%	5.5%	11.4%
C1	52	54	50	50	52	50	30	31*	***
C2	52	50	49	***	52	48	24*	***	***
C3	47	50	52	25	49	47	24*	***	
C4	46	48	48	30	50**	47**	***	28*	
Scatter of C	6.6%	6.9%	4.5%	42.9%	3.4%	4.2%	53.8%	5.1%	
D1	60	60	***	***					
D2	67	***	***						
D3	62	***	***						
D4	61	52							
Scatter of D	7.2%	7.1%							
E1	52	49	50	49	31**	48	48	31**	34**
E2	50	51	46	46	45	35*	39	40	33**
E3	49	51	48	51	51	31**	30*	***	36**
E4	51**	48	44**	49	49	47	48	40	37**
Scatter of E	3.0%	3.5%	6.4%	15.9%	29.5%	23.0%	27.3%	16.2%	5.7%

Note:

A= WC-Co on stainless steel substrate

B= Stainless steel powder on stainless steel substrate

C= Tool steel match powder (composition close to D2 tool steel) on stainless steel substrate

D= WC-Co on D2 tool steel substrate

E= Tool steel powder on D2 tool steel substrate.

* failure occurred within the coating (cohesive failure)

** glue failure

*** coating failure prior to bonding test

Table 13 Bond Strength (MPa) And Failure Mode Of Samples

Figure 54 shows the bond strength of various coatings on stainless steel substrate. Figure 55 details bond strength test results for WC-Co and Tool steel base powder on D2 tool steel substrates. It can be seen from Figure 54 that the coating thickness of less than 2mm has little effect on the bond strength of both stainless steel and D2 coatings. Bond strength of these two types of coatings only starts to reduce at thicknesses greater than 2mm. For stainless steel the reduction is relatively linear, but quite a lot of scatter in bond strength was found using D2 match material to higher thicknesses. It was not possible to produce a WC-Co coating of thickness greater than 2mm.

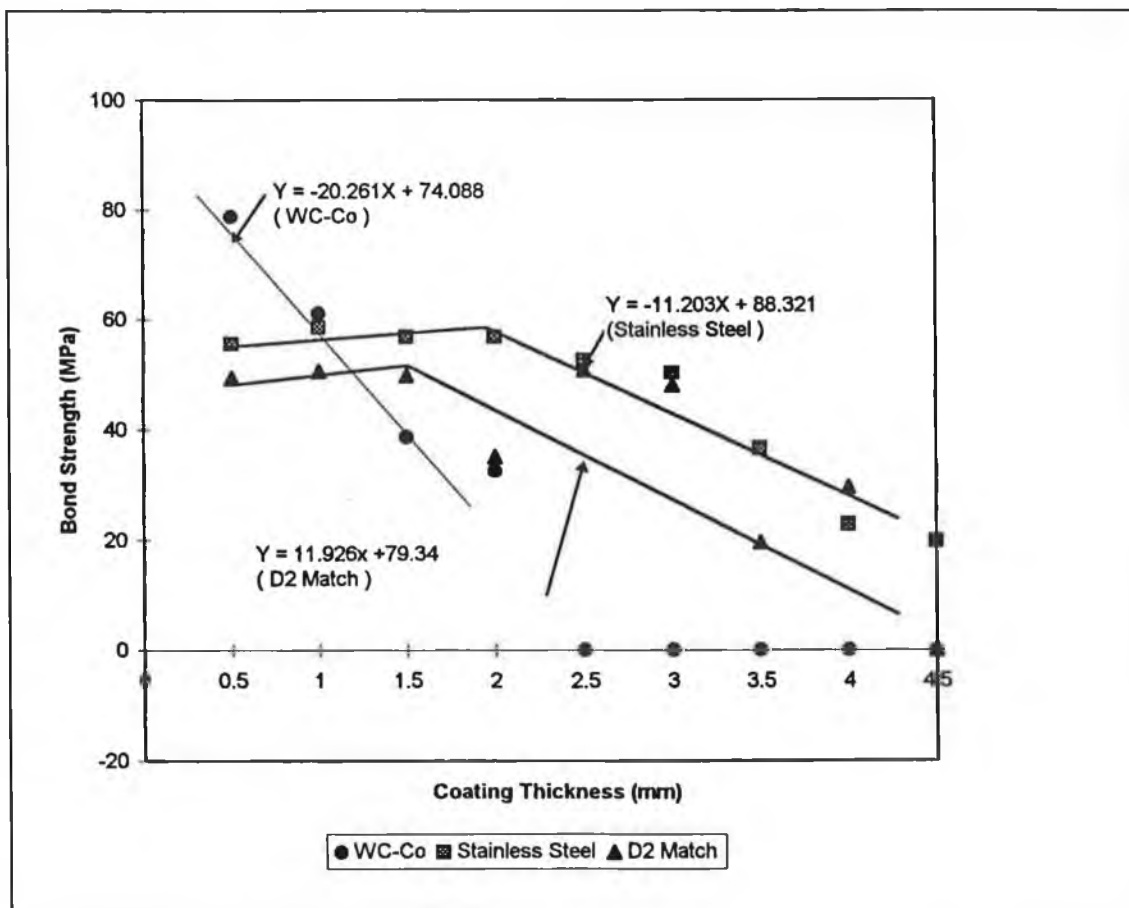


Figure 54 Bonding Strength Vs Coating thickness for stainless steel substrate

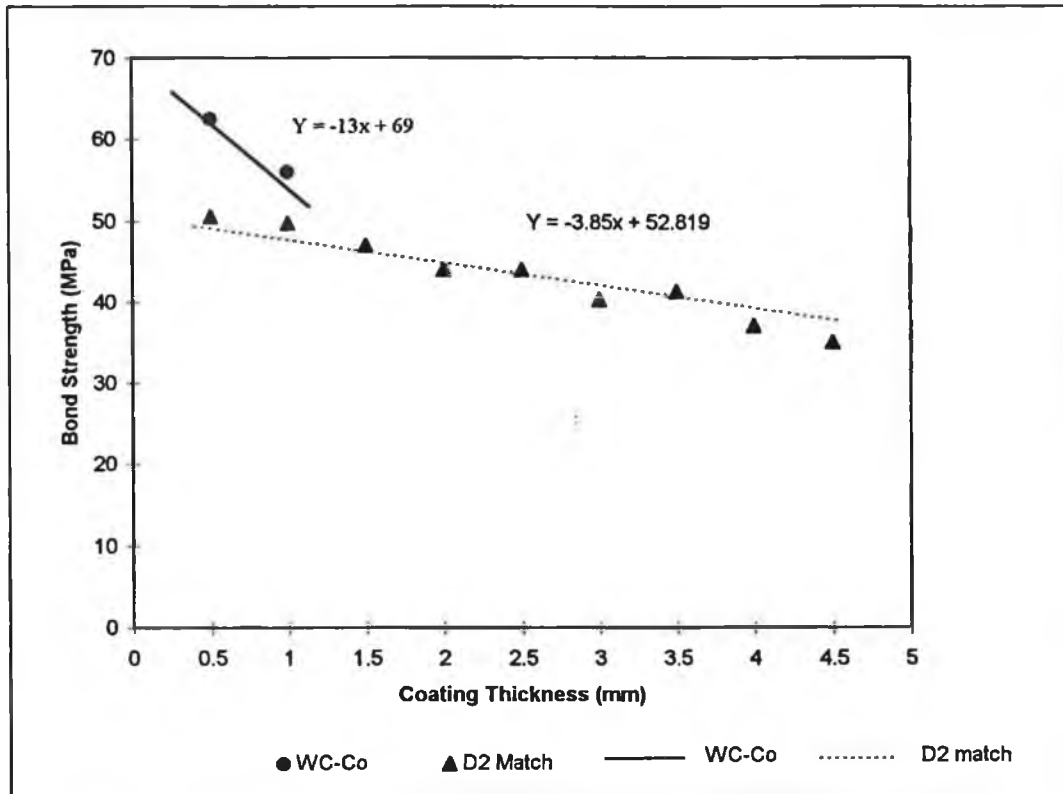


Figure 55 Bonding Strength Vs Coating thickness for D2 tool steel substrate

Discussion of results

Tensile bond strength tests using ASTM standard 633-79 measure the bonding strength of a coating to a substrate, when failure occurs at the coating to substrate interface. In such cases, the parameters that influence the strength are usually correlated with material sprayed, spraying process technique and substrate thermophysical properties. If the failure occurs in the coating, usually called cohesive failure, it may be concluded that the coating is weaker than its coating bonding strength to the substrate.

From the results table in Table 13, (samples A & D) it can be seen that in coating with WC-Co powder, it is very difficult to build up a coating of more than 1.5mm; 50% of coatings with coating thickness more than 1.5mm spalled off or cracked before the

bonding test could be carried out. Because the build up of tensile residual stresses during spraying of thick coatings can be greater than the bond strength between the coating and the substrate, the coating may fracture also due to these residual stresses within the hard and brittle material like tungsten carbide. Tensile bond strengths of WC-Co coatings of >100MPa have been achieved by work carried out by Kreye et.al [94] on mild steel substrate. They paid a lot of attention to substrate surface preparation and cooling techniques during spraying in order to achieve this. Other work carried out by Matsubara et. al. and Beczkowail et. al [95-96] achieved average values of bond strength at approximately 60MPa for WC-Co coatings on a mild steel substrate. The current bond strength values for WC-Co coatings with thickness of <1.5mm. compare well with these results.

For the stainless steel coatings on stainless steel substrate Sample B, (Table 13), the average bond strength of the coatings only started to drop significantly when the coating thickness reached 3.5mm. The residual stresses generated within the thick coating have weakened the bond strength of the coatings. There were also consistent occurrences of cohesive failure for coatings thicker than 3.5 mm. Results showed that 50% of samples with coating thickness of 3.5mm were cohesive failure and all samples above this thickness failed in a similar way. This weakness in the coating is thought to be the result of interruptions to the spraying process which have to be made in order to avoid overheating of the coating. This interruption of spraying causes the coating to build up in layers, and too many layers in a coating will lead to poor cohesive strength within the coating. However, it is not possible to identify there under microscope.

The positive influence of similarities in thermophysical properties is evident from the results. Coatings where the substrate and coating material are similar (eg. D2 coated with D2 powder) can be built up to 4.5mm in thickness (Table 13).

The bond strength results were averaged and are plotted in Figures 54 and 55. For the WC-Co coatings on stainless steel, the highest coating thickness attained was 2.0mm

but with the bond strength value 60% less than that for a coatings of thickness 0.5mm. Scatter between values for similar specimens was small (<4.8%) for coating thickness' of less than 1.5mm, but was 12.1% for coatings of 1.5mm. The stainless steel coatings on stainless steel substrates showed a small but constant decrement in bond strength up to the thickness value of 3mm. Scatter of between 2.6% and 13.5% were found for coating thickness up to this range. There was a 30% decline in bond strength for coatings with thickness increase from 3.0mm to 3.5mm.

For the WC-Co coatings on D2 steel substrates with coating thickness of 1.5 mm sample D (Figure 55), only half of the experiments were carried out with success. However, the tool steel base coatings on D2 steel substrates showed a steady decrease in the average bond strength. Scatter of between 3% - 6.4% was found for these coatings with thickness' up to 1.5mm. The scatter was large for coatings with thicknesses from 2.0mm to 4.0mm (15%-30%), this was due to the different types of test failure modes of coatings.

Figure 54 shows lines fitted for each type of coating. It can be seen that WC-Co coatings show the steepest slope. This confirms once again that the coating thickness has more influence on the bond strength of hard material like tungsten carbide. By ranking the different combinations of coatings and substrates, it can be said that tungsten carbide coating on stainless steel substrate shows the least strength match, while D2 match powder on D2 substrate shows the ideal combination.

(c) Residual stress test

Two types of Residual Stress techniques were employed, the: 1) Hole Drilling method and 2) X-ray Diffraction method.

Only the coatings of stainless steel on stainless steel substrates were used for these residual stress test. This type of coating is the most suitable material for the hole drilling equipment available. Since there is no minimum coating thickness requirement for running this test, all samples prepared were between 0.2mm and 0.6mm thick. The objective of the hole drilling tests was to establish the effect of different preheating temperatures, and of coating thickness on the residual stress of HVOF coatings. In addition the effect of varying the depth of the drilled hole for the measuring method was assessed.

The coating was drilled only up to the depth (approximately 100 micron) above the coating and the substrate interface. The maximum relative strain value was recorded for the stress calculation. This maximum strain usually occurred at a depth near the interface layer of the substrate and coating.

The interface layer itself usually has lower stress values, because the shot peening effect of the sprayed particles on the substrate surface generates compressive residual stress on the substrate surface [88]. In addition the substrate usually suffers compressive stress from the grit blasting process. Work carried out by Greving et.al. (Figure 56) showed that grit blasted specimens without a coating sustain compressive residual stress [97].

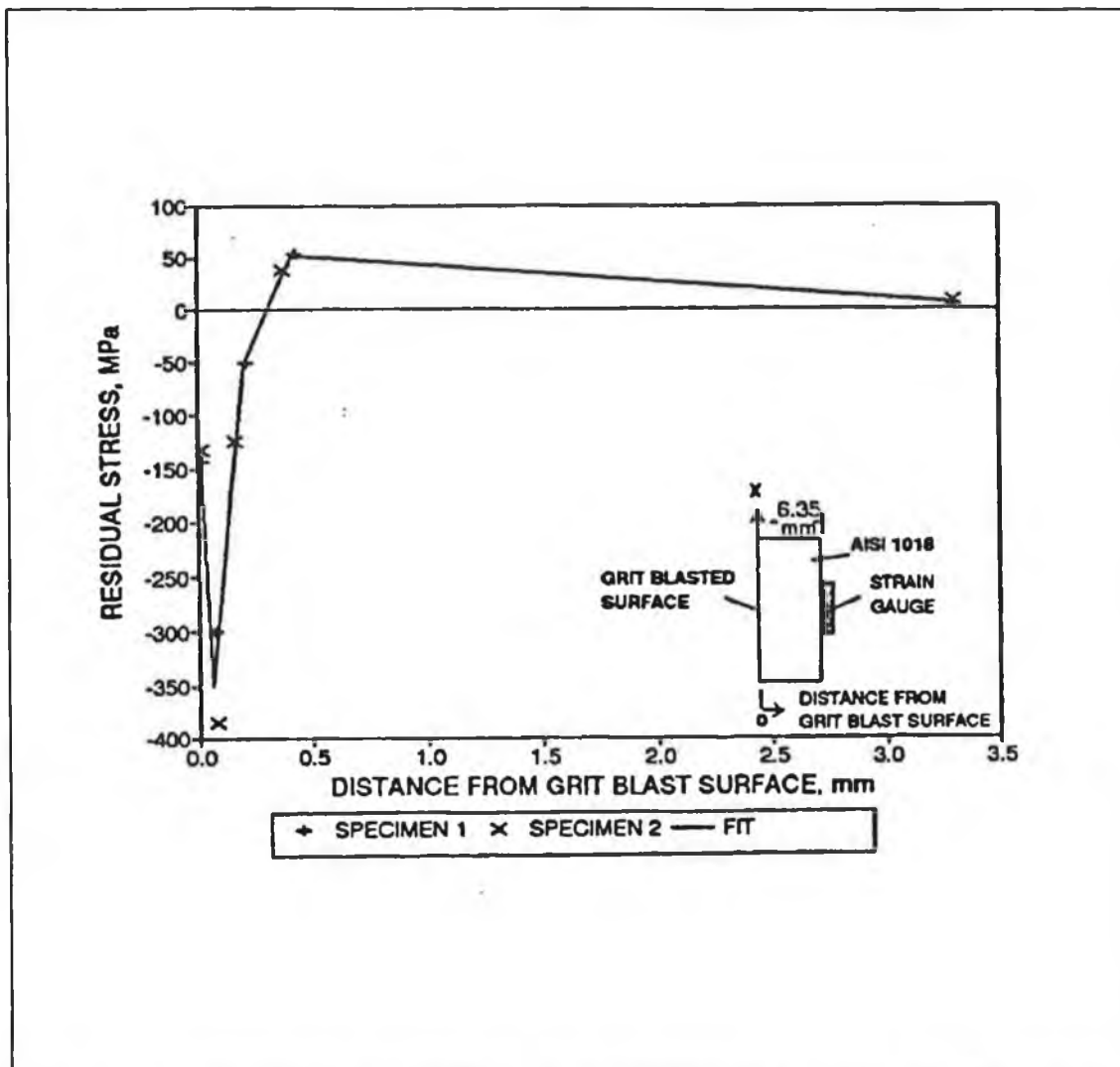


Figure 56 Residual stress distribution for grit blasted AISI 1018 steel specimens without coating [97].

Samples were coated using four different pre-spray heating temperature values: 20°C, 100°C, 150°C and 200°C and three different thicknesses: 0.2mm, 0.35mm and 0.6mm. The pre-spray heating temperatures of this range were chosen because temperatures higher than 200°C have been found to cause excess build up of an oxide layer [91]. All samples were sandblasted prior to spraying. The sand blasting process enhances bonding of the coating to substrate [39].

The X-Ray Diffraction Method was used to provide a comparison with the results of the hole drilling method. All samples were prepared with the spraying parameters according to the spraying data sheet in Appendix A for stainless steel powder.

Both the residual stress measurement methods and stress calculation procedure have been described in detail in Chapter 4.

For the hole drilling method, the carbide cutter used for drilling the holes has a diameter D_0 of 1.6mm, while the mean gauge circle diameter of the strain gauge, D , is 5.14mm, therefore the ratio of D_0/D is 0.3113. From the table supplied by the strain gauge manufacturer

$$\bar{a} = 0.11903 \text{ and } \bar{b} = 0.30718$$

Using equations 5 and 6 (section 4.6.2.4) with $E= 140000\text{N/mm}^2$ and $\nu= 0.3$:

$$A= -5.52639 \times 10^{-7} \text{ mm}^2/\text{N}$$

$$B= -1.09707 \times 10^{-6} \text{ mm}^2/\text{N}$$

The strain indicator reads the value of each strain in $\mu\epsilon$ after drilling. Strain values are recorded as soon as the drill penetrates the substrate; therefore the residual stress of each sample can be calculated according to the equation:

$$\sigma_{\min}, \sigma_{\max} = \frac{\epsilon_3 + \epsilon_1}{4A} \pm \frac{\sqrt{[(\epsilon_3 - \epsilon_1)^2 + (\epsilon_3 + \epsilon_1 - 2\epsilon_2)^2]}}{4B}$$

The equivalent stresses are then calculated with the following formula, within 10% of scatter error:

$$\sigma_{\text{eq}} = \sqrt{\sigma_{\max}^2 + \sigma_{\min}^2 - \sigma_{\max} \cdot \sigma_{\min}}$$

Results of the effect of different annealing temperature and coating thickness on residual stresses shown in Table 14 were based on the average of 4 samples.

Sample	Pre-spray temperature °C	Coating thickness		
		0.2mm	0.3mm	0.6mm
		σ_{eq} (MPa)	σ_{eq} (MPa)	σ_{eq} (MPa)
A	none	479.2	501	536
B	100	400.1	380	411
C	150	341.7	361	351
D	200	320.6	318	306

Table 14 Hole Drilling results for stainless steel coating on stainless steel substrate.

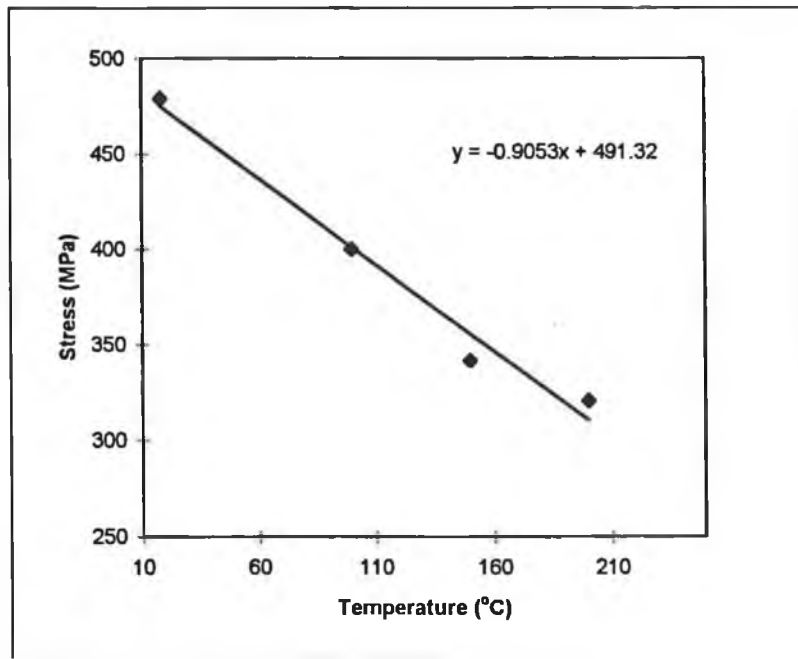


Figure 57 Effect of different pre-spray heating temperature on stresses for coating thickness of 0.2mm

Effect of Pre-spray Temperature

Figure 57 shows how the equivalent tensile residual stress varied with the substrate annealing temperature for a coating thickness of 0.2mm. It can be seen that as the substrate annealing temperature increases, the equivalent residual stress decreases. With no pre-spray heat treatment, the equivalent stress was measured as 479.2 MPa, whereas with a high pre-spray temperature (200° C), the σ_{eq} was at 320.6 MPa. The decrease in stress is due to the reduction in the absolute thermal expansion difference between the coating and substrate with the higher preheating temperature.

The residual stress can be further reduced if the pre-spray temperature is increased [90], but in this test, the ideal pre-spray temperature using the flame from the gun was found to be limited to 200°C. High preheating temperatures generated using the gun will usually encourage the build up of undesirable oxide residuals which are detrimental to the quality of the coating produced. The oxide layer will decrease the coating bond strength and hardness, as explained on the previous section. It would be better to use an alternative heating device eg. electric transfer arc in order to achieve higher substrate temperature. The optimum substrate preheat temperature is one for which the resulting bonding is just sufficient for the residual stresses to be at the lowest level possible. If the preheat temperature is too low, the coating will peel off along the interface, because of the build up of residual stresses due to the absolute thermal expansion difference between the material sprayed and the substrate material. The coating will sometimes crack in the direction vertical to the surface because the stresses exceed the ultimate tensile strength of the coating [90]. The optimum substrate pre-spraying temperature will also greatly depend on the coating and substrate materials [91].

Effect of Coating Thickness

Tests were also carried out to examine the effect of different coating thickness' on the residual stress of a coated sample, while all other spraying parameters were maintained constant.

The effect was investigated for four different pre-spray heating temperatures and all samples were then measured for their residual stress using the hole drilling method.

As seen in Figure 58 at temperatures over 100 °C there is not much variation in the stresses measured for coating thickness' of 0.2mm to 0.6mm. There is an overlap in stress values for different coating thicknesses, eg. The coating with the thickness of 0.3 mm at a pre-spray temperature of 150°C and a scatter of 8%, overlaps the stress results measured for the 0.6mm coatings at a similar pre-spray temperature. This is consistent with other work [91] which suggests that as long as the spray temperature is kept within 50°C of the pre-spray temperature, the increase in coating thickness has little effect on the residual stress within the coating. WC-Co coating, 2.5mm thick has been deposited on a stainless steel substrate with the use of a CO₂ liquid cooling system to control the spraying temperature [29].

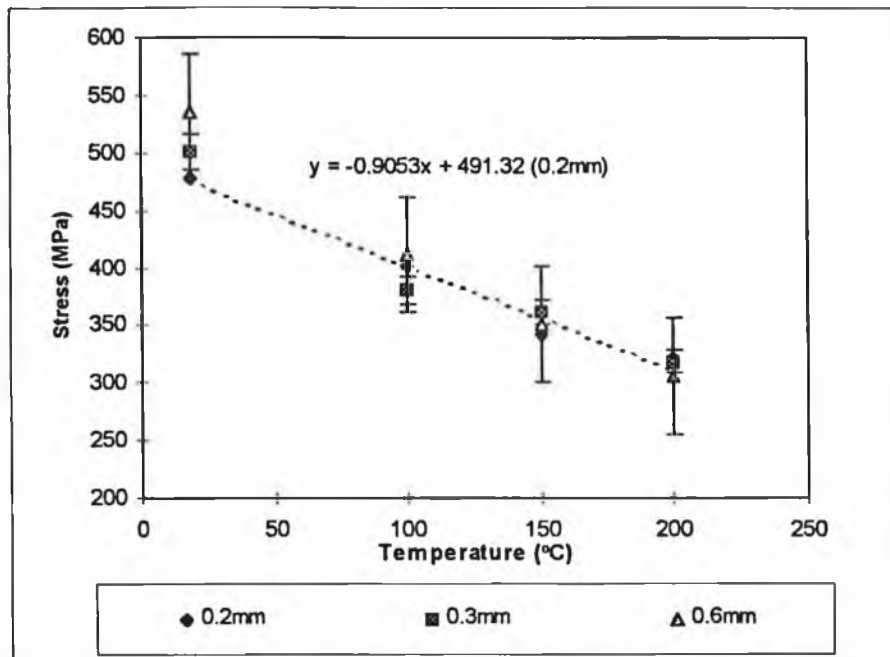


Figure 58 The effect of different pre-spray heating temperature on residual stress for various coating thickness.

The effect of drilling hole depth on residual stress measurements

A sample with coating of thickness of 2.5mm was prepared to identify the effect of the drilling hole depth on residual stress measurement. According to ASTM standard E837-92 [80], the residual stresses measured for the above tests were determined on the assumption that the stresses within the coating do not vary significantly with depth. The hole was drilled only up to a depth very close to the coating and substrate interface. In such cases, experimental relaxed strain calibration data from test specimen with known uniform stress fields provided by the strain gauge manufacturer can be used directly [98]. According to standard ASTM E 837-92, the residual stresses determined by this method may be expected to exhibit a bias not exceeding $\pm 10\%$.

It is suggested that in the case where the coating thickness is less than $1.2D$ (D is the diameter of the cutter; 1.6mm in our case), that the hole be drilled through the entire

thickness of the coating [80]. A test was carried out to find the variation of equivalent stress measurement with hole depth for a coating thickness of 2.5mm. When applying the hole drilling method on thick coatings, the residual stress is fully relieved when the hole is drilled approximately to a "full depth". A "full depth". means that the hole is drilled to a depth which is equal to the diameter of the cutter.

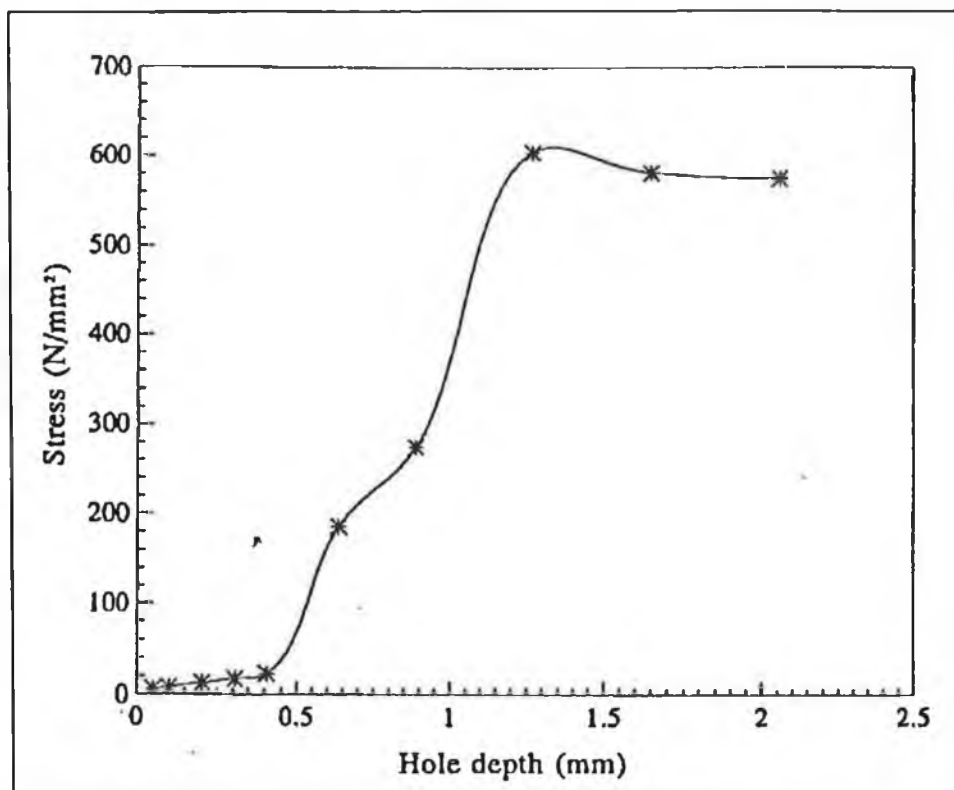


Figure 59 Stresses relieved Vs drilled hole depth

Figure 59 shows that up to a depth of 0.5 mm, σ_{eq} is almost constant, then as the hole depth increases, the equivalent stress increases rapidly up to maximum at 1.25 mm. It can be seen that the stress remains almost constant up to the final 2.0 mm hole depth. The stress in the coated sample are considered to be fully relieved at this depth. It is

not necessary to drill any further because the strain values will remain constant after this depth .

Comparison of XRD and Hole Drilling Stress Measurements

The aim of this stage of experimental work was to compare the results of two different residual stress measurement methods. It must be emphasized that precise agreement of XRD and Hole Drilling method cannot be expected since they each average the local stresses which they measure over different volumes. The depth of penetration of XRD is usually about 0.015mm, which is usually several times shallower than the depth samples by hole drilling method. Further, the areas of specimen measured by the two methods are usually different, with XRD normally sampling an area of 1mm² and hole drilling about 10 times that area [99].

Sample type	Heat Treatment	XRD method (MPa)	Hole Drilling method (MPa)
Stainless steel powder coated 316L	no pre-spray heat treat	510.8	479.2
Stainless steel powder coated 316L	200°C pre-spray heat treat	323.6	320.6

Table 15 Comparison of XRD and Hole Drilling Stress Measurements

Despite the differences in both measurement methods, correlation between the two methods of residual stress measurement was reasonably good. For both specimen types the XRD method indicates larger tensile stresses, although the difference between the two methods at approximately 6%, is within the range of scatter for XRD stress measurements. Confidence in the XRD stress data derived for WC/Co components was increased on the basis of this correlation. The effect of pre-spray heat treatment was confirmed by both methods was to reduce the residual tensile stress significantly (by approximately 30%).

Summary:

From the tests carried out on the effect of coating thickness and pre-spray heat treatment on residual stress, it was found that residual stress on the coating can be reduced by at least 33% if the substrate is annealed at 200°C prior to the deposition. The coating thickness has very little effect on the residual stress provided the temperature variation during spraying is kept low. Such control is very difficult for thick coatings unless proper cooling system is used.

The experimental work has been carried out on the effect of spraying distance, sprayed coating thickness and pre-spray heat treatment on coating properties including hardness, bonding strength and residual stresses. Based on the results, it was found that there is a strong correlation between the bond strength, coating thickness and residual stress in coatings. The bond strength and the residual stress are both greatly influenced by the temperature of the spray process. It is seen from the results that tensile residual stresses coupled with increasing coating thickness cause the degradation of bond strength.

A possible mechanism for this coupling is described in Figure 60, suggested by Greving et. al. [97]. A free body diagram of a coating containing residual stress is shown with the edge effect in this diagram. In the diagram (a), for a thin coating, a tensile residual stress is generated in the X-direction. The edge effect is a stress distribution in the Z-direction with tension at the edge and compression away from the edge. The shape of the σ_z stress distribution satisfies the equilibrium of the free body diagram. Two characteristics of the σ_z stress distribution are important. The first is that moment equilibrium about point B of the free body diagram requires that the σ_z stress distribution be tensile at the free edge. The second important characteristics is that if the coating is thicker, the moment caused by the residual stress in the coating as shown in Figure 60-b is larger. Therefore, the σ_z stress distribution must increase to balance this larger moment. The result is a higher tensile σ_z stress at the edge as shown in

Figure 60-b. The conclusion is that the thicker coating causes higher tensile edge stresses and will increase the tendency for debonding and hence reduce the applied stress required to cause debonding. It is also noted that this behaviour occurs without an increase in coating residual stress for thicker coatings. Therefore, a thicker coating will be more likely to have a lower bond strength than a thinner coating with the same level of residual stress.

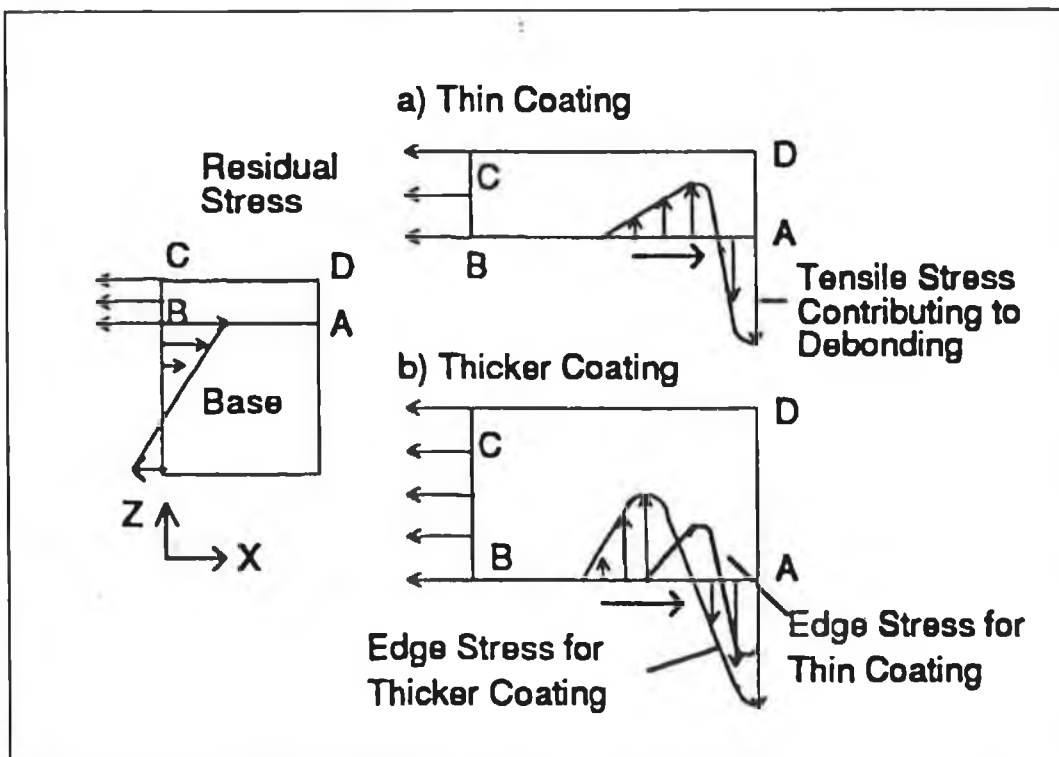


Figure 60 The effect of coating thickness and tensile residual stresses on the free edge debonding tensile stresses [97].

5.3 Repair of damaged components using the HVOF Process

HVOF thermal spraying is potentially a cost effective means for component dimension restoration following service induced wear. New surfaces may be provided without the material property distortion caused by welding, or the expense of special plating techniques. Furthermore the new surface may be created using the same material as the base material, or with a more wear or corrosion resistant material.

Prior to spraying, the surface of the damaged components are usually machined to prepare the substrate surface for the coating. Undercutting or grooving is the most common machining operation, this will remove previously hardened surface, chemical contamination, oxidation or previously applied sprayed material. For example, at each undercut section on a cylindrical part, the shoulders should be cut at a slight obtuse angle ($>15^\circ$) [100]. The undercut section should not extend to the end of a shaft, as shown in Figure 61.

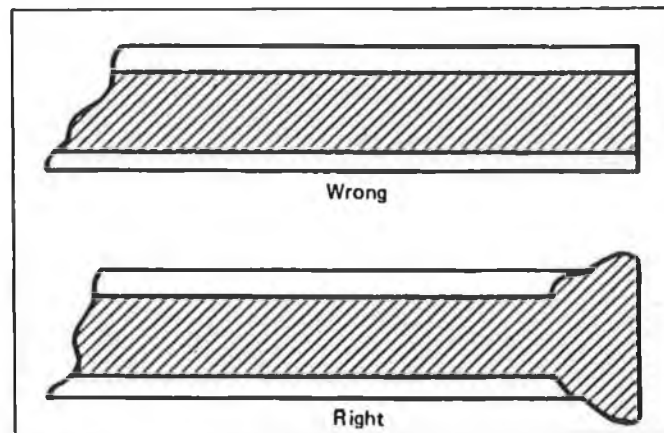


Figure 61 Shaft with proper and improper undercut section [100].

As tight control on depth and spread of deposited material is not possible in HVOF spraying, a finishing process is therefore required for components repaired using the technique.

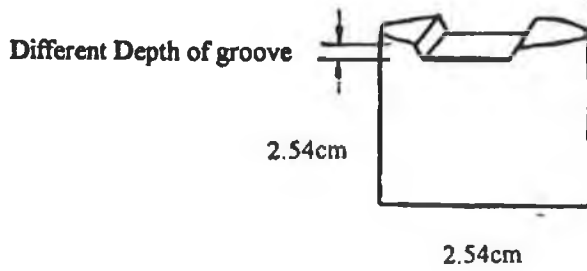
The main objectives of this part of study were to optimise the repair of damaged tools using the HVOF process, and also to establish the machinability of these repaired components using various machining methods.

Several experiments were carried out in order to study and establish the optimum method for carrying out the repair work.

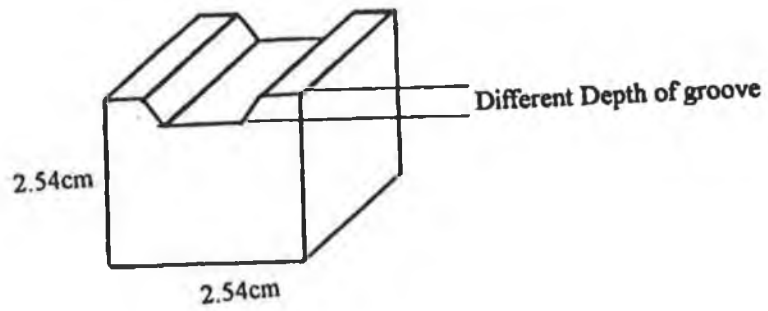
Austenitic stainless steel was chosen initially as a repair material for this study in order to match the repair material to a substrate of reasonable toughness, restoring the damaged component to its original state. The experimental scope was then extended to using hard D2 tool steel and nitrided D2 tool steel substrates. These were repaired using either a 'tool steel matching' powder (commercial name: Diamalloy 4010), or Tungsten Carbide-Cobalt repair materials. D2 steel is a common material used for industrial tools. Nitrided tool steel samples were also included in the tests as industrial components are often case-hardened by the nitriding process to improve wear and corrosion resistance, and this hardening is expected to make repair adhesion more difficult. The nitriding process parameters for the tool steel sample is described in Appendix A.

All stainless steel samples had the same overall dimensions as shown in Figure 62a. Tool steel samples were rectangular blocks of dimension 25.4mm x 25.4mm, and stainless steel samples were cylindrical blocks of dimension 25.4mm in diameter by 25.4mm in height. A groove of certain depth (minimum 1mm) was machined on each sample with certain shoulder (wall) angle as shown in Figure 62c. Each sample was then degreased and sand blasted with aluminium oxide grit prior to coating. Immediately before spraying the samples were pre-heated to 250°C using the flame from the HVOF gun to reduce the thermal expansion difference between the sprayed repair material and the substrate. The groove was then sprayed with the repair material until the whole top face of the sample was covered with the deposited material up to

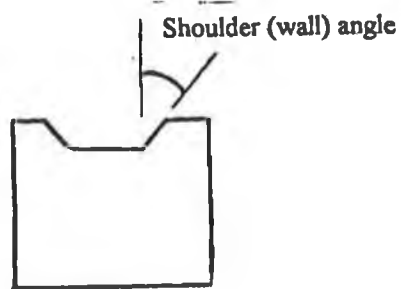
thicknesses in the range 1.5mm to 4.2mm. The repaired samples were then final finished using either grinding, turning, milling or EDM.



(a)



(b)



(c)

Figure 62 Schematic diagram of a)Stainless steel sample b) D2 tool steel sample and c) Sample with an angled shoulder (wall).

The spraying processes were carried out according to the spraying parameters listed in Appendix A for the particular powder material.

Table 16 details the experimental matrix. Samples in group A are stainless steel components repaired with stainless steel material and samples B are D2 tool steel components repaired with matching tool steel powder. Samples C are nitrided tool steel components also repaired with tool steel powder.

Sample No	Machining Method	Depth Of Groove	Depth of built- up repair
A1(a),1(b)	Milling	1.5mm	3mm
A2	Milling	1.5mm	5.5mm
B1(a),1(b),1(c), 1(d)	Milling	1.5mm	3mm
C1(a),1(b),1(c)	Milling	1.5mm	3mm
A4	Grinding	1mm	2.2mm
A5	Grinding	1.5mm	3.5mm
B2 (a), 2(b)	Grinding	1.5mm	3mm
C2(a), 2(b)	Grinding	1.5mm	3mm
A3	Turning	1.5mm	2.5mm
A6	Spark Erosion	1.5mm	5.5mm
B3	Spark Erosion	1.5mm	3.5mm
C3	Spark Erosion	1.5mm	3.5mm

A = stainless steel powder on stainless steel substrate

B = tool steel match powder on tool steel substrate

C = tool steel match powder on nitrided tool steel substrate

Table 16 Experimental Matrix for Machinability Tests.

5.3.1 Machining of repaired components

The machining of thermally sprayed material can be a difficult task. Sprayed coatings are composed of a collection of lenticular splats, and have poor thermal conductivity compared to the same material in wrought form. Heat transfer away from the cutting point is slow. The acceptable methods, practices and techniques used for machining materials in their wrought form do not apply to the same materials when sprayed. Intrinsically, materials which are abrasion resistant are difficult to machine. In order that the repair 'plug' does not come away from the component, the adhesion of the repair material to the substrate has to be strong enough to resist the forces involved in cutting. Also, the bond between the sprayed particles is primarily mechanical, therefore individual particles can be pulled out if cutting pressures are excessive. For certain applications where surface finish is important, highly reflective finishes are difficult to achieve for sprayed materials with a relatively porous structure. Factors which influence a choice of finishing method include type of material to be finished, the shape of the part, finish and tolerance required, and economics.

Carbide tools are generally used for machining of hard coating materials such as ceramics, carbides and cermets. Tool angles, surface speed and feeds are critical in the success of machining these coatings. Improper tool angles and tool pressure can result in excessive particle pull-out and destruction of the coating substrate bond.

Discussion of results from all the repaired components is presented under the type of final finish machining process used on the repaired area. Machining operations were carried out according to general machining procedures for the particular machining operation. As the tungsten carbide-cobalt repair material failed to adhere to any of the substrates, these samples were not available for machining, and are therefore not included in the body of the discussion of results. The 1mm depth of the groove introduced in samples exceeded the coating thickness limit for tungsten carbide-cobalt material (thickness limit 0.64mm [70]). The tensile residual stresses within the built-up

material caused it to debond from the substrate component. The substrate and repair material had different expansion rate due to their dissimilar physical properties.

The repair of all samples with the other two types of repair material (stainless steel and tool steel) were carried out successfully, with the built up thicknesses ranging from 2.2 mm to 5.5 mm. The repair built-up thickness of 5.5mm was achieved with the help of a cool air jet stream to dissipate the heat during the deposition. Interruption of spraying is also needed in order to achieve thicknesses of this magnitude.

Figures 63 and 64 show the pictures of some of the repaired samples produced in this study.

Milling machining

Two identical damaged samples (Sample No A1a and A1b) both are stainless steel substrates repaired with stainless steel repair material. They were sprayed to the same built up thickness of 3mm. Both samples were sectioned and mounted for inspection under microscope, one without any final finishing, the other being final finished with a milling machine. The first sample was used as a comparison for any damage on the repaired area that might be induced by the milling machining.

Pictures of the pre-machining and post-machining repaired samples were taken and compared. The cross sections indicate very little difference under microscope (x100 magnification). There are no signs of damage to the coating caused by the machining process (Micrograph No 1)

The cross section micrograph indicated good adherence of coating to the substrate. A bond line - possibly an oxide layer in between the coating and substrate can be seen. This oxide inclusion was caused by the flame from the gun when the sample was heated to the temperature of 250 °C before the repaired material was sprayed onto it. This pre-spray heat treatment of the sample reduce the thermal expansion difference of the coated layer and the substrate, and hence reducing the tensile stress on the coated

material which might lead to coating failure. This heat treatment process will also increase the coated material bonding strength to the substrate by encouraging more diffusion between the coated material and the substrate.

Sample No.A2, also stainless steel sprayed onto stainless steel, was machined from an original built up thickness of 5.5mm to a depth 1mm on the substrate. Observation of the cross section micrograph reveals good adherence of the repair material to the substrate, even though a large volume of the repaired material was machined away by the milling process (Micrograph No 2). This test proves that the repaired area can withstand an aggressive machining process.

Samples No. B1(a), B1(b), B1(c) and B1(d) are all damaged D2 samples repaired with matching tool steel material which underwent different types of milling processes after being built up to 3mm thickness. The top face of sample B1(a) was machined off ; whereas one side of sample B1(b) was machined in steps, and sample B1(c) was machined to an angle of 45 degree. Some of the repaired samples are shown in Figure 64. These samples prove that the repaired area with D2 material could withstand machining processes of different geometries and depths of cut. The cross section of the repaired samples indicates good adherence of coating to the substrate (Micrograph 3). All the repaired material on sample B1(d) was machined away completely, the original dimension prior to the repair process being restored. This test proves that it is possible to reverse any repair action if desired. The substrate surface integrity was not affected by the heat from the HVOF process. A good repair result was also observed on the nitrided D2 sample (sample C1) under similar tests.

Turning

Sample A3 was machined by turning, the top face of the sample was turned until both the repaired area and the substrate were exposed. Two bond lines were observed on the turned surface, coinciding with the edge of the repaired groove. These lines were investigated under higher magnification and were found to be areas where the repair material consists of smaller grains and more oxide inclusion compared with the rest of the coating area. This is because some of the deposited particles were deflected by the

angled (45 degree) wall. It is generally recommended to have the direction of deposition perpendicular to the substrate for best spraying result for thermal spraying process.

Grinding

Samples A4, A5, B2(a), B2(b) and C2 were machined using a diamond grinding wheel, all samples showed good adherence of repaired material to the substrate. Sample B2(b) was ground to remove all the repaired material. The cross section and the top face of these samples observed under the microscope were found to be quite similar to the other samples. Micrographs 4 show the cross sectioned view of sample A4.

Spark Erosion

Samples A6, B3 and C3 were all machined using the spark erosion process. This is quite a different machining process to those used on the other samples, but aside from the typical EDM heat affected area, the quality of the repaired area when inspected under the microscope appeared to be as good as those which underwent other machining processes. Micrograph No 5 show the cross section view of the sample A6.

Summary:

The HVOF thermal spraying process has successfully been used to repair stainless steel and D2 tool steel substrates with different depths of damage, to a built-up thickness of up to 5.5 mm. This thickness can only be achieved if the substrate and the repair material have similar or matching physical properties, and an air cooling system is utilised during spraying. Repair was not possible using WC-Co repair material on either of the substrates, within the range of spraying parameters used. For all the successful repairs, the sprayed material shows good adherence to the substrate when inspected under microscope, even following various types of aggressive machining processes. This is true even when a large section of the repaired area is removed. The repair action can also be reversed, if necessary, as shown on sample B1(d).

A longer spraying time is required to accomplish repair work on the nitrided components compared to others, due to the hardened nitrided surface deflecting some of the deposited material away from its surface during the spraying process.



Sample A1, milling
(from depth of 3mm)

Sample A2, milling
(from depth of 5.5mm)

Sample A3, turning



Sample A4, grinding

Sample A5, grinding

Sample A6, spark erosion

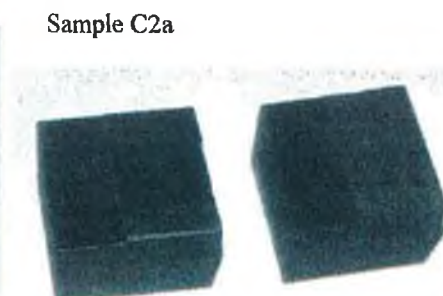
Figure 63 Stainless steel substrates, repaired using stainless steel material, and machined with various machining processes.



(a)

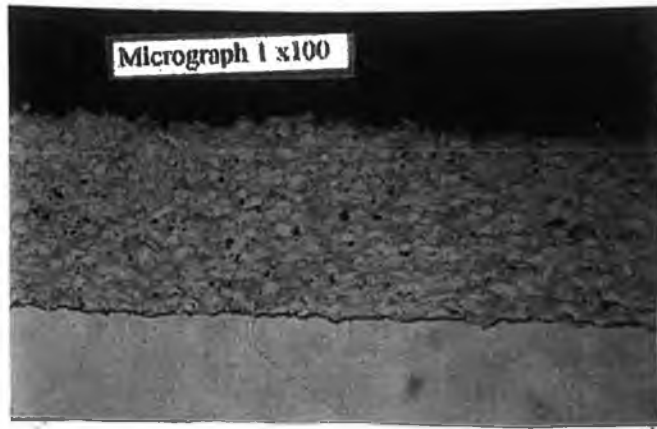


(b)

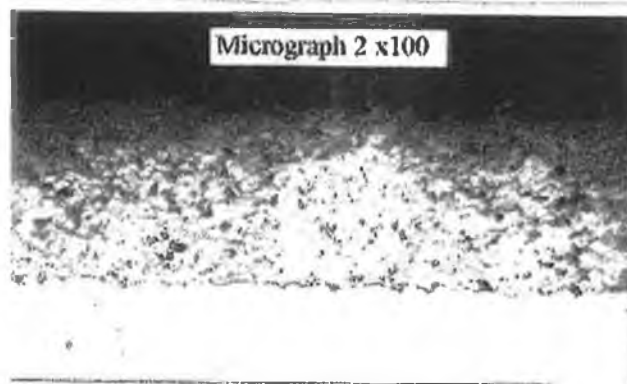


(c)

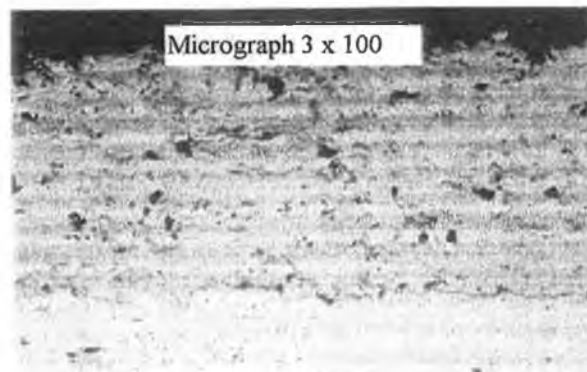
Figure 64 Tool steel substrate repaired with tool steel matching powder and subsequently machined by a) milling, b) spark erosion and c) grinding.



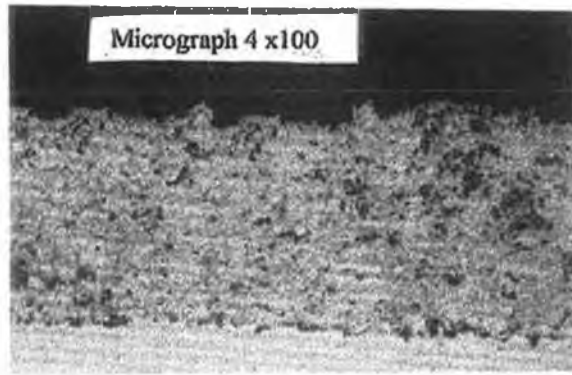
Micrograph 1. Sample A1, stainless steel on stainless steel; milling machining.



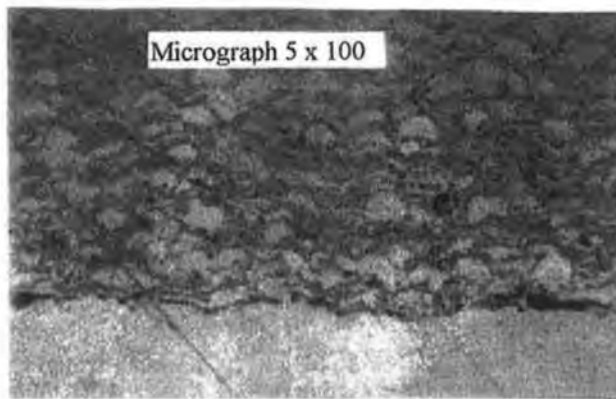
Micrograph 2. Sample A2, stainless steel on stainless steel; milling machining.



Micrograph 3. Sample B1a, tool steel matching powder on tool steel; milling machining.



**Micrograph 4. Sample A4, stainless steel on stainless steel;
grinding.**



**Micrograph 5. Sample A6, stainless steel on stainless steel;
EDM .**

5.3.2 The optimisation of HVOF repair process

To optimise the HVOF repair process, several spraying conditions were varied, including: (1) repair thickness (2) pre-repair and post repair heat treatment (3) repair wall angle and (4) substrate surface preparation.

All the repair work carried out using the HVOF spraying process is grouped and discussed here according to the type of test carried out. For example the results, discussion and summary for adhesion tests are presented under one section for all types of repair thickness and geometry of damaged. Additional tests were also carried out for the effect of various substrate surface treatments on the bond strength, and the effect of different post spray heat treatments on the bond strength.

All of the spraying was carried out using parameters according to the powder spraying data sheet in Appendix A, unless otherwise stated.

Experimental matrix

The experimental matrix for the repair work is categorised into four groups:

- 1) Bond strength test
- 2) Surface treatment effect on bond strength
- 3) Post spray heat treatment effects on the bond strength.
- 4) Three point bend test

1) Bond strength experimental matrix

Sample Type	Sample no	Method of Characterisation	Repair Thickness	Pre-spray heat treatment	Wall angle
WC-Co on Stainless Steel	A	Bond Strength	0.5 mm 1.0 mm 1.5 mm 2.0 mm	Five pre-spray temperatures: 1) Room Temp. 2) 100°C 3) 150°C 4) 200°C 5) 250°C	60 degree
Stainless steel powder on Stainless Steel	B	Bond Strength	0.5 mm 1.0 mm 1.5 mm 2.0 mm	Five pre-spray temperatures: 1) Room Temp. 2) 100°C 3) 150°C 4) 200°C 5) 250°C	60 degree
Tool steel base powder on D2 Steel	C	Bond Strength	0.5 mm 1.0 mm 1.5 mm 2.0 mm	Five pre-spray temperatures: 1) Room Temp. 2) 100°C 3) 150°C 4) 200°C 5) 250°C	60 degree
WC-Co on Stainless Steel	D	Bond Strength	0.5 mm 1.0 mm 1.5 mm 2.0 mm	200°C	Two types of wall angle 1)60 degree 2)45 degree
Stainless steel powder on Stainless Steel	E	Bond Strength	0.5 mm 1.0 mm 1.5 mm 2.0 mm 2.5 mm 3.0 mm 3.5 mm 4.0 mm	200°C	Three types of wall angle 1)60 degree 2)45 degree 3)15 degree
Tool steel base powder on Stainless Steel	F	Bond Strength	0.5 mm 1.0 mm 1.5 mm 2.0 mm 2.5 mm 3.0 mm 3.5 mm	200°C	Three types of wall angle 1)60 degree 2)45 degree 3)15 degree
WC-Co on D2 Steel	G	Bond Strength	0.5 mm 1.0 mm 1.5 mm 2.0 mm	200°C	Two types of wall angle 1)60 degree 2)45 degree
Tool steel base powder on D2 Steel	H	Bond Strength	0.5 mm 1.0 mm 1.5 mm 2.0 mm 2.5 mm 3.0 mm 3.5 mm 4.0 mm	200°C	Three types of wall angle 1)60 degree 2)45 degree 3)15 degree

I

2) Three point bend test experimental matrix

Sample Type	Sample no	Method of Characterisation	Repair Thickness	Pre spray heat treatment	Wall Angle
Stainless steel powder on Stainless Steel	I	Bend Test	0.5 mm 1.0 mm 1.5 mm 2.0 mm 2.5 mm	Three types of Pre spray temperatures 1) 100°C 2) 200°C 3) 250°C	Four types of wall angles 1) 90 degree 2) 60 degree 3) 45 degree 4) 15 degree
Tool steel base powder on D2 tool Steel	J	Bend Test	0.5 mm 1.0 mm 1.5 mm 2.0 mm 2.5 mm	Three types of Pre spray temperatures 1) 100°C 2) 200°C 3) 250°C	Three types of wall angles 1) 60 degree 2) 45 degree 3) 15 degree

3) Experimental matrix for various substrate surface treatments

Sample Type	Sample Group	Sample no	Method of Characterisation	Repair Thickness	Pre spray heat treatment
Tool steel base powder on D2 Steel	Sand Blasted roughened surface	K	Bond Strength	0.5 mm 1.0 mm 1.5 mm 2.0 mm 2.5 mm 3.0 mm	200°C
Tool steel base powder on D2 Steel	EDM roughened surface	L	Bond Strength	0.5 mm 1.0 mm 1.5 mm 2.0 mm 2.5 mm 3.0 mm	200°C

4) Experiment matrix for different post spray heat treatments

Sample Type	Sample no	Method of Characterisation	Repair Thickness	Post spray heat treatment
Tool steel base powder on D2 Steel	M	Bond Strength	0.5 mm 1.0 mm 1.5 mm 2.0 mm	Three types of post spray heat treatments: 1) Room Temperature 2) 450 °C for 3 hrs 3) 450 °C, for 5 hrs
Stainless steel powder on Stainless Steel	N	Bond Strength	0.5 mm 1.0 mm 1.5 mm 2.0 mm	Three types of post spray heat treatments: 1) Room Temperature 2) 450 °C for 3 hrs 3) 450 °C, for 5 hrs
WC-Co on Stainless Steel	O	Bond Strength	0.5 mm 1.0 mm 1.5 mm 2.0 mm	Three types of post spray heat treatments: 1) Room Temperature 2) 450 °C for 3 hrs 3) 450 °C, for 5 hrs

5.3.2 Results:

1) Repair bond strength test

All samples (except for sample group A, B, C, I and J as shown in experiment matrix) were prepared with pre-spray temperature of 200°C. For any repair work, it is very important for the repair material to have good adhesion strength with the substrate. In order to carry out the repair work on a damaged component, its surface has to be machined and prepared for the spraying process, sometimes a groove has to be created or machined away,. The wall angle of this groove is very important because for any HVOF spraying, the deposition angle has to be a minimum of 45 degrees to the substrate in order for the deposited particles to splat fully, creating a mechanical interlock between each deposited layer.

Tensile bond strength tests using standard ASTM 633-69 measure the bonding strength between a coating and the substrate. If failure occurs at the coating and substrate interface, the parameters that influence the bond strength are correlated with:

- sprayed material (especially thermophysical material properties that determine the contact temperature such as latent heat of fusion, specific heat, thermal conductivity and diffusivity), and the substrate material size and method of preparation, (which determine the size of contact area between the lamellae and substrate).
- processing technique: the selection of parameters, which determine the velocity of particles at impact, and the temperature prior to processing,
- substrate thermophysical properties (thermal diffusivity and conductivity) and
- surface condition(roughness and or the way of roughening).

If the failure occurs in the coating it may be concluded that the coating cohesion is weaker than the coating bond strength to its substrate.

Tests were carried out to study the effect that different repair wall angles and pre-spray temperature on the bonding strength of the repaired material, including 1) WC-Co powder on stainless steel substrate 2) Stainless steel powder on stainless steel substrate 3) Matching tool steel powder (composition close to D2 tool steel) on stainless steel 4) WC-Co on D2 tool steel substrate and, 5) Matching tool steel powder on D2 tool steel substrate.

The results are plotted using the average values of four samples.

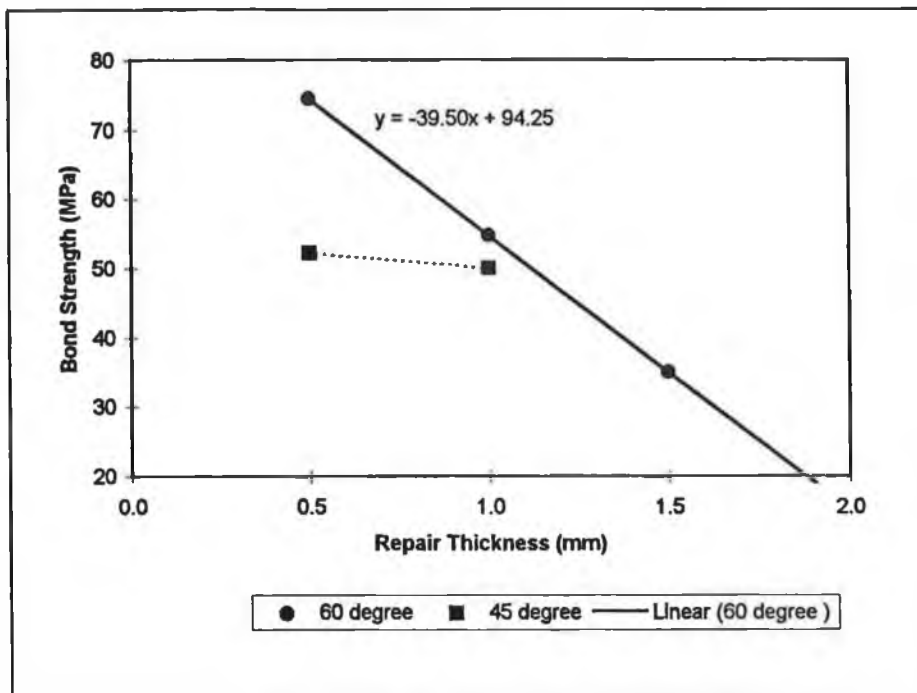


Figure 65 Bond Strength Vs Repair thickness for Stainless steel substrate repaired with WC-Co material for different repair wall angle.

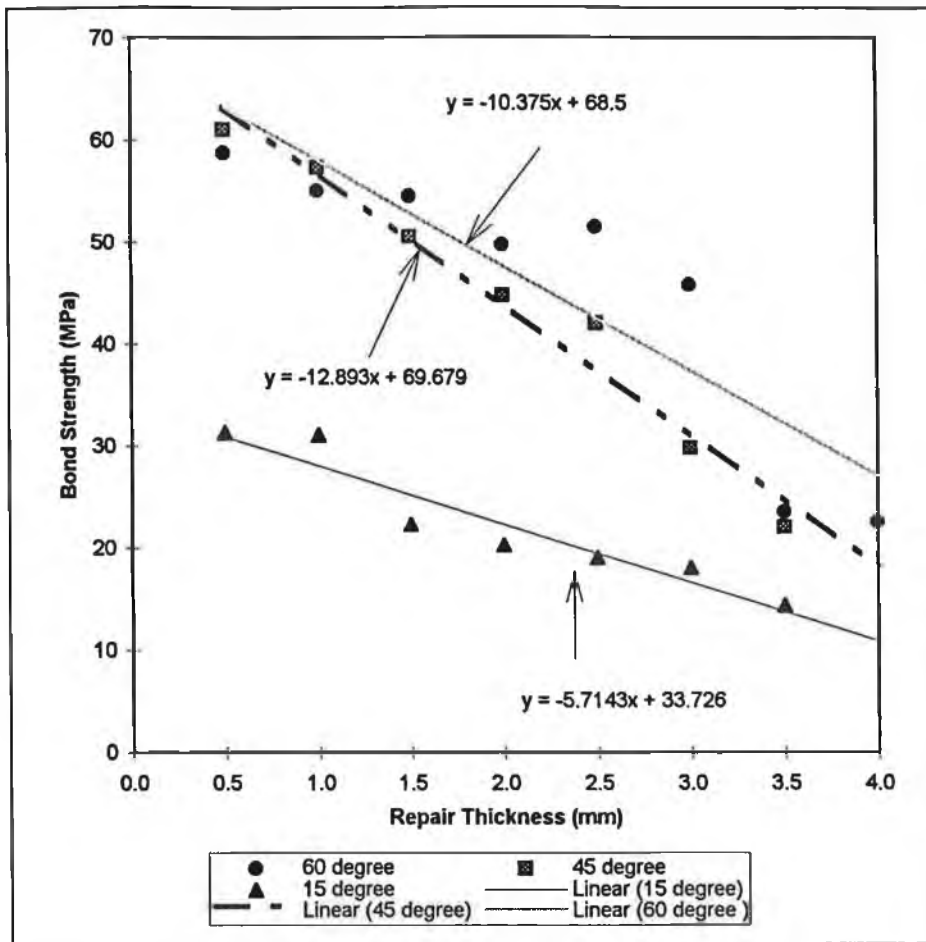


Figure 66 Bond Strength Vs Repair thickness for Stainless steel substrate repaired with stainless steel material for different repair wall angle.

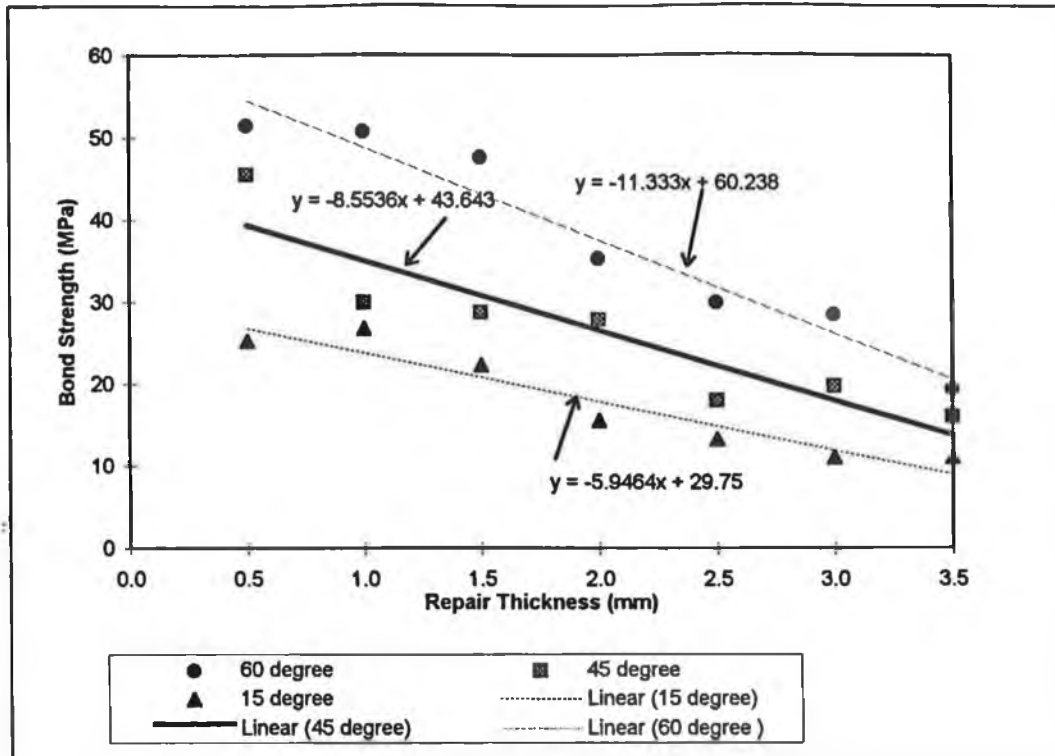


Figure 67 Bond Strength Vs Repair thickness for stainless steel substrate repaired with D2 tool steel material for different repair wall angle.

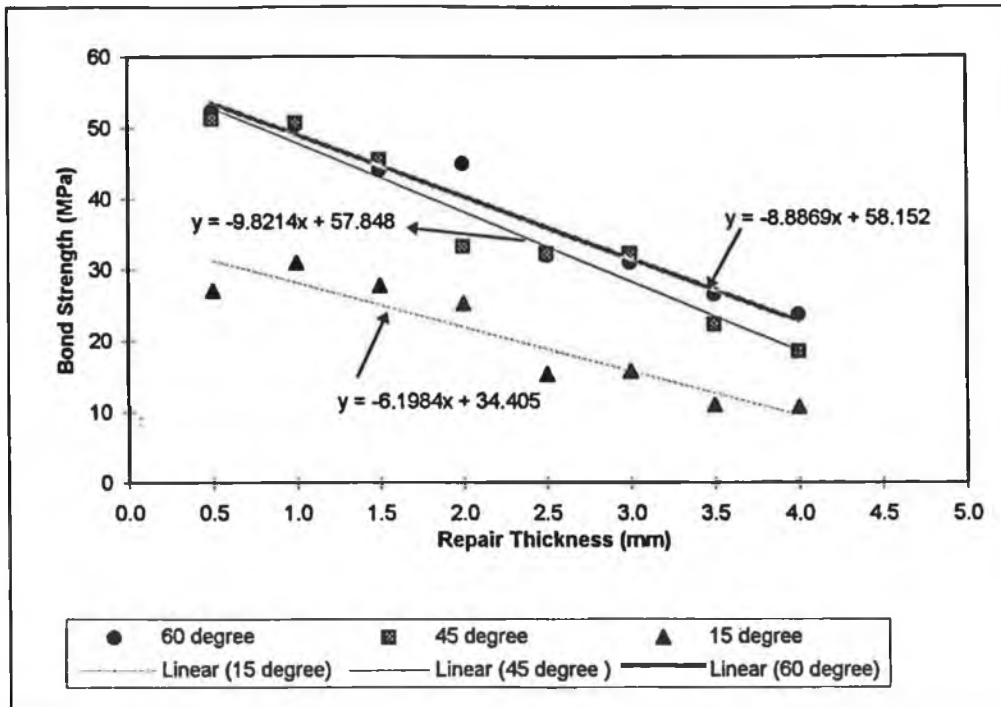


Figure 68 Bonding Strength Vs Repair thickness for D2 tool steel substrate repaired with D2 tool steel material for different repair wall angle.

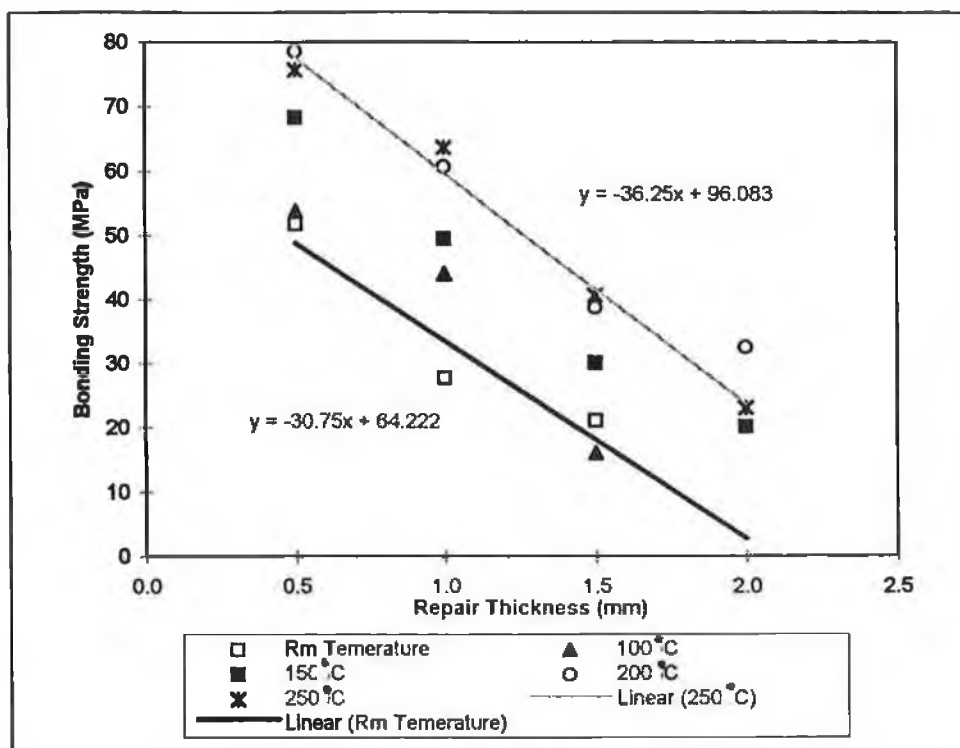


Figure 69 Bond Strength Vs repair thickness for various pre-spray heat treatment for stainless steel substrate repaired with WC-Co material.

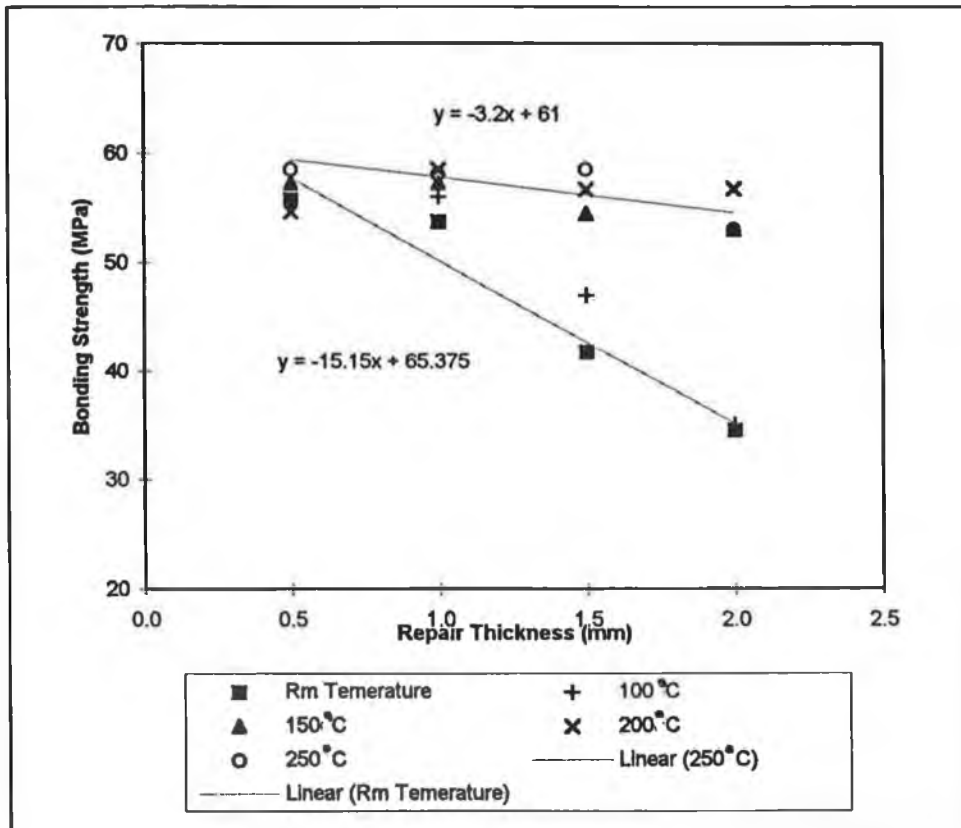


Figure 70 Bond Strength Vs repair thickness for various pre-spray heat treatment for stainless steel substrate repaired with stainless steel material.

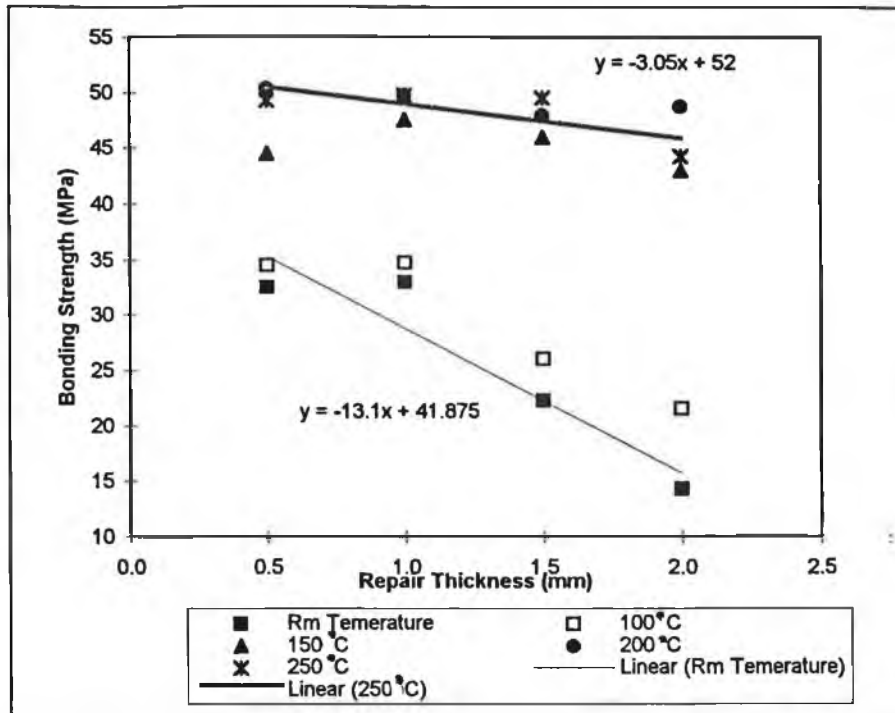


Figure 71 Bond Strength Vs repair thickness for various pre-spray heat treatment for D2 tool steel substrate repaired with D2 tool steel material

Discussion of results:

1) Effect of sample wall angle on the bond strength

All samples for this group of experiments were prepared using the same spraying parameter those designated by the manufacturer for the individual type of powder. The same pre-spray heating temperature, 200°C, was used to all the samples.

From the results plotted in Figures 65 to 67, for stainless steel substrates repaired with D2 matching powder, WC-Co and stainless steel powder, all components showed an average of about 35% increase in bond strength for components with a bigger wall angle. It is important for the sprayed particles to impact on a substrate surface of minimum 45 degree to the direction of deposition in order to produce better results. A narrow wall angle can also cause the sprayed particles to bounce off the substrate surface, and this can be observed from all the samples with 15 degree wall angle. From

the results in Figure 65, it can be seen that the repair with WC-Co powder was very difficult; for a build up of more than 1mm, 50% of the repairs were spalled off before the bonding test. Due to the mismatch in the properties of the coating and the substrate materials, the build up of tensile residual stresses during spraying for thick coatings is usually greater than its coating adhesion strength. For the repair with stainless steel powder, there are more occurrences of cohesive failure for coatings thicker than 3.5 mm. This happened because, with the present facility, in order to build up thick coatings, spraying process have to be interrupted to avoid overheating of the coatings and build up of residual stresses. This interruption of spraying will cause the coating to build up in layers, and too many layers will reduce the cohesive strength within the coating.

From Figures 66 and 68, it can be seen that repairs with substrate and repair material of similar type (eg. D2 coated with D2 match powder or Stainless steel coated with stainless steel) can be built up to a thickness of 3.5mm or greater. This is because both the substrate and the repair material have similar thermophysical properties, and residual stresses for similar type substrates and coating material combinations are lower compared to those with dissimilar substrate and coating materials.

In the test carried out on the repair of D2 steel substrate using WC-Co powder, none of the repair were successful for a repair wall angle of less than 45 degree, where it was observed that the sprayed particles bounced off the substrate. The hard WC-Co will bounce off the hard D2 tool steel substrate unless it is sprayed with a deposition angle of 90 degrees to the substrate. No graph could be plotted for these samples due to insufficient data.

2) Effect of pre-spray temperature on bond strength

All the test samples in this category were repaired using the spraying parameters designed for each individual type of powder. Only the pre-spray temperature was varied. All samples had a 60 degree wall angle, as this wall angle was shown to produce the highest bond strength in the previous section of this work.

From the results of the bond tests carried out with components of varying pre-spray temperature (Figure 69 to Figure 71), it was found that the bond strength was increased by 15 % to 28 % if the temperature of the substrate was increased from without any pre-spray temperature to 250°C. The tool steel match powder had a similar chemical composition and hardness to the D2 steel substrate. Due to the almost identical physical properties of these two materials, the repair work was carried out with a 100% success rate, there were no coatings failure prior to the bond strength test. However, with repair work carried out on the stainless steel substrate with WC-Co powder, the success rate was reduced to about 50%, mainly due to the mismatch in physical properties of these two materials leading to the formation of residual stress within the coatings.

It was found that for the repair of D2 steel with tool steel match powder there were only two cases of cohesive failure, and two cases of glue failure out of 80 samples. The repair of stainless steel with stainless steel powder, there were two cases of glue failure out of 80. But in the repair of stainless steel with WC-Co all the coating with coating thickness of 2mm debonded from the substrate before the test, the bond strength of 1.5 mm repair thickness was improved by almost 50% with pre-spray temperature of 250°C, but this value was only half the bond strength of the 0.5mm repair thickness.

The scatter was large for results on WC-Co repair, (36%-48%), this was due to the mismatch of the substrate and repair material. But scatter of between 2.5% - 7 % was found for those repairs which have been carried out on the substrate and repair material of the similar type.

From results presented, it can be concluded that an undercutting wall angle of 60 degrees usually produced the highest bonding strength, as it is always recommended that, if possible, the spraying direction should be kept at right angles to the substrate surface in order for the sprayed particles to splat fully. Spraying with a lesser angle will cause the sprayed particles to deflect away or not splat properly. The splat formation of sprayed particles has also been linked to the residual stresses on the coating produced [101]. Leger et. al [102] carried out test on the particle splat formation of ZrO_2 powder on stainless steel substrate tilted at 60 degree, found that the sprayed particles formed a long narrow splat, as shown in Figure 72.

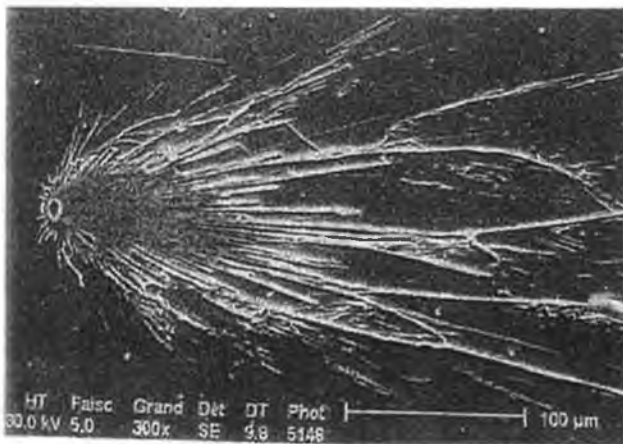
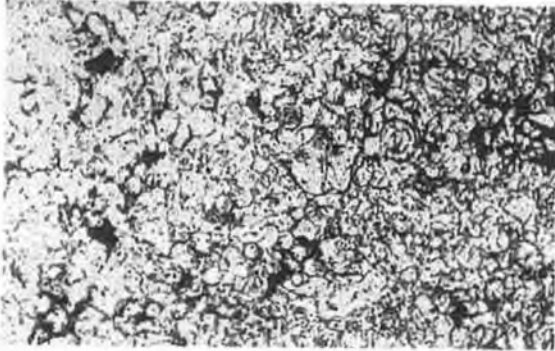


Figure 72 Zirconia particle sprayed on stainless steel substrate tilted at 60 degree [102].

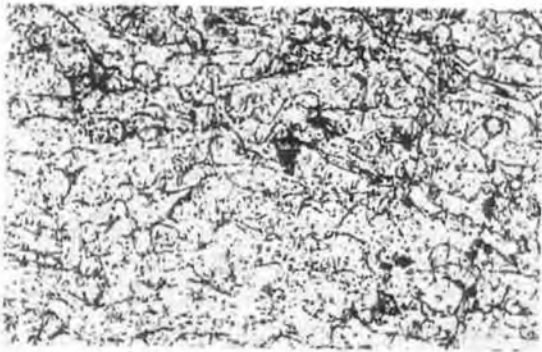
All the repaired material on sample with small wall angle had a weaker bond strength compared with those with wider angle. This confirmed that the way that the sprayed particles splat at impact on the substrate surface have direct effect on the mechanical interlocking of each layer of lamellae sprayed. Two samples were prepared, both are tool steel match powder on D2 steel substrate but with 15 and 60 degrees deposition angle respectively. The cross section microstructure of each coating was studied using a high power optical microscope. It was observed that the sample which was sprayed with a deposition direction of 60 degrees to the substrate has larger splat of deposited

material as compared to the sample sprayed with a 15 degrees wall angle. Photographs taken for these samples are shown in Figure 73 and 74. More voids and oxide inclusion were also found in sample sprayed with 15 degree deposition angle (Figure 73) due to the excessive splat of the sprayed particle.



X150 magnification

Figure 73 Cross section view of coating sprayed with 15 degree deposition angle.



X150 magnification

Figure 74 Cross section view of sample sprayed with 60 degree deposition angle.

From the above results, it was also found that the substrate pre-spray heat temperature also affects the bond strength of the repaired material. According to Bianchi et.al.[103], a fully spread sprayed particle has a higher cooling rate which will cause less residual stress within each lamella layer. Additionally, a fully spread particle will give a higher bonding area between each sprayed layer. Figure 75 shows a picture of single splat of Zirconia on substrates with different pre-spray temperature [102]. On diagram a, the splat is almost perfectly lenticular with substrate pre-spray temperature of 300°C. In diagram b, the shape is close to disk shape with few "fingers" corresponding probably to the cooling down of the particle surface resulting in a bursting of the underneath liquid upon impact. When the particles were sprayed on a

relatively cold substrate (pre-spray temperature of 75°C), diagram c, the splat was extensively fingered with a good contact with substrate only in their central part. In the a & b case, the mean diameter of the splat is about $100\mu\text{m}$ as against $60\mu\text{m}$ in the case of C.

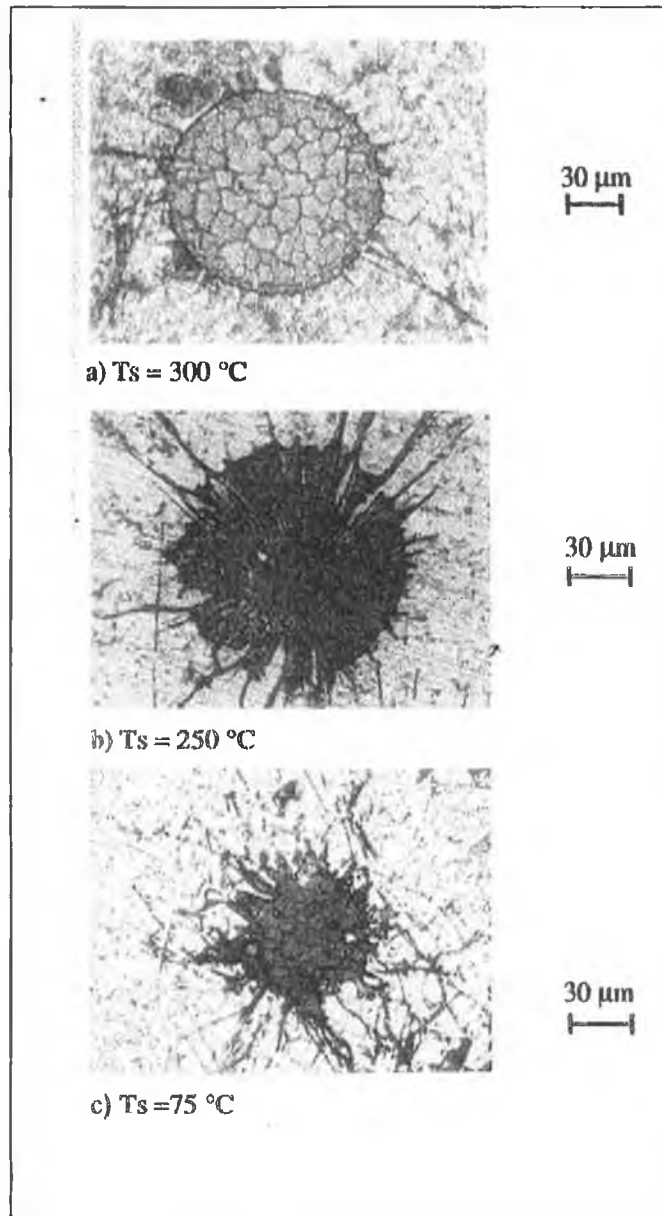


Figure 75 Splats collected on smooth ($R_a=0.2\mu\text{m}$) substrate at different temperature [102].

2) Three point bending test

The bend test adopts a fracture mechanics approach to the evaluation of crack propagation and is based on defining adhesion in terms of a stress intensity factor, K , or strain energy release rate, G . The experimental method and related theory are described in Chapter 4. Tests were carried out to study the fracture resistance strength of repaired components using the three point bend test, for both stainless steel powder on stainless steel substrate and D2 match powder on D2 tool steel substrate.

All samples were repaired with spraying parameters according to the spraying data table in Appendix A, unless otherwise stated. All specimens have the dimension of 75mm x 10mm x 3.5mm (length x width x thickness). A groove of different depth, from 0.5mm to 2.5mm was machined on each sample. After spraying, the samples were ground on all sides adjacent to the surface of the deposit, in order to eliminate rounded edges. Maximum load was recorded when the test sample started to fracture. Figure 76 shows a picture of some of the test specimens. Measurements were taken for six samples in each category and the average of the six values were used to graph results.

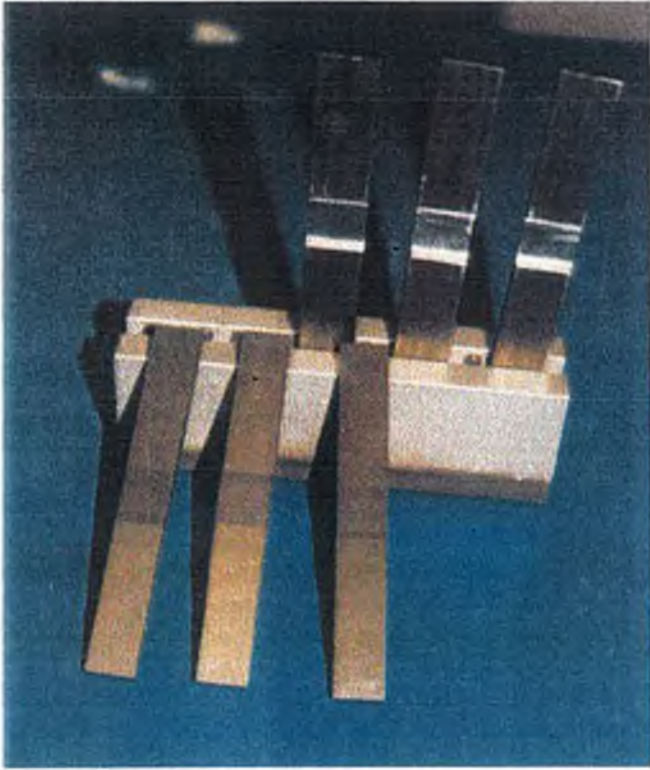


Figure 76 Specimens for three point bend tests.

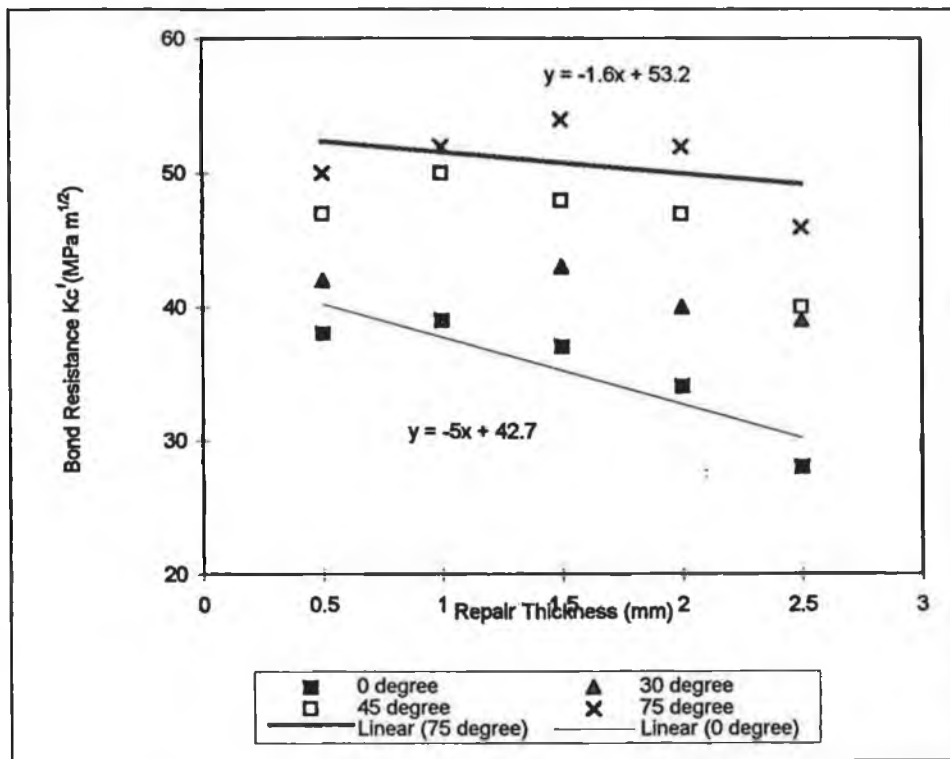


Figure 77 Bond resistance Vs repair thickness at pre-spray temperature of 100°C for various wall angles, stainless steel powder on stainless steel substrate.

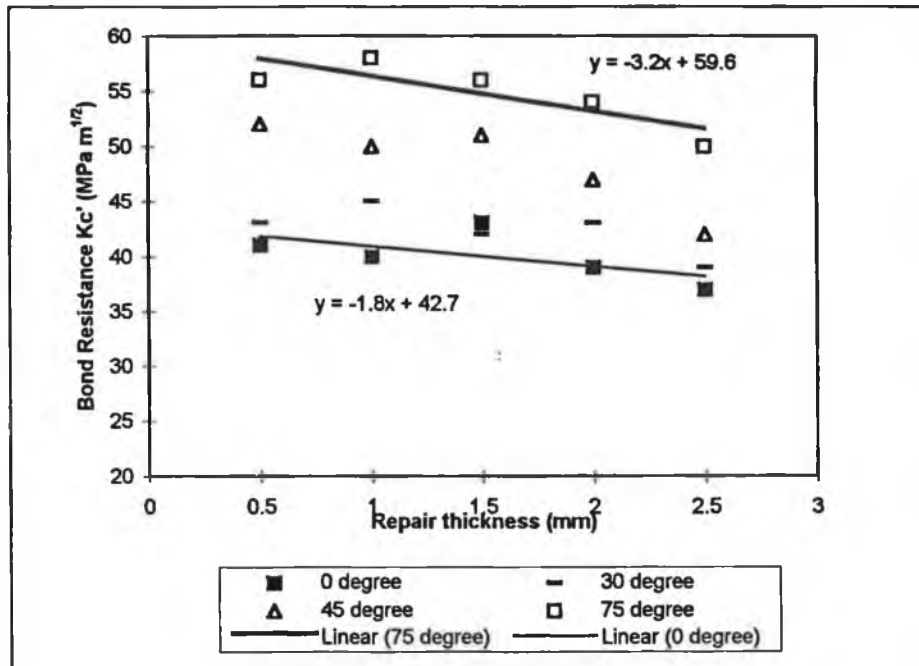


Figure 78 Bond resistance Vs repair thickness at pre-spray temperature of 200°C for various wall angles, stainless steel powder on stainless steel substrate

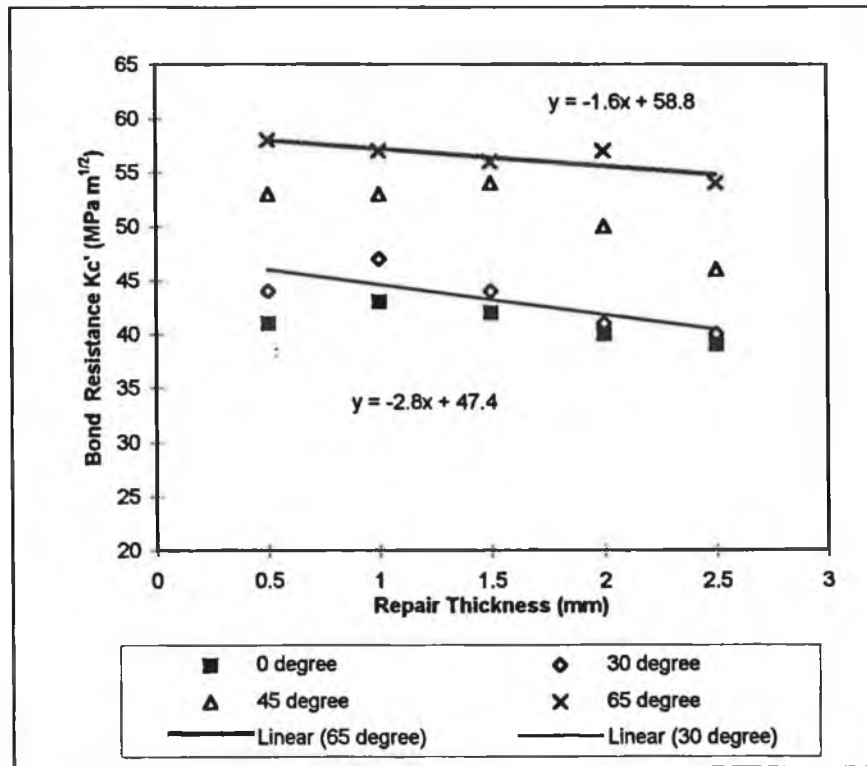


Figure 79 Bond resistance Vs repair thickness at pre-spray temperature of 250°C for various wall angles, stainless steel powder on stainless steel substrate

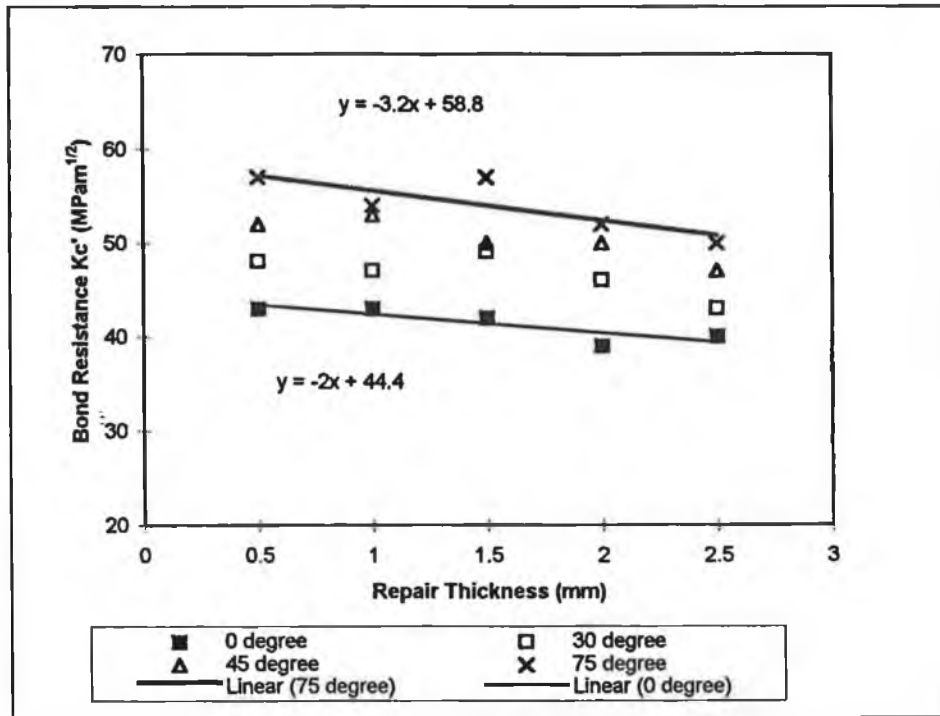


Figure 80 Bond resistance Vs repair thickness at pre-spray temperature of 100°C for various wall angles, D2 tool steel powder on D2 tool steel substrate

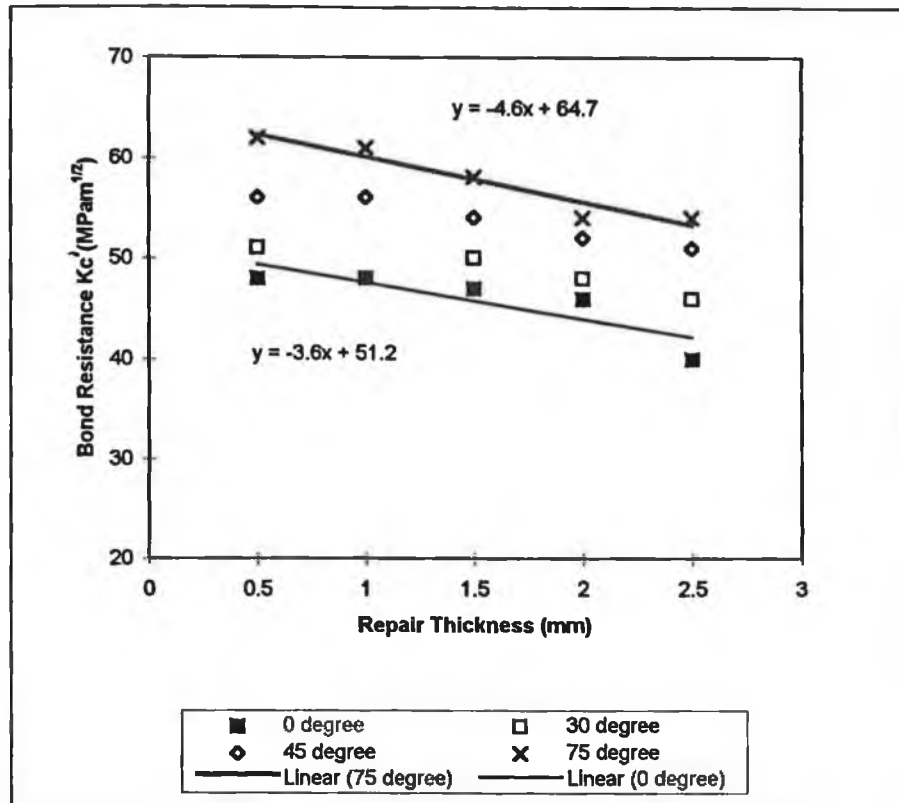


Figure 81 Bond resistance Vs repair thickness at pre-spray temperature of 200°C for various wall angles, D2 tool steel powder on D2 tool steel substrate

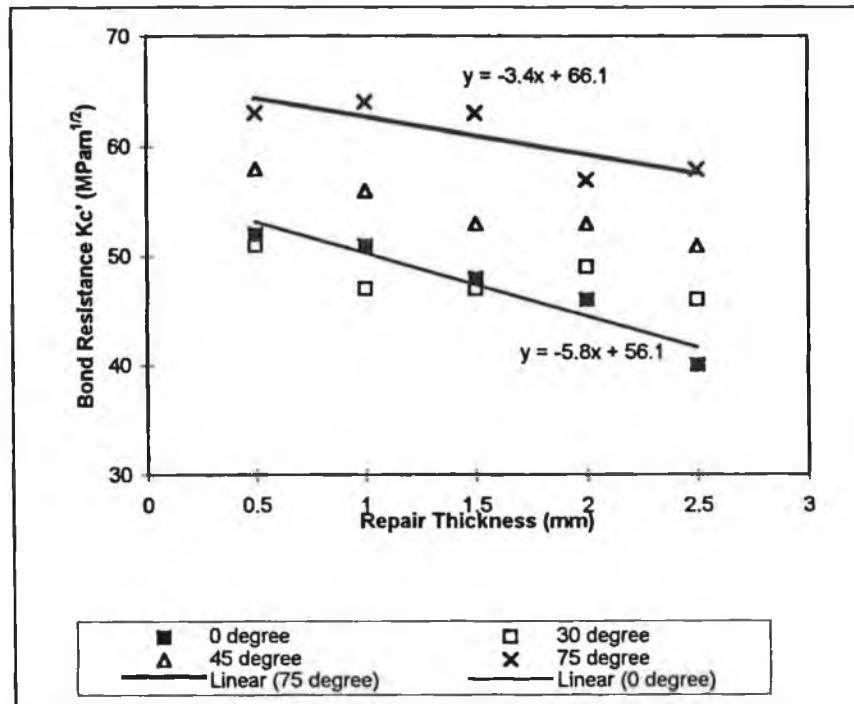


Figure 82 Bond resistance Vs repair thickness at pre-spray temperature of 250°C for various wall angles, D2 tool steel powder on D2 tool steel substrate

Discussion of results

This three point bend test uses the concept of fracture mechanics to determine the adherence of a coating to its substrate. Figure 77 to 79 show the results of bend tests for the repair of stainless steel substrate with stainless steel powder for different pre-spray temperatures. It was observed that for the samples with 100°C pre-spray heat treatment (Figure 76), there was an average increase of 30% in fracture resistance by increasing the sample wall angle from 0 degree to 75 degree wall angle. There was an even bigger increase in fracture resistance (40%) for the similar condition if the pre-spray temperature was increased to 250°C. For all the results, there was a general decrease in fracture resistance value for repairing wall angle of 0 degree and 30 degree, as the repair thickness was increased from 0.5mm to 2.5mm. For 0 degree wall angle,

3) Effect of various surface treatment on bond strength

Substrate surface preparation plays a very important role in the bond strength of thermally sprayed coatings. Tests were carried out to compare the bond strength of similar repairs with two different types of surface preparation 1) Sand blast roughened surface and 2) Electrode discharge machining roughened surface. The roughness of grit blasted surface is between Ra 6-15 μ m. The roughness of this EDM created surface is approximately between Ra 400-750 μ m. All other spraying parameters were kept constant. The results are presented using the average values of four samples.

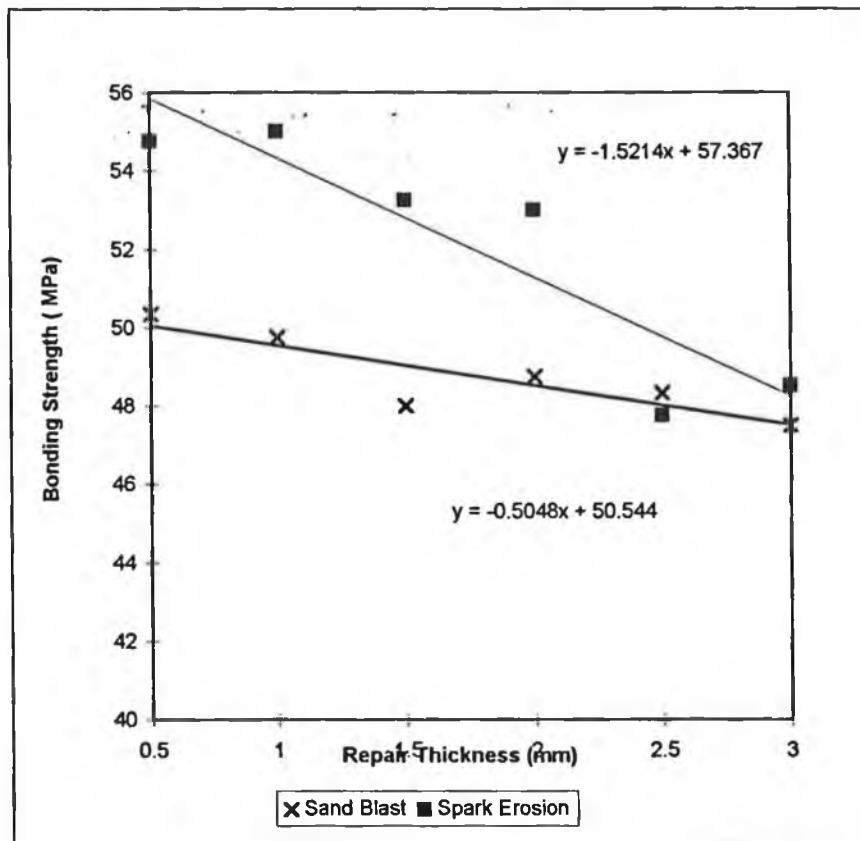


Figure 83 Bond Strength Vs repair thickness for two types of substrate surface preparation, D2 base powder on D2 tool steel substrate.

Discussion of results

In thermal spray coatings, substrates to be coated are usually sand blasted with alumina grit to roughen the surface. Many lamellae on the roughened surface are, to a degree attached to the substrate by the force resulting from the shrinkage of the liquid wrapped around surface irregularities as shown in Figure 84. As the deposited material shrinks, the lamellae tend to interlock the peak of the roughened surface and hence improve the bond strength. A rougher substrate also allow the possibility of diffusion between the substrate and the deposited lamellae on certain substrate material eg. aluminium

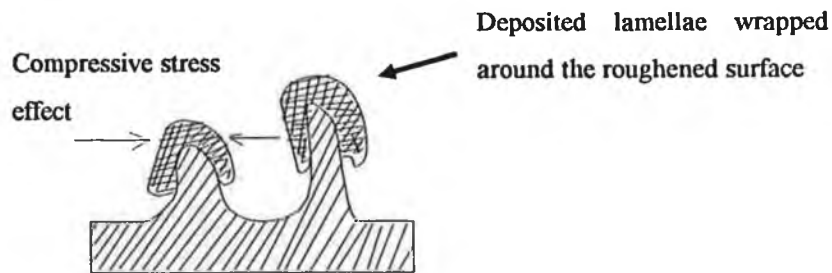


Figure 84. Mechanical interlocking effect of sprayed lamellae on roughened surface.

The effect of the EDM roughened surface on the bond strength results were compared with the sample roughened by the sand blasting procedure. It was found that (Figure 83) the bond strength of the samples with the surface roughened by the EDM method obtained an average increase of 10% in the bond strength, but when the coating thickness 2.5mm or greater, the surface preparation had very little effect on the bonding strength.

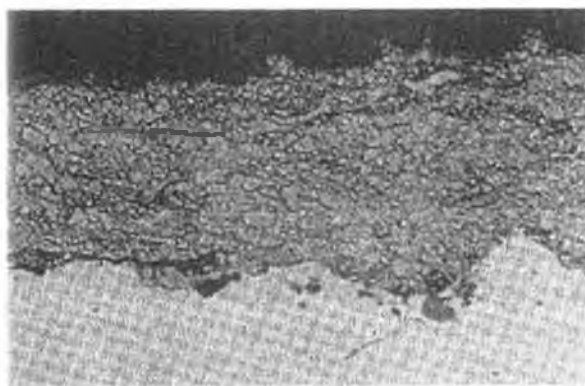
Figure 85 shows a cross section tool steel base powder coating on D2 tool steel for a normal sand blasting roughened substrate surface. Figure 86 shows a similar coating on a EDM roughened substrate surface. It can be seen on Figure 86 that on the EDM roughened substrate, the sprayed particles spread around the wider crest surfaces

created by the EDM process. The bond strength is higher on such surface because the residual stresses on such surfaces is usually in favour to the coatings because stresses have been broken into smaller components, along each side of each groove, they react on the opposite direction and can cancel each other. (Figure 87)



x 150 magnification

Figure 85 Tool steel base powder Coating on D2 Steel with sand blasting surface roughened



x150 magnification

Figure 86 Tool steel base powder Coating on D2 steel with EDM spark eroded substrate surface

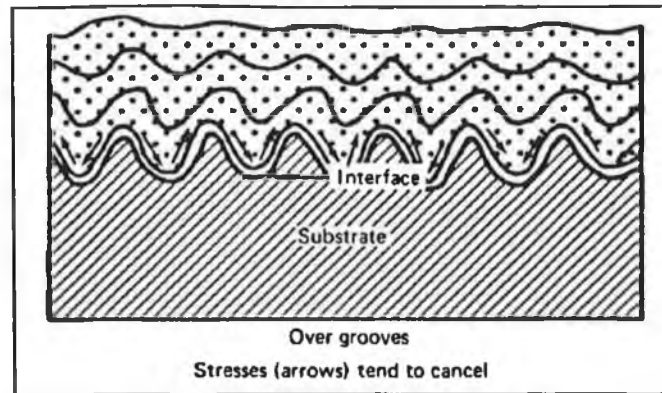


Figure 87 Schematic diagram of direction of stresses in a grooved surface.

4) Effect of different post spray heat treatment on the bondstrength.

Post repair heat treatment plays an important role in preventing the generation of sudden internal stresses after spraying due to the different contraction rates of the substrate and the coating in air. Tests were carried out to study the effect of different post spray heat treatments on the bond strength of the repaired material to the substrate. All the repaired samples for this test were transferred immediately after the repair work to a pre-heated furnace (450°C) for heat treatment, as the temperature of the spraying process is usually between 400-500 °C. All the repair work was carried out using parameters according to the spraying data parameter table in Appendix A. All damaged components were heat treated to 200°C prior to deposition.

The results were plotted in Figure 88-90 using the average values of four samples.

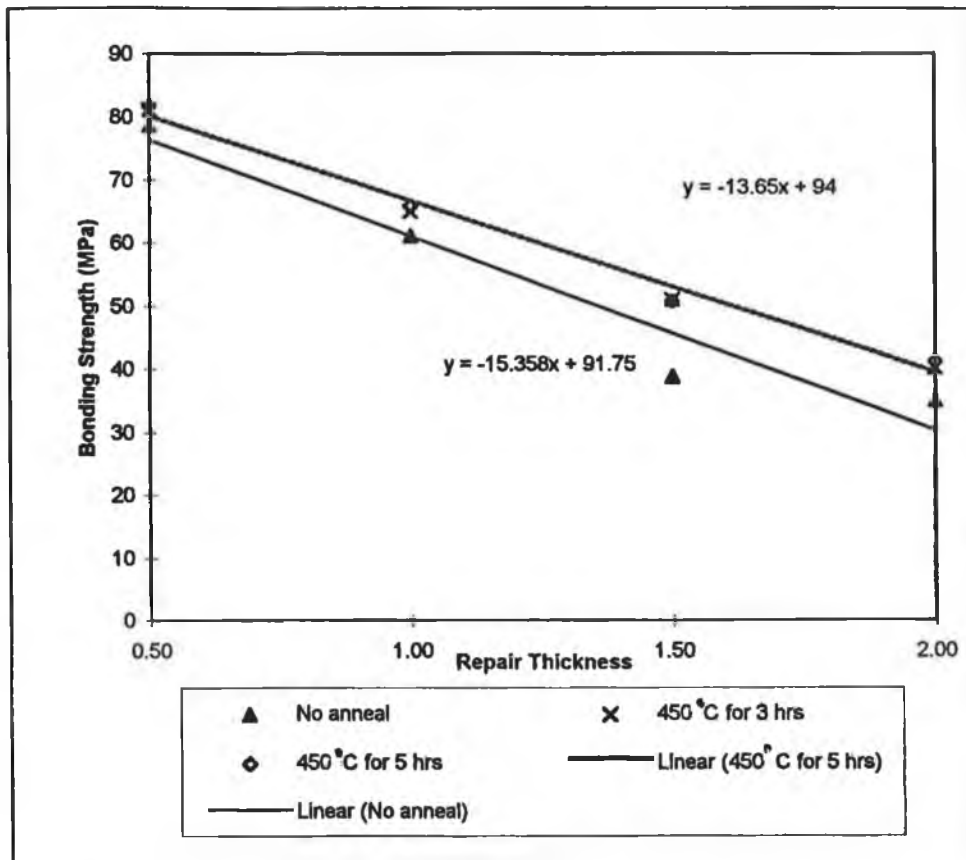


Figure 88 The effect of post spray heat treatment on bond strength for WC-Co on stainless steel substrate.

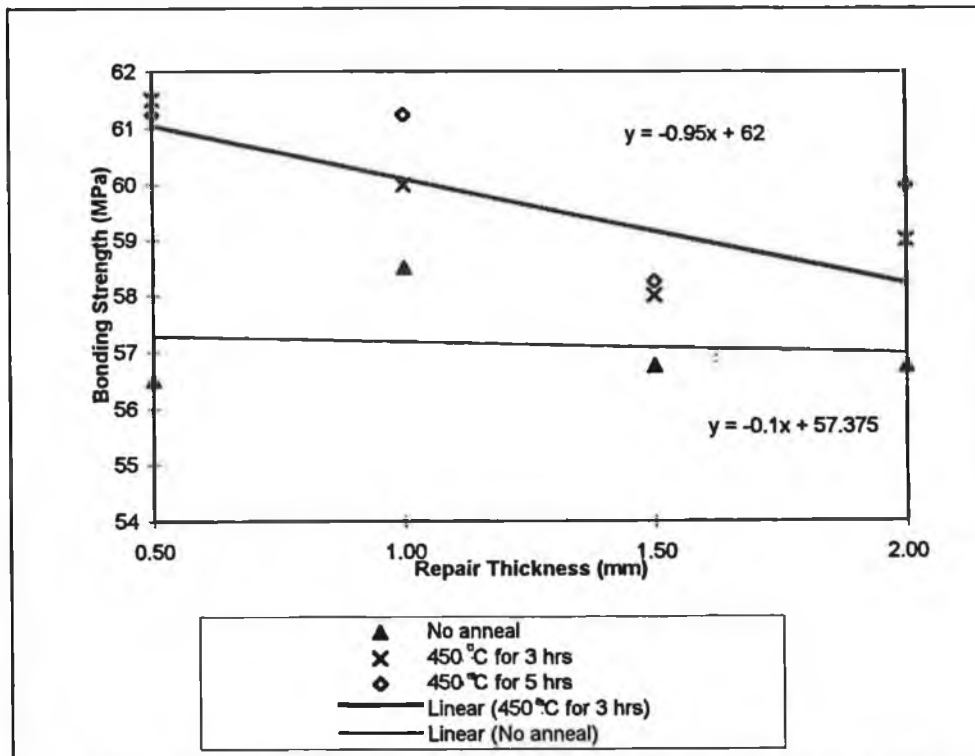


Figure 89 The effect of post spray heat treatment on bond strength for stainless steel powder on stainless steel substrate.

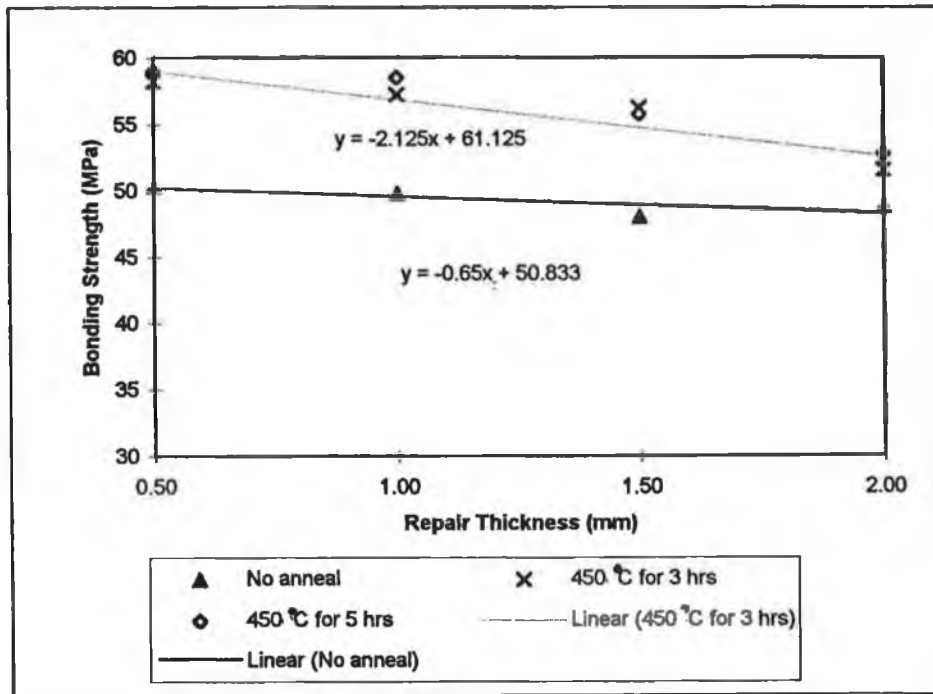


Figure 90 The effect of Post spray heat treatment on Bond strength for Tool steel base powder on D2 tool steel substrate.

Discussion of results

From the results (Figure 88 to 90) it can be seen that there is an increase of average 5-10 % in the bonding strength for samples post spray heat treated for 450°C for 3 hrs. Only samples of stainless steel substrate and coating showed an improvement for post spray heat treatment for 5 hrs. The results scatter value is between 10-18%.

The thermal stresses are generated when the coating and the substrate cool down after the deposition process and are due to the mismatch of their thermal expansion coefficients (TEC). The sudden change in the thermal expansion mismatch will lead to coating failure. This stress can be minimized if the cooling process of the coated samples can be controlled. One of the most effective ways is to transfer the coated material into a preheated furnace immediately after the spraying process.

5.4 Statistical Analysis of Results

This section provides a summary of all the tests carried out in this thesis. All the experimental data obtained from various tests on the characterisation of the coating or repair quality were input into SPSS (Statistical Package for Social Science) for statistical analysis.

SPSS is a comprehensive statistical analysis and data management system. Each column in SPSS representing a variable, and has to be assigned a value label, eg.

1= coating with combination of WC-Co powder on Stainless Steel substrate

2= coating with combination of Stainless Steel powder on Stainless Steel substrate

A full detail of the all coded variables are shown in Appendix A.

Summary of experimental investigation:

A total of 977 samples were analysed using the SPSS. Graphs were then plotted in order to give a view of general changes in coatings properties as the spraying parameters are altered.

One way analysis of variance (ANOVA) was also used to rank the degree of influence of each varying parameters on the individual coating property such as bond strength, residual stress. In the one way analysis of variance, the following assumptions were made:

- Each of the groups is an independent random sample from a normal population.
- In the population, the variances of the groups are equal.

One way analysis of variance test calculates two estimates of variability in a population: the within-group mean square and the between-group mean square. The within-group mean square is based on how much the observation within each group vary. The between-group mean square is based on how much the group means vary among themselves. The statistical test for the null hypothesis that all group have the same mean in the population is based on the ratio, called an F statistic. This F-ratio is the value of the ratio of the between-group mean square value to the within -group mean square value. This F- ratio is used to rank the impact of each spraying parameter on the coating property.

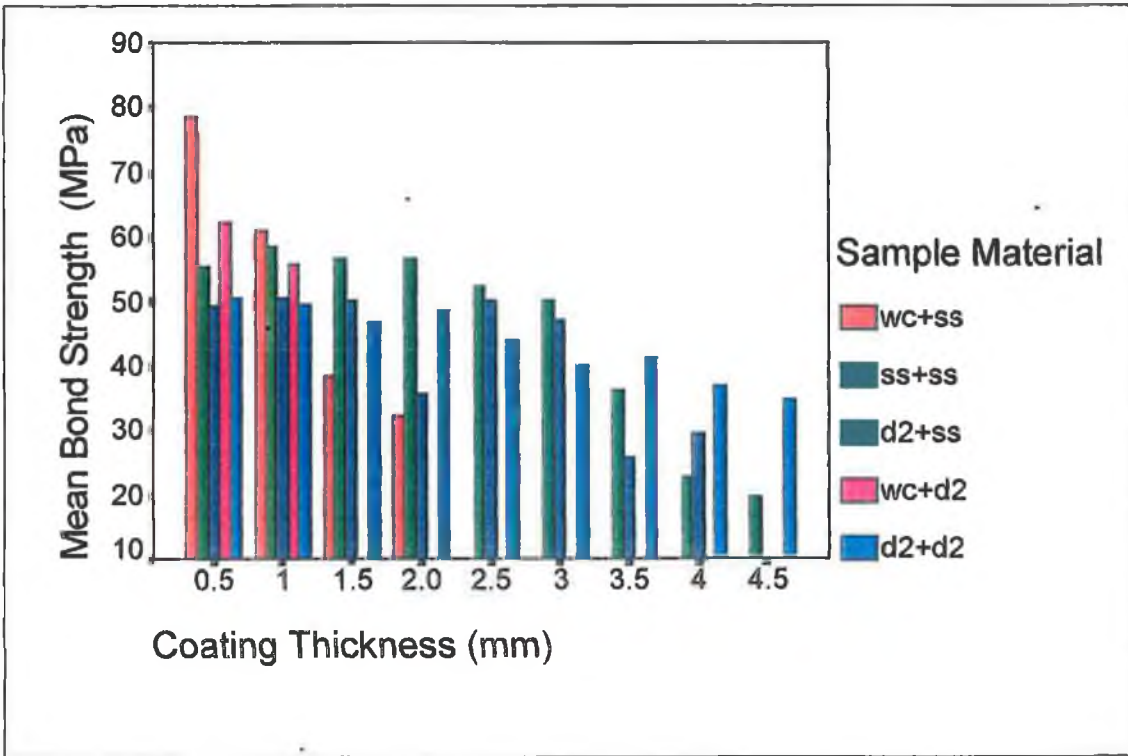


Figure 91 Relationship of coating thickness against mean bond strength for various spraying powder and substrate combinations.

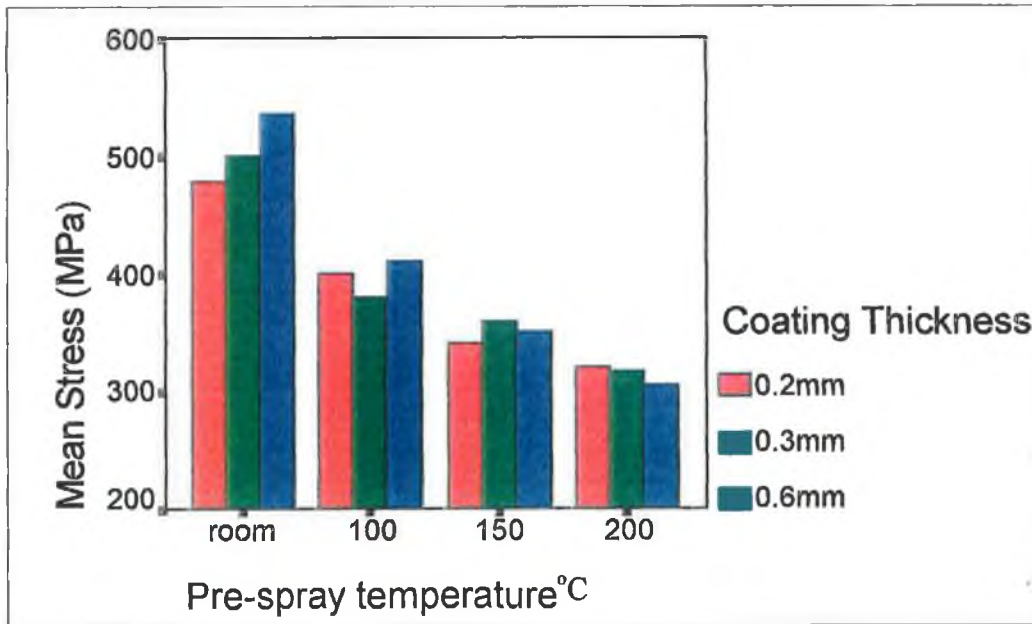


Figure 92 The effect of pre-spray temperature on the mean stress value for various coating thickness for all combinations of substrate and coating materials.

The general relationship of the coating thickness against the mean bond strength for various combination of substrate and the coating material is shown in the Figure 91. As the influence of coating thickness is the main concern here, the mean bond values calculated for the particular thickness is the average value of all bond strength measured. Other spraying parameters which have influence on the bond strength value are discounted. The bond strength values at the Y-axis are the average bond strength for each type of material combination. From the results it can be seen that only coatings with similar material both substrate and coating (tool steel match powder on tool steel substrate and stainless steel powder on stainless steel substrate) were successfully deposited up to a thickness of 4.5mm. The mean bond strength for these two material combinations also show a constant gradual decrease as the thickness of the coating increases. The WC-Co coating shows the highest mean bond strength but the coating thickness is the dominant factor affecting its bonding strength.

Figure 92 shows the general behaviour of the residual stress as the coating thickness increases for various pre-spray substrate temperatures. Results show a general stress decrease as the pre-spray temperature increases. There is an average of 20% decrease in stress when the pre-spray substrate heat temperature of 100°C is introduced.

Analysis of variance (ANOVA) was carried out to determine which is the more influential factor on the stress in the coating: the coating thickness or the pre-spray substrate temperature. The results shows that the pre-spray substrate temperature has a higher F-ratio, is therefore more influential on the residual stress than the sprayed coating thickness. The results of the ANOVA analysis is shown in Appendix C.

The dependence of average bond strength value on various spraying parameters for all the repaired samples are shown in Figure 93 to 97.

Figure 93 shows the effect of coating thickness on the mean bond strength of repaired material for all combinations of substrate and sprayed material. As the influence of coating thickness is the main interest here, the mean bond values calculated for the

particular thickness is the average value of all bond strength measured. Other spraying parameters which have influence on the bond strength value were disregarded.

It can be seen that the WC-Co spray material can only be built up to a thickness of 2.0mm, whereas those samples of similar material for the substrate and repair material can be repaired up to a thickness of 4mm. As the repair thickness increases the bond strength of the repair material to the substrate decreases, eg. the bond strength of stainless steel substrate repaired with stainless steel material shows about 50% reduction in bond strength as the repair thickness was increases from 0.5mm to 4mm.

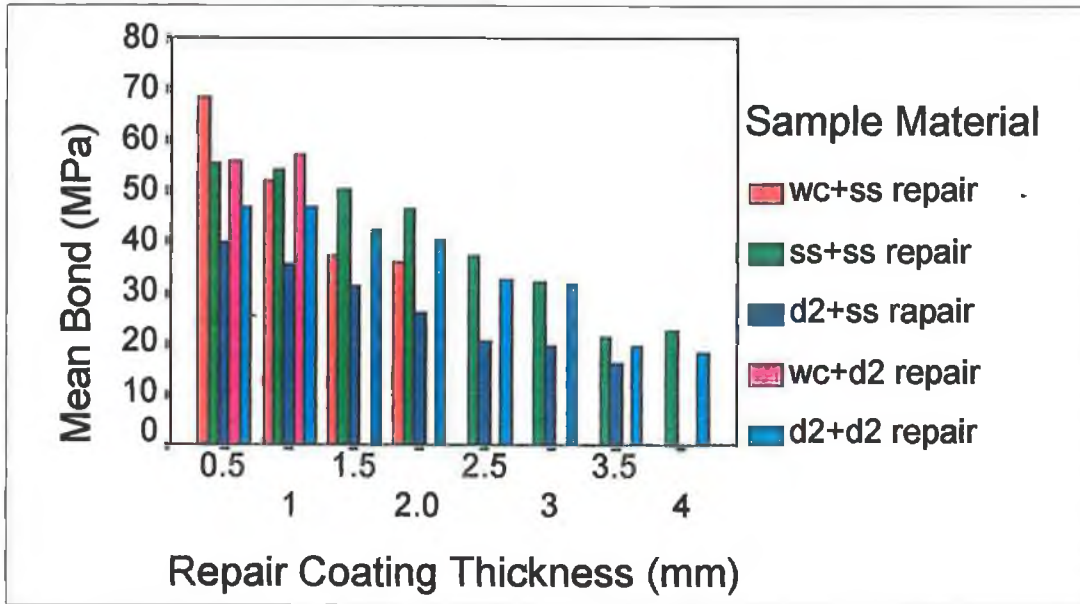


Figure 93 Relationship of coating thickness against mean bond strength for various spraying powder and substrate combinations repair sample

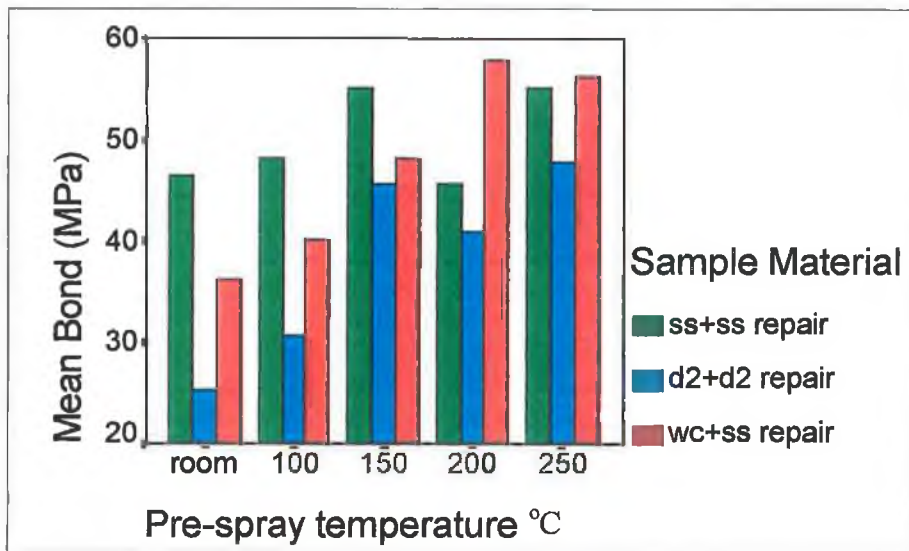


Figure 94 The effect of pre-spray substrate temperatures on the mean bond strength of various sample materials.

Figure 94 shows the effect of different pre-spray substrate temperatures on the mean bond strength for three substrate and repair material combinations. The average bond strength was greater as the pre-spray temperature was increased.

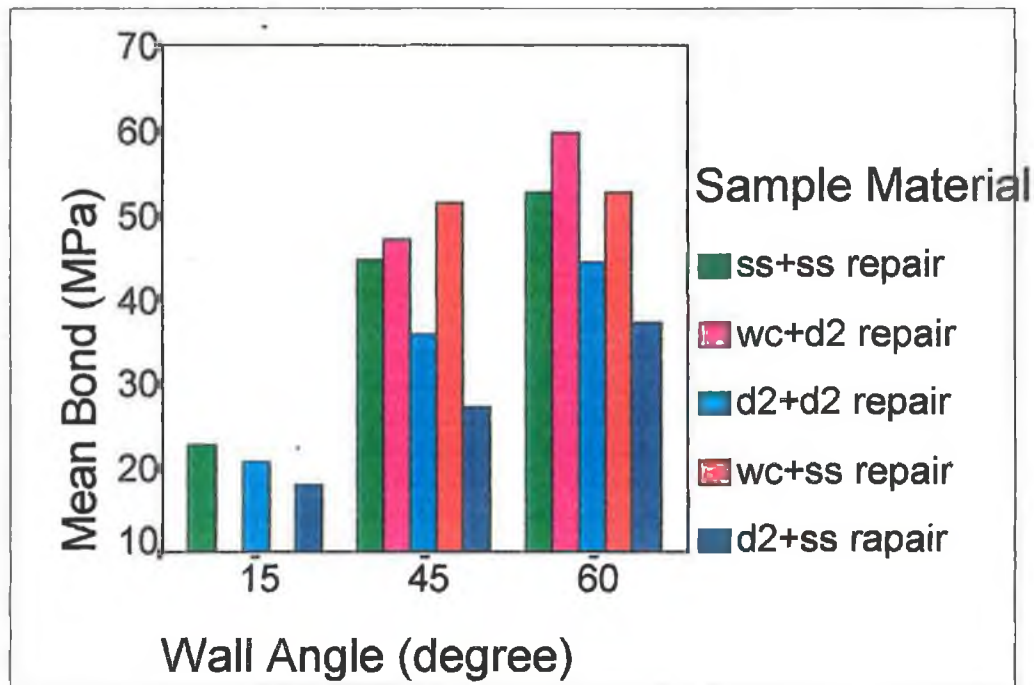


Figure 95 The effect of sample wall angle on the mean bond strength for various sample materials.

It can be seen from the above graph that bigger wall angle of the repair sample is essential for obtaining higher bond strength of the repaired material onto the substrate. All the samples for WC-Co repair material cracked prior to bond strength tests for the wall angle of 15 degree. As undercutting is necessary on mechanical parts that are to be rebuilt, the wider angle of the machined groove will produce higher bond as seen in the above graph for all combinations of substrate and repair materials.

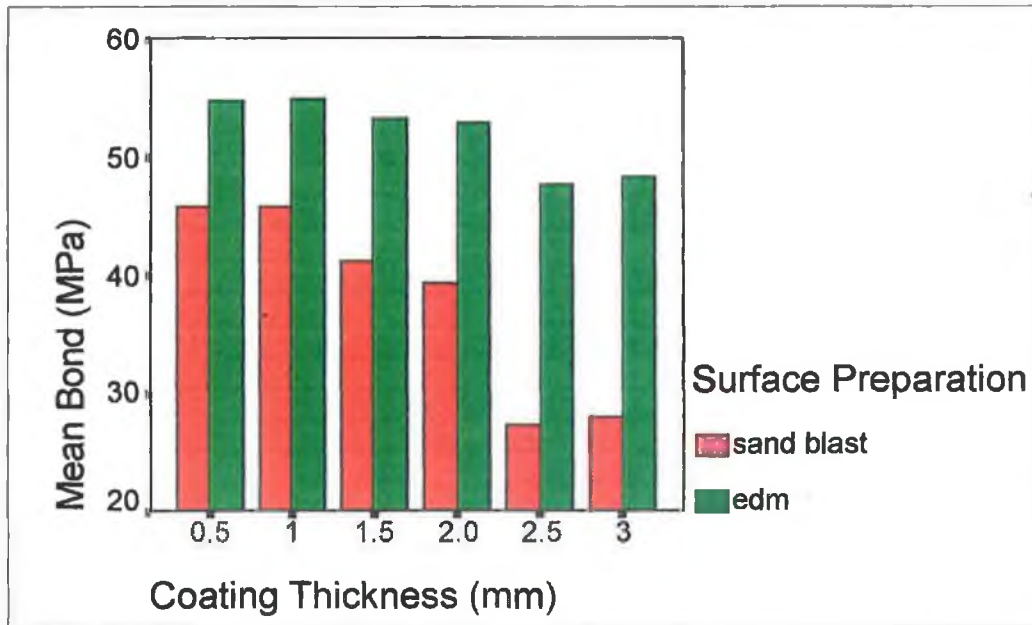


Figure 96 The effect of sample wall angle on the mean bond strength for D2 substrate repaired with D2 match powder material.

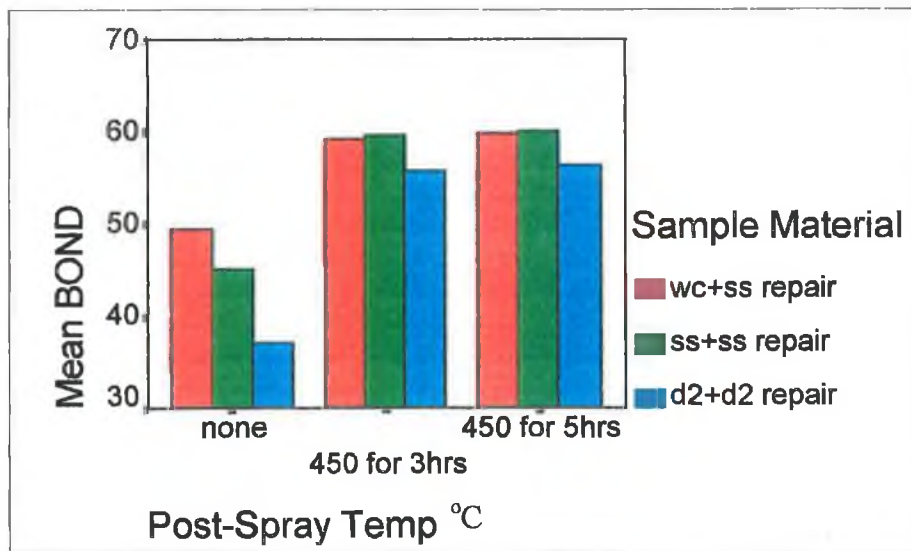


Figure 97 The effect of post-spray heat treatment on the mean bond strength for various sample materials.

Figure 96 and 97 show the effect of the two different substrate surface preparation and sample post-spray heat treatment on the average bond strength of the repaired material. In Figure 96, samples with the EDM roughened surface show larger increase in mean bond strength for higher repair thickness. Figure 97 shows the effect of post-spray heat treatment on the average bond strength. The mean bond strength was found to be higher for samples treated in the furnace after the repair was carried out. This process will reduce the sudden changed of contraction rate of the coating and the substrate material which will generate residual stress if the repaired sample is cool down slowly in the furnace.

Analysis of variance (ANOVA) was carried out on all the repair samples to determine which spraying parameter influences most the bond of the repaired material to its substrate. The following table summarises the results of the ANOVA at a confidence level of 95%. The influence of the spray parameters have been ranked from the most influential (rank #1) to the least according to the F-ratio obtained from the ANOVA analysis. The results from the three point bend test on the fracture resistance of the repair samples is also included in the table below. Detail results is shown in Appendix C.

Sample parameter	Bond Strength (MPa)	Fracture Toughness (MPam ^{1/2})
Substrate wall angle	#1	#1
Repair thickness	#2	#3
Sample post-spray heat treatment	#3	
Pre-spray substrate temperature	#4	#2
Sample surface preparation	#5	

Table 15. Results of ANOVA analysis for all the repair samples.

By running the ANOVA analysis on the experimental data on the fabrication of free standing components, it was found that the sprayed powder flow rate is the more influential parameter compare with the spraying distance in affecting the residual stress within the fabricated component

CHAPTER 6 CONCLUSIONS AND RECOMMENDATIONS

6.1 Conclusion:

In this study, the experimental investigation to optimise the High Velocity Oxy-Fuel thermal spray process for coating, forming and repair of components were conducted. The conclusions resulting from the current study are summarised as follows:

- The use of HVOF process to fabricate free standing components of various sizes and shapes is possible.
- Residual stresses in solid components can be controlled by annealing.
- The average bond strength greatly reduces as the thickness of coating increases from 0.5 to 4 mm
- Coatings can be successfully deposited to a thickness of 4mm or greater on substrate of similar material.
- Residual stress can be greatly reduced if the substrate is heated prior to spraying.
- Residual stress increases as the coating thickness increases. There is a strong correlation between residual stress and bond strength as they are both affected by coating thickness.
- For the repair of damaged components, the shape of the prepared surface is the most influential parameter.
- Post sprayed heat treatment and substrate surface preparation increase the bond strength of coatings.

6.2 Thesis Contribution

This work has furthered understanding of the HVOF process and parameters required for optimising the quality of coatings and formed and repaired components. The work also demonstrates that the HVOF process can be used to produce free standing components of industrial relevance. Furthermore, this thesis suggests that the process can be used for component repair upto a limited extent of damage.

6.2 Recommendations for future work

- As the current HVOF process is manually control, repeatability and consistency of spraying process are greatly restricted. The development of an automated spraying process would be of benefit. Other factor such as measurement of temperature, coating thickness, spraying distance and powder flow rate could be improved through the use of computerised data acquisition.
- An investigation into the use of alternative cooling devices may provide a means of overcoming residual stress and overheating problems.
- The spraying parameters which affect the coating properties have been optimised in this work. By developing computer software which utilises these data to model the process whereby coatings with desired properties may be produce at low cost.
- The use of Finite Element Analysis to predict the properties of coating may also prove beneficial.

References:

1. Chapman B.N. & Anderson T.C. " Science and Technology of Surface Coating " Academic Press, London, 1974.
2. Halling J. " Introduction : Recent Developments In Surface Coating and Modification Processes" MEP, London 1-2, 1985.
3. Bushan B. " Handbook of Tribology", Mc Graw Hill, New York, 1991.
4. Herman H., Adv. Mat. Proc. 137 (4), pp 86-92, 1990.
5. Ingham H.S., et.al, " Metco Spray Handbook (8th Edn.) Vol 1, "The Wire Process "1969.
6. Gartner F.W., et.al, Proceedings 9th Int. Thermal Spraying Conf., The Hague, p20, 1980.
7. Marantz D.E. " The Basic Principles of Electrical Arc Spraying" Chapman B.N., p308, 1974.
8. Steffens H.D., et.al, Proc. 12th Int. Thermal Spraying Conf. London, Vol 2 p61, 1989.
9. Vardelle A., et.al, " Measurements of the Plasma and Condensed Particle Parameters in a D.C. Plasma Jet" IEEE, Transaction on Plasma Science, Vol PS-8, 4, pp 417-424, 1980.
10. Vardelle M. et.al, " Study of the Trajectories and Temperature in a D.C. Plasma Jet - Correlation With Alumina Sprayed Coatings" DVS, Dusseldorf, pp 88-92, 1983.
11. Stefen H.D. et.al, Mat. Sc. Forum, Vol 163-165, pp 559-572, 1994.
12. Stefen H.D. et.al, Metall-Verlag Gmbh, Band 42, pp 236-249, Berlin/Heidelberg, 1986.
13. Ingham H.S., et.al, " Metco Flame Spray Handbook Vol 2, The Powder Process " 1967.
14. Smith R.G. " The Basic Principle of Detonation Coating " Union Carbide UK Ltd., 1988
15. Gill B., Surface Engineering, Vol 6, pp 96, 1990.
16. Heinrich P. Conf. Proc. SURTEC '91, pp 233-245, Berlin 1991.

17. Nusum P., " Application of Thermal Spraying " Proc. of NTSC, Cincinnati OH., pp 449-454, 1988.
18. Crawmer D.C. et.al, " Coating Development of HVOF Process Using Design of Experiments" Proc. Int. Thermal Spraying Conf. Florida, pp 729-734, 1992.
19. Jarosinski W.J., et.al, " Characterisation of Tungsten Carbide Cobalt Powder and HVOF Coatings " Proc. 5th National Thermal Spray Conf., California, pp 153-158, 1993.
20. Roa K.V., et.al, " Properties and Characterisation of Coatings Made Using Jet Kote Thermal Spray Technique " Proc. 11th Int. Thermal Spray Conf., Montreal, Canada, pp 873-882, 1986.
21. Provox X., et.al, "Comparative Studies of Microstructure, Residual Stress Distribution and Wear Properties for HVOF and APS WC-Co Coatings " Proc. 5th National Thermal Spray Conf., Anaheim, California, pp 159-166, 1993.
22. Miller Thermal Inc. Brochure of HVOF Spray System. 1988.
23. Kowalsky K.A., Marantz D.R., et. al " HVOF Particle, Flame Diagnostics and Coating Characteristics " Proc. 3rd National Thermal Spray Conf., CA, pp 587-596, 1990.
24. Thrope M.L, Richter H.S. " Pragmatic Analysis and Comparison of The HVOF Process " Proc. Int. Thermal Spray Conf., Florida, pp 137-148, 1992.
25. Thrope R.J. and Thorpe M.C. " High Pressure HVOF - An Update " Proc. 5th National Spray Conf. CA, pp 199-204, 1993.
26. Wagner, et.al " Particle Velocity In Hypersonic Flame Spraying of WC-Co" Surface Technology, 22, pp 67-71, 1984.
27. Hackett C.M., et.al " on The Gas Dynamics of HVOF Thermal Sprays " Proc. 5th National Thermal Conf. CA, pp 167-172, 1993.
28. Weber T.H. " HVOF Spraying" Mat. Sc. Forum, Vols 163, pp 573-578, 1994.
29. Greffield G.K. et.al, ' Process Gases for HVOF Spraying " Nat. Thermal Spray. Conf., Boston, pp 233-238, 1994.
30. Heinrich P., et.al "Linde Industrial Gases Brochure for Customers: Know How " Vol 1, pp 3-5, 1993.

31. Helali M. et. al " A comparative Study of Plasma Spraying and HVOF Thermal Spraying "Proc. (IMC-10), pp 377-387, Galway, Sept 1992.
32. Elsing R. et.al " Investigation of Thermal Spraying Processes Using Simulation Methods" Journal of Mat. Proc. Tech. pp 26, 1991.
33. Nicoll A.R., et. al. " The Application of High Velocity Combustion Spraying " Proc. ITSC'92, Orlando, 1992.
34. Parker D.W. et.al " HVOF Spray Technology: Poised for Growth." Adv. Mat. & Proc. Vol 4, pp 68-74, 1991.
35. Scott K.T. et.al " Thermal Spraying : Advance Surface Coating Handbook of Surface Engineering " Chapman and Hall, New York, 1991.
36. Bushan B. et.al , Handbook of Tribology, Mc Graw Hill, New York, 1991.
37. Bushah R.F." Deposition Technologies for Films and Coatings" Noyes Publication, New Jersey, 1982.
38. Pawlowski Lech. " The Science and Engineering. of Thermal Spray Coatings" Publisher Wiley, 1994.
39. C.K.Lin & C.C.Berndt "Measurement and Analysis of Adhesion Strength for Thermally Sprayed Coatings" J. Thermal Spray Tech., Vol 3, pp 75-104, 1994.
40. Datta P.K. et.al " Surface Eng. Vol 3: Fundamentals of Coatings" Royal Soc. of Chemistry, Cambridge, 1985.
41. Levistein M.A. et.al " Properties of Plasma Sprayed Material" Welding Journal, Vol 40, pp 234-245, 1961
42. Ault N.N." Some Characteristics. of WC Weld Deposits" Welding Journal Vol 30, pp 144-160, 1991.
43. Berger LM. et.al " Influence of Carbide Powder Composition on Decarburization and Properties of Air Plasma Sprayed Coating" Proc. of Int. Thermal Spray Conf., Florida, pp 375-380, 1992.
44. Beczkowiak J, et.al " Tailoring Carbides and Oxides for HVOF " Proc. of Forth National Thermal Spray Conf., Pennsylvania, pp 121-126, 1991.
45. Kaufold R. et.al " Deposition of Coatings Using A High Velocity Combustion Spray Gun" Proc. Third Nat. Thermal Spray Conf., CA, pp 561-569, 1990.

46. Stover D. et.al " Residual Stress In Low Pressure Plasma Sprayed Chromia Coatings" Proc. Fourth Nat. Thermal Spray Conf. PA, USA, pp 421-426, 1991.
47. Takuichi S. et.al " Modelling of Residual Stress In Plasma Sprayed Coatings: Effect of Substrate Temperature" Surf. Coating Tech. Vol 42, pp 35-41, 1990.
48. Kawan et.al " Study on Elastics Contact and Residual Stress Measurements During Ceramic Coatings" Proc. Third National Thermal Spray Conf., CA, pp339-342, 1990.
49. Kitahara S. et.al " A Study of The Bonding Mechanism of Sprayed Coatings" J. Vac. Sc. Tech., 11, pp 747-754, 1974.
50. Nicola M.G. and Scott K.T. Surface Journal, Vol 12 (1), 1982.
51. Moss A.R. and Young W.J. "Arc Plasma Spraying" in Chapman B.N. & anderson T.C. " Science and Technology of Surface Coating " Academic Press, London, p287, 1974.
52. Baxtor C.F. and Reiter H. Proc. of Advances in Surface Coating Tech., Welding Inst., London, p23 1978.
53. Fukanuma H. "Methemathical Modelling of Flattening Process on Rough Surfaces in Thermal Spraying" Proc. of 9th NTSC, Cincinatti, Ohio, pp 647-656, Oct 1996.
54. Engel O.G., Journal of Reaserch of Nat. Bureau of Standard, Vol-54, pp 281-298, May 1995
55. Fukanuma F., Journal of Thermal Spray Tech, vol 3(1), pp 33-44, March, 1994.
56. Moreau, et.al. Journal of Thermal Spray Technology, Vol 4(1), pp 25-33, 1995.
57. Trapaga G. et. al. "Mathematical Modelling of the Isothermal Impingement of Liquid Droplets in Spraying Process" Metallurgical Transaction B, 22B, pp901-914, 1991.
58. Solomenko O.P. "Advanced Thermophysical Fundamental of Melt Microdroplets Flattening and Solidfication on a Substrate" Proc. 8th NTSC, Houston, pp 237-242, 1995.
59. Houben J. "Relation of Adhesion of Plasma Sprayed Coating to the Process Parameter: Size, Velocity and heat Content of the Sprayed Particles" PhD thesis, Technical University of Eindhoven, Holland, 1993.
60. Gruner H " Vacuum Plasma Spray Quality Control " Thin Solid Film, 118, pp 409-420, 1984.

61. Henne R, et.al " Low Pressure Plasma Spraying - Properties and Potential for Manufacturing Improved Electrolysis " Thin Solid Films, 119, pp 141-152, 1984.
62. Nakahira et.al " Anisotropy of Thermally Sprayed Coating " Proc of Int. Thermal Spray Conf., Orlando, Florida, pp 1011-1018, 1992.
63. Lewis R.E., et.al " Microstructural & Properties Improvements In 7075 and 8090 Aluminium Alloys By Spray Forming " Proc of P/M Aerospace and Defense Technologies Symposium " Metal Powder Ind. Fed., Princeton, NJ, USA, pp 185-192, 1991
64. Hayman C., Brit. Cer. Soc. Proc. No 34, pp 175, 1984.
65. Scott K.T. & Cross A.G. " Neat Net Shape Fabrication By Thermal Spraying " British Ceramic Proc., Vol 38, pp 203-211, 1986.
66. Helali M.D. Phd. Thesis, Dublin City University, Ireland, 1994.
67. Tan J.C., et.al " Fabrication and Residual Stress Measurement of Free Standing Component By HVOF Process: A Critical Review " Proc. of Advances In Materials and Processing Technologies 95, pp 1537-1547, Dublin, 1995.
68. Lewis R.E., Lawley A. " Spray Forming of Metallic Material: An Overview " Proc of P/M Aerospace and Defense Technologies Symposium " Metal Powder Ind. Fed., Princeton, NJ, USA, pp 173-184, (1991).
69. Metco / Perkin Elmer " Diamond Jet System and Gun Manual " 1989.
70. Metco/ Perkin Elmer " Hand Note " 1989.
71. Pawlowski L. " The Sc. of Thermal Spray Coatings" Publisher Wiley, 1994.
72. ANSI " Safety Document for Welding and Thermal Spraying" Z49.1, 1994.
73. Metco / Perkin Elmer "Diamond Jet Safety Measures" Diamond Jet Gun Manual, 1989.
74. ASTM E376-69 " Standard Practice for Measuring Coating Thickness By Magnactic-Field Eddy-Current Test Method" 1969.
75. Yost F.G. " On The Definition of Microhardness " Metallurgical Transaction, Vol 14A, pp 947-952, 1983.
76. ASM Handbook, Vol 8: Mechanical Testing, Ninth Edition, American Society for Metals, 1992.

77. ASTM C633-79 " Standard Test method for Adhesion or Cohesive Strength of Flame Spray Coatings" 1979.
78. SAE Information Report, Methods of Residual Stress Measurement- SAE J 936 " Dec. 1965.
79. Rendler N.J., et.al " Hole Drilling Strain Gauge Method of Measuring Residual Stresses" Experimental Mechanics, Vol 6, pp 577-586, 1966.
80. ASTM E837-92 " Standard Test method for Determining Residual Stresses by Hole Drilling Strain Gauge Method" 1992.
81. Prasad C.B., et.al "Determination of Calibration Constant for Hole Drilling Residual Stress Measurement Technique Applied To Orthotropic Composites" Composite Structure, Vol 8, pp 105-118, 1987
82. Suga T., Kervernes I. and Elssner, Z. Wersktofftch, 15, pp 371-377, 1984.
83. Evans A.G. "Fracture Mechanics Determination" Fracture Mechanics of Ceramics, Vol 1, Plenum Press, pp 17-48, 1974.
84. Bergmann C.P. " Influence of the Substrate Roughness on the Adhesion of Plasma Sprayed Ceramics Coatings" Proc. 7th NTSC, Boston, pp683-686, 1994.
85. Helali M, et.al " Production of Free Standing Objects By High Velocity Oxy-Fuel (HVOF) Thermal Spraying Process" Proc. of Advances In Materials and Processing Technologies, Dublin, pp 1315-1322, 1993.
86. Vardelle M, et.al " Dynamic of Splat Formation and Solidification In Thermal Spraying Processes" Proc. of 7th National Thermal Spray Conference, Boston, pp 555-562, 1994.
87. Metco / Perkin Elmer "Application Data Charts. " (1989).
88. Brandt O.C. "Measuring Residual Stress in Thermally Sprayed Coatings " Proc 8th NTSC, pp451-455, 1995.
89. Kraak T, et.al " Influence of Different Gases on The Mechanical and Physical Properties of HVOF Sprayed WC-Co" Proc. International Thermal Spray Conf., Orlando, pp 153-158, 1992.

90. J.Disam, et.al "The Influence of Coating and Substrate Temperature on the Stresses Generated at the Interface on a Stellite 21 Coating on a 13% Cr Steel During and After the LPPS Process: Theory and Experiment" Proc.of Fourth National Thermal Spray Conference, Pittsburgh, Pa USA, pp 229-236, 1991.
91. A Itoh, et.al "The Effect of Substrate Temperature During Spraying on The Properties of Sprayed Coating " Proc. 1993 National Thermal Spray Conf. Anaheim CA, pp 593-600, 1993.
92. Borisov Y., et. al. " Structure and Properties of Stainless Steel Coatings Produced by Supersonic Plasma spraying Method" Proc. 9th NTSC, Ohio, pp 757-763, 1996.
93. Voggenreiter H., et. al. " Influence of Particle Velocity and Molten Phase on the Chemical and Mechanical Properties of HVOF Sprayed Structural Coating of Alloy 316L" Proc. 8th NTSC, Houston, pp303-308, 1995.
94. Kreye H. et. al. " Microstructure and Bond Strength of WC-Co Coatings Deposited by Jet Kote Process " 11th ITSC, Montreal, Canada, pp 121-128, 1986.
95. Matsubara Y. and Tomiguchi A. " Surface Testure and Adhesive Strength of HVOF Sprayed Coatings for Rolls of Steel Mills " 13th ITSC, Orlando, pp 637-641, 1992.
96. Beczkowiak J. et. al. " Characterisation and Selection of Powder for Thermal Spraying " 2nd PlasmO, Technik Symposium, Lucerne, Switzerland, pp323-331, 1991.
97. Greving D.J., et. al. " Effect of Coating Thickness and Residual Stresses on Bond Strength of C633-79 Thermal Spray Coating Test Specimens " Proc. 7th NTSC, Boston, pp639-649, 1994.
98. Schajer G.S. " Measurement of Non-Uniform Residual Stress Using the Hole Drilling Method. Part 1 - Stress Calculation Procedure " Transaction of ASME, Vol 110, pp338-343, Oct 1988.
99. Ruud C.O., et. al. " Comparison of Three Residual Stress Measurement Methods on a Mild Steel Bar " Journal of Experimental Mechanics, pp 338-343, Dec 1985.
100. American Welding Society, " Thermal Spraying: practices, Theory and Application" 1985.
101. Fukanuma H, et. al. " Behaviour of Molten Droplets Impinging on Flat Surfaces " Proc. of 7th NTSC, pp 563-568, 1994.
102. Leger A.C., et. al. " Plasma Spray Zirconia : Relationship Between Particle Parameters, Splat Formation and Deposition Generation - Part 1: Impact and Solification " Proc. of 9th NTSC, Ohio, pp623-628, 1996.

103. Bianchi L., et. al. " Effect of Particles Velocity and Substrate Temperature on Aluminium and Zirconia Splat Formation " Proc. 7th NTSC, Boston, pp569-574, 1994.

Publications:

- 1) J.C. Tan, L.Looney & M.S.J. Hashmi “ *Fabrication and Residual Stress Measurement of Free Standing Solid Components By HVOF Process: A Critical Review*” International Conference on Advances in Materials and Processing Technologies, Dublin, Ireland, August 1995.
- 2) J.C. Tan & M.S.J. Hashmi “ *HVOF Thermal Spray: Prospect and Limitation for Engineering Application*”6th Cairo University Int. Mechanics, Design and Production Conference, Cairo, June 1996.
- 3) J.C. Tan, L.Looney & M.S.J. Hashmi “*Residual Stress Analysis of WC-Co solid Components Formed by the HVOF Thermal Spraying Process*”1996 World Congress on Powder Metallurgy and Particulate Materials, Washington D.C., USA, June 1996.
- 4) J.C. Tan, L.Looney & M.S.J. Hashmi “*Components Repair Using HVOF Thermal Spraying*” International Conference on Advances in Materials and Processing Technologies, Portugal, 1997.

Appendix A

Table A. Flow rate and pressure of different gases required by HVOF Thermal Spray System

System Unit	Type of gas	Working Pressure (Bar)	Flow Rate Required (SLPM)
Spray Gun	Oxygen	10.3	284
	Propylene	6.9	81
	Nitrogen	8.6	20
	Air	5.2	415
Powder Feeder	Air	1.4	20
Grit Blaster	Air	2 - 9	1500

Table B. Gun Setting and Spraying Parameters for different types of powder materials

	Powder Material		
	Stainless Steel	WC-Co	Tool Steel Match
Gun Setting			
Siphon Plug	2	2	2
Shell	A	A	A
Insert	3	2	2
Injector	3	2	2
Air Cap	2	3	3
Spraying Parameters			
Oxygen Pressure (Bar)	10.3	10.3	10.3
Oxygen Flow (SLPM)	265.0	278.0	265.0
Propylene Pressure (Bar)	6.9	6.9	6.9
Propylene Flow (SLPM)	71.0	74.0	73.0
Air Pressure (Bar)	5.2	5.2	5.2
Air Flow (SLPM)	318	338	325
Spraying Distance (mm)	200	150-200	220-275
Spray Rate (g/min)	38	38	38
Coverage (m ² /hr/0.1mm)	3.4	1.2	1.7
Deposit Efficiency	87%	70%	60%

Table C. Chemical Compositions of powder material

Type of Material	Chemical Composition
Tungsten Carbide- Cobolt Powder	Tungsten - 88.5% Carbide - 11.5% Cobalt
Stainless Steel Powder* (Similar to 316 stainless steel)	Nickel ✓ Manganese ✓ Silicon ✓ Molybdenum ✓ Iron ✓ Chromium ✓
Tool Steel Matching Powder	Molybdenum - 3.0% Manganese - 0.5% Iron - Balance Carbon - 1.8%

✓ Percentage not known

Table D. Chemical Compositions substrate material.

316LStainless Steel	Carbon - 0.03% Manganese - 2% Silicon - 16-18% Chromium - 10-14% Nickel - 0.045 Iron - Balance
D2 Tool Steel	Carbon - 1.4-1.6% Manganese - 0.6% Silicon - 0.6% Chromium - 11-13% Nickel - 0-3% Molybdenum - 0.7-1.3%

Appendix B

Scotch Weld Structural Adhesive EC-1386 Product Specification

Product Description:

Colour Light Cream
Solvent: None
Base: Modified Epoxy Resin

Adhesive Application:

EC-1386 can be applied by a spatula, knife coat or by extruding into place. Standard equipment is available which allow pumping directly from five gallon pails. A lower viscosity for ease of application can be obtained by warming EC-1386 to 100-120°F. Note: EC-1386 may start to thicken if held at 120°F for more than 4 hours.

Caution: Care should be taken not to incorporate air into the adhesive during application. Included air can expand during cure lead to a porous and weaken bond.

Cure Cycle:

General cure requirements:

Flow and Cure Temperature:

Normal flow and cure initiation temperature for EC-1386 are as follows:

Flow temperature: 60°F
Cure Initiation temperature: 325 - 335°F

Cure Pressure:

The only pressure required during the cure of EC-1386 is that needed to keep parts in alignment and to overcome distortion and thermal expansion in the adherents

Cure Temperature

The cure temperature may varied from 330 - 600°F, depending on the materials being bonded, equipment available and bond properties desired. EC-1386 will wet the surface to which it has been applied. Heating at temperature above 326°F will chemically converts the adhesive into a high strength solvent resistant bond.

Cure Time

Cure time depend on the cure temperature used, methods of heat application, production limitation and bond properties required. Since no two bonding operations are exactly the same, it is suggested that a few sample experiments be conducted varying both temperature and cure time to determine optimum conditions for the particular application.

Appendix C

Derivation strains and residual stress formula

To establish a relationship between the relieved strains and residual stress according to Kirsch's theory, a plane plate with a stress defined by main tension σ_1 and σ_2 (σ_1 (σ_2) is considered. ξ , and η are the directions for σ_1 and σ_2 respectively, with O as their axis origin.

Without a hole, at a point P using polar co-ordinates r , α , the stresses are (Figure.A):

$$\sigma_r = \frac{\sigma_1 + \sigma_2}{2} + \frac{\sigma_1 - \sigma_2}{2} \cdot \cos(2\alpha) \quad \text{Eqn 1}$$

$$\sigma_t = \frac{\sigma_1 + \sigma_2}{2} - \frac{\sigma_1 - \sigma_2}{2} \cdot \cos(2\alpha) \quad \text{Eqn 2}$$

$$\tau_{rt} = \frac{\sigma_1 - \sigma_2}{2} \cdot \sin(2\alpha) \quad \text{Eqn 3}$$

Where

σ_r , σ_t = normal stress component in the directions of r and t ,

τ_{rt} = shear stress normal to directions r and t

With a hole, the stresses in P become:

$$\sigma_{rf} = \frac{\sigma_1 + \sigma_2}{2} \cdot \left(1 - \frac{a^2}{r^2}\right) + \frac{\sigma_1 - \sigma_2}{2} \left(1 - \frac{4a^2}{r^2} + \frac{3a^4}{r^4}\right) \cdot \cos(2\alpha) \quad \text{Eqn 4}$$

$$\sigma_{rt} = \frac{\sigma_1 + \sigma_2}{2} \cdot \left(1 + \frac{a^2}{r^2}\right) - \frac{\sigma_1 - \sigma_2}{2} \left(1 + \frac{3a^4}{r^4}\right) \cdot \cos(2\alpha) \quad \text{Eqn 5}$$

$$\tau_{rtf} = \frac{\sigma_2 - \sigma_1}{2} \left(1 + \frac{2a^2}{r^2} - \frac{3a^4}{r^4}\right) \cdot \sin(2\alpha) \quad \text{Eqn 6}$$

The residual stresses relieved after the generation of a hole are:

$$\Delta\sigma_r = \sigma_{rf} - \sigma_r \quad \text{Eqn 7}$$

$$\Delta\sigma_t = \sigma_{tf} - \sigma_t \quad \text{Eqn 8}$$

$$\Delta\tau_t = \tau_{rf} - \tau_R \quad \text{Eqn 9}$$

The radial strain (produced by residual stresses relaxed is:

$$\varepsilon = \frac{\Delta\sigma_r - \nu\Delta\sigma_t}{E} \quad \text{Eqn 10}$$

Where:

ν = Poisson's ratio

E = Young's modulus

Equations 1,2,4,5,7 and 8 give

$$\varepsilon = \frac{\sigma_1 + \sigma_2}{E} \cdot \left(-(1 + \nu) \cdot \frac{a^2}{2r^2} \right) + \frac{\sigma_1 - \sigma_2}{E} \left((1 + \nu) \cdot \frac{3a^4}{2r^4} - \frac{2a^2}{r^2} \right) \cdot \cos(2\alpha) \quad \text{Eqn 11}$$

This is radial strain in P, a function of residual stresses, and can be written as:

$$\varepsilon_r = \frac{A_0}{E} (\sigma_1 + \sigma_2) + \frac{B_0}{E} (\sigma_1 - \sigma_2) \cdot \cos(2\alpha) \quad \text{Eqn 12}$$

with $A_0 = A'_t$; $B_0 = B'_t$, where:

$$A'_t = -(1 + \nu) \cdot \frac{a^2}{2r^2} \quad \text{Eqn 13}$$

$$B'_t = -\frac{2a^2}{r^2} \left(1 - \left(\frac{3a^2}{4r^2} \right) \cdot (1 + \nu) \right) \quad \text{Eqn 14}$$

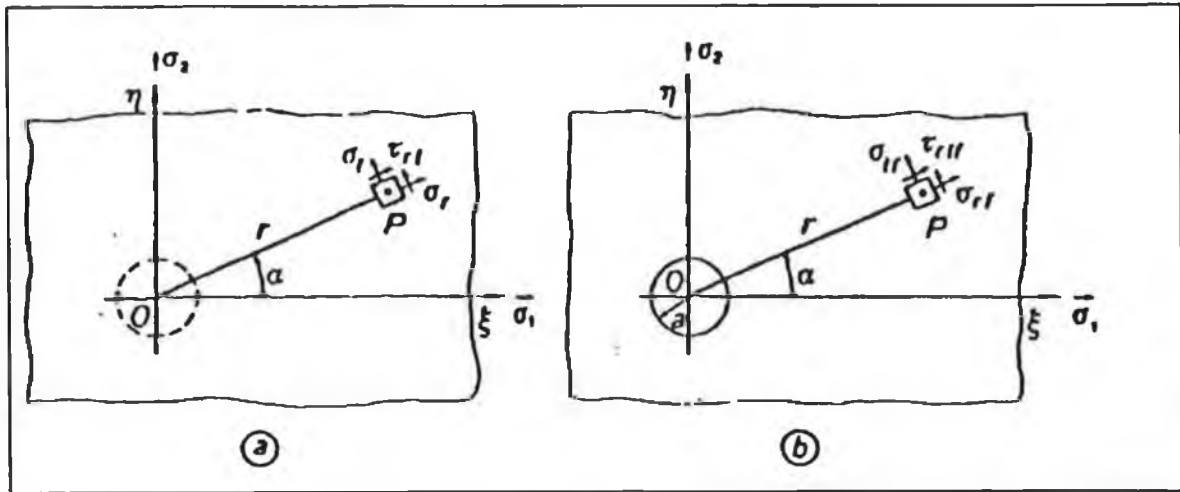


Figure A Stresses at point P (a) before and (b) after the drilling of the hole.

A strain gauge radially disposed measures the average deformation along the base

$l_0 = r_2 - r_1$ (see Figure. 36a) that is:

$$\epsilon = \frac{1}{r_2 - r_1} \cdot \int_{r_1}^{r_2} \epsilon_r dr \quad \text{Eqn 15}$$

Therefore the Eqn 12 can be written as:

$$\epsilon_r = \frac{\sigma_1 + \sigma_2}{E} \cdot \frac{1}{r_2 - r_1} \cdot \int_{r_1}^{r_2} A'_t dr + \frac{\sigma_1 - \sigma_2}{E} \cdot \frac{1}{r_2 - r_1} \cdot \int_{r_1}^{r_2} B'_t dr \quad \text{Eqn 16}$$

By integrating this equation and substitute A_0 and B_0 from Eqn 12 and A_t and B_t :

$$A_t = \frac{1}{r_2 - r_1} \cdot \int_{r_1}^{r_2} A'_t dr = -\frac{(1+\nu)}{2} \cdot \left(\frac{a}{r_1}\right)^2 \cdot \frac{r_1}{r_2} \quad \text{Eqn 17}$$

$$B_t = \frac{1}{r_2 - r_1} \cdot \int_{r_1}^{r_2} B'_t dr = -\left(\frac{a}{r_1}\right)^2 \cdot \frac{r_1}{r_2} \cdot \left[2 - \frac{(1+\nu)}{2} \cdot \left(\frac{a}{r_1}\right)^2 \cdot \left[\left(\frac{r_1}{r_2}\right)^2 + \frac{r_1}{r_2} + 1 \right] \right] \quad \text{Eqn 18}$$

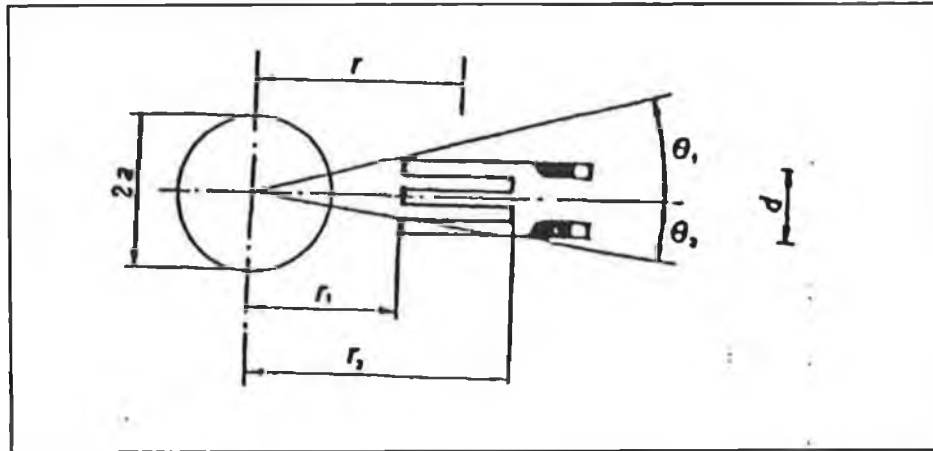


Figure B(a) Strain gauge geometry

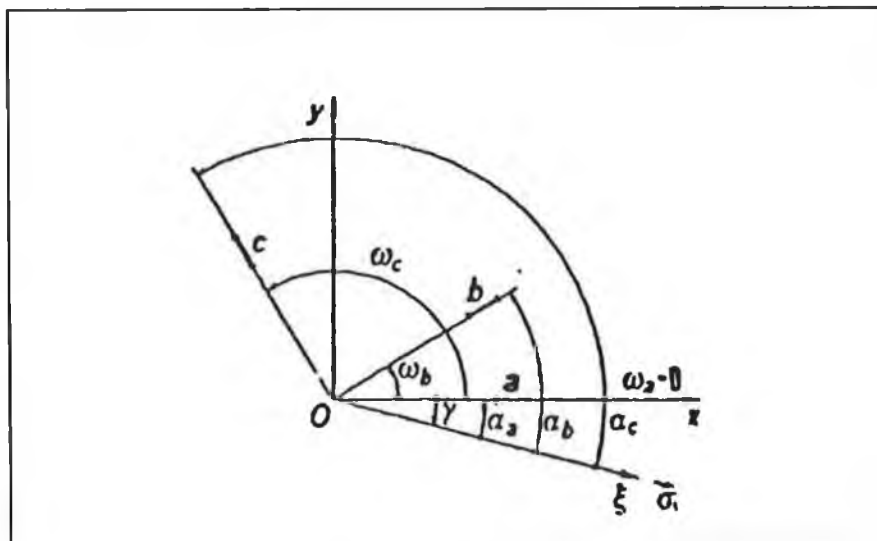


Figure B(b) Geometry of generic rosette

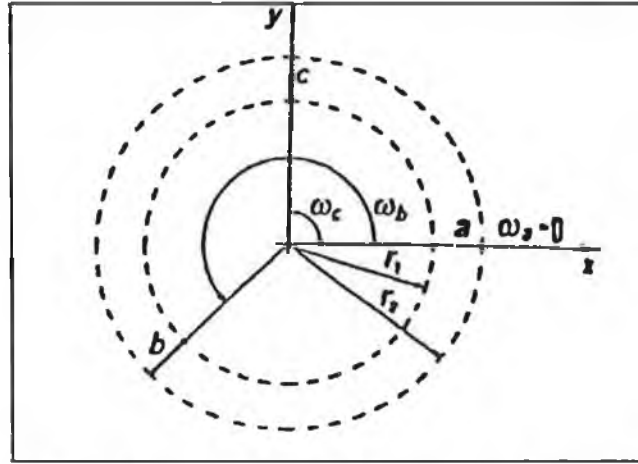


Figure B(c) Geometry of rectangular rosette

Finally, if the grid width of the rosette is not negligible, the integration at the surface occupied by the grid must be extended. Therefore, A_0 and B_0 from the Eqn 12 must be replaced with A''_t and B''_t where:

$$A''_t = -(1+\nu) \frac{a^2}{d(r_2 - r_1)} \cdot (\vartheta_1 - \vartheta_2) \quad \text{Eqn 19}$$

$$B''_t = \frac{-(1+\nu)a^2}{2d(r_2 - r_1)} \cdot \left[\frac{4(1-\nu)}{1+\nu} \cdot (\vartheta_1 - \vartheta_2) + \sin(2\vartheta_1) - \sin(2\vartheta_2) + \left(\frac{a}{r_1} \right)^2 \cdot \sin(2\vartheta_1) \cdot \cos(2\vartheta_1) + \left(\frac{a}{r_2} \right)^2 \cdot \sin(2\vartheta_2) \cdot \cos(2\vartheta_2) \right] \quad \text{Eqn 20}$$

$$\text{with } \vartheta_1 = \arctg \frac{d}{r_1} \text{ and } \vartheta_2 = \arctg \frac{d}{2r_2} \quad \text{Eqn 21}$$

To calculate the residual stresses σ_1 and σ_2 and their orientation, three strains must be measured, therefore a three elements strain gauge is used.

w_a , w_b and w_c are the angles that the three grids a, b and c of the rosette form with an x-axis, Figure B(b).

Assuming the x-axis coincides with the longitudinal axis of the grid ($w_a = 0$)

$$\alpha_a = -\gamma \quad \alpha_b = -\gamma + w_b; \quad \alpha_c = -\gamma + w_c; \quad \text{Eqn 22}$$

where γ is the angle between grid a and stress σ_1 , measured counter clockwise from grid a.

Eqn 12 gives the relation between the strains measured by strain gauge and residual stresses:

$$\varepsilon_i = \frac{A_0}{E}(\sigma_1 + \sigma_2) + \frac{B_0}{E}(\sigma_1 - \sigma_2) \cdot \cos(2\alpha_i) \quad (i = a, b, c) \quad \text{Eqn 23}$$

For a rectangular rosette (Figure 36c) with x-axis coinciding with the axis of the grid a, the grid form the angles:

$$w_a = 0^\circ; \quad w_b = 225^\circ \text{ (or } 45^\circ) \text{ and} \quad w_c = 90^\circ$$

Therefore:

$$\alpha_a = -\gamma; \quad \alpha_b = -\gamma + 225^\circ; \quad \alpha_c = -\gamma + 90^\circ.$$

The system (23) gives:

$$\sigma_{1,2} = \frac{E}{4A_0}(\varepsilon_a + \varepsilon_c) \pm \frac{E}{4B_0} \cdot \sqrt{(\varepsilon_c - \varepsilon_a)^2 + (\varepsilon_a - 2\varepsilon_b + \varepsilon_c)^2} \quad \text{Eqn 24}$$

$$\tan 2\gamma = \frac{\varepsilon_a - 2\varepsilon_b + \varepsilon_c}{\varepsilon_c - \varepsilon_a} = \frac{N}{D} \quad \text{Eqn 25}$$

Where the minus sign is for the main major stress σ_1 and the positive sign is for the main less stress σ_2

To allocate the corrected value of γ the sign of N and D must be considered in accordance to the following table by the gauge manufacturer:

$N \geq 0, D > 0$	$0 \leq \gamma \leq 45^\circ$	$\gamma = 1/2 \operatorname{tng}^{-1} (N/D)$
$N > 0, D = 0$	$\gamma = 45^\circ$	$\gamma = 1/2 \operatorname{tng}^{-1} (N/D)$
$N \geq 0, D < 0$	$45^\circ < \gamma \leq 90^\circ$	$\gamma = 1/2 \operatorname{tng}^{-1} (N/D) + \pi/2$
$N < 0, D < 0$	$90^\circ < \gamma < 135^\circ$	$\gamma = 1/2 \operatorname{tng}^{-1} (N/D) + \pi/2$
$N < 0, D \geq 0$	$135^\circ \leq \gamma < 180^\circ$	$\gamma = 1/2 \operatorname{tng}^{-1} (N/D) + \pi$
$N = D = 0$	γ indeterminate, plane isostatic state $\sigma_1 = \sigma_2$	

Appendix D

Results of Anova Analysis

- - - - - O N E W A Y - - - - -

Variable	STRESS	stress value			
By Variable	PREHEAT	Pre-spray temperature			
Analysis of Variance					
Source	D.F.	Sum of Squares	Mean Squares	F Ratio	F Prob.
Between Groups	3	61488.8867	20496.2956	67.0800	.0000
Linear Term	1	57177.4140	57177.4140	187.1295	.0000
Deviation from Linear	2	4311.4727	2155.7363	7.0553	.0171
Within Groups	8	2444.4000	305.5500		
Total	11	63933.2867			

Variable	STRESS	stress value			
By Variable	THICKNES	coating thickness			
Analysis of Variance					
Source	D.F.	Sum of Squares	Mean Squares	F Ratio	F Prob.
Between Groups	1	42.3200	42.3200	.0076	.9335
Linear Term	1	42.3200	42.3200	.0076	.9335
Within Groups	6	33569.2600	5594.8767		
Total	7	33611.5800			

Figure A ANOVA analysis results for various coating samples.

- - - - - O N E W A Y - - - - -

Variable BOND
By Variable PREHEAT Pre-spray temperature

Analysis of Variance

Source	D.F.	Sum of Squares	Mean Squares	F Ratio	F Prob.
Between Groups	4	8506.2810	2126.5702	8.3322	.0000
Unweighted Linear Term	1	6114.6886	6114.6886	23.9583	.0000
Weighted Linear Term	1	3063.3877	3063.3877	12.0028	.0006
Deviation from Linear	3	5442.8933	1814.2978	7.1087	.0001
Within Groups	611	155940.8602	255.2224		
Total	615	164447.1412			

Variable BOND
By Variable THICKNES coating thickness

Analysis of Variance

Source	D.F.	Sum of Squares	Mean Squares	F Ratio	F Prob.
Between Groups	7	65005.2701	9286.4672	56.7786	.0000
Weighted Linear Term	1	62860.4139	62860.4139	384.3364	.0000
Deviation from Linear	6	2144.8562	357.4760	2.1857	.0428
Within Groups	608	99441.8711	163.5557		
Total	615	164447.1412			

- - - - - O N E W A Y - - - - -

Variable BOND
By Variable ANGLE wall angle

Analysis of Variance

Source	D.F.	Sum of Squares	Mean Squares	F Ratio	F Prob.
Between Groups	2	59097.7835	29548.8917	171.9372	.0000
Unweighted Linear Term	1	55213.8942	55213.8942	321.2750	.0000
Weighted Linear Term	1	58632.0045	58632.0045	341.1641	.0000
Deviation from Linear	1	465.7789	465.7789	2.7102	.1002
Within Groups	613	105349.3577	171.8587		
Total	615	164447.1412			

Figure B. ANOVA analysis for all the repair samples.

- - - - - O N E W A Y - - - - -

Variable BOND
By Variable POSTHEAT post heat

Analysis of Variance

Source	D.F.	Sum of Squares	Mean Squares	F Ratio	F Prob.
Between Groups	2	26803.3156	13401.6578	59.6846	.0000
Weighted Linear Term	1	25777.7252	25777.7252	114.8017	.0000
Deviation from Linear	1	1025.5904	1025.5904	4.5675	.0330
Within Groups	613	137643.8256	224.5413		
Total	615	164447.1412			

Variable BOND
By Variable SURFACE substraee surface treatment

Analysis of Variance

Source	D.F.	Sum of Squares	Mean Squares	F Ratio	F Prob.
Between Groups	1	1918.6295	1918.6295	7.2482	.0073
Within Groups	614	162528.5118	264.7044		
Total	615	164447.1412			

Figure B ANOVA analysis for all the repair samples (continue).

- - - - - O N E W A Y - - - - -

Variable BEND bending test
By Variable ANGLE wall angle

Analysis of Variance

Source	D.F.	Sum of Squares	Mean Squares	F Ratio	F Prob.
Between Groups	3	3530.8667	1176.9556	63.1503	.0000
Linear Term	1	3484.8600	3484.8600	186.9825	.0000
Deviation from Linear	2	46.0067	23.0033	1.2343	.2948
Within Groups	116	2161.9333	18.6374		
Total	119	5692.8000			

- - - - - O N E W A Y - - - - -

Variable BEND bending test
By Variable PREHEAT Pre-spray temperature

Analysis of Variance

Source	D.F.	Sum of Squares	Mean Squares	F Ratio	F Prob.
Between Groups	2	515.8500	257.9250	5.8292	.0039
Linear Term	1	514.8214	514.8214	11.6351	.0009
Deviation from Linear	1	1.0286	1.0286	.0232	.8791
Within Groups	117	5176.9500	44.2474		
Total	119	5692.8000			

27 Jun 97 SPSS for MS WINDOWS Release 6.0

Page 78

- - - - - O N E W A Y - - - - -

Variable BEND bending test
By Variable THICKNES coating thickness

Analysis of Variance

Source	D.F.	Sum of Squares	Mean Squares	F Ratio	F Prob.
Between Groups	4	487.2167	121.8042	2.6909	.0345
Linear Term	1	371.7893	371.7893	8.2134	.0049
Deviation from Linear	3	115.4274	38.4758	.8500	.4694
Within Groups	115	5205.5833	45.2659		
Total	119	5692.8000			

Figure C ANOVA analysis for all the three point bend test samples.